1974

Laminar flow heat transfer in ordinary and augmented tubes

Shun-Wu Hong
Iowa State University

INFORMATION TO USERS

This material was produced from a microfilm copy of the original document. While the most advanced technological means to photograph and reproduce this document have been used, the quality is heavily dependent upon the quality of the original submitted.

The following explanation of techniques is provided to help you understand markings or patterns which may appear on this reproduction.

1. The sign or "target" for pages apparently lacking from the document photographed is "Missing Page(s)". If it was possible to obtain the missing page(s) or section, they are spliced into the film along with adjacent pages. This may have necessitated cutting thru an image and duplicating adjacent pages to insure you complete continuity.

2. When an image on the film is obliterated with a large round black mark, it is an indication that the photographer suspected that the copy may have moved during exposure and thus cause a blurred image. You will find a good image of the page in the adjacent frame.

3. When a map, drawing or chart, etc., was part of the material being photographed the photographer followed a definite method in "sectioning" the material. It is customary to begin photoing at the upper left hand corner of a large sheet and to continue photoing from left to right in equal sections with a small overlap. If necessary, sectioning is continued again — beginning below the first row and continuing on until complete.

4. The majority of users indicate that the textual content is of greatest value, however, a somewhat higher quality reproduction could be made from "photographs" if essential to the understanding of the dissertation. Silver prints of "photographs" may be ordered at additional charge by writing the Order Department, giving the catalog number, title, author and specific pages you wish reproduced.

5. PLEASE NOTE: Some pages may have indistinct print. Filmed as received.

Xerox University Microfilms
300 North Zeeb Road
Ann Arbor, Michigan 48106

Laminar flow heat transfer in ordinary and augmented tubes

by

Shun-Wu Hong

A Dissertation Submitted to the
Graduate Faculty in Partial Fulfillment of
The Requirements for the Degree of
DOCTOR OF PHILOSOPHY

Major: Mechanical Engineering

Approved:

Signature was redacted for privacy.

In Charge of Major Work

Signature was redacted for privacy.

For the Major Department

Signature was redacted for privacy.

For the Graduate College

Iowa State University
Ames, Iowa
1974

TABLE OF CONTENTS

LIST OF TABLES

LIST OF FIGURES

NOMENCLATURE

Latin Symbols

A	cross-sectional flow area, $\pi D^2/4$
$\underline{A}$	matrix
A_s	cross-sectional flow area with twisted tape, $A - \delta D_i$
a	tube radius
a_i, b_i, c_i, d_i	elements of vector
Be	viscosity parameter, $-\frac{1}{\mu}\left(\frac{d\mu}{dT}\right)\Delta T$
C	axial pressure gradient or element of vector
C_1	coefficient, $Nu/Ra^{\frac{1}{4}}$; constant
C_p	constant pressure specific heat
D, D_i	inside tube diameter
D_o	outside tube diameter
e	thermocouple voltage reading
f	dummy variable; Darcy friction factor, $2 g_c D_i \Delta P/(L \rho \bar{W}^2)$
g	gravitational acceleration
G	mass flux, $\dot{m}/A_s$
g_c	gravitational constant in Newton's law
Gr	Grashof number, $g\beta\rho^2 a^3 \Delta T/\mu^2$
Gr_a^*	modified Grashof number, $g\beta\rho^2 a^3 \Delta T^*/\mu^2$
Gr^{∇}	Grashof number for Non-Newtonian fluid, Eq. (F-14)
Gr_D	Grashof number based on diameter, $g\beta\rho^2 D^3 \Delta T/\mu^2$
h	enthalpy; local heat transfer coefficient, $q''/(T_w - T_b)$

$\bar{h}$	circumferential average heat transfer coefficient, $q''/(\bar{T}_w - T_b)$
H	pitch for 180° rotation of tape; enthalpy
I	electric current
K	fluid thermal conductivity
k_f	tape thermal conductivity
k_w	tube wall thermal conductivity
K	consistency index, Eq. (F-1)
L	length along tube axis
L_s	tube length from onset of heating to measuring section
L_T	total heated length of test section
M	number of divisions in R-direction
$\dot{m}$	mass flow rate
N	number of divisions in θ-direction
Nu	Nusselt number, $\bar{h}(2a)/k$
Nu_s	Nusselt number for swirl flow, $\bar{h}(D_i)/k$
P	pressure
P_d	pressure due to motion
P_s	hydrostatic pressure
P_e	Peclet number, Re Pr
Pr	Prandtl number, $\mu C_p/k$
P_w^*	tube wall parameter, $k D/(k_w t)$
ΔP	pressure drop
q	rate of heat transfer
q'	rate of heat transfer per unit length
q''	rate of heat transfer per unit area

q'''	rate of volumetric heat generation
R, θ, Z	dimensional cylindrical coordinates
r, θ, z	dimensionless cylindrical coordinates
Ra	Rayleigh number, Gr Pr
Ra_a	Rayleigh number, Gr_a Pr
Ra_a^*	modified Rayleigh number, Gr_a^* Pr
Ra_D	Rayleigh number based on diameter, Gr_D Pr
Re	Reynolds number, $\frac{\bar{W}\, a\, \rho}{\mu}$
Re_D	Reynolds number based on diameter, $\frac{\bar{W}\, D\, \rho}{\mu}$
Re_s	Reynolds number for swirl flow, $\frac{G\, D}{\mu}$
S	pipe circumference, $2\pi a$
T	local fluid temperature
t	tube wall thickness
T_b	bulk average temperature
T_w	temperature at wall
T^+	temperature in the core region
ΔT	temperature difference, $\bar{T}_w - T_b$
ΔT^*	modified temperature difference, q"a/k
U, V, W	dimensional velocities in R, θ, Z directions or in X, Y, Z directions of boundary layer region
u, v, w	dimensionless velocities in R, θ, z directions or in x, y, z directions of boundary layer region, U/U_c, V/V_c, $W/\bar{W}$
U^+, V^+, W^+	dimensional velocities in X^+, Y^+, Z directions of core

u^+, v^+, w^+ — dimensionless velocity in x^+, y^+, z directions of core region

U_c — characteristic velocity, α/a ; $\frac{\mu}{\rho a}\left(\frac{Gr}{Pr}\right)^{1/2}$

U_c^+ — characteristic velocity in core region, $\frac{\mu}{\rho a}\left(\frac{Gr}{Pr}\right)^{1/4}$

V_c — characteristic velocity, $\frac{\mu}{\rho a}\left(\frac{Gr}{Pr}\right)^{1/4}$

$\bar{W}$ — bulk average velocity in axial direction

X, Y, Z — dimensional boundary layer coordinates: circumferential direction, perpendicular to the wall direction, and axial direction

X^+, Y^+, Z — dimensional core region coordinates: horizontal direction, vertical direction, and axial direction

x, y — dimensionless boundary layer coordinates: circumferential and perpendicular to the wall

x^+, y^+ — dimensionless core region coordinates: horizontal and vertical

y — twist ratio, H/D

z — reduced axial direction distance, $Z/a\ Re_a\ Pr$

Z_c — characteristic length in axial direction, $a\ Re_a\ Pr$

Greek Symbols

α — thermal diffusivity, $k/\rho\ C_p$

β — coefficient of thermal expansion, $\frac{-1}{\rho}\left(\frac{\partial \rho}{\partial T}\right)_p$

γ — coefficient of viscosity variation due to temperature change, $\frac{-1}{\mu}\left(\frac{d\mu}{dT}\right)$

δ thickness of the thermal boundary layer or thickness of twisted tape

Δ characteristic parameter for thermal boundary layer, $a/(Gr\ Pr)^{1/4}$

Δ_h characteristic parameter for hydrodynamic boundary layer

Δ_T characteristic parameter for thermal boundary layer

ϵ a prescribed error

η dimensionless position, y/δ

θ angle measured from top of the tube in Chapters II, V; from bottom of tube in Chapter III

μ viscosity

ν kinematic viscosity, μ/ρ

ξ vorticity function

ρ density

ϕ dimensionless temperature, $\frac{T - T_b}{\Delta T}$ or $\frac{T - T_b}{\Delta T^*}$

ϕ_w dimensionless temperature in core region evaluated at wall, $\frac{T^+ - T_b}{\Delta T}$

Ψ stream function

ω relaxation factor

∇ three-dimensional Laplacian operator,

$$\frac{\partial^2}{\partial r^2} + \frac{1}{r}\frac{\partial}{\partial r} + \frac{\partial^2}{r^2 \partial\, \theta^2} + \frac{\partial^2}{\partial z^2}$$

∇_1 two-dimensional Laplacian operator,

$$\frac{\partial^2}{\partial r^2} + \frac{1}{r}\frac{\partial}{\partial r} + \frac{\partial^2}{r^2 \partial \theta^2} \quad \text{or} \quad \frac{\partial^2}{\partial x^2} + \frac{\partial^2}{\partial y^2} .$$

Subscripts

b	bulk mean value
c	characteristic value
f	evaluated at fluid film temperature, $(\bar{T}_w + T_b)/2$
h	across heated section
i, j	space subscripts of grid points in R and θ directions
i	inside or inlet
o	outside, outlet, empty tube, or twisted tape of $y = \infty$
s	swirl flow
t	total
w	evaluated at tube wall temperature
∞	asymptotic value

Superscripts

k	space superscripts of grid point in z direction
n	nth iteration

CHAPTER I. INTRODUCTION

Laminar Flow Heat Transfer in Tubes

Laminar flow heat transfer in tubes is encountered in a wide variety of engineering situations. The following examples can be cited: heating or cooling of viscous liquids in the chemical and food industries, heating of oils so that they can be transported, cooling of space suits, heating of the circulating fluid in solar collectors, heat transfer in compact exchangers, and cooling or warming of blood during surgical operations. One potential application of great magnitude involves the heating of oil from the Arctic oil fields so that it can be transported south. It is estimated that more than $100 million annually is involved in heat exchangers associated with laminar flow. In addition, in cases where normal heat exchanger operation is in turbulent flow, off-design operation and operation during start-up or shut-down periods may result in laminar flow conditions. When laminar flow heat transfer occurs, it usually represents the dominant thermal resistance in a heat exchanger.

In the discussion of the heat transfer activity in the present decade, Sabersky [1] emphasized that even though laminar flow heat exchangers have been and are now being used widely, there is a lack of precision in the prediction of the laminar flow heat transfer coefficients. It has been recognized that laminar flow heat transfer is dependent on many variables, including tube geometry, flow inlet velocity profile, fluid properties, tube orientation, tube wall properties, and heat flux boundary conditions. With the demands of modern technology, more accurate predictions of laminar heat transfer are required. In recent years, the solutions available for

laminar flow have been extended by sophisticated experiments and analysis. Today, by the application of modern computer technology, analysis has exceeded experimental verification to some degree.

Literature Survey

A tabular survey of the current and past literature relating to laminar flow will be given here for the purpose of general orientation. The existing analytical solutions for the heat transfer and pressure drop parameters for laminar-flow systems can be classified according to axial thermal boundary condition, fluid property variation, tube geometry, orientation, and tube thermal boundary conditions. Neglecting fluid property variation and orientation effects, Shah and London [2] reviewed the available analytical solutions up to December, 1970, for laminar flow. Only the forced convection, steady laminar flow of constant-property Newtonian fluids through stationary ducts was considered. However, in any convective heat transfer process within a gravitational force field, density differences arising from differences in temperature are responsible for natural convection effects, and, in most practical situations, both forced and free convection modes are present. For completeness, then, the present survey includes variable properties and tube orientation.

Emphasis is given to the analytical solutions for laminar flow heat transfer in straight and stationary tubes. The primary literature up to May, 1974, is presented in Table 1.1. Letters and numbers are used to represent different conditions, as follows:

G. Geometry

1. Circular Tubes

2. Rectangular Channels, etc.

O. Orientation

1. Horizontal

2. Inclined

3. Vertical

B. Thermal Boundary Condition

1. Constant heat flux axially, but uniform wall temperature around circumference

2. Constant heat flux axially and circumferentially

3. Constant wall temperature

A. Axial Thermal Condition

1. Developing

2. Fully developed

P. Fluid Property Variation

1. Constant property

2. Variable density

3. Variable viscosity

4. Non-Newtonian behavior

G1, O1, B1 and B2, A1 , and P1 for example, represents the analytical solution for the entrance region, assuming constant fluid properties, in a horizontal circular tube with the uniform heat flux boundary condition.

As indicated in Table 1.1, many important problems have not been considered. Since it is still not possible to solve a general formulation of the problem, future analytical studies will continue to fill in the gaps in this table. Two such problems of practical interest which are analytically tractable consider the effects of free convection on entrance region heat

Table 1.1. Laminar flow heat transfer in tubes

Investigators	(Year)	[Reference]	Considerations	Method
Constant Property, Fully Developed				
Marco and Han	(1955)	[3]	G1 and G2, O1, B1, A2, P1	Analogy with deflection of thin plates
Sparrow and Siegel	(1959)	[4]	G1, O1, B1, A2, P1	Variational method
Reynolds	(1960)	[5]	G1, O1, B1, A2, P1	Series expansion
Cheng	(1966)	[6]	G2, O1, B1, A2, P1	Analogy with deflection of thin plates
Faris and Viskanta	(1969)	[7]	G1, O1, B2, A2, P1	Perturbation
Constant Property Entrance Region				
Graetz	(1883)	[8]	G1, O1, B1 and B3, A1, P1	Series expansion
Clark and Kays	(1953)	[9]	G2, O1, B1 and B3, A1, P1	Numerical
Kays	(1955)	[10]	G1, O1, B1, A1, P1	Numerical
Sellars, Tribus, and Klein	(1956)	[11]	G1 and G2, O1, B1 and B3, A1, P1	Eigen function
Siegel, Sparrow, and Hallman	(1958)	[12]	G1, O1, B1, A1, P1	Series expansion
Singh	(1958)	[13]	G1, O1, B3, A1, P1	Eigen function
Sparrow and Siegel	(1960)	[14]	G1 and G2, O1, B1, A1, P1	Variational method
Tien and Dawelek	(1964)	[15]	G1, O1, B3, A1, P1	Series expansion
Hwang and Fan	(1964)	[16]	G2, O1, B1 and B3, A1, P1	Numerical
Ulrichson and Schmitz	(1965)	[17]	G1, O1, B2 and B3, A1, P1	Numerical

Table 1.1 (Continued)

Investigators	(Year)	[Reference]	Considerations	Method
Hornbeck	(1965)	[18]	G1, 01, B1 and B3, A1, P1	Numerical
Roy	(1966)	[19]	G1, 01, B1 , A1, P1	Numerical
McMordie and Emery	(1966)	[20]	G1, 01, B1, A1, P1	Numerical
Montgomery and Wilbulswas	(1966)	[21]	G2, 01, B1 and B3, A1, P1	Numerical
Butterworth and Hazell	(1969)	[22]	G1, 01, B1, A1, P1	Series expansion
Manohar	(1969)	[23]	G1, 01, B2, B3, A1, P1	Numerical
Hsu	(1971)	[24]	G1, 01, B1, A1, P1	Series expansion
Fully Developed with Density and/or Viscosity Variation				
Deissler	(1951)	[25]	G1, 01, B1, A2, P3	Series expansion
Morton	(1959)	[26]	G1, 01, B1, A2, P2	Perturbation
Kettleborough	(1960)	[27]	G2, 01, B2 and B3, A2, P2 and P3	Numerical
Koppel and Smith	(1962)	[28]	G1, 01, B2, A2, P2 and P3	Series expansion
Bradley and Entwistle	(1965)	[29]	G1, 01, B3, A2, P2 and P3	Numerical
Mori and Futagami	(1967)	[30]	G1, 01, B1, A2, P2	Boundary layer integration
Siegwarth, Mikesell, Readal, and Hanratty	(1969)	[31]	G1, 01, B1, A2, P2	Boundary layer integration
Cheng and Hwang	(1969)	[32]	G2, 01, B1, A2, P2	Numerical

Table 1.1 (Continued)

Investigators	(Year)	[Reference]	Considerations	Method
Newell and Bergles	(1970)	[33]	G1, 01, B1 and B2, A2, P2	Numerical
Siegwarth and Hanratty	(1970)	[34]	G1, 01, B1, A2, P2	Numerical
Hwang and Cheng	(1970)	[35]	G1, 01, B1, A2, P2	Boundary vorticity
Martin and Fargie	(1972)	[36]	G1, 01, B1, A2, P3	Numerical
Entrance Region With Density and/or Viscosity Variation				
Yang	(1962)	[37]	G1, 01, B1 and B3, A1, P3	Series expansion
Rosenberg and Hellums	(1965)	[38]	G1, 01, B3, A1, P3	Numerical
Test	(1968)	[39]	G1, 01, B1, A1, P3	Numerical
Hwang and Hong	(1970)	[40]	G2, 01, B1, A1, P3	Series expansion
Schade and McEligot	(1971)	[41]	G1, 01, B2 and B3, A1, P2 and P3	Numerical
Swearingen and McEligot	(1971)	[42]	G2, 01, B2, A1, P2 and P3	Numerical
Cheng, Hong, and Hwang	(1972)	[43]	G2, 01, B1, A1, P2	Numerical
Non-Newtonian Fluid Flow				
Metzner and Gluck	(1960)	[44]	G1, 01, B3, A2, P4	Series expansion
Oliver and Jenson	(1964)	[45]	G1, 01, B3, A1, P3 and P4	Series expansion
Mikillop	(1964)	[46]	G1, 01, B2 and B3, A1, P4	Numerical

Table 1.1 (Continued)

Investigators	(Year)	[Reference]	Considerations	Method
DeYoung and Scheele	(1970)	[47]	G1, 03, B2, A2, P2, and P4	Series expansion
Vertical Tubes and Channels				
Hallman	(1956)	[48]	G1, 03, B1, A2, P2	Series expansion
Lu	(1960)	[49]	G1, 03, B2, A2, P2	Series expansion
Tao	(1960)	[50]	G2, 03, B2, A2, P2	Complex functions
Rosen and Hanratty	(1961)	[51]	G1, 03, B3, A1, P1 and P3	Series expansion
Lawrence	(1965)	[52]	G1, 03, B2 and B3, A1, P2 and P3	Numerical
Marner	(1968)	[53]	G1, 03, B3, A1, P4	Numerical
Allen and Finn	(1970)	[54]	G1, 03, B3, A1, P2	Numerical
Zeldin and Schmidt	(1971)	[55]	G1, 03, B3, A1, P2	Numerical
Iqbal, Aggarwala, and Khatry	(1972)	[56]	G2, 03, B1, A2, P2	Series expansion
Inclined Tubes				
Iqbal and Stachiewicz	(1966)	[57]	G1, 02, B1, A2, P2	Perturbation
Iqbal and Stachiewicz	(1967)	[58]	G1, 02, B1, A2, P2	Perturbation
Hong	(1971)	[59]	G1, 02, B1, A2, P2	Numerical
Cheng and Hong	(1972)	[60]	G1, 02, B1, A2, P2	Numerical

transfer in horizontal circular tubes (G1, O1, B2, A1, P2) and the effects of the temperature dependency of both density and viscosity on heat transfer in fully developed flows in circular tubes (G1, O1, B1 and B2, A2, P2 and P3).

Several attempts have been made to determine the effect of free convection on a fully developed laminar tube flow. In many cases, the entrance region is quite short; hence, the fully developed case is of practical interest. None of the analyses for fully developed laminar flows have considered temperature-dependent density and viscosity, yet most fluids used in laminar flow exhibit a pronounced variation of viscosity with temperature. Of the various analytical techniques used for studying fully developed combined forced and free convection (perturbation [26, 57, 58], boundary vorticity [35, 59, 60], boundary layer [30, 31, 34], and finite difference [33]), the boundary layer technique appears to be the most promising for inclusion of viscosity effects.

Laminar Flow Heat Transfer Augmentation in Tubes

It has been realized that laminar flow heat transfer coefficients in ordinary tubes are generally low. In recent years, the requirement for more efficient heat transfer systems has stimulated interest in augmentative heat transfer methods. Use of artificially roughened surfaces, use of extended surfaces, use of inlet vortex generators, vibration of the surface or fluid, application of electrostatic fields, and the insertion in tubes of objects such as twisted tapes, coiled wire, or spinners are a few examples of such augmentative techniques. Existing systems can often be improved by using an augmentative method, while in other applications,

such as the design of heat exchangers for use in space vehicles, an augmentative scheme may be mandatory in order for the system to function properly and meet the size limitations imposed. The given augmentative methods are frequently accompanied with increases in cost, weight, pumping power, and extra parts. It is necessary for the designer to understand the mechanism involved in augmentation and to evaluate the performance of the method in terms of applicable design constraints. A detailed survey and evaluation of the many augmentative methods presently employed is given by Bergles [61, 62].

The present investigation is focused on laminar flow heat transfer augmentation in tubes. For this objective, the primary available literature is summarized in Table 1.2.

Devices which establish a swirl in the fluid in order to increase the heat transfer coefficient are particularly attractive augmentative schemes for forced convection systems. However, there appears to be no data for swirl flow of liquids in laminar flow. Swirl flows generated by twisted tapes running the entire length of the heat transfer tube appear to offer significant benefits since improvements in heat transfer are obtainable at relatively low cost. Tape inserts can be easily employed to improve the performance of existing systems. Twisted tapes, of course, involve increased pressure drop and thus pumping power. The benefits of twisted-tape inserts must be viewed in terms of the constraints of the particular application: fixed flow rate, fixed pressure drop, fixed pumping power, etc.

Table 1.2. Laminar flow heat transfer augmentation in tubes

Techniques	Investigators	Test Arrangement	Test Parameters	Conclusions
1. Surface Roughness and Treatment	Cope (1941) [63]	Cooling of water in internally knurled tubes.	Re = 10^3 - 10^5	Roughness increases h in transition and laminar region, but has little effect on h for turbulent flow.
	Nunner (1956) [64]	Two-dimensional attached roughness rings of rectangular or round shape inserted with various spacings in tubular test section. Heating of air.	Re = 500 - 80,000	Up to 280 percent improvement in laminar range with most effective roughness configuration.
	Koch (1958) [65]	Circular disks or rings inserted into tube with various spacings. Heating of air.	Re = 100 - 10^5 L/e: 4-196	Optimum L/e ratio at about 10. Turbulent characteristics at very low Re. 15 - 200 percent improvement.
	Blumenkrantz and Taborek (1971) [66]	Heating and cooling of Alta-Vis-530 in Turbotec deep spirally grooved tubes.	ID = 0.93 in. Re = 3-4500	h increased up to 450 percent for heating and 120 percent for cooling.
	Zappa and Geiger (1971) [67]	Heating of transformer oil in horizontal annulus with inner tube having circumferential fins.	Ratio of spacing to height of fin: 3-40 Re = 200 - 700	h increased up to 83 percent

Table 1.2 (Continued)

Techniques	Investigators	Test Arrangement	Test Parameters	Conclusions
2. Internal Extended Surface	De Lorenzo and Anderson (1944) [68]	Longitudinal fins, in annular gap of double pipe exchanger. Heating of SAE 40, 50 lube oil, and 43° API kerosene.	Re = 20 - 10,000 Numbers of fin = 24, 28, 36	Transition between laminar and turbulent flow begins at Re < 400. h with 24 fins is higher than h with 36 fins about 45 percent.
	Kun (1970) [69]	V fins in straight tubes. Analytical solution for UWT, assuming fully developed, constant property flow.	Variable fin angle and length	Nu_H varies between 1.7 and 4.6.
	Hu and Chang (1973) [70]	Internally finned tubes. Analytical solution for UHF assuming fully developed, constant property flow.	Variable number and length of fins	22 fins extended to 80 percent of radius is the optimum condition, Nu_D = 85.2.
	Watkinson, Miletti and Kubanek (1974) [71]	Heating of SAE 10w30 motor oil in Forge-Fin tubes.	Re = 50 - 3,000 Pr = 180 - 450	Up to 187 percent improvement in h based on constant pumping power comparison.
3. Swirl Flow	Koch (1958) [65]	Heating of air in tubes with loose-fitting twisted tapes.	y = 11, 4.3, 2.5 Re = 100 - 70,000	Up to 50 percent increase in h in laminar range with y = 2.5.
	Siegel and Perlmutter (1958) [72]	Analytical entrance region solution with inlet swirl flow. UHF and constant fluid properties		Nu is higher with swirl flow case than without swirl in entrance region.

Table 1.2 (Continued)

Techniques	Investigators	Test Arrangement	Test Parameters	Conclusions
	Penney (1965) [73]	Twisted-tape is installed loosely and secured at downstream end in a bearing ("Spiraltor"). Heating of corn syrup solution.	Tape rotation up to 100 rpm	h increased up to 95 percent with the rotating tape.
	Kiya and Fukusako (1971) [74]	Analytical region solution with inlet swirl. UWT and constant fluid properties.	Pr = 0.72 K = $\Omega a/w$ = 0, 1.0, 1.5	Entrance swirl increases Nu about 15 percent
	Date and Singham (1972) [75]	Numerical solution of UHF with constant fluid properties.	Pr = 1, 10, 100, 500 Re = 300 - 2,000	Nu increases sharply as Pr and Re/y increase. Nu up to 1250 for Pr = 500, Re/y = 600.
4. Displaced Promoters	Koch (1958)[65]	Disks, propellers, Raschig rings, and balls as tube inserts. Heating of air.	Re = 100 - 70,000	Up to about 200 percent increase with all inserts in laminar region.
	Sununu (1971) [76]	Static Mixer loosely inserted in tube. Heating of silicone oil, water, and lubricating oil.	Re = 0.05 - 500 Pr = 1 - 10,000	Nu increases in both entrance and fully developed region.
	Genetti and Priebe (1973) [77]	Static Mixer, steam heating, motor oil, 10W.	Re = 10 - 2,100	Nu increased with static mixer up to 70.
5. Curved Tubes	Truesdell and Adler (1970) [78]	Numerical solution for helically coiled tubes.	De = 1 - 295	Nu increases as De increases.

Table 1.2 (Continued)

Techniques	Investigators	Test Arrangement	Test Parameters	Conclusions
	Dravid, Smith, Merrill and Brian (1971) [79]	Helically coiled tubes. Entrance region solution, assuming UWT and constant fluid properties.	Pr = 4 - 6 De = 87 - 1950	De shortens entrance length, increases Nu.
	Akiyama and Cheng (1971) [80]	Numerical solution for curved pipe, assuming UHF and constant fluid properties.	Nu = f (De, Pr)	Nu increases with increasing De and Pr.
	Singh (1973) [81]	Helically coiled tubes, electrically heated. Water and Dowtherm G.	Re = 70 - 8,000	Improvement is higher for laminar flow than for turbulent flow. Nusselt number up to 100.
6. Rotating Tubes	Mori and Nakayama (1967) [82]	Analytical solution for a straight pipe rotating around a parallel axis. Fully developed flow, UWT, and constant fluid properties assumed.		Coriolis force increases Nu.
	Mori and Nakayama (1968) [83]	Theoretical analysis of a straight pipe rotating around an axis perpendicular to its own axis.		Nu increases as rotational speed increases.
	Miyazaki (1971) [84]	Analytical solution for a rotating curved pipe. UHF, fully developed flow and constant fluid properties assumed.		Gr, De, and Coriolis forces have significant effect on increasing Nu, but radius ratio has minor effect.

Table 1.2 (Continued)

Techniques	Investigators	Test Arrangement	Test Parameters	Conclusions
7. Vibration	Scanlan (1958) [85]	Forced convection in a rectangular channel with long, heated side vibrated transversely. Heating of water.	a = 0.0005 - 0.002 in. f = 20 - 75 Hz Re = 360 - 2,170	Up to 180 percent increase in h below cavitation intensity.
	Raben (1961) [86]	Transverse vibration of a pipe with water flowing on the outside of the pipe in an annular space.	Re_f = 541 - 16,000 Re_v = 600 - 6,000	Up to 450 percent improvement in h in laminar range.
	Nevill, Commerford and Raben (1963) [87]	Annulus with inner tube laterally oscillating. Heating of water.	a = 0.5 in. f = 20 - 100 Hz q = 4,500 - 13,000 Btu/hr-ft^2	Reduction in h.
	Ogle and Engel (1963) [88]	Annular test section with water flowing in inner tube. Transversely vibrated inner tube.	a = 0.042 - 0.208 in. f = 4 - 450 Hz Re = 417 - 629	Up to 70 percent increase in overall coefficient for laminar flow.
8. Electro-static Fields	Schmidt and Leidenfrost (1953) [89]	Flow of oil in annular test section with inner surface heated. Electric field applied to annular gap.	Re = less than 3,000 E = 0 - 32 kvdc	Up to 400 percent improvement in h.
	Velkoff (1963) [90, 91]	Heating of air inside a tube having a wire electrode suspended concentrically in tube.	E = 0 - 75 kvdc	Up to 100 percent increase in h.

Table 1.2 (Continued)

Techniques	Investigators	Test Arrangement	Test Parameters	Conclusions
	Levy (1963) [92]	Heating of silicon oil in annular test section. Electric field applied to annular gap.	ID = 0.5 in., OD = 0.79 in. E = 0 - 15 kvdc	Up to 140 percent increase in h.
	Moss and Grey (1966) [93]	Heating of nitrogen inside a tube having a wire electrode located concentrically in tube.	Re = 1,200 - 10,000	Up to 95 percent improvement in h for laminar flow; negligible improvement for turbulent flow.

Scope of Investigation

The preceding discussion has indicated several unresolved areas in laminar flow heat transfer. In accordance with the practical need for new information in this area, an analytical and experimental program was undertaken. The present report on this program is organized mainly into four chapters. Chapter II concerns free convection effects in the thermal entrance region for laminar flow in horizontal circular tubes. The literature review reveals that an analytical solution is not available for this problem. As indicated by the experimental work of Petukhov and Polyakov [94, 95] and Bergles and Simonds [96], the developing length for the combined forced and free convection flow can be much shorter than that required in the absence of free convection effects. The disagreement between these experimental investigations and the traditional analytical prediction of entrance length and heat transfer coefficient in the fully developed region encourages an analytical solution of the secondary motion effect in the entrance region. The objective in Chapter II is, therefore, to obtain a more realistic analytical solution which can be used for design purposes.

Chapter III describes the temperature-dependent viscosity effect on combined forced and free laminar convection in horizontal tubes. Morcos and Bergles [97] recently reported that the available analytical solutions could not accurately predict the heat transfer results. The disagreement is especially noticeable for fluids with highly temperature-dependent viscosities, such as ethylene glycol. The usual purely empirical correlations which employ bulk to wall viscosity ratios or evaluate the fluid properties

at the film temperature are not derivable from the governing differential equation or dimensional analysis. A new parameter which can be derived directly from the governing equation must be introduced. In order to complete the study of fluid property variation, non-Newtonian fluid flow, together with variable density and constituency, in horizontal tubes is discussed briefly in Appendix E.

Chapter IV describes a theoretical study which supports the experimental twisted tape studies presented in Chapter V. This analytical solution for constant-property flow in the entrance region of a semi-circular tube is a limiting solution for twisted tape flow which is used to verify that experimental data were obtained under fully developed conditions.

CHAPTER II. ANALYTICAL SOLUTIONS FOR COMBINED FORCED AND FREE LAMINAR CONVECTION IN THE ENTRANCE REGION OF HORIZONTAL TUBES

Introduction

Heat transfer from a solid surface to a fluid is influenced by two modes of induced fluid motion when a pump is used to produce circulation. The primary mode is called forced convection. Motion due to density differences occurring throughout a fluid under the influence of gravity is called free or natural convection. For laminar flow heat transfer in a horizontal tube, the body forces are characterized by the Grashof number and the forced flow by the Reynolds number. The tube diameter is conventionally used as the characteristic dimension in both dimensionless parameters. The fluid properties associated with Prandtl number are usually coupled with Grashof number and Reynolds number as Rayleigh number and Peclet number, respectively. In most physical situations, both forced and free convection modes are present, and the relative magnitude of the forces associated with these modes determines whether the flow can be classified as pure forced, combined forced and free, or free convection.

Three boundary conditions are generally considered for analytical solutions of laminar heat transfer in circular tubes: uniform wall temperature (UWT), uniform heat flux (UHF), and uniform temperature difference. For pure forced convection, the thermally fully developed analyses for these boundary conditions are well known. The heat transfer analysis in the developing thermal region is given for uniform wall temperature (classical Graetz problem) in Refs. 8, 10, 11, 18, and 21, for uniform heat flux in Refs. 10, 11, 12, 18, 19, and 21, and for constant temperature

difference in Ref. 10 (refer to Table 1.1).

In the real physical situation, however, when a flowing fluid is heated in a horizontal tube, the fluid near the wall is warmer, and therefore lighter, than the fluid farther removed from the wall. This lighter fluid thus flows upward along the wall and continuity requires a downflow of the heavier fluid near the center of the tube. As a result, there is a secondary fluid motion established which is symmetrical about a vertical plane passing through the axis of the tube; combined with the axial flow, the three-dimensional streamlines exhibit a spiraling character.

In situations where natural convection effects are not negligible, the tube orientation becomes important, with the two major alignments being vertical and horizontal. In vertical tubes, the velocity caused by buoyant forces is in parallel to the direction of the main flow. It is relatively straightforward to solve the momentum and energy equations analytically including free convection because rotational symmetry is retained. Detailed results for upward and downward fully developed flow in vertical tubes are given by Hallman [48]. In the case of horizontal tubes, however, the buoyant and inertial forces are perpendicular to each other, which results in loss of rotational symmetry and a more difficult analysis. In some operating conditions, the tube may be inclined. When this occurs, the tube inclination angle is seen to be an important parameter. As indicated recently by Cheng and Hong [60] the Nusselt number increases considerably with increasing tube inclination angle from zero to 10 degrees for high Rayleigh number flow due to strong secondary flow. For tube inclinations larger than 10 degrees, the Nusselt number increases slightly and reaches a maximum at 90 degrees of tube inclination. A maximum Nusselt

number does not exist for some intermediate tube inclinations, which is contrary to the results obtained by Iqbal and Stachiewicz [57] using a perturbation method.

Morton [26], del Casal and Gill [98] and Iqbal and Stachiewicz [57] considered series solutions of fully developed combined forced and free convection in horizontal tubes using various quantities for a perturbation parameter. Applying Boussinesq's approximation [99], all of these investigators assumed constant properties except for density variation with temperature in the buoyancy term. These results, which include both first-order and second-order perturbation analyses, are, however, contrary to experimental results for even moderate values of the expansion parameters. Mori and Futagami [30] utilized an integral approach which was in fair agreement with limited experimental results for air. An early boundary layer solution by Mikesell [100] was unsuccessful; however, a later boundary layer analysis by Siegwarth and co-workers [31] agreed well with data for ethlene glycol at larger Rayleigh numbers. With this method the flow is divided into two regions: a boundary layer region close to the wall and a core region. Since intense circulation is required for this model, the boundary layer solution is only good for larger Rayleigh numbers.

In order to accurately solve the horizontal tube problem, Newell and Bergles [33] employed finite-difference techniques and a large-scale digital computer to obtain the fully developed laminar flow solution (UHF) for two limiting boundary conditions: zero circumferential heat conduction in the tube wall ("Glass tube" or "ZC") and uniform temperature around the tube circumference ("Infinite conductivity tube" or "IC"). The finite-difference approach appears to be the only method which will yield accurate

predictions over a wide range of conditions. Siegwarth and Hanratty [34] applied a finite-difference solution and obtained detailed flow and temperature profiles for several cases with ethylene glycol. Cheng and Hwang [32] recently developed a more economical boundary vorticity method to obtain solutions for horizontal and inclined tubes. This method is restricted to lower values of the Rayleigh number. Among these analytical studies, several hundred percent Nusselt number increases were reported for high Rayleigh numbers.

Martin and Fargie [36] and Test [39] considered the effects of temperature-dependent viscosity and reported that heat transfer coefficients were further enhanced by viscous heat generation within the fluid. Viscous effects were negligible for Prandtl numbers of 100 or less. Test further indicated that errors of more than 50 percent in both f and Nu were predicted when the $\partial\nu/\partial r \cdot \partial u/\partial r$ term in the momentum equation was eliminated. For most liquids, the heat transfer coefficent increases with increasing temperature due to decreasing viscosity. However, the increase in most cases is seen to be less than 100 percent. It is clear at this stage that temperature-dependent density has a greater effect on the heat transfer coefficient than Temperature-dependent viscosity.

A distinction between variable density and variable viscosity effects can easily be made in an analytical formulation; however, it is difficult to sort out the two effects in an experiment. At present, a number of empirical correlations have been proposed for heating or cooling of various fluids in horizontal tubes with approximately constant wall temperature [101-104]. In most of these investigations, the data correlations were attempted with a view toward obtaining average Nusselt numbers via various

modifications of the Graetz solution which applies to the uniform wall temperature situation. For the constant heat flux boundary condition, the free convection persists throughout the tube. Experimental data for the heating of air [105-108], water [94, 95, 109-112] and ethylene glycol [111, 112] are available at present. Good agreement between analytical predictions and experimental results was reported for air and ethylene glycol by Mori and Futagami [30] and Siegwarth et al. [31], respectively. A single parameter, Rayleigh number or Grashof number, was found to correlate most of the data satisfactorily.

Experimental results from Petukhov and Polyakov [94, 95] and Petukhov et al. [110] show that the constant property solution in the entrance region is valid only for very low Rayleigh numbers. The only analytical confirmation of this effect is a recent study for rectangular channels with uniform heat flux [43] The pure forced convection approximation is shown to be applicable only when the Rayleigh number is less than about 10^3. An analytical solution for the entrance region of circular tubes with free convection effects is not yet available.

In earlier investigations [94, 95, 105, 111], it has been established that experimental works directed towards the assessment of the free convection effect in the tube inlet will be inhibited by the number of parameters to be controlled, by a lack of knowledge regarding the form of the function needed to correlate the data, by the difficulty of obtaining the precise measurements required for laminar flow, and by the difficulty of maintaining the specified thermal boundary conditions. Experimental data for the entrance region are very limited. These considerations suggest

that an analytical solution for the entrance region with buoyancy effects is an appropriate subject for the first part of this study.

Formulation of the Problem

Statement of Problem

Consideration is given to a steady, hydrodynamically fully developed, but thermally developing, laminar flow of a viscous Newtonian fluid in a horizontal tube where a step change in uniform wall heat flux is imposed starting at Z = 0. See Fig. 2-1. The problem involves determining the temperature development and the variation in heat transfer coefficient along the axial and circumferential directions. The variation of the density in the presence of the earth's gravitational field provides, of course, the motive force for the secondary flow that is under consideration. However, when the density is primarily a function of temperature, as was pointed out by Boussinesq [99], the variability of the density can be ignored in all of the analytical expressions except the body force term. This effects a considerable simplification in mathematical formulation of the problem since part of the non-linearities associated with the material derivatives are circumvented. The free convection has a major influence on the heat transfer coefficient.

The analysis will start with the derivation of the governing equations valid for any Prandtl number. A Newtonian fluid is assumed and the viscosity is assumed to be constant.

Governing Equations

Referring to the coordinate system shown in Fig. 2-1, the continuity

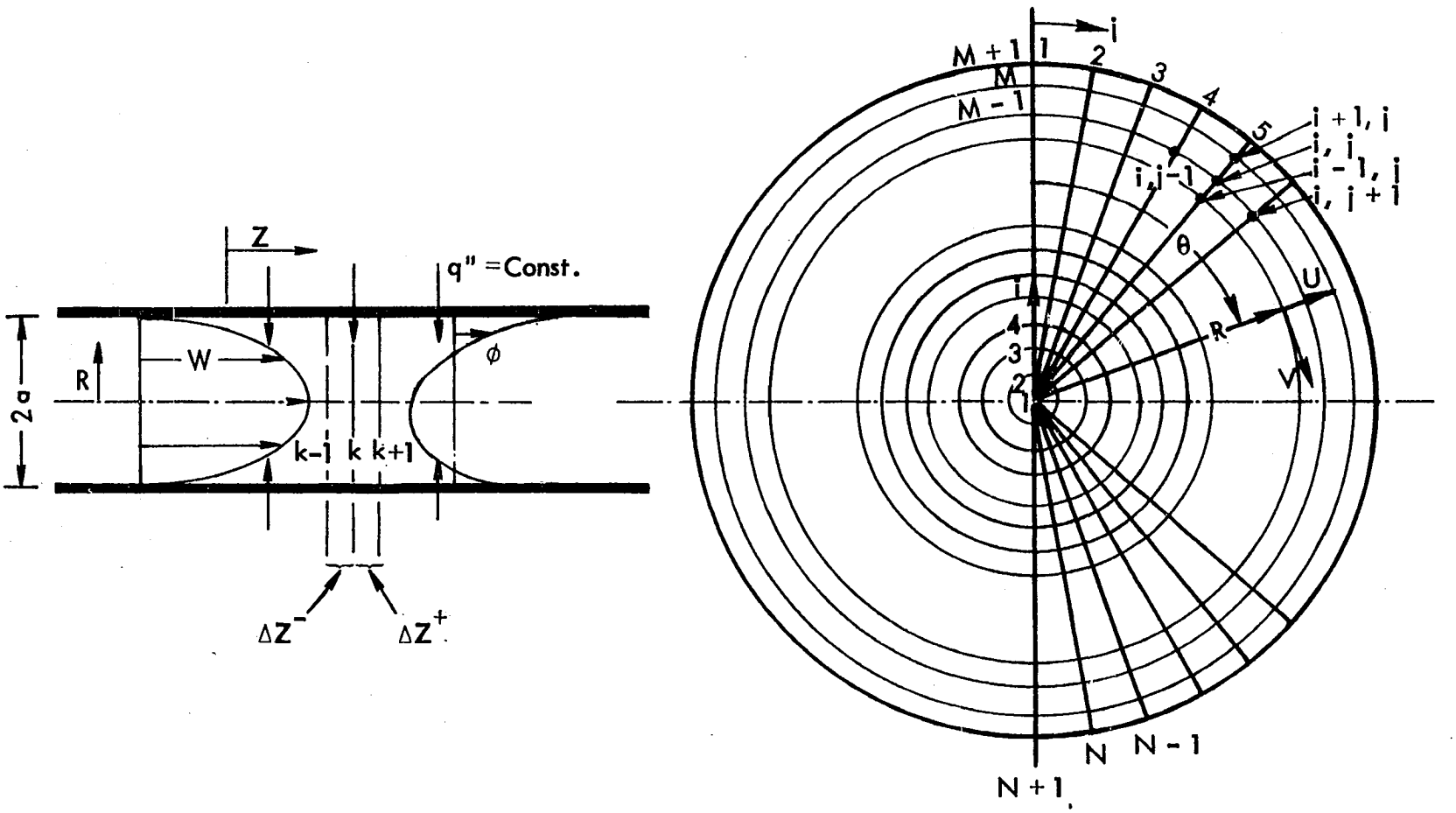

Fig. 2-1 Coordinate system and numerical grid for circular tube.

equation, the complete Navier-Stokes equations, and the energy equation in cylindrical coordinates become

Continuity:

$$\frac{1}{R}\frac{\partial}{\partial R}(RU) + \frac{1}{R}\frac{\partial V}{\partial \theta} + \frac{\partial W}{\partial Z} = 0 \tag{2-1}$$

Axial direction momentum equation:

$$\rho_b\left(U\frac{\partial W}{\partial R} + \frac{V}{R}\frac{\partial W}{\partial \theta} + W\frac{\partial W}{\partial Z}\right) = -\frac{\partial P}{\partial Z} + \mu\nabla^2 W \tag{2-2}$$

Radial direction momentum equation:

$$\rho_b\left(U\frac{\partial U}{\partial R} + \frac{V}{R}\frac{\partial U}{\partial \theta} - \frac{V^2}{R} + W\frac{\partial U}{\partial Z}\right) = -\frac{\partial P}{\partial R} + \mu\nabla^2 U - \rho g\cos\theta \tag{2-3}$$

Circumferential direction momentum equation:

$$\rho_b\left(U\frac{\partial V}{\partial R} + \frac{V}{R}\frac{\partial V}{\partial \theta} + \frac{UV}{R} + W\frac{\partial V}{\partial Z}\right) = \frac{-1}{R}\frac{\partial P}{\partial \theta} + \mu\nabla^2 V + \rho g\sin\theta \tag{2-4}$$

Energy equation:

$$\rho_b C_p\left(U\frac{\partial T}{\partial R} + \frac{V}{R}\frac{\partial T}{\partial \theta} + W\frac{\partial T}{\partial Z}\right) = k\nabla^2 T + \mu\Phi \tag{2-5}$$

where ∇^2 is the Laplacian operator

$$\nabla^2 = \frac{\partial^2}{\partial R^2} + \frac{1}{R}\frac{\partial}{\partial R} + \frac{1}{R^2}\frac{\partial^2}{\partial \theta^2} + \frac{\partial^2}{\partial Z^2}$$

For the laminar incompressible fluid flow with heat transfer, the heat generation due to viscous dissipation $\mu\Phi$ can be neglected. This is due to the low Reynolds number and the low Eckert number in laminar flow. As shown in Ref. 39, including the dissipation term did not appear to cause more than a one percent change in the value of Nu. In order to compare the

order of magnitude of other terms in Eqs. (2-1) to (2-5), appropriate characteristic variables are introduced to nondimensionalize each term:

$$R = ar,\ Z = Z_c z,\ U = U_c u,\ W = \bar{W} w,\ V = V_c v,\ P = P_c p,$$

$$\phi = \frac{T - T_b}{\Delta T^*},\ \Delta T^* = \frac{q''a}{k} \tag{2-6}$$

It is noted that the conventional ΔT is taken as the difference between the average wall temperature and the bulk temperature at a specified location. However, since $\bar{T}_w - T_b$ varies with axial position in the tube inlet region, this is not an appropriate reference temperature difference for the analysis. By contrast, ΔT^*, defined as q"a/k, is constant along the tube axis for the uniform heat flux boundary condition.

As indicated in many investigations [33, 35, 60], the pressure drop in the momentum equation can be treated in the following way. It is assumed that the pressure can be separated into two components

$$P(R, \theta, Z) = P(Z) + P(R, \theta) \tag{2-7}$$

where P(Z) is assumed to be a linear function of axial direction Z. Moreover, $P(R, \theta)$ is due to motion and hydrostatic effects, i.e.,

$$P(R, \theta) = P_d(R, \theta) + P_s(R, \theta) \tag{2-8}$$

The hydrostatic pressure in Eq. (2-8) is assumed to be a function of average density and local position, relative to the center of the tube, that is,

$$P_s(R, \theta) = - \rho_b g R \cos \theta \tag{2-9}$$

By introducing Eqs. (2-7), (2-8) and (2-9) into pressure gradient terms

appearing in the momentum equation and combining with the gravitational force, the following expressions are obtained:

$$- \frac{\partial P}{\partial Z} = - \frac{\partial P(Z)}{\partial Z} = \text{Constant}$$

$$- \frac{\partial P}{\partial R} - \rho g \cos \theta = (\rho_b - \rho) g \cos \theta - \frac{\partial P_d}{\partial R} \tag{2-10}$$

$$\frac{-1}{R} \frac{\partial P}{\partial \theta} + \rho g \sin \theta = (\rho - \rho_b) g \sin \theta - \frac{1}{R} \frac{\partial P_d}{\partial \theta}$$

The term $(\rho - \rho_b) g \sin \theta$ represents the buoyancy force which is generated by density gradients.

The density difference in Eq. (2-10) can be further simplified by introducing an isobaric thermal expansion coefficient, β, which is defined as

$$\beta = - \frac{1}{\rho} \left(\frac{\partial \rho}{\partial T} \right)_p \tag{2-11}$$

and can be approximated as

$$\beta \approx \frac{-1}{\rho_b} \left(\frac{\rho - \rho_b}{T - T_b} \right)_p \tag{2-12}$$

This approximation is exact for an ideal gas and represents a reasonable expression for real gases. It is also found that Eq. (2-12) is valid for most liquids. A higher order expression for the equation of state $\rho(T)$ may be utilized for fluids subject to large temperature differences. After substitution of the characteristic variables and Eqs. (2-10) and (2-12), Eqs. (2-1) to (2-5) become

$$\frac{1}{r} \frac{\partial}{\partial r} (ru) + \frac{1}{r} \frac{\partial r}{\partial \theta} + \left[\frac{\bar{W}a}{U_c Z_c} \right] \frac{\partial w}{\partial z} = 0 \tag{2-13}$$

$$\nabla_1^2 w + \left(\frac{a}{Z_c}\right)^2 \frac{\partial^2 w}{\partial z^2} = \left(\frac{a^2}{\mu \bar{W}}\right) \frac{\partial P(Z)}{\partial Z} + \left[\frac{U_c a}{\nu}\right]\left(u \frac{\partial w}{\partial r} + \frac{v}{r} \frac{\partial w}{\partial \theta}\right)$$

$$+ \left(\frac{\bar{W} a^2}{\nu Z_c}\right)\left(w \frac{\partial w}{\partial z}\right) \tag{2-14}$$

$$\nabla_1^2 u + \left(\frac{a}{Z_c}\right)^2 \frac{\partial^2 u}{\partial z^2} = \left(\frac{aP_c}{\mu U_c}\right) \frac{\partial P}{\partial r} + \left(\frac{U_c a}{\nu}\right)\left(u \frac{\partial u}{\partial r} + \frac{v}{r} \frac{\partial u}{\partial \theta} - \frac{v^2}{r}\right)$$

$$+ \left(\frac{\bar{W} a}{\nu Z_c}\right) W \frac{\partial u}{\partial z} + \left(\frac{g \beta \Delta T^* a^2}{\nu U_c}\right) \cos \theta \phi \tag{2-15}$$

$$\nabla_1^2 u + \left(\frac{a}{Z_c}\right)^2 \frac{\partial^2 v}{\partial z^2} = \left(\frac{aP_c}{\mu U_c}\right) \frac{1}{r} \frac{\partial P}{\partial \theta} + \left(\frac{U_c a}{\nu}\right)\left(u \frac{\partial v}{\partial r} + \frac{v}{r} \frac{\partial v}{\partial \theta} + \frac{vu}{r}\right)$$

$$+ \left(\frac{\bar{W} a^2}{\nu Z_c}\right) w \frac{\partial v}{\partial z} - \left(\frac{g \beta \Delta T^* a^2}{\nu U_c}\right) \sin \theta \phi \tag{2-16}$$

$$\nabla_1^2 \phi + \left(\frac{a}{Z_c}\right)^2 \frac{\partial^2 \phi}{\partial z^2} = \left(\frac{U_c a}{\alpha}\right)\left(u \frac{\partial \phi}{\partial r} + \frac{v}{r} \frac{\partial \phi}{\partial \theta}\right) + \left(\frac{\bar{W} a^2}{\alpha}\right) w \frac{\partial \phi}{\partial z}$$

$$+ \left(\frac{\bar{W} a^2}{\Delta T^* \alpha}\right) w \frac{\partial T_b}{\partial Z} \tag{2-17}$$

where

$$\nabla_1^2 = \frac{\partial^2}{\partial r^2} + \frac{1}{r} \frac{\partial}{\partial r} + \frac{1}{r^2} \frac{\partial^2}{\partial \theta^2}$$

By appropriately choosing U_c and Z_c, it is possible to obtain from the reduced equations familiar parameters, such as Rayleigh number, Reynolds number, and Grashof number. The choice of U_c and Z_c should be such that the least number of parameters is obtained so as to facilitate correlation.

$Z_c = a\,Re_a Pr$ is seen to be a suitable choice, since the dimensionless variable z will be on the order of unity and $Re_a Pr$ will not appear in the governing equations. With this choice and the uniform axial heat flux

boundary condition for the term $\partial T_b/\partial Z$ in Eq. (2-17), Eq. (2-17) can be reduced to

$$\nabla_1^2\phi + \left(\frac{1}{Re_a Pr}\right)^2 \frac{\partial^2\phi}{\partial z^2} = \left(\frac{U_c a}{\nu}\right)\left(u\frac{\partial\phi}{\partial r} + \frac{v}{r}\frac{\partial\phi}{\partial\theta}\right) + w\left(\frac{\partial\phi}{\partial z} + 2\right) \tag{2-18}$$

where

$$Re_a = \frac{\bar{W}a}{\nu} \quad \text{and} \quad Pr = \frac{\nu}{\alpha}$$

The second term in the left hand side of Eq. (2-18) takes into account heat conduction in the axial direction. Whether or not the term can be neglected apparently depends on the magnitude of $Re_a Pr$; large values of this parameter suppress the term. The differential equation alone is insufficient to tell how large this parameter must be in order to neglect axial conduction, but investigations [24, 113] have indicated that, as a general rule, the term is negligible for $Re_a Pr \geq 50$. For the present analysis, this term and similar terms appearing in Eqs. (2-14) to (2-16) will be neglected with this reservation. Thus the energy equation becomes

$$\nabla_1^2\phi = \left(\frac{U_c a}{\nu}\right)\left(u\frac{\partial\phi}{\partial r} + \frac{v}{r}\frac{\partial\phi}{\partial\theta}\right) + w\left(2 + \frac{\partial\phi}{\partial z}\right) \tag{2-19}$$

It is noted that if thermally fully developed flow is assumed, $\partial\phi/\partial z$ becomes zero in Eq. (2-19). This assumption of fully established profiles can, however, be fulfilled only provided that the tube is long enough; the fully developed result is the asymptotic solution of the present analysis.

Employing the hypothesis that each term in the continuity equation is of the same order of magnitude, the following relationship is obtained:

$$\frac{\bar{W}a}{U_c Z_c} = 1 \tag{2-20}$$

It is thus convenient to choose $U_c = \bar{W}a/Z_c$ for a characteristic variable. When the choice of U_c and Z_c as stated above is utilized, the momentum equations, Eqs. (2-14) to (2-16), can be reduced to

$$\nabla_1^2 w = \left(\frac{a^2}{\mu \bar{W}}\right) \frac{\partial P(Z)}{\partial Z} + \left(\frac{1}{Pr}\right)\left(u \frac{\partial w}{\partial r} + \frac{v}{r} \frac{\partial w}{\partial \theta} + w \frac{\partial w}{\partial z}\right) \tag{2-21}$$

$$\nabla_1^2 u = \left(\frac{aP_c}{\mu U_c}\right) \frac{\partial P}{\partial r} + \left(\frac{1}{Pr}\right)\left(u \frac{\partial u}{\partial r} + \frac{v}{r} \frac{\partial u}{\partial \theta} - \frac{v^2}{r} + w \frac{\partial u}{\partial z}\right) + \left(\frac{g\beta \Delta T^* a^2}{\nu U_c}\right) \cos \phi \tag{2-22}$$

$$\nabla_1^2 v = \left(\frac{aP_c}{\mu U_c}\right) \frac{1}{r} \frac{\partial P}{\partial \theta} + \left(\frac{1}{Pr}\right)\left(u \frac{\partial v}{\partial r} + \frac{v}{r} \frac{\partial v}{\partial \theta} + \frac{uv}{r} + w \frac{\partial v}{\partial z}\right) - \left(\frac{g\beta \Delta T^* a^2}{\nu U_c}\right) \sin \theta \phi \tag{2-23}$$

Since Prandtl number is assumed to be very large, the inertia term in the momentum equations, Eqs. (2-21) to (2-23), can be neglected. Physically, Prandtl number expresses relative speeds at which momentum and energy are propagated through the system. The high Prandtl number assumption is expected to be valid for most liquids, including water. This large Prandtl number assumption simplifies the differential equations considerably. As mentioned earlier, the flow is assumed to be hydrodynamically fully developed before entering the heat section. This assumption is not considered to be very restrictive since for high Prandtl number fluids the hydrodynamic profiles develop more rapidly than the thermal profiles.

As pointed out above, the characteristic variable U_c is chosen to be $\bar{W}a/Z_c$, which can be further simplifed to

$$U_c = \frac{a\bar{W}}{aRe_a Pr} = \frac{\alpha}{a} \tag{2-24}$$

When U_c is introduced, Eqs. (2-21) to (2-23) can be reduced to a simpler form with Re_a as the only parameter, that is

$$\frac{g\beta\Delta T^{*2}a}{\nu U_c} = Gr_a^* \cdot Pr = Ra_a^*$$

where Gr_a^* and Ra_a^* are modified Grashof and Rayleigh number, respectively, and are defined as

$$Gr_a^* = \frac{g\beta\Delta T^* a^3}{\nu^2}$$

$$Ra_a^* = Gr_a^* Pr \tag{2-25}$$

Note that the Rayleigh number and the Grashof number utilized subsequently in this chapter are defined in this manner instead of in the conventional way using diameter and tube wall bulk temperature difference.

Normalized Governing Equations and Boundary Conditions

The pressure terms in Eqs. (2-22) and (2-23) can be eliminated by cross-differentiation. A stream function and vorticity function can also be defined, such that

$$ru = \frac{\partial\psi}{\partial\theta}$$

$$v = -\frac{\partial\psi}{\partial r} \tag{2-26}$$

$$\xi = \nabla_1^2\psi$$

thereby satisfying the continuity condition. The momentum and energy equations can now be restated in the following dimensionless forms:

Axial momentum equation:

$$\nabla_1^2 w = \frac{a^2}{\mu \bar{W}} \frac{\partial P(Z)}{\partial Z} = C = \text{constant} \tag{2-27}$$

Momentum equation for secondary flow:

$$\nabla_1^2 \xi = Ra_a^* \left(\cos\theta \frac{1}{r} \frac{\partial \phi}{\partial \theta} + \sin\theta \frac{\partial \phi}{\partial r} \right) \tag{2-28}$$

Vorticity equation:

$$\nabla_1^2 \psi = \xi \tag{2-29}$$

Energy equation:

$$\nabla_1^2 \phi = u \frac{\partial \phi}{\partial r} + \frac{v}{r} \frac{\partial \phi}{\partial \theta} + w \left(2 + \frac{\partial \phi}{\partial z} \right) \tag{2-30}$$

It is recalled that the effect of the temperature field on the flow field depends strongly on the value of Prandtl number which appears in Eqs. (2-21) to (2-23). The effect of Pr on the primary flow becomes insignificant as the Prandtl number increases. This is a consequence of the kinetic viscosity being much greater than the thermal diffusivity. From Eq. (2-27), it is evident that for $Pr \to \infty$ the secondary flow does not affect the velocity field in the axial direction. This conclusion is also reached in Ref. [31], where the investigators utilized ethylene glycol in their experiments to support their analytical results. Furthermore, it should be noted that as $Pr \to \infty$, the primary forced flow is unaffected by the secondary flow generated by free convection. The solution of Eq. (2-27) is thus simply Poiseuille flow; that is,

$$w = 2(1 - r^2)$$

The axial pressure drop associated with friction is then given by Poiseuille's relation [114].

Due to mathematical difficulty, virtually all of the heat transfer solutions reported to date have been obtained by neglecting the secondary flow. These traditional constant-property solutions will represent the limiting case of the results to be obtained here with $Ra_a^* = 0$.

Equations (2-28) and (2-29) are second-order elliptic partial differential equations. Equation (2-29) can be substituted into Eq. (2-28) to obtain the stream function in biharmonic form. When vorticity is introduced into (2-28), the stream function of fourth order is reduced to second order. As indicated in previous investigations [35, 60], the boundary vorticity method required fewer than one hundred iterations to obtain the converged solution of Eqs. (2-28) and (2-29). When the original fourth-order biharmonic equation is utilized, it will take several thousand iterations as reported in Ref. [33]. The boundary vorticity method is preferred as considerably less computer time is required.

Equation (2-30) is a parabolic equation, and the solution can be obtained by employing the available stable explicit DuFort-Frankel method [115]. The ADI (Alternating Direction Implicit) method [116, 117] also can be utilized to solve the three-dimensional parabolic equation, Eq. (2-30). However, more computing time is required for the ADI method than for the DuFort-Frankel method.

Through symmetry, it is necessary to consider only one half of the circular region as shown in Fig. 2-1. Applying the non-slip condition at the wall and symmetry about vertical centerline, the flow field boundary conditions for Eqs. (2-27) to (2-29) are

$$U = V = W = \psi = 0 \qquad \text{at the pipe wall, } r = 1$$

$$V = \psi = \xi = 0 \qquad \text{at the vertical centerline, } \theta = 0, \pi \qquad (2\text{-}31)$$

The most reasonable thermal boundary condition that can be physically imposed with the Joulean heating of cylindrical tubes is that of insulating the outer tube surface. The problem, then, requires the simultaneous solution of the fluid and solid tube material regions. This can be achieved, but the number of independent parameters that must be considered is also prohibitively increased unless a specified experimental situation is alluded to. Thus, the heat transfer results are strongly dependent on tube wall boundary conditions.

Newell and Bergles [33] pointed out that the inner tube wall boundary conditions can be bracketed by two bounds. In the first case, it is the fluid system that determines the circumferential temperature distribution at the tube wall; mathematically, this corresponds to zero circumferential heat conduction in the tube wall. In practice, this can be approximated by electrically heated glass tubes or metal tubes with very thin walls. In the second case, it is assumed that the tube material exhibits an infinite thermal conductivity; hence there are no circumferential temperature gradients at the tube wall. In this latter case, the heat flux varies around the circumference even though the average heat flux is uniform. Experimental data would be expected to be bracketed by solutions utilizing these two boundary conditions. The present solution will be carried out for the lower limit of zero circumferential conduction. The solution for the other boundary condition can be achieved by employing a technique

similar to that described in this chapter.

The mathematical thermal boundary conditions can be restated as follows:

$$\frac{\partial \phi}{\partial \theta} = 0 \qquad \text{at the vertical centerline or } \theta = 0, \pi$$
$$\frac{\partial \phi}{\partial r} = 1 \qquad \text{at the tube wall, } r = 1 \tag{2-32}$$

The initial conditions are

$$U = V = \phi = 0, \quad W = 2(1 - r^2) \qquad \text{at } z = 0 \tag{2-33}$$

It does not appear that a closed form solution of Eqs. (2-28), (2-29), (2-30), (2-32), and (2-33) is possible. However, the finite-difference scheme which has been employed in many previous investigations can be used.

Numerical Solution Using Boundary Vorticity and DuFort-Frankel Methods

Application of boundary vorticity method to momentum equation

By use of three-point, central-difference operators, Eqs. (2-28) and (2-29) can be transformed into a set of algebraic finite-difference equations. These equations can be regarded as having the following form:

$$\frac{\partial^2 f}{\partial r^2} + \frac{1}{r}\frac{\partial f}{\partial r} + \frac{1}{r^2}\frac{\partial^2 f}{\partial \theta^2} = G \tag{2-34}$$

where f is a dummy variable and G represents the remaining terms in the equations. It is noted that Eq. (2-34) is a Poisson equation. With reference to the coordinate system and numerical grid shown in Fig. 2-1, the finite-difference formulation of Eq. (2-34) can be written as

$$\frac{f_{i-1,j} + f_{i+1,j} - 2f_{i,j}}{\Delta r^2} + \frac{f_{i+1,j} - f_{i-1,j}}{2r_i \Delta r}$$

$$+ \frac{f_{i,j-1} + f_{i,j+1} - 2f_{i,j}}{\left(r_i \Delta\theta\right)^2} = G_{i,j} \qquad (2\text{-}35)$$

where

$$G_{i,j} = \xi_{i,j}$$

for Eq. (2-29) and

$$G_{i,j} = Ra_a^* \left(\cos \theta_j \frac{\phi_{i,j+1} - \phi_{i,j-1}}{2r_i \Delta\theta} + \sin \theta_j \frac{\phi_{i+1,j} - \phi_{i-1,j}}{2\Delta r}\right)$$

Multiplying by $(\Delta r)^2$ and rearranging changes Eq. (2-35) to

$$\left(1 - \frac{\Delta r}{2r_i}\right) f_{i-1,j} - 2\left[1 + \left(\frac{\Delta r}{r_i \Delta\theta}\right)^2\right] f_{i,j} + \left(1 + \frac{\Delta r}{2r_i}\right) f_{i+1,j}$$

$$= G_{i,j}(\Delta r)^2 - \left(\frac{\Delta r}{r_i \Delta\theta}\right)^2 f_{i,j-1} - \left(\frac{\Delta r}{r_i \Delta\theta}\right)^2 f_{i,j+1} \qquad (2\text{-}36)$$

where

$$a_i = 1 - \frac{\Delta r}{2r_i}$$

$$b_i = -2\left[1 + \left(\frac{\Delta r}{r_i \Delta\theta}\right)^2\right]$$

$$c_i = 1 + \frac{\Delta r}{2r_i}$$

and

$$d_i = G_{i,j}(\Delta r)^2 - \left(\frac{\Delta r}{r_i \Delta\theta}\right)^2 f_{i,j-1} - \left(\frac{\Delta r}{r_i \Delta\theta}\right)^2 f_{i,j+1}$$

Eq. (2-36) can be reduced to

$$a_i f_{i-1,j} + b_i f_{i,j} + c_i f_{i+1,j} = d_i \qquad (2\text{-}37)$$

Equation (2-37) is seen to be a general finite-difference expression applicable to Eqs. (2-28) and (2-29) and is a typical relation for two-dimensional elliptic equations. In calculating the secondary velocity components using $U = 1/r \cdot \partial\psi/\partial\theta$ and $V = -\partial\psi/\partial r$, a five-point central-difference formula has been employed to obtain more accurate results. The expressions are as follows:

$$\frac{\partial f_{i,j}}{\partial r} = \frac{1}{12\Delta r}\left(f_{5,j} - 6f_{4,j} + 18f_{3,j} - 10f_{2,j} - 3f_{1,j}\right) \quad \text{for } i = 2$$

$$= \frac{1}{12\Delta r}\left(f_{i-2} - 8f_{i-1,j} - 8f_{i+1,j} + f_{i+2,j}\right)$$

$$\text{for } i = 3, 4, \ldots, M - 1$$

$$= \frac{1}{12\Delta r}\left(f_{M-3,j} - 6f_{M-2,j} + 18f_{M-1,j} - 10f_{M,j} - 3f_{M+1,j}\right)$$

$$\text{for } i = M \qquad (2\text{-}38)$$

$$\frac{\partial f_{i,j}}{\partial \theta} = \frac{1}{12\Delta\theta}\left(- f_{i,2} + 8f_{i,3} - f_{i,4}\right) \quad \text{for } j = 2$$

$$= \frac{1}{12\Delta\theta}\left(f_{i,j-2} - 8f_{i,j-1} + 8f_{i,j+1} - f_{i,j+2}\right)$$

$$\text{for } j = 3, 4, \ldots N - 1$$

$$= \frac{1}{12\Delta\theta}\left(f_{i,N-2} - 8f_{i,N-1} + f_{i,N}\right) \quad \text{for } j = N \qquad (2\text{-}39)$$

Note that $\partial f_{i,j}/\partial\theta = 0$ at $j = 1$ and $N + 1$ due to symmetry about the vertical centerline. In order to avoid the singularity at the origin of the cylindrical coordinates which appears in Eq. (2-35) when $r = 0$, a finite-difference equation in Cartesian coordinates is employed at the origin as follows:

$$f_{1,1} = \frac{1}{4}\left(f_{2,1} + f_{2,N+1} + 2f_{2,N/2+1} - G_{i,j}\Delta r^2\right) \tag{2-40}$$

The flow field boundary condition in Eq. (2-31) can also be written in finite-difference form as

$$\begin{aligned} &\psi_{i,j} = u_{i,j} = v_{i,j} = w_{i,j} = 0 && \text{for } i = M + 1 \\ &\psi_{i,j} = \xi_{i,j} = 0 && \text{for } j = 1 \text{ and } N + 1 \\ &\psi_{i,j} = \xi_{i+1,j} && \text{for } i = M + 1 \end{aligned} \tag{2-41}$$

When the above boundary conditions are used, a set of finite-difference equations may be written, after applying Eq. (2-37) to the grid points along the radial line j, as

$$\begin{aligned} &b_1 f_{1,j} + c_1 f_{2,j} = d_1 && i = 1 \\ &a_i f_{i-1,j} + b_i f_{i,j} + c_i f_{i+1,j} = d_i && i = 2, 3, \ldots, M - 1 \\ &a_M f_{M-1,j} + b_M f_{M,j} = d_M && i = M \end{aligned} \tag{2-42}$$

Equation (2-42) can be written in matrix form as

$$\underline{A}\,\underline{f} = \underline{d}$$

or

$$\begin{bmatrix} b_1 & c_1 & & & & \\ a_2 & b_2 & c_2 & & 0 & \\ 0 & a_3 & b_3 & c_3 & & \\ & & - & - & - & \\ & & & - & - & - \\ & 0 & & & a_{M-1} & b_{M-1} & c_{M-1} \\ & & & & & a_M & b_M \end{bmatrix} \begin{bmatrix} f_1 \\ f_2 \\ f_3 \\ \cdot \\ \cdot \\ f_{M-1} \\ f_M \end{bmatrix} = \begin{bmatrix} d_1 \\ d_2 \\ d_3 \\ \cdot \\ \cdot \\ d_{M-1} \\ d_M - c_{M+1} f_{M+1} \end{bmatrix} \tag{2-43}$$

Here $\underline{A}$ is seen to be a tridiagonal matrix. This system can be solved explicitly for the unknowns, thereby eliminating any matrix operations. This method has been discovered independently by many and has been called the Thomas algorithm [118]. The following procedure using forward elimination and backward substitution is utilized:

$$p_1 = c_1/b_1$$

$$p_i = c_i/(b_i - a_i p_{i-1}) \qquad i = 2, 3, \ldots, M - 1$$

$$q_1 = d_1/b_1$$

$$q_i = (d_i - a_i q_{i-1})/(b_i - a_i p_{i-1}) \qquad i = 2, 3, \ldots, M$$

$$f_M = q_M$$

$$f_i = q_i - p_i f_{i+1} \qquad i = M - 1, M - 2, \ldots, 1$$

The above algorithm can be applied to Eq. (2-29), with the boundary conditions given in Eq. (2-41), but the boundary condition for the equation is unknown. On the other hand, two boundary conditions are available for Eq. (2-29). The success of the boundary vorticity method is based on the observation that a linear relationship exists between the vorticity $\xi_{M+1,j}$ and the stream function $\psi_{M+1,j}$ at the boundary. A more detailed discussion of the boundary vorticity method is given in Ref. [35]. Only a summary of the procedures used in this calculation is described in subsequent paragraphs.

Use of the boundary condition of $\psi_{i-1,j} = \psi_{i+1,j}$ for $i = M + 1$ replaces some elements of the matrix equation [Eq. (2-43)], such as a_M, b_M, f_M, and $d_M - c_{M+1} f_{M+1}$, by $a_{M+1} + c_{M+1}$, b_{M+1}, f_{M+1} and d_{M+1}, respectively.

Assuming arbitrary values $\xi_w^{(1)}$ and $\xi_w^{(2)}$ for $\xi_{M+1,j}$ and solving the finite-difference equations [Eqs. (2-28) and (2-29)], $\psi_w^{(1)}$ and $\psi_w^{(2)}$ are obtained for the boundary condition $\partial\psi/\partial r = 0$ at wall. The boundary values for the vorticity $\xi_{M+1,j}$ and stream function $\psi_{M+1,j}$ are related by the following equation:

$$\xi_w^{(3)} = \frac{\xi_w^{(2)} - \xi_w^{(1)}}{\psi_w^{(2)} - \psi_w^{(1)}} \left(\psi_w^{(3)} - \psi_w^{(2)}\right) + \xi_w^{(2)} \tag{2-44}$$

By using this linear relation between ξ and ψ and noting that the correct stream function at the boundary is $\psi_w^{(3)} = 0$, the vorticity $\xi_w^{(3)}$ can be computed. After the boundary vorticity is numerically determined, the numerical solution of Eqs. (2-28) and (2-29) can be carried out by a line-iterative relaxation procedure using the following equation:

$$f_{i,j}^{(n+1)} = f_{i,j}^{(n)} + \omega\left[f_{i,j}^{(n+1)} - f_{i,j}^{(n)}\right] \tag{2-45}$$

where ω is a relaxation factor. The numerical solution of the set of secondary flow equations [Eqs. (2-28) and (2-29)] can be started by using previous upstream values for $\psi_{i,j}^{k-1}$, $\xi_{i,j}^{k}$ and $\psi_{i,j}^{k-1}$. The numerical solution is continued until the dependent variables $\psi_{i,j}$, $\xi_{i,j}$ satisfy the following prescribed error:

$$e = \sum_{i,j} \left|f_{i,j}^{n+1} - f_{i,j}^{n}\right| / \sum_{i,j} \left|f_{i,j}^{n}\right| < 10^{-5} \tag{2-46}$$

It is observed that the final average Nusselt number at each axial location differs less than 0.01 percent from the previous calculated value when the prescribed error of Eq. (2-46) is reached. The secondary velocity components, $u_{i,j}$ and $v_{i,j}$ can be obtained by using the five-point finite-

difference for the first derivatives as expressed in Eq. (2-39).

A method of determining an optimum relaxation factor is not available for the present problem. However, it was found in Ref. [35] that the influence of over-relaxation [$\omega > 1$] or under-relaxation ($\omega < 1$) on computing time is not appreciable. Consequently, the relaxation factor of unity was used in most of the present calculations.

The rate of convergence for the line-iteration method depends on the values of the parameters Ra_a^* and z. For the calculation as $Ra_a^* = 5 \times 10^4$, for example, 120 iterations are required close to the tube inlet but only 30 iterations are required in the fully developed region (for mesh size of 20 by 20). Details of the computer program are given in Appendix A.

Application of DuFort-Frankel method to energy equation

The energy equation [Eq. 2-30] is a parabolic-type, second-order differential equation. The Alternating Direction Implicit (ADI) method has been recently reported as an effective means of solving the comparable equation for a rectangular channel [43]. Dividing the tube entrance calculation into two steps, Dravid et al. [79] utilized the ADI method to solve the energy equation in helically coiled tubes with some degree of success. The ADI method is seen, however, to be more complicated to program and requires more computing time than the explicit DuFort-Frankel method. In addition, the stability criterion of the ADI method does not appear to be available for solving this non-linear, cylindrical coordinate system. To solve the energy equation and compare the different finite-difference schemes, the DuFort-Frankel method was tried.

The stable, explicit DuFort-Frankel method [115] has been employed in

this study. The main advantage of this explicit method over the implicit methods is one of the directness and simplicity (explicit methods are generally algebraically simpler than implicit methods, thus saving computing time). It has been shown [119] that the DuFort-Frankel method, just like the implicit methods, is unrestricted in the choice of streamwise step size in boundary-layer type equations because of stability considerations.

The original DuFort-Frankel scheme, based on a uniform grid in the axial direction, proceeds as follows:

The first-order derivative for the energy equation is represented by

$$\left(\frac{\partial \phi}{\partial z}\right)^k = \frac{\phi_{i,j}^{k+1} - \phi_{i,j}^{k-1}}{2\Delta z} + 0\left[\Delta z^2\right] \tag{2-47}$$

where $0[\Delta z^2]$ indicates that the truncation error incurred by using this scheme is of the order of magnitude of Δz^2. Equation (2-47) is applicable only when the streamwise step size is taken equally. In the present calculation, however, the maximum step size is taken within the stability criterion to accelerate the computation. Step size is changed in each calculation. The axial gradient $(\partial\phi/\partial z)^k$ is then evaluated using the following equation with non-equal step size, Δz^+ for the present step and Δz^- for the previous step, obtained by applying the Taylor series expansion:

$$\left(\frac{\partial \phi}{\partial z}\right)^k = \frac{\left(\Delta z^-\right)^2 \phi_{i,j}^{k+1} - \left(\Delta z^+\right)^2 \phi_{i,j}^{k-1} + \phi_{i,j}^{k}\left(\Delta z^{+2} - \Delta z^{-2}\right)}{\Delta z^- \Delta z^+ \left(\Delta z^- + \Delta z^+\right)} + 0\left[\Delta z^{+2}\right] \tag{2-48}$$

where $\Delta z^- = z^k - z^{k-1}$, $\Delta z^+ = z^{k+1} - z^{k-1}$. Following the DuFort-Frankel scheme, the energy equation [Eq. (2-30)] can be written in finite-difference form as

$$w_{i,j}\left[2 + \frac{\Delta z^{-2}\phi^{k+1}_{i,j} - \Delta z^{+2}\phi^{k-1}_{i,j} + \phi^{k}_{i,j}\left(\Delta z^{+2} - \Delta z^{-2}\right)}{\Delta z^{-}\Delta z^{+}\left(\Delta z^{-} + \Delta z^{+}\right)}\right]$$

$$= \frac{1}{r_i}\frac{1}{\Delta r}\left[\left(\frac{r_i + r_{i+1}}{2\Delta r}\right)\left(\phi^{k}_{i+1,j} - \frac{\phi^{k+1}_{i,j} + \phi^{k-1}_{i,j}}{2}\right)\right.$$

$$\left. - \left(\frac{r_i + r_{i-1}}{2\Delta r}\right)\left(\frac{\phi^{k+1}_{i,j} + \phi^{k-1}_{i,j}}{2} - \phi^{k}_{i-1,j}\right)\right]$$

$$+ \frac{1}{r_i^2}\left[\frac{\phi^{k}_{i,j+1} + \phi^{k}_{i,j-1} - \phi^{k+1}_{i,j} - \phi^{k-1}_{i,j}}{\Delta\theta^2}\right]$$

$$- U^{k}_{i,j}\left(\frac{\phi^{k}_{i+1,j} - \phi^{k}_{i-1,j}}{2\Delta r}\right) - \frac{v^{k}_{i,j}}{r_i}\left(\frac{\phi^{k}_{i,j+1} - \phi^{k}_{i,j-1}}{2\Delta\theta}\right) \qquad (2\text{-}49)$$

where

$$\phi^{k}_{i,j} = \phi(i\Delta r,\ j\Delta\theta, z_k)$$

and

$$W_{i,j} = 2\left(1 - r_i^2\right)$$

As a further simplification, Eq. (2-49) can be reduced to an explicit form which requires no iteration, as follows:

$$\phi^{k+1}_{i,j} = \frac{1}{A_1}\left[A_2\phi^{k}_{i+1,j} + A_3\phi^{k}_{i-1,j} + A_4\phi^{k}_{i,j+1} + A_5\phi^{k}_{i,j-1}\right.$$

$$\left. + A_6\phi^{k-1}_{i,j} + A_7\phi^{k}_{i,j} + A_8\right] \qquad (2\text{-}50)$$

where

$$A_1 = \frac{w_{i,j}\left(\Delta\bar{z}\right)^2}{\Delta z^{-}\Delta z^{+}\left(\Delta z^{-} + \Delta z^{+}\right)} + \frac{r_{i+1} + 2r_i + r_{i-1}}{4r_i\Delta r^2} + \frac{1}{\left(r_i\Delta\theta\right)^2}$$

$$A_2 = \frac{r_i + r_{i+1}}{2r_i\Delta r^2} - \frac{u^{k}_{i,j}}{2\Delta r}$$

$$A_3 = \frac{r_i + r_{i-1}}{2r_i\Delta r} + \frac{u^k_{i,j}}{2\Delta r}$$

$$A_4 = \frac{1}{(r_i\Delta\theta)^2} - \frac{v^k_{i,j}}{2r_i\Delta\theta}$$

$$A_5 = \frac{1}{(r_i\Delta\theta)^2} + \frac{v^k_{i,j}}{2r_i\Delta\theta}$$

$$A_6 = \frac{w_{i,j}\Delta z^{+2}}{\Delta z^-\Delta z^+(\Delta z^- + \Delta z^+)} - \frac{r_{i+1} + 2r_i + r_{i-1}}{4r_i\Delta r^2} - \frac{1}{(r_i\Delta\theta)^2}$$

$$A_7 = - w_{i,j}\frac{\Delta z^{+2} - \Delta z^{-2}}{\Delta z^-\Delta z^+(\Delta z^- + \Delta z^+)}$$

$$A_8 = - 2w_{i,j}$$

If uniform wall heat flux along the tube circumference is assumed, the boundary condition of Eq. (2-32) can be restated in finite-difference form as

$$\begin{aligned} \phi^k_{i,0} &= \phi^k_{i,2} && \text{at } \theta = 0, \pi \\ \phi^k_{M+i,j} &= \phi^k_{M,j} + \Delta r && \text{at } r = 1 \end{aligned} \tag{2-51}$$

Since the DuFort-Frankel method requires three levels of temperature information, it may not be possible to start the calculation by using the DuFort-Frankel technique. However, a standard explicit scheme which requires only two levels of temperature information can be utilized to overcome the difficulty. The energy equation is formulated according to a standard explicit scheme as follows:

$$w_{i,j}\frac{\phi^{k+1}_{i,j}-\phi^{k}_{i,j}}{\Delta z}=\frac{1}{\Delta r^2}\left[\phi^{k}_{i+1,j}+\phi^{k}_{i-1,j}-2\phi^{k}_{i,j}\right]$$
$$+\frac{1}{r^{i}}\left[\frac{\phi^{k}_{i+1,j}-\phi^{k}_{i-1,j}}{2\Delta r}\right]+\frac{1}{r_i^2}\left[\frac{\phi^{k}_{i,j+1}+\phi^{k}_{i,j-1}-2\phi^{k}_{i,j}}{\Delta\theta^2}\right]$$
$$-u^{k}_{i,j}\frac{\phi^{k}_{i+1,j}-\phi^{k}_{i-1,j}}{2\Delta r}-\frac{v^{k}_{i,j}}{2r_i\Delta\theta}\left(\phi^{k}_{i,j+1}-\phi^{k}_{i,j-1}\right)-2w_{i,j} \quad (2\text{-}52)$$

The initial conditions for Eq. (2-52) at z = 0 are

$$u_{i,j}=v_{i,j}=\phi_{i,j}=0 \quad (2\text{-}53)$$

Since no heat flux is assumed at $z = 0^-$, it is reasonable to assume that there is no secondary flow at z = 0. Following the procedure used for the momentum equation at r = 0, a finite-difference equation in Cartesian coordinates is employed at the origin to avoid the singularity at the center of tube. By using Cartesian coordinates instead of cylindrical coordinates at the origin, the energy equation can be written in finite-difference form for the standard explicit and DuFort-Frankel methods as follows:

Standard explicit:

$$w_{i,j}\frac{\phi^{k+1}_{i,j}-\phi^{k}_{i,j}}{\Delta z}=\left(\frac{1}{\Delta r}\right)^2\left[\phi^{k}_{i+1,j}+\phi^{k}_{i-1,j}-2\phi^{k}_{i,j}\right]$$
$$+\left(\frac{1}{\Delta r}\right)^2\left[\phi^{k}_{i,j+1}+\phi^{k}_{i,j-1}-2\phi^{k}_{i,j}\right]$$
$$-v^{k}_{i,j}\left[\frac{\phi^{k}_{i,j+1}-\phi^{k}_{i,j-1}}{2\Delta r}\right]-2w_{i,j} \quad (2\text{-}54)$$

DuFort-Frankel method:

$$w_{ij}\left[\frac{\Delta z^{-2}\phi_{i,j}^{k+1} - \Delta z^{+2}\phi_{i,j}^{k+1} + \phi_{i,j}^{k}\left(\Delta z^{+2} - \Delta z^{-2}\right)}{\Delta z^{-}\Delta z^{+}\left(\Delta z^{-} + \Delta z^{+}\right)}\right]$$

$$= \left(\frac{1}{\Delta r}\right)^2\left(\phi_{i+1,j}^{k} + \phi_{i-1,j}^{k} - \phi_{i,j}^{k+1} - \phi_{i,j}^{k-1}\right)$$

$$+ \left(\frac{1}{\Delta r}\right)^2\left(\phi_{i,j+1}^{k} + \phi_{i,j-1}^{k} - \phi_{i,j}^{k+1} - \phi_{i,j}^{k-1}\right)$$

$$- v_{i,j}^{k}\left(\frac{\phi_{i,j+1}^{k} - \phi_{i,j-1}^{k}}{2\Delta r}\right) - 2w_{i,j} \qquad \text{for } i = j = 1 \qquad (2\text{-}55)$$

The fluid temperature can be easily determined from Fig. (2-50) with Eq. (2-51) as the boundary condition and Eq. (2-53) as the initial condition. The computation is continued until the fully developed condition is reached. The fully developed point is defined as the point after which the dimensionless temperature profile does not change appreciably. The average axial dimensionless temperature gradient is then zero. That is

$$\overline{\frac{\partial \phi}{\partial z}} = 0 \qquad (2\text{-}56)$$

It is noted that although the bulk fluid temperature keeps increasing after passing through the fully developed point, the average wall and bulk fluid temperature difference will remain constant; thus, the Nusselt number is at the asymptotic value for the constant heat flux case. Going further downstream in the tube, however, the fluid will eventually start to boil. Also, the viscosity may decrease to the point where the flow becomes turbulent. The laminar flow assumption will fail to cover these regions.

To summarize the computation process, the following steps are taken to obtain the heat transfer results:

(1) With standard explicit techniques, the solution of the energy equation [Eq. (2-30)] is started by assuming $u = v = \phi = 0$ at $z = 0$ as the initial condition.

(2) The secondary flow associated with the stream and vorticity equations [Eqs. (2-28) and (2-29)] at $k = 1$ can be solved with the given temperature value obtained from step (1).

(3) With two levels of u, v and ϕ at $k = 0, 1$, the DuFort-Frankel method can be applied to solve the energy equation [Eq. (2-30)]. The marching process is continued until the fully developed condition is reached.

(4) The average Nusselt number at any point can be evaluated using the local bulk fluid temperature and the local average wall temperature.

(5) When the fluid temperature at step k is known, the stream function and the secondary velocity at step k can be obtained by using the boundary vorticity method.

(6) Processes (3) to (5) are repeated until the fully developed condition is achieved.

It is possible to obtain heat transfer results in the entrance region within 10 minutes for Rayleigh numbers smaller than 10^5 on the Iowa State University IBM 360/65 system. However, for high Rayleigh numbers, $Ra_a^* = 10^6$, for example, it takes around 15 minutes to obtain the heat transfer results in the entrance region.

Consistency and Stability of the Numerical Solution

Two concerns with the finite-difference solution are convergence and stability. Convergence is generally studied by expanding the dependent variables in Taylor series expansions in a manner such that the difference between the partial differential equations and the finite-difference representation can be observed. This difference is known as the truncation error of the equations, and, if it vanishes in the limit as the mesh size is reduced, the finite-difference representation is said to be consistent. This technique also can be used to compare various difference formulations by observing the order of the corresponding truncation errors. Stability implies that round-off errors, or errors from any other source, are not amplified or allowed to grow in subsequent steps in the solution. Stability is a very important consideration in the present study. Often the best scheme in terms of truncation error is completely unstable and must be altered.

A stable, consistent scheme is said to be convergent in the limit as the mesh size reduced. In dealing with stability and convergence, the ideas of Von Neumann [120] and Lax and Richtmyer [121] were used. Examples of first- and second-order derivatives in the momentum equation can be approximated on a uniform grid. The truncation error of the derivatives can be shown by using three-point central finite-difference operators as follows:

First derivatives:

$$\left(\frac{\partial f}{\partial r}\right)_{i,j} = \frac{f^{k}_{i+1,j} - f^{k}_{i-1,j}}{2\Delta r} + O(\Delta r^2) \qquad (2\text{-}57)$$

Second derivatives:

$$\left(\frac{\partial^2 f}{\partial r^2}\right)_{i,j} = \frac{f^k_{i+1,j} + f^k_{i-1,j} - 2f^k_{i,j}}{\Delta r^2} + 0\left(\Delta r^2\right) \tag{2-58}$$

The truncation error is seen to be of the order of Δr^2 in Eqs. (2-57) and (2-58). It is clear that there is less truncation error as the grid size is reduced. Equations (2-57) and (2-58) are considered to be standard approximations for convergence and accuracy.

For the DuFort-Frankel method, the second derivatives are approximated as:

$$\frac{\partial^2 f_{i,j}}{\partial r^2} = \frac{f^k_{i+1,j} + f^k_{i-1,j} - f^{k+1}_{i,j} - f^{k-1}_{i,j}}{\Delta r^2} + \left(\frac{\Delta z}{\Delta r}\right)^2 \frac{\partial^2 f}{\partial z^2}$$

$$- \frac{1}{12}(\Delta r)^2 \frac{\partial^4 f}{\partial r^4} + \ldots \tag{2-59}$$

Comparison of Eqs. (2-58) and (2-59) shows that the DuFort-Frankel representation of the second derivative is obtained by replacing the $f^k_{i,j}$ term in the standard explicit representation by $\left(f^{k+1}_{i,j} + f^{k-1}_{i,j}\right)\Big/2$. The truncation error in Eq. (2-59) is $0[(\Delta z/\Delta r)^2] + 0[\Delta r^2]$. To provide a mathematically correct representation of $\partial^2 f/\partial r^2$ and $\partial^2 f/\partial \theta^2$ the mesh must be refined in such a way that

$$\lim_{\substack{\Delta z \to 0 \\ \Delta r \to 0}} \left(\frac{\Delta z}{\Delta r}\right) = 0$$

It is also desirable that $\Delta z/\Delta r$ be small in a given calculation so that the finite-difference approximation is reasonably accurate. However, the

leading term in truncation error is really $(\Delta z/\Delta r)^2 \cdot \partial^2 f/\partial z^2$. It is also known that $\partial^2 f/\partial z^2$ is negligibly small compared to the other second derivatives indicated in the energy equation [Eq. (2-17)], $\partial^2 f/\partial r^2$ and $1/r^2 \cdot \partial^2 f/\partial \theta^2$. Thus, the finite-difference representation in Eq. (2-59) would be expected to be a good approximation even for $\Delta z/\Delta r$ and $\Delta z/\Delta\theta$ approximately equal to unity.

The stability criterion of the DuFort-Frankel method in this nonlinear, cylindrical, three-dimensional coordinate system has not been pointed out in previous investigations. However, the stability criterion can be obtained by employing Von Neumann's ideas [120]. Using equal grid spacing in the r, θ, and z directions to simplify the derivation, the energy equation in finite-difference form as follows:

$$w\left(\frac{\phi_{i,j}^{k+1} - \phi_{i,j}^{k-1}}{2\Delta z}\right) + u\frac{\phi_{i+1,j}^{k} - \phi_{i-1,j}^{k}}{2\Delta r} + \frac{v}{r}\frac{\phi_{i,j+1}^{k} - \phi_{i,j-1}^{k}}{2\Delta\theta}$$
$$= \frac{\phi_{i+1,j}^{k} + \phi_{i-1,j}^{k} - \phi_{i,j}^{k} - \phi_{i,j}^{k}}{\Delta r^2} + \frac{\phi_{i+1,j}^{k} - \phi_{i-1,j}^{k}}{2r\Delta r}$$
$$+ \frac{\phi_{i,j+1}^{k} + \phi_{i,j-1}^{k} - \phi_{i,j}^{k+1} - \phi_{i,j}^{k-1}}{r^2\Delta\theta^2} \qquad (2\text{-}60)$$

where

$$w = w_{i,j}^{k},\ u = u_{i,j}^{k},\ v = v_{i,j}^{k}$$

and the 2w term shown in Eq. (2-30) has been neglected, since a constant term will not have an effect on the stability analysis.

When it is assumed that the error due to the finite-difference approximation will be of the same form as the function ϕ, the error should satisfy Eq. (2-60).

Let the error δ be

$$\delta_{i,j}^{k} = e^{\alpha z} e^{i\beta\gamma} e^{i\gamma\theta} \tag{2-61}$$

where $i = \sqrt{-1}$, and α, β, and γ are eigenvalues. Substituting this expression into Eq. (2-60), this equation becomes

$$\left[\frac{w}{2} + \frac{\Delta z}{\Delta r^2} + \frac{\Delta z}{(r\Delta\theta)^2}\right]\eta - \left[\frac{w}{2} - \frac{\Delta z}{\Delta r^2} - \frac{\Delta z}{(r\Delta\theta)^2}\right]\eta^{-1}$$

$$= \frac{2\Delta z}{\Delta r^2} \cos \beta\Delta r + 2\frac{\Delta z}{(r\Delta\theta)^2} \cos (\gamma\Delta\theta) + 2i \left[\frac{\Delta z}{2r\Delta r} - \frac{u\Delta z}{2\Delta r} \sin (\beta\Delta r)\right.$$

$$\left. - v \frac{\Delta z}{2r\Delta\theta} \sin (\gamma\Delta\theta)\right] \tag{2-62}$$

where

$$\eta = e^{\alpha\Delta z}$$

To insure that the error should not be magnified as z increases, it is necessary and sufficient that

$$|\eta| \leq 1 \tag{2-63}$$

Equation (2-62) can be solved with any value of β and γ and the condition that $|\eta| \leq 1$ defines the stability criterion as

$$\Delta z \leq \frac{w}{\left|\frac{u}{\Delta r} + \frac{v}{r\Delta\theta} - \frac{1}{r\Delta r}\right|} \tag{2-64}$$

In the present calculation Δz is taken as 0.9 Δz given by the equation in Eq. (2-64) to be on the safe side. The streamwise step Δz is therefore controlled by this stability condition. It appears that for larger

secondary flow, larger Rayleigh numbers, for example, Δz becomes smaller. This stability condition of Eq. (2-64) must be satisfied if the solution is to be stable. This was, in fact, verified during early computations by deliberately choosing to cause a step size and observing the computation to go unstable. Clearly, even for the implicit method, there is an upper limit on the size of the streamwise step beyond which the numerical solutions no longer bear reasonable resemblance to the exact solutions to the governing partial differential equation. It is suggested that it is necessary to examine stability conditions before the solutions can be trusted, even in the ADI method used in Ref. 79.

Heat Transfer Results

Thermal and Hydrodynamic Development

For the present Newtonian laminar flow heat transfer problem with uniform heat flux axially and circumferentially, the thermal and hydrodynamic fields depend on Rayleigh number, and dimensionless axial position.

The dimensionless temperature for example, depends on Ra_a^* and z. The development of temperature along the vertical centerline is illustrated in Fig. 2-2 for a typical high value of $Ra_a^* = 5 \times 10^4$. The fluid temperature before the heated section is uniform and heating starts at $z = 0$. The secondary flow is weak at the tube inlet; thus, the temperature profile is initially symmetric about the center. The symmetric temperature profile is destroyed by the stronger secondary flow further downstream. The top fluid temperature near the wall is warmer than the bottom fluid temperature as a result of the secondary motion. The minimum temperature occurs on the vertical centerline below the tube axes at radii between 0.25 and 0.5. The

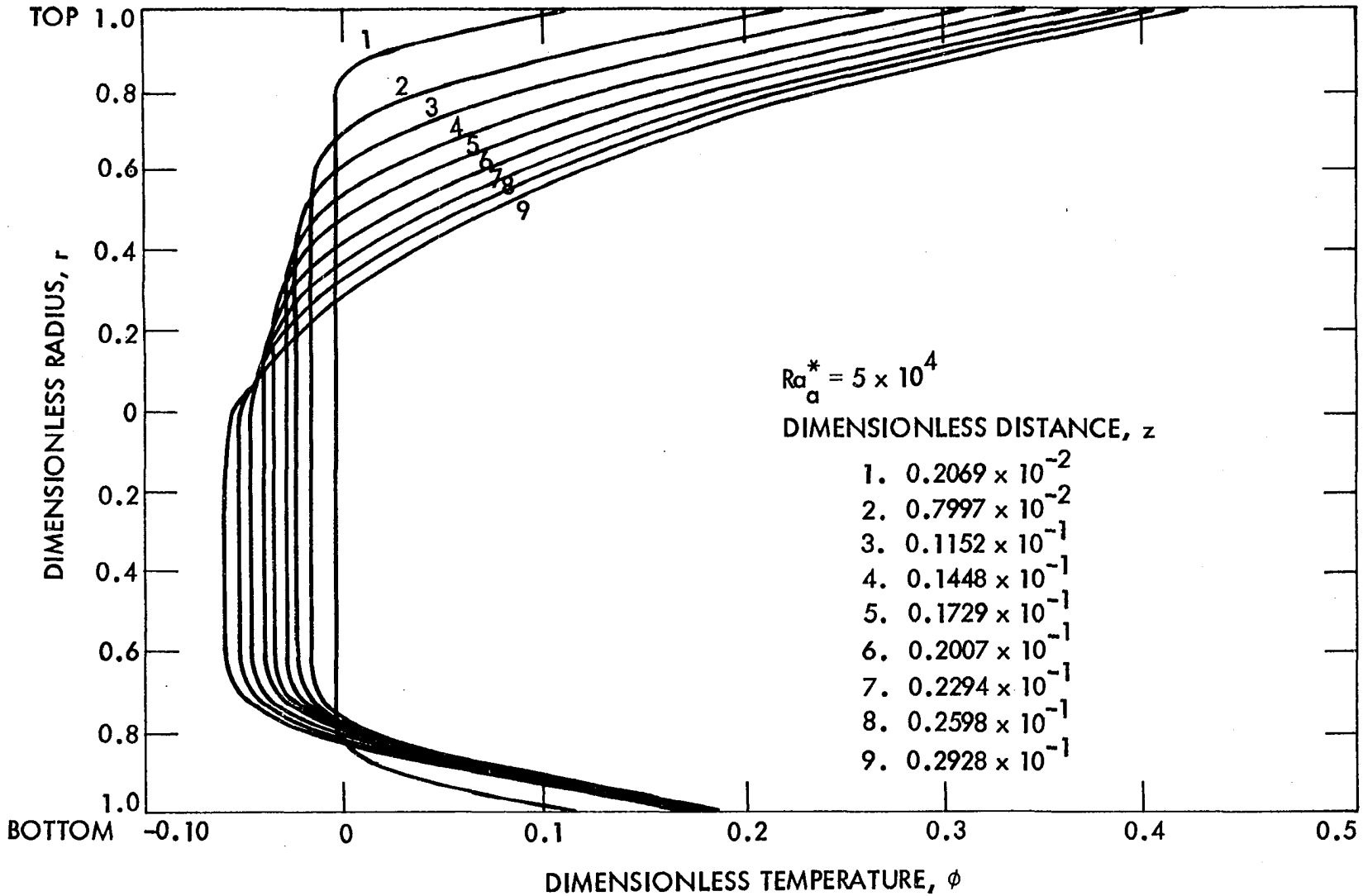

Fig. 2-2 Typical temperature development along vertical centerline for $Ra_a^* = 5 \times 10^4$

maximum and minimum temperature at each cross-section can be seen more clearly in Figs. 2-6 and 2-7. The temperature profile will remain nearly constant after reaching the fully developed condition.

Figure 2-3 shows the development of the horizontal centerline temperature profile for $Ra_a^* = 5 \times 10^4$. It is clear that uniform temperature appears between radii 0 and 0.5. The thermal boundary layer thickness varies from 0 at the tube inlet to about 0.4 of the radius at $z = 0.293 \times 10^{-1}$, which will be shown in Fig. 2-12 to be near the fully developed region. The boundary layer approximation employed in Refs. 30 and 31, which neglects temperature gradients in the horizontal direction in the central core region for high Rayleigh number flow, is thus found to be valid even in the entrance region.

Figure 2-4 presents the circumferential variation in the tube wall temperature, again for $Ra_a^* = 5 \times 10^4$ with z as a parameter. These circumferential tube wall temperature profiles are in qualitative agreement with experimental data [97]. The maximum wall temperature is located at the top of the tube, and this maximum temperature increases as z increases. The temperature around tube wall rises gradually from the bottom of the tube until θ equals about 60° and then increases sharply from this point to the top of the tube. The temperature variation along the tube wall will be pronounced when the secondary flow becomes dominant.

Values of the secondary flow velocities u and v are presented in Figs. 2-5 and 2-6, respectively. The radial velocity is negative at the top of the tube due to downward fluid flow. Figure 2-5 demonstrates that the radial velocity along the vertical centerline increases from an initial value of zero to a maximum value at approximately $z = 0.0173$, and decreases

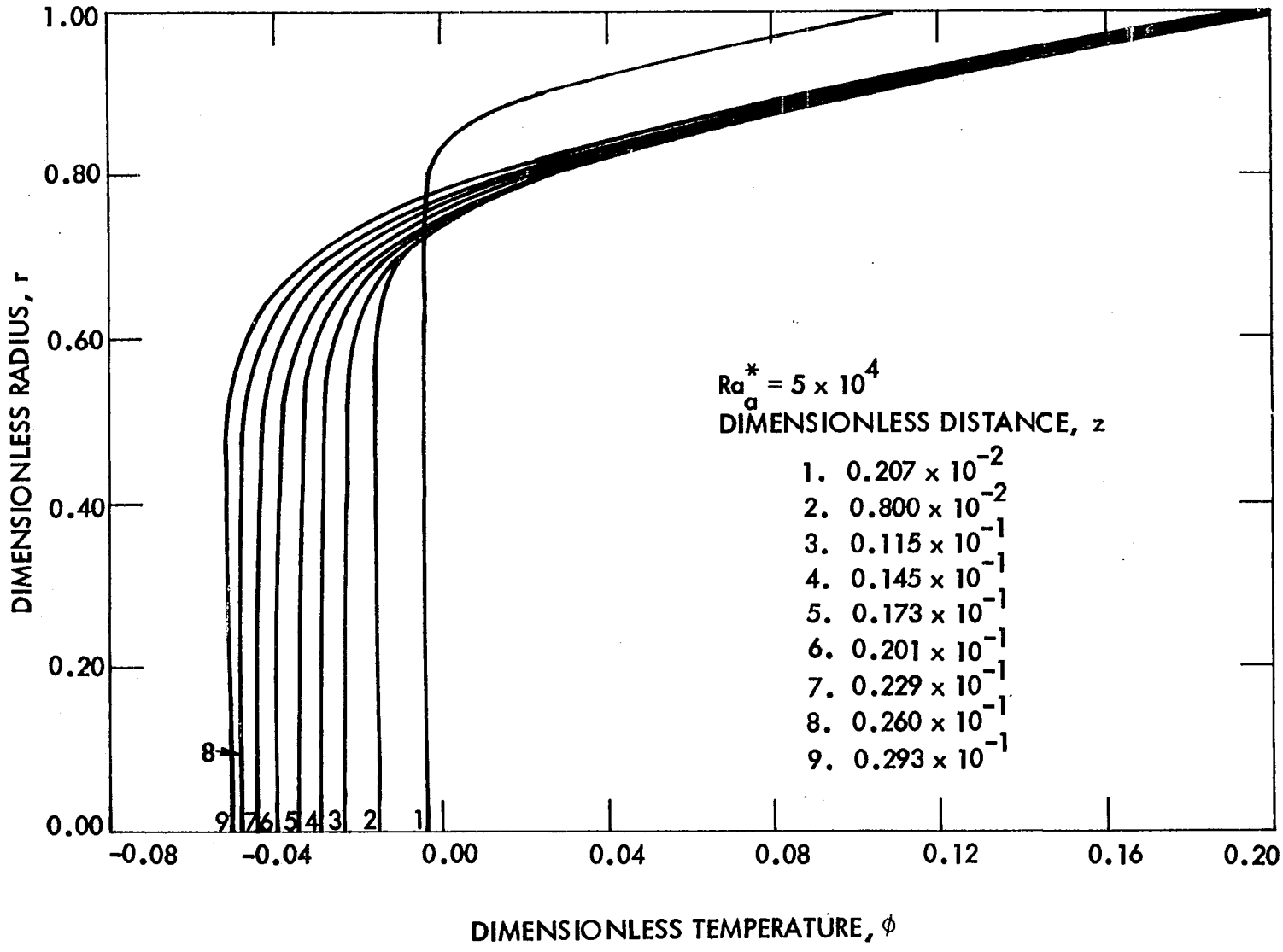

Fig. 2-3 Typical temperature development along horizontal centerline for $Ra_a^* = 5 \times 10^4$

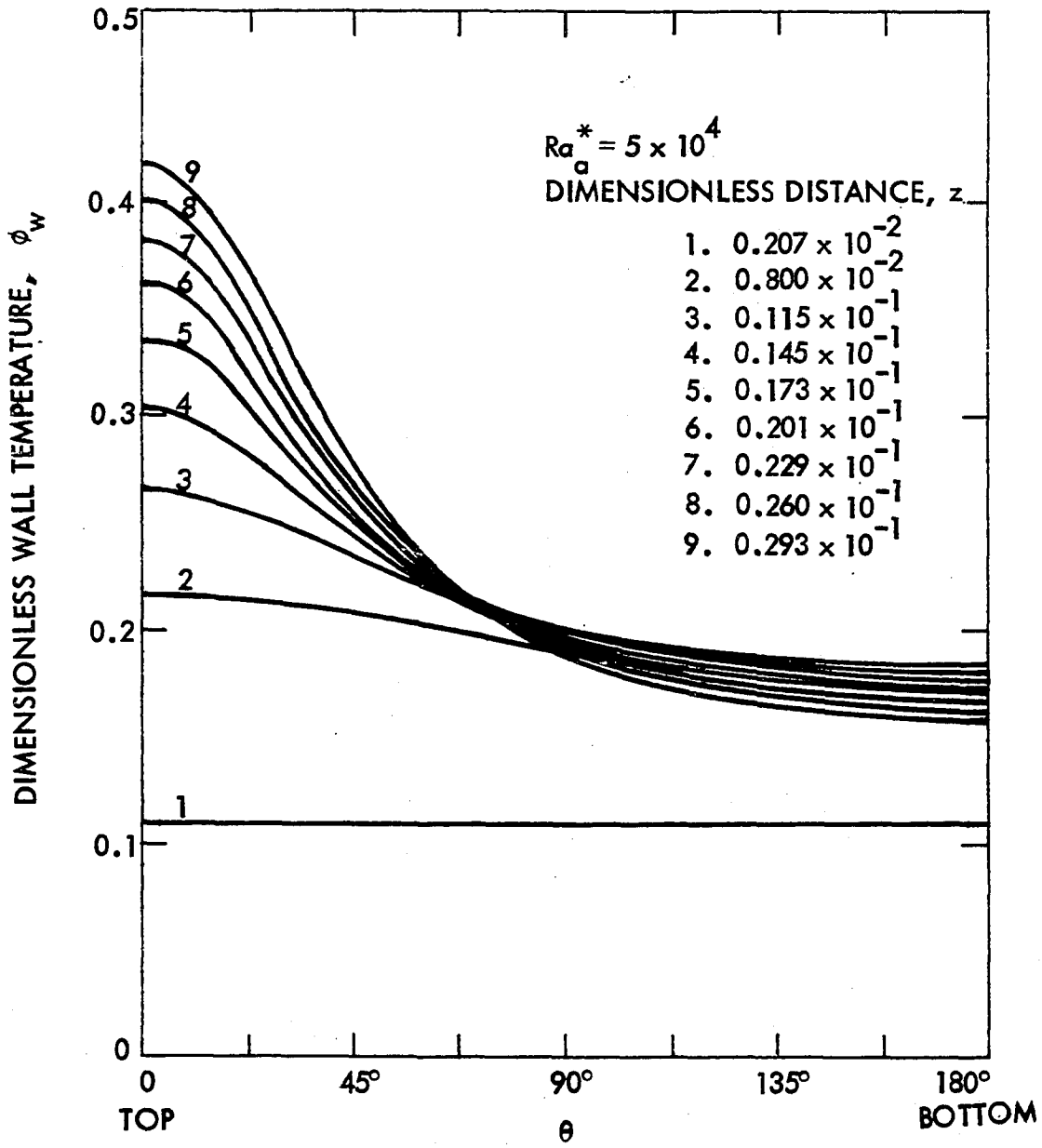

Fig. 2-4 Tube wall temperature development for $Ra_a^* = 5 \times 10^4$

after that until the fully developed condition is reached. The increasing and decreasing phenomena of radial velocity at the vertical centerline, however, occurs only at high Rayleigh numbers. For low Rayleigh numbers, $Ra_a^* = 10^3$, for example, the secondary velocity at the vertical centerline increases steadily from zero to a maximum at the fully developed condition. The secondary flow develops sooner for high Rayleigh numbers because of the larger differences in density between the wall and core regions.

Figure 2-6 depicts the distribution of the circumferential secondary velocity. The maximum secondary motion occurs within about 1/5 of the tube radius from the wall. The natural convection development along tube axis is also shown clearly. Unlike the radial velocity at the vertical centerline, the circumferential velocity increases from the initial zero value to about the maximum value at the fully developed condition. Inflection points of velocity in the θ-component are seen to occur at the same location, which is about half of tube radius from the centerline. The boundary layer approximations reported by Mori and Futagami, in which the vertical direction velocity distribution in the core region was assumed to be uniform, are observed to be fairly good approximations for high Rayleigh number fully developed flows.

Lines representing constant temperature and lines representing constant values of the stream functions are shown in Figs 2-7a and 2-7b. As mentioned earlier, the maximum temperatures occur at the top of the tube. The minimum temperatures for this Ra_a^* occur on the vertical centerline below the tube axis at the radius of 0.5 for $z = 0.5424 \times 10^{-2}$ and at a radius of 0.4 for $z = 0.02759$ for the fully developed region. A study of the isotherms at the tube inlet for any Rayleigh number reveals that the isotherms

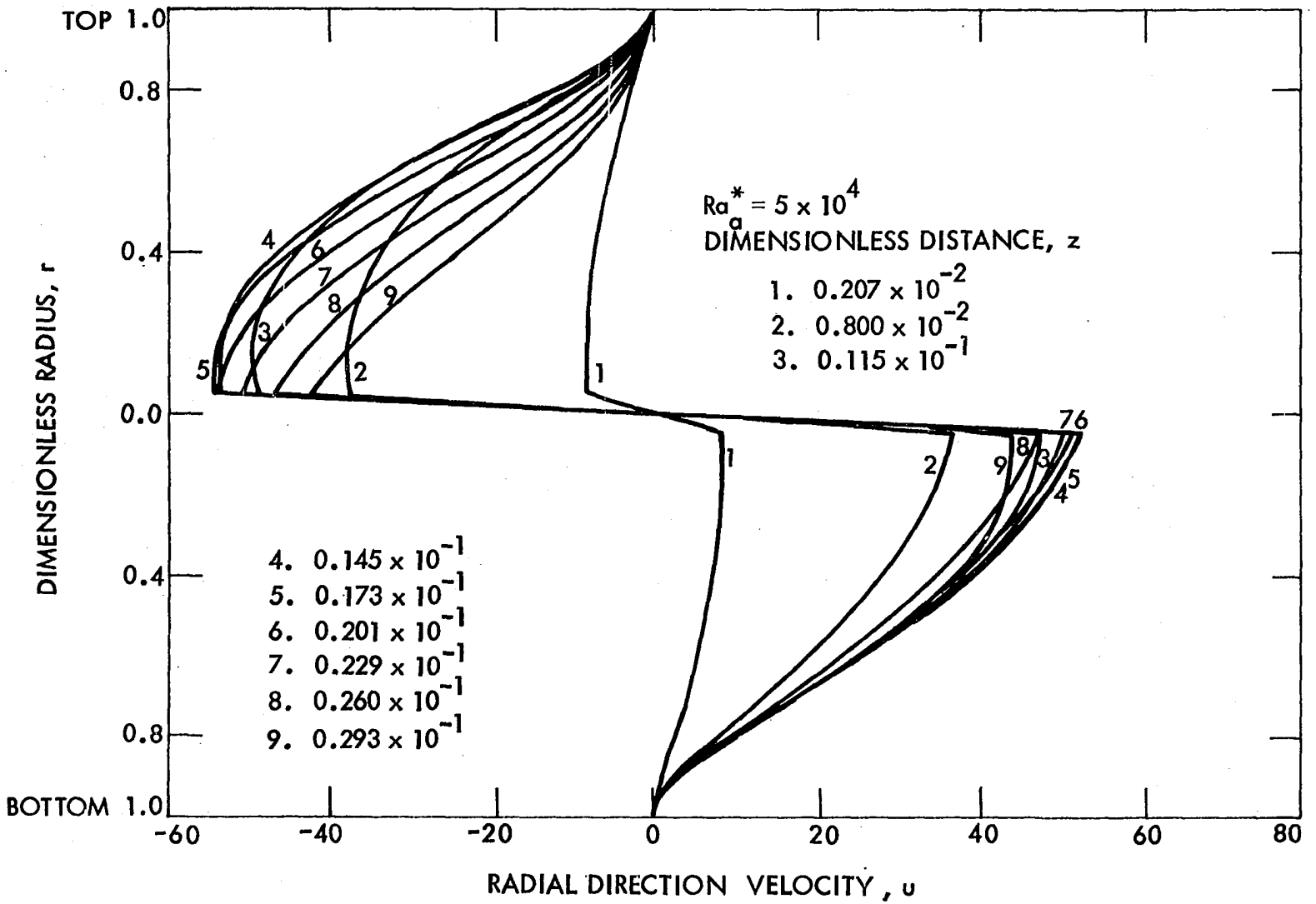

Fig. 2-5 Radial velocity development along vertical centerline for $Ra_a^* = 5 \times 10^4$

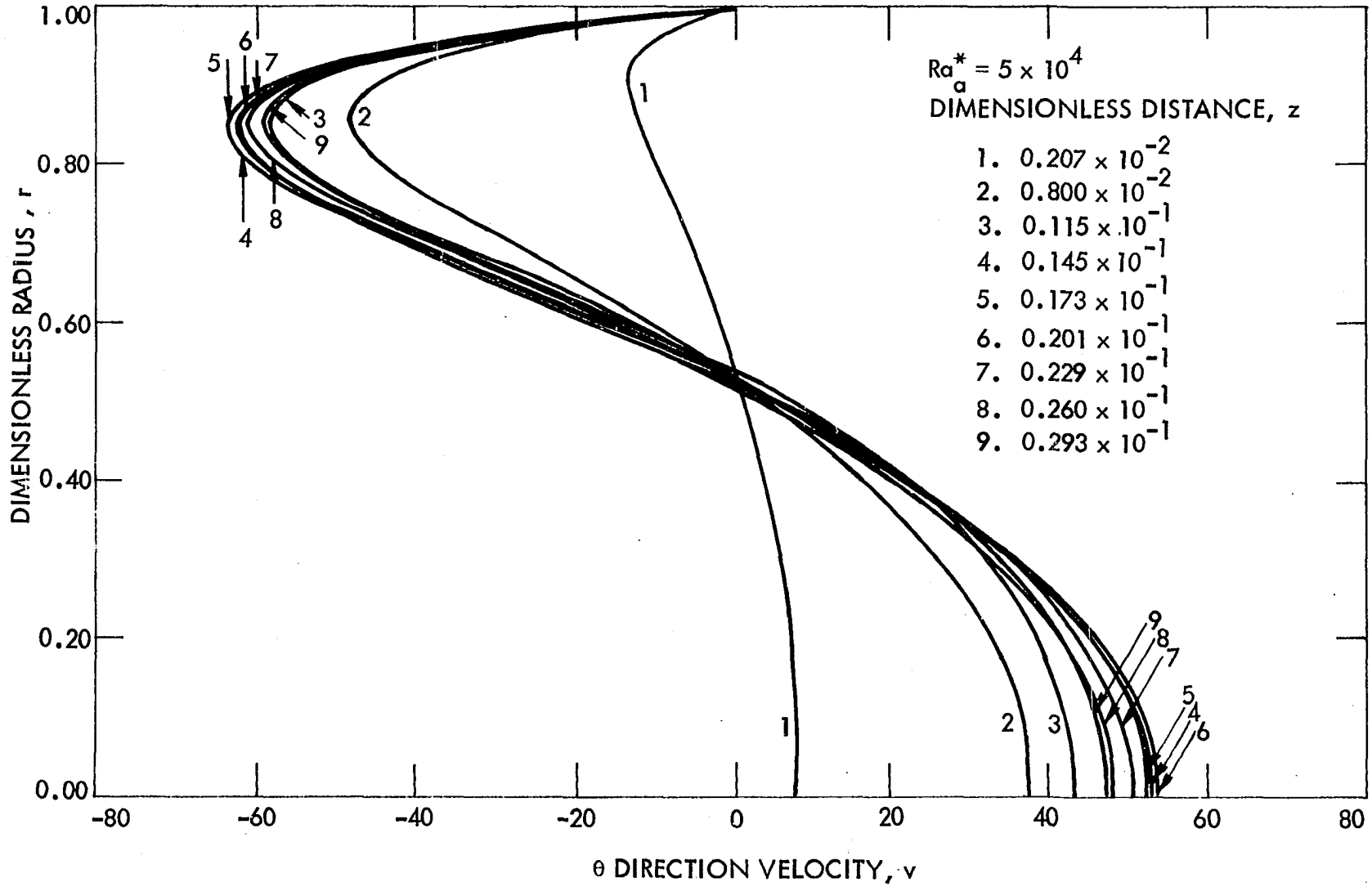

Fig. 2-6 Circumferential velocity development along horizontal centerline for $Ra_a^* = 5 \times 10^4$

are nearly circular and concentric. This behavior can also be seen from the temperature profiles shown in Figs. 2-2 and 2-3. The concentric isotherms will be gradually distorted and finally become fully developed. At a lower Rayleigh number, $Ra_a^* = 10^3$, for example, the fully developed isotherms are nearly concentric due to a weak secondary flow. As shown here in the high Rayleigh number region, the isotherms are distorted faster and will eventually exhibit fully developed patterns similar to those reported in previous investigations of the fully developed case [33, 35, 59].

There are two symmetric streamline patterns for the secondary flow; one pattern is presented in Figs. 2-7a and 2-7b. By studying the centers of circulation and their absolute values, the development of the secondary flow can be visualized. The centers of circulation first appear on the radial line $\theta = \pi/2$ at $z = 0.5425 \times 10^{-2}$. With increasing distance from the inlet, these centers tend to move upward and slightly toward the tube vertical centerline. With further increases of tube length, these centers move downward and toward the wall. The absolute value of the stream function at the "eye" increases from 0 at $z = 0$ to a maximum value of 18.36 at $z = 0.01448$ and then decreases to 16.88 at the fully developed condition. This behavior is also observed at extremely high Rayleigh numbers. For $Ra_a^* = 5 \times 10^5$, for example, the eye of the stream function moves upward from $\theta = \pi/2$, $r = 0.55$ ($z = 0.691 \times 10^{-2}$) to $\theta = 81^o$, $r = 0.55$ ($z = 0.691 \times 10^{-2}$) and falls to $\theta = 99^o$, $r = 0.65$ for the fully developed condition. The increasing and decreasing stream functions at the eye indicate the growth and decay of the secondary motion in the tube inlet region. For $Ra_a^* = 10^3$, for example, the eye of the stream function stays at $\theta = \pi/2$, $r = 0.55$, and the absolute stream function value at the eye increases from

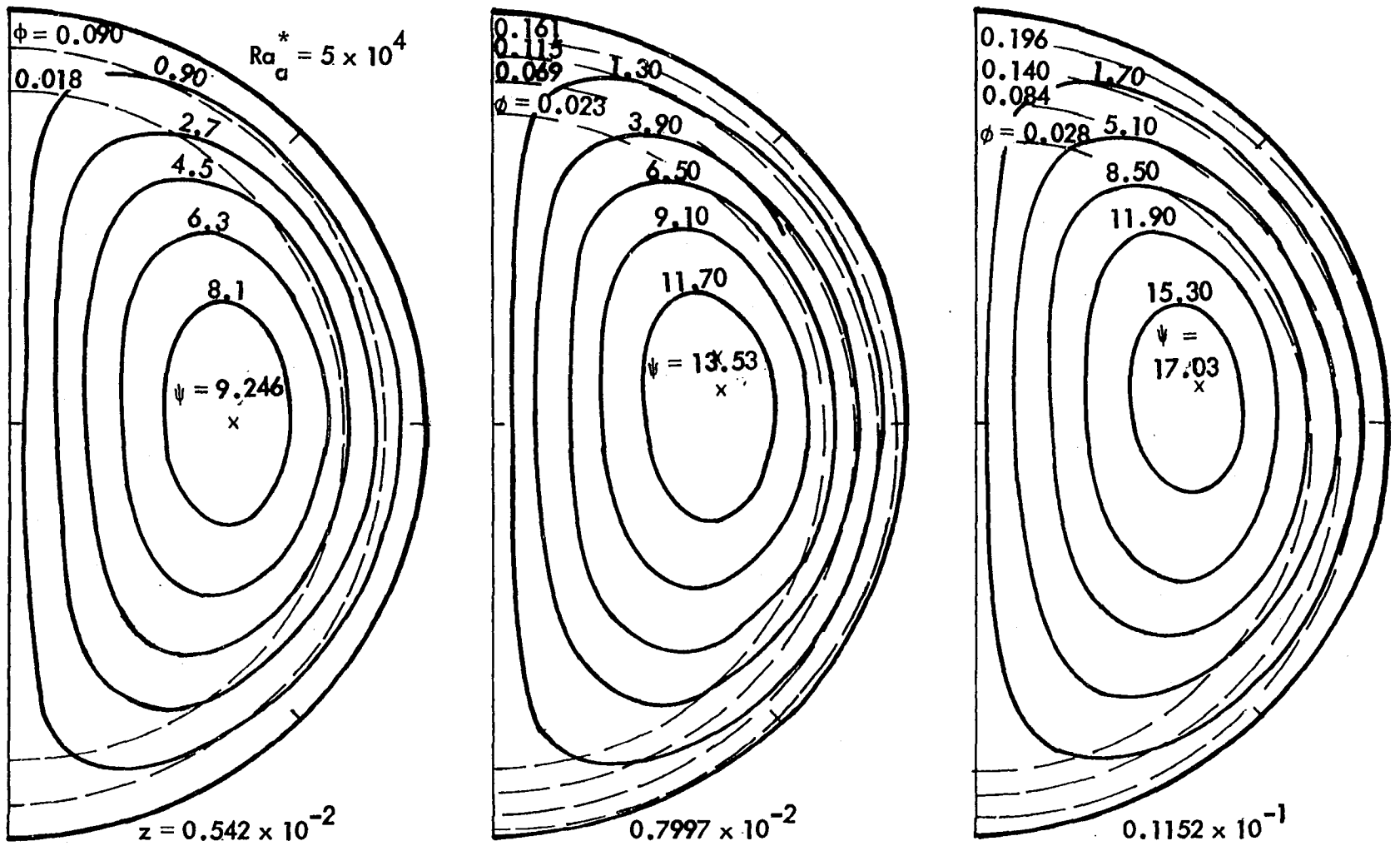

Fig. 2-7(a) Streamlines and isotherms at various axial positions for $Ra_a^* = 5 \times 10^4$

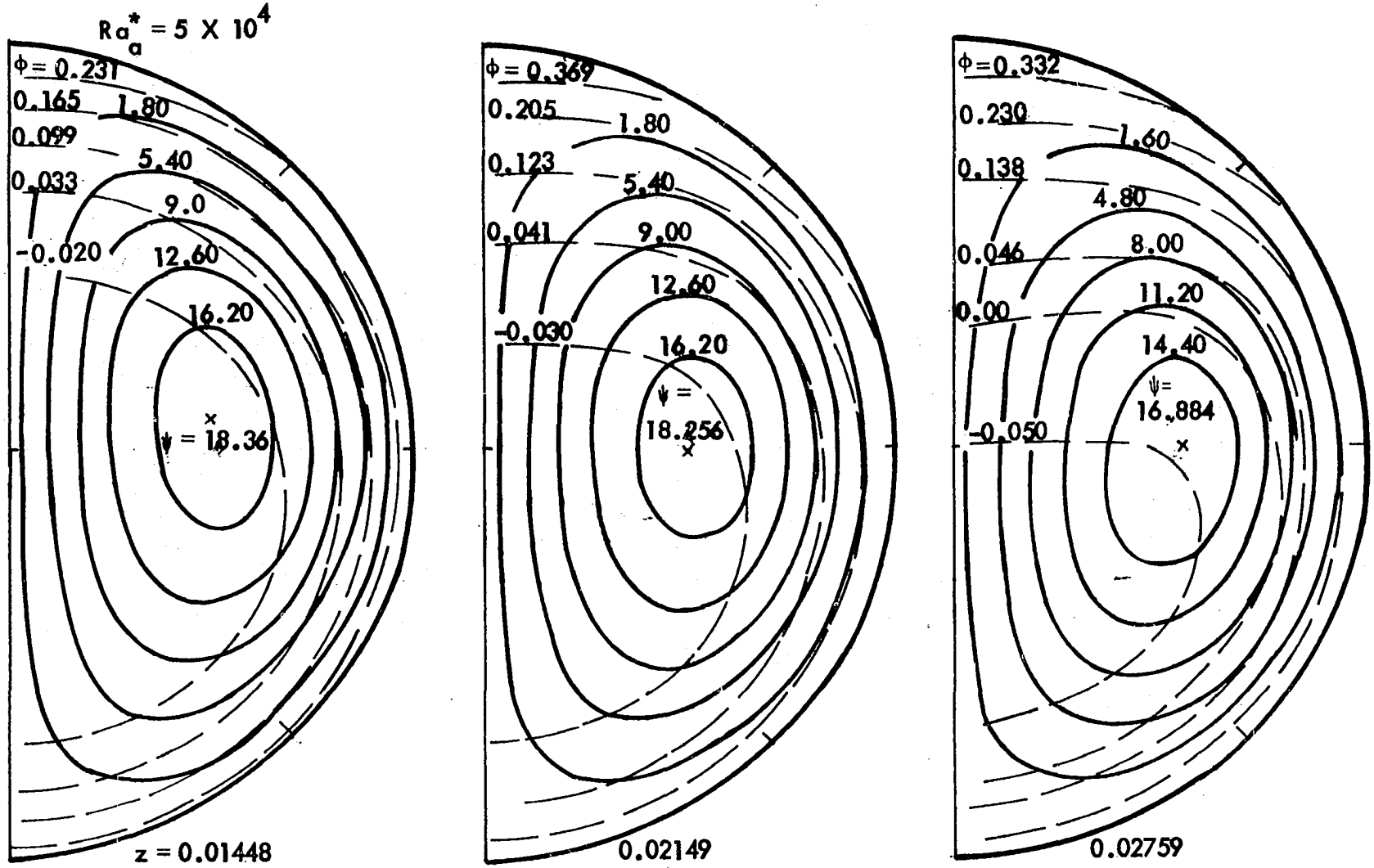

Fig. 2-7(a) (Continued)

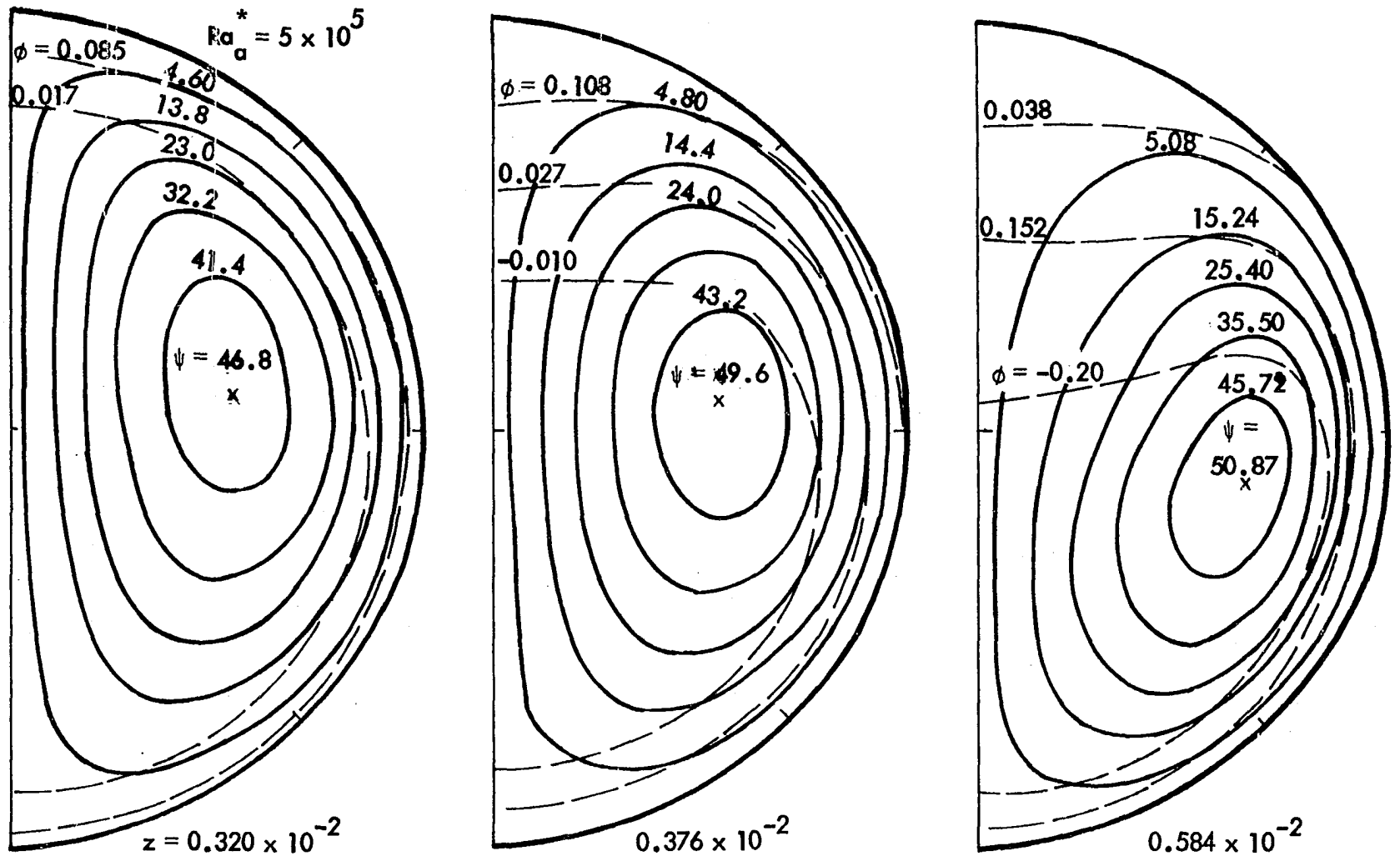

Fig. 2-7(b) Streamlines and isotherms at various axial positions for $Ra_a^* = 5 \times 10^5$

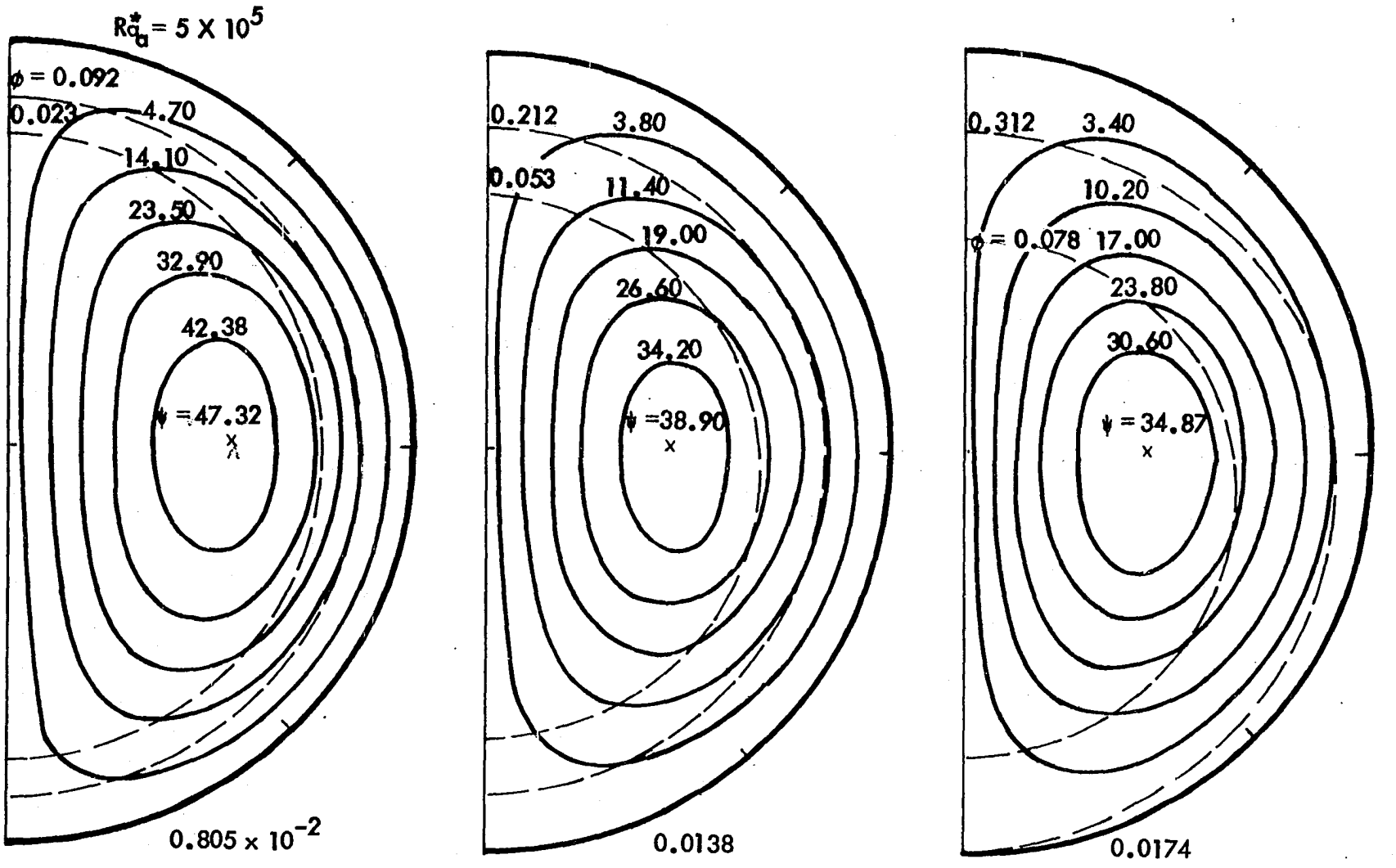

Fig. 2-7(b) (Continued)

0 to a maximum of 1.97 after the asymptotic condition has been reached. However, since the heat transfer coefficient is obtained from temperature profile, the growth and decay of the secondary motion does not necessarily imply the increase and decrease of heat transfer coefficient.

Figure 2-8 presents the local tube wall temperatures versus z for $Ra_a^* = 5 \times 10^4$. The average wall temperature and bulk mean temperature shown in this figure are defined as follows:

Average wall temperature

$$\overline{\phi}_w = \frac{\overline{T}_w - T_b}{\Delta T^*} = \frac{\int_0^{\pi} \phi_w \, d\theta}{\pi} \tag{2-65}$$

Bulk mean temperature

$$\phi_b = \frac{\iint_A \phi w dr d\theta}{\iint w dr d\theta} \tag{2-66}$$

Since ϕ_b is identically equal to zero it is possible to verify numerical computations by checking the computed ϕ_b. The temperature difference between the top and bottom of the tube wall is negligible at the tube inlet. However, the difference becomes considerable further downstream. The tube wall temperature increases gradually from the bottom to $\theta = \pi/2$ and increases rapidly from $\theta = \pi/2$ to the top of the tube.

The fully developed point is defined as the axial position after which the dimensionless temperature profiles remain constant. For practical application, however, the fully developed condition defined in Eq. (2-56)

$$\overline{\frac{\partial \phi}{\partial z}} = 0$$

indicates a reasonable asymptotic bound to represent hydrodynamic

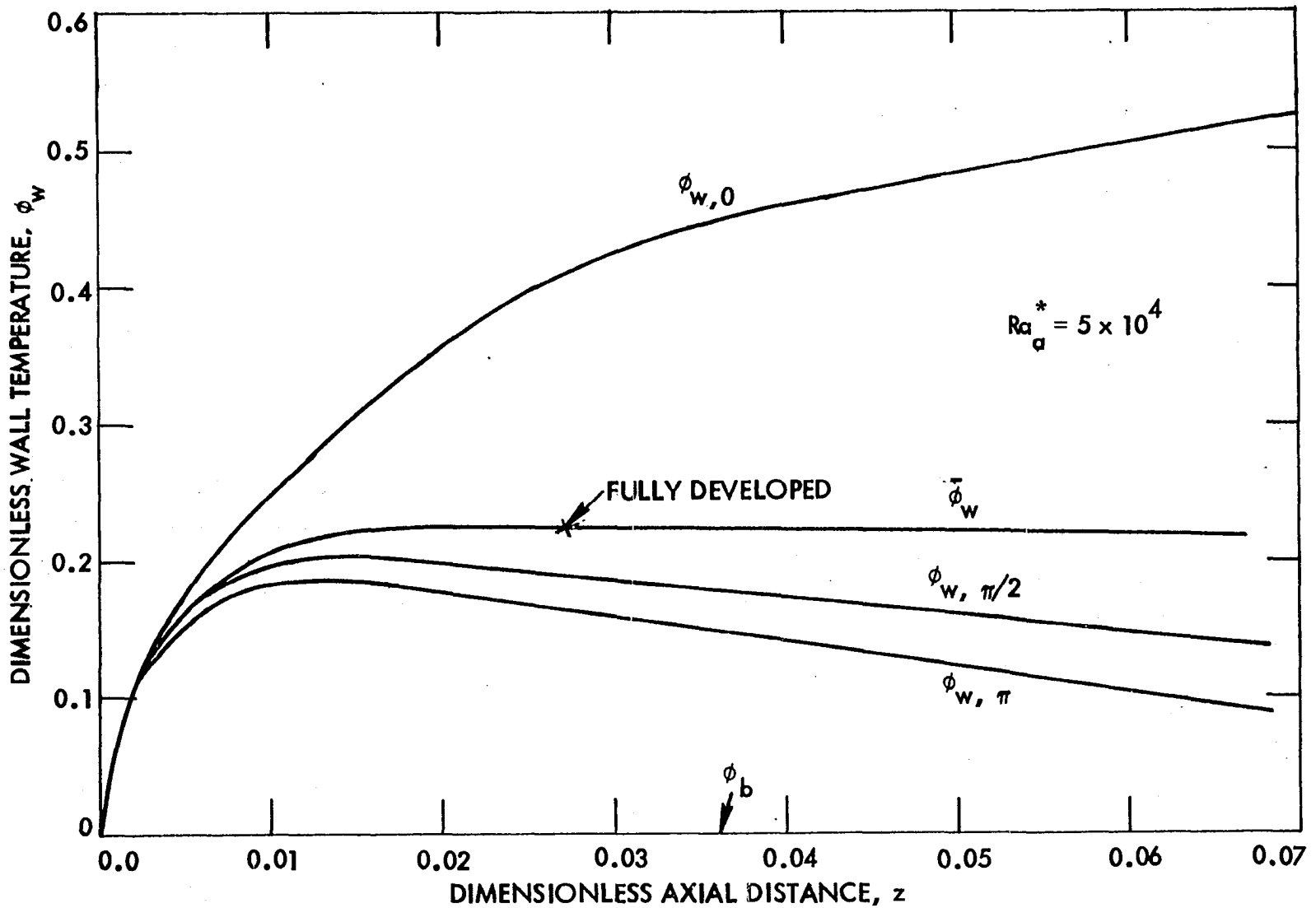

Fig. 2-8 Tube wall temperature versus reduced axial length at various locations for $Ra_a^* = 5 \times 10^4$

and heat transfer results after the flow reaches the asymptotic condition. It is noted that the top and bottom tube wall temperature difference keeps on increasing after the fully developed point, although $\bar{\phi}_w - \phi_b$ remains constant.

Nusselt number

The heat transfer results are presented in terms of Nusselt number, which can be obtained in two independent, but equivalent, ways. One way is to consider the temperature gradient at the wall, and the other way is to consider the overall energy balance for the axial length dz. The Nusselt number is defined as

$$Nu = \frac{\bar{h}\ 2a}{k} \tag{2-67}$$

Utilizing the temperature gradient at wall, the average heat transfer coefficient $\bar{h}$ can be written as

$$\bar{h}(\bar{T}_w - T_b)\cdot S\cdot dZ = k\left(\frac{\partial T}{\partial R}\right)_{R=a}\cdot S\cdot dZ = S\cdot q''\cdot dZ$$

Thus,

$$\bar{h} = \frac{k\left(\frac{\partial T}{\partial R}\right)_{R=a}}{\bar{T}_w - T_b} \tag{2-68}$$

Substituting this average heat transfer coefficient $\bar{h}$ into Eq. (2-67), the Nusselt number is obtained in terms of average dimensionless temperature as

$$(Nu)_I = \frac{2}{\bar{\phi}_w} \tag{2-69}$$

Another possibility is to consider the overall energy balance, which can be stated as follows:

$$\rho C_p \int_W \frac{\partial T}{\partial Z} dA \cdot dZ = \bar{h}(\bar{T}_w - T_b) \cdot S \cdot dZ \tag{2-70}$$

Consequently, Eq. (2-70) can be expressed as

$$(Nu)_{II} = \frac{\overline{\left(\frac{\bar{\partial}\phi}{\partial z}_w\right)} + 2}{|\overline{\bar{\phi}_w - \phi)w}|} \tag{2-71}$$

Since the prescribed error ϵ in Eq. (2-46) was set to be less than 10^{-5}, it was expected that the numerical results for the Nusselt number would be valid up to four significant figures. It was found that the Nusselt number obtained from these two alternative definitions agreed with each other up to the third significant digit. The final Nusselt numbers presented in this chapter were taken as the average value of these two alternative Nusselt numbers to reduce the uncertainty. It is thus believed that the 20 by 20 mesh size at each cross-section is satisfactory. The computer program and some numerical results are given in Appendix A and B respectively.

As indicated in the governing differential equations [Eqs. (2-28), (2-29) and (2-30)] and the boundary conditions [Eq. (2-31)], one obtains $\psi = 0$ and thus $u = v = 0$ in the tube for $Ra_a^* = 0$. Without the secondary velocities u and v, the energy equation [Eq. (2-30)] reduces to the traditional constant-property version. Moreover, when secondary flow motion is neglected, the momentum and energy equations are uncoupled. Therefore, one can solve those equations separately. Without the influence of secondary motion, the dimensionless temperature profile becomes symmetric about the origin and Eq. (2-30) is reduced to a two-dimensional (r and z) equation, which is much easier to solve analytically.

The comparison of the present numerical solution for $Ra_a^* = 0$ with

previous constant property solution is depicted in Fig. 2-9. The present results using a 20 by 20 mesh, are in satisfactory agreement with the well known constant-property analytical solutions.

It is of interest to examine the behavior of circumferential local Nusselt numbers, which are given by

$$Nu' = \frac{2}{\phi_w} \tag{2-72}$$

Figure 2-10 presents typical circumferential local Nusselt numbers at different axial locations. The Nusselt numbers around the tube circumference distribute uniformly at the tube inlet and are gradually distorted along the tube. As would be expected from the circumferential wall temperature distributions, the Nusselt number at the top of the tube is lower than that at the bottom. The local Nusselt numbers around tube perimeter are in qualitative agreement with the experimental results given in Ref. 121 for water in thin-walled metal tubes. The lower heat transfer coefficient at the top of the tube is due to substantially reduced circulation resulting from thermal stratification. A negative Nusselt number at the tube wall is also possible, as is pointed out in Ref. 97; however, no such phenomena were observed in this analytical study.

Figure 2-11 indicates the stability and convergence of the numerical solution where secondary flow is involved. These factors are examined most conveniently on the average Nusselt number plot. Recall that the truncation error of each finite-difference representation as shown in Eqs. (2-57) and (2-58) is of the order of magnitude of Δr^2 or $\Delta\theta^2$. With finer grids, one obtains more accurate solutions. The sensitivity of the solution to mesh size is demonstrated by the calculations for $Ra_a^* = 10^5$. The change from

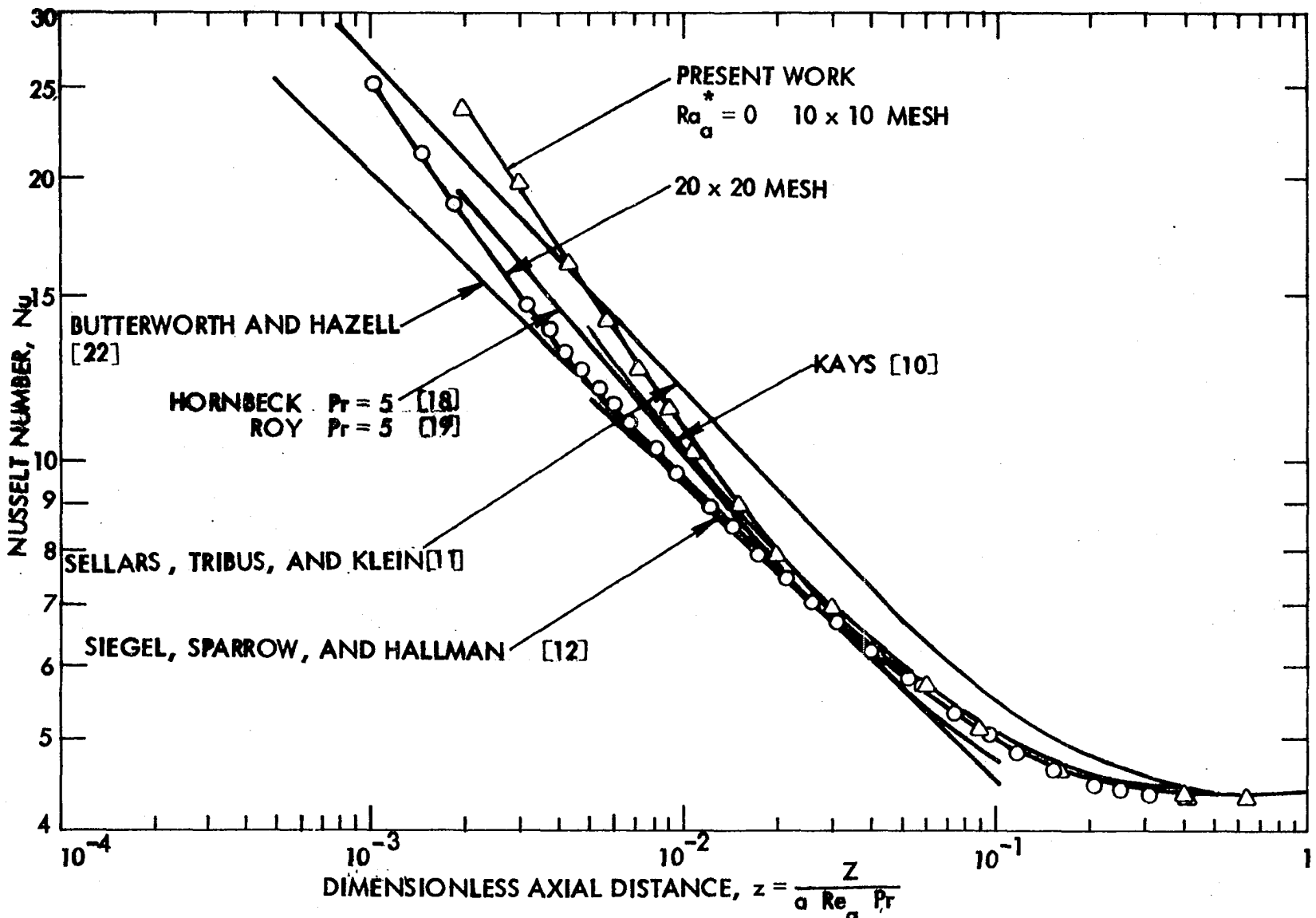

Fig. 2-9 Comparison of present limiting results ($Ra_a^* = 0$) with traditional constant property thermal entry solutions

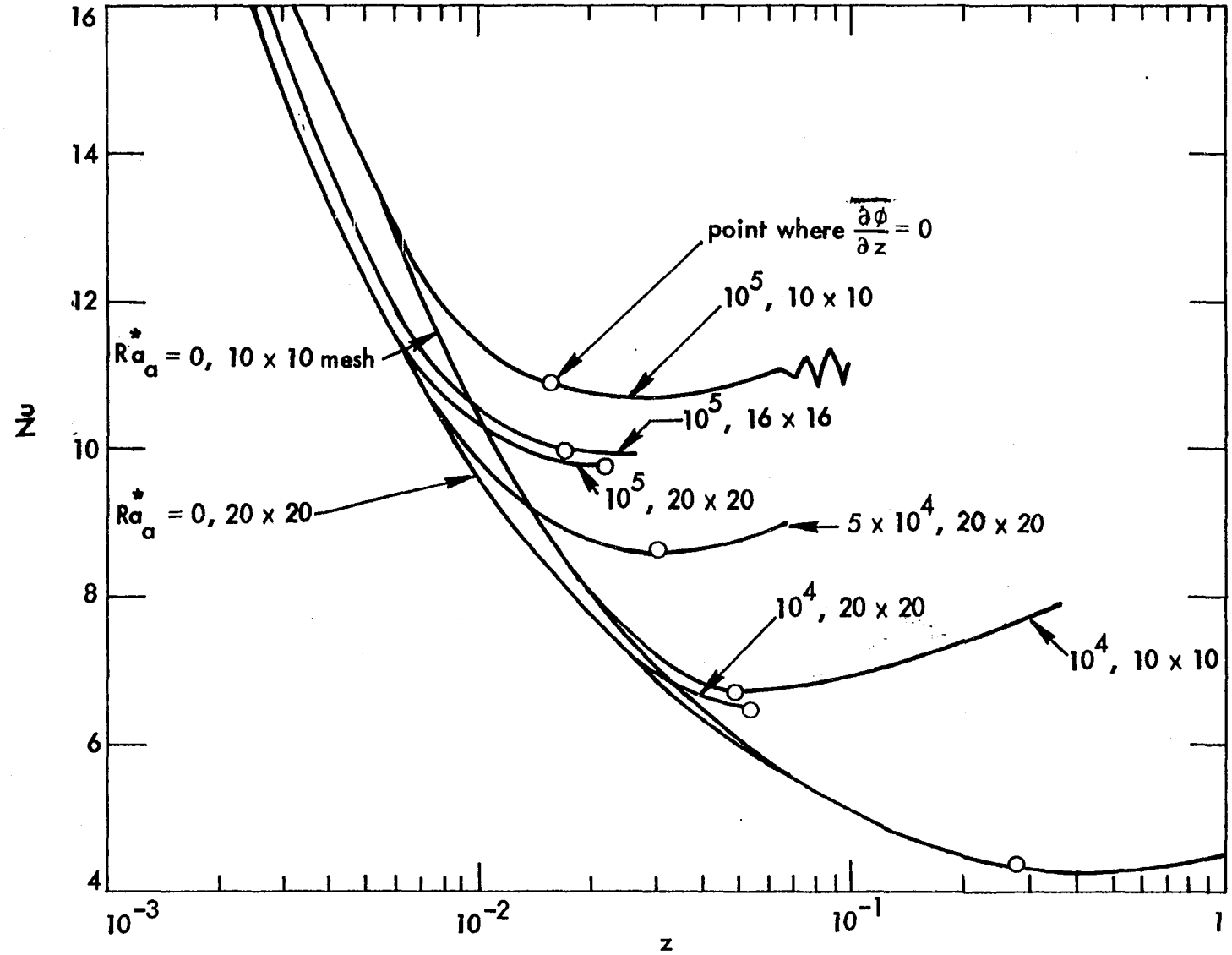

Fig. 2-11 Stability behavior of computation in thermal entrance region for various mesh sizes and Ra_a^*.

16 by 16 to 20 by 20 mesh is relatively small; hence, the 20 by 20 mesh is considered to be a sufficiently fine grid. This choice is supported by the good agreement with previous exact solution for $Ra_a^* = 0$ given in Fig. 2-9.

To illustrate what happens as the calculation proceeds beyond the defined fully developed point, the computed results for $Ra_a^* = 10^5$, 5×10^4 and 10^4 are shown in Fig. 2-11. The "accurate" 20 by 20 mesh calculations were not extended beyond the fully developed point for all cases. It takes more than an hour of computing time for the 20 by 20 mesh, in contrast to the 5 minutes of computing time required for the 10 by 10 mesh, to get to $z = 0.1$ for $Ra_a^* = 10^5$. As mentioned earlier, the step size in the axial direction is controlled by Eq. (2-64) to satisfy the stability criterion. Beyond the fully developed point the Nusselt number starts to increase or oscillate. The oscillation appears to be caused by computational instability. It is recalled that temperature and secondary velocity profiles keep on changing after the fully developed condition has been reached. Eventually, this temperature or secondary flow variation will make the matrix in the momentum equation or the stability criterion in the energy equation unstable. Brian et al. [79] reported that a similar oscillation occurred in the numerical solution of the helically coiled tube problem when the ADI method was employed. Nevertheless, they argued that this was a real flow oscillation instead of a computational instability. This seems highly unlikely.

A similar minimum in the Nusselt number, shown in the Nu - z plot for constant Rayleigh number, was presented in one of the authors' previous reports [43] in which the ADI technique was applied. At this time the computed data were considered to be valid as there was a lack of knowledge of

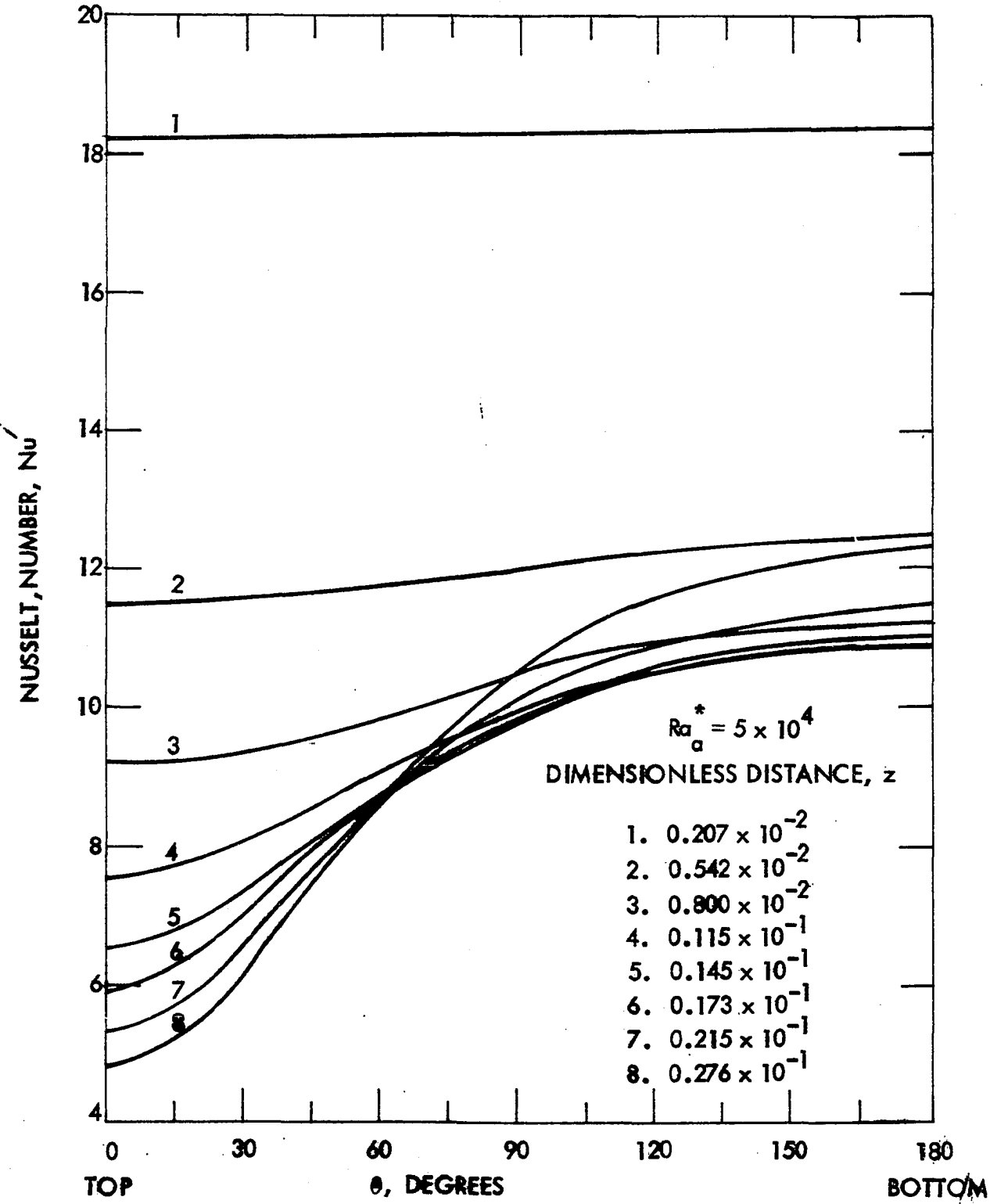

Fig. 2-10 Local Nusselt numbers at various axial positions for $Ra_a^* = 5 \times 10^4$

the stability criterion and of a suitable method for predicting the fully developed condition. On the basis of the present study it is suggested that the heat transfer result at the fully developed condition defined in Eq. (2-56) represents the asymptotic solution. In order to further examine the proper definition of Eq. (2-56) for the fully developed condition and the unlikely Nusselt number which occurred in the Nu - z plot, a numerical solution for $Ra_a^* = 0$ was carried out to z = 1.0, as shown in Fig. 2-11. The fully developed point predicted by Eq. (2-56) occurred at z = 0.278 and the Nusselt number at that point was 4.366, as compared to 4.364 for the exact solution. It is thus believed that the definition of Eq. (2-50) is suitable for the present study.

Figure 2-12 presents the final results for the free convection effect on Nusselt number in the thermal entrance region. The numerical data are tabulated in Appendix B. In Fig. 2-2 constant property solutions are demonstrated to be valid only for $Ra_a^* = 0$ and are accurate within 5 percent for Rayleigh numbers less than 10^3. For $Ra_a^* = 10^6$, the developed Nusselt number is about 250 percent above the constant property value, and the entrance length is about one tenth of the constant property prediction. Rayleigh number is seen to decrease the thermal entrance length and increase the Nusselt number. The right hand dashed line in Fig. 2-12 shows the theoretical prediction of the exact thermal entrance length [according to Eq. (2-56)]. The left hand dashed line in the same figure represents the entrance length where the Nusselt number is five percent higher than the asymptotic prediction. Comparison of the present analytical solution with the experimental data for water reported by Petukhov et al. [94, 95] is also shown in Fig. 2-12. The present numerical solution is seen to be in good

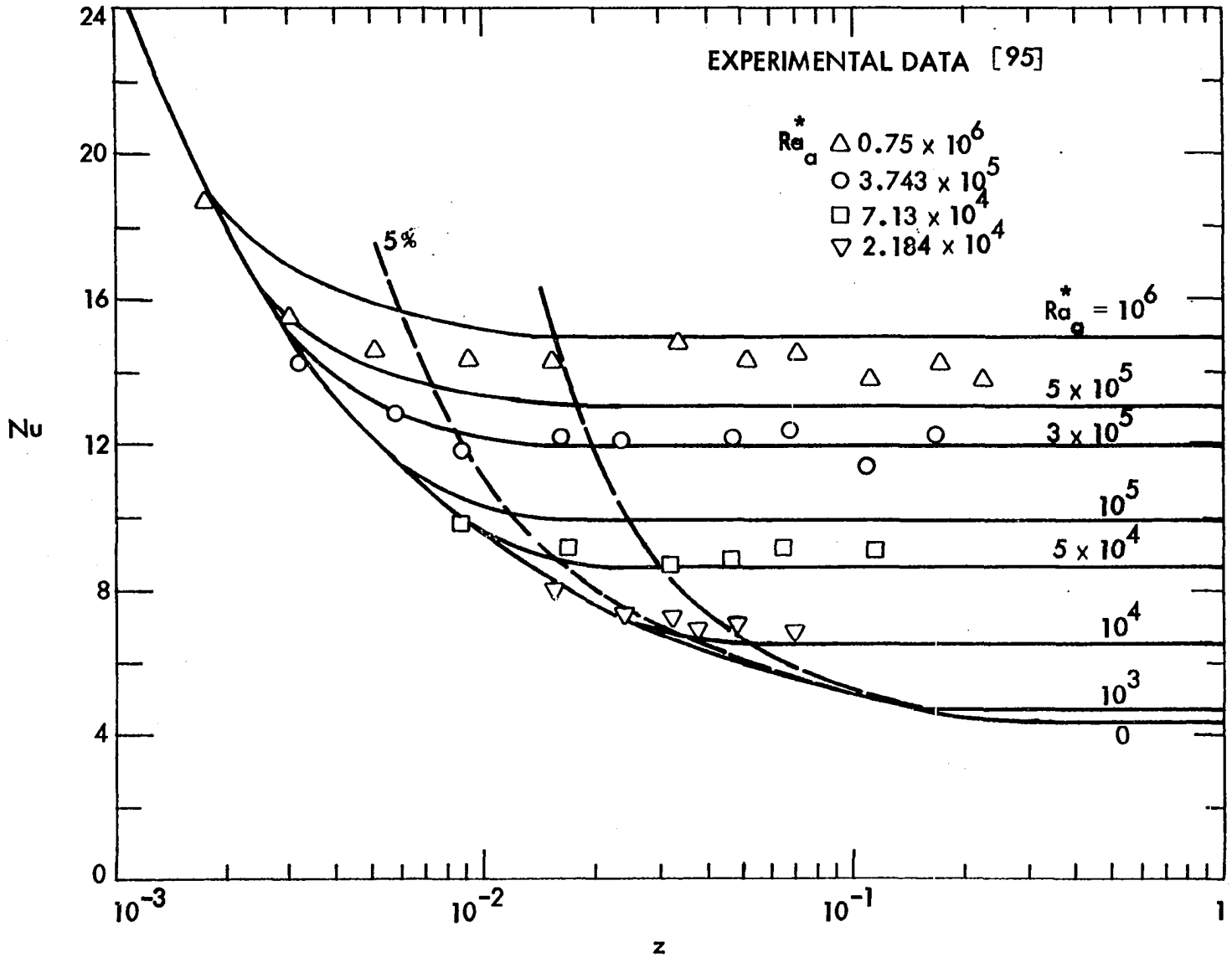

Fig. 2-12 Comparison of present results with experimental data for water

agreement with the experimental data. This substantiation of the analytical results indicates that the Prandtl number assumption is valid even for water.

Figure 2-13 shows various values of the thermal entrance length versus Rayleigh number. It indicates more clearly that the Rayleigh number associated with secondary flow reduces the thermal entrance length. Experimental predictions from Petukhov and Polyakov [94, 95] are low, generally bracketed by the present curves.

The present solutions for fully established Nusselt numbers are compared with some available analytical solutions in Fig. 2-14. The present Nusselt number predictions appear to be lower than the integral solution of Siegwarth et al. [31] which also assumes large Prandtl number, but also has the infinite thermal conductivity boundary condition.

The numerical solutions from Newell and Bergles [33] for water with both tube wall boundary conditions are also shown in Fig. 2-14. The present solutions for the fully developed condition fall between the two limited bounds proposed by Newell and Bergles [33] in the high Rayleigh number region. The difference between the present solution and the solutions from Newell and Bergles [33] at lower Rayleigh numbers may be a result of the large Prandtl number assumption being inadequate for water, which was used in their computations. In general, the present asymptotic solutions are qualitatively in good agreement with these analytical solutions for high Rayleigh number. The asymptotic Nusselt number can be estimated by Eq. (2-73) with 99 percent confidence for $Ra_a^* \geq 4 \times 10^3$

$$Nu_\infty = 1.287\ Ra_a^{*0.177} \tag{2-73}$$

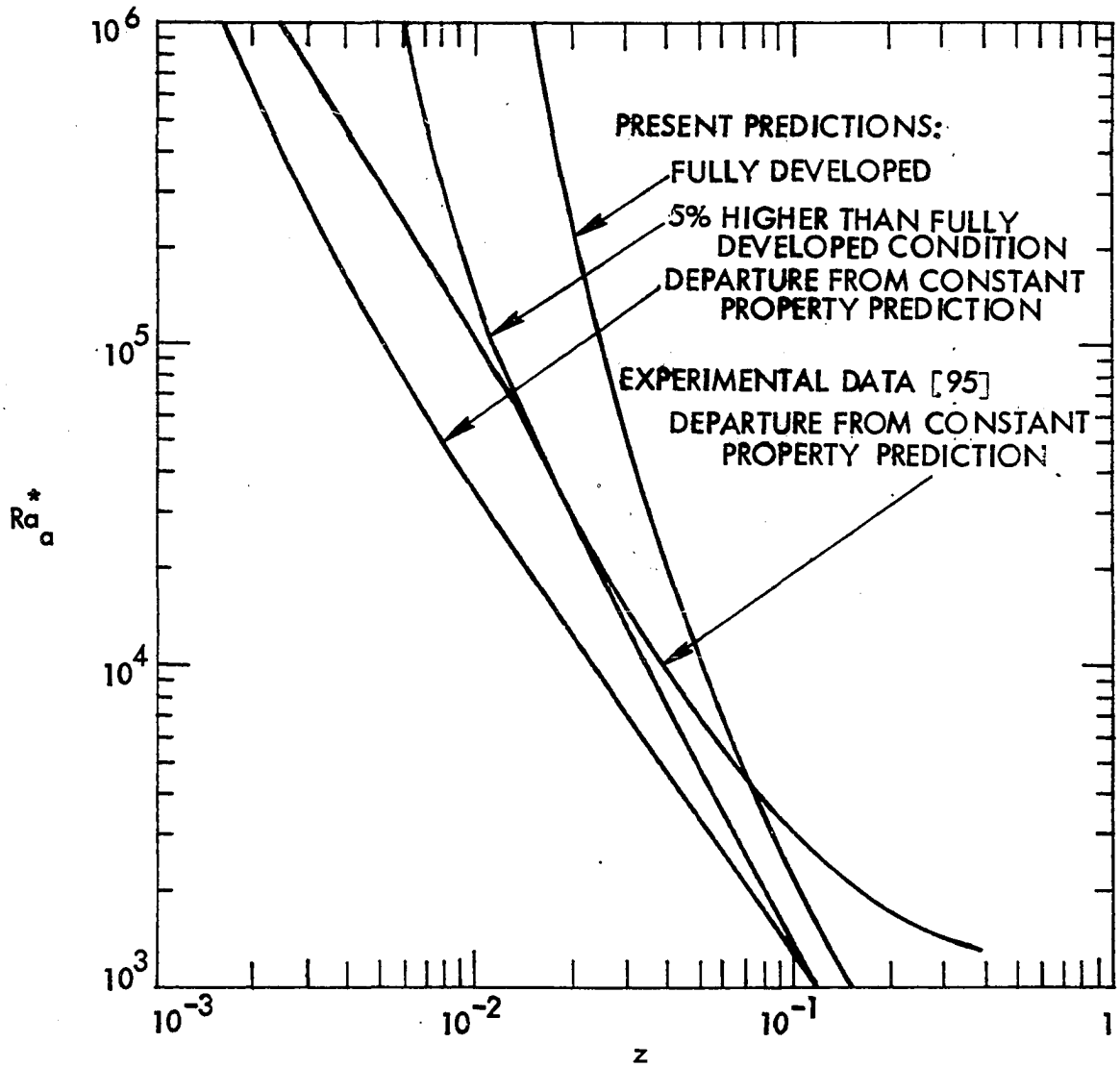

Fig. 2-13 Thermal entrance lenth versus Ra_a^* for different definitions of entrance length- comparison with experimental data for water

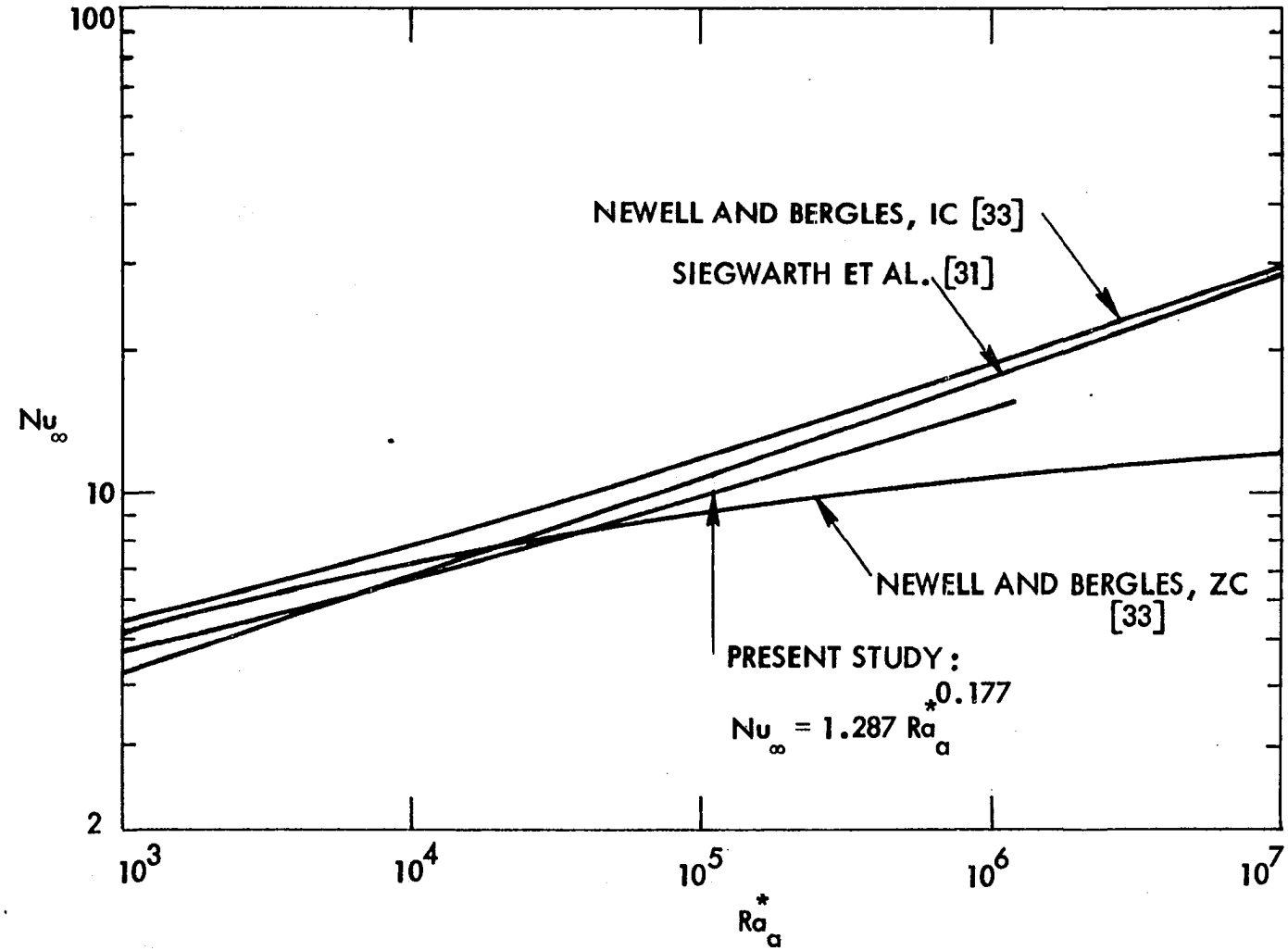

Fig. 2-14 Comparison of present fully developed heat transfer results with results of previous analytical investigations

Concluding Remarks

1. The classical Graetz problem for laminar forced convection in a horizontal tube with uniform wall heat flux is extended by taking buoyancy effects into consideration. The Graetz problem with free convection is formulated in general, and the limiting case of large Prandtl number is solved by the DuFort-Frankel and boundary vorticity methods.

2. Figure 2-12 represents the behavior of the Nusselt number in the entrance region. Good agreement of the analytical solutions with available experimental data suggests that water is included in the "large" Prandtl number class.

3. The present numerical results provide confirmation that the traditional constant property solutions are valid only for the very low heat fluxes associated with low Rayleigh numbers (less than 10^3). For $Ra_a^* = 10^6$, the Nusselt number in the fully developed region is about 200 percent above the constant property solution, and the thermal entrance length is about one tenth of that indicated by the constant-property solution. At larger Ra_a^* the transition region between the constant property Nu and the fully developed forced and free convection Nu is considerable. The present solution clearly defines this region. Increasing Rayleigh number decreases the thermal entrance length and increases the Nusselt number.

4. A simple correlation for the asymptotic Nusselt number and Rayleigh number has been established as

$$Nu_\infty = 1.287\ Ra_a^{*\,0.177} \tag{2-73}$$

for $Ra_a^* \geq 4 \times 10^3$ within 1 percent error. This correlation is in reasonable agreement with available analytical solutions.

5. Oscillation and divergence behavior appearing in Ref. 79 and the present investigation raises questions of stability and convergence in applying either the ADI or DuFort-Frankel method to nonlinear, cylindrical, three-dimensional, parabolic partial differential equations. A further study in numerical stability is suggested to verify the limits of the available numerical schemes.

6. The friction factor in the present solution is not affected by secondary flow, since the primary flow is assumed not to change (large Prandtl number assumption).

7. The variation of local Nusselt numbers along the tube for uniform wall heat flux shows that the buoyancy effect is negligible up to a certain entry length z, depending on the magnitude of the Rayleigh number. The dip in the curves for the local Nusselt numbers in Ref. 43 would be avoided if the present fully developed definition were applied. It can be considered to be a general rule that the Nusselt number decreases as tube length increases.

8. Other three-dimensional laminar heat transfer problems can be approached by the present analytical techniques. These include curved pipes subject to centrifugal force effects and rotating pipes subject to coriolis forces. Combined forced and free convection in inclined pipes can also be solved by similar numerical techniques. It should be pointed out that the entrance region in many applications is very short; hence, the developing or three-dimensional solutions may not be required.

CHAPTER III. THEORETICAL SOLUTIONS FOR FULLY DEVELOPED LAMINAR COMBINED FORCED AND FREE CONVECTION IN HORIZONTAL TUBES WITH TEMPERATURE-DEPENDENT VISCOSITY

Introduction

The prediction of laminar heat transfer coefficients, with density variation taken into account, has been generally discussed in the previous chapter. In actual application, however, experimental data may exhibit considerable deviations from these analytical predictions. This is in large part due to the inaccuracy of the constant transport property assumption in the analytical formulation and the improper tube wall boundary conditions in the corroborating experiments. Most previous analytical investigations focus on determining the effects of either variable density or temperature-dependent viscosity. The present study extends previous analyses to include variable viscosity effects on combined forced and free laminar convection in horizontal tubes.

To account for transport property variation, three empirical methods are often employed to correlate experimental data for laminar and turbulent tube flow. In one of these methods, all properties are evaluated at the mean film temperature [$T_f = 1/2(T_w + T_b)$]. This method is usually adequate when the fluid properties are weak functions of temperature. The second traditional method is to consider viscosity temperature variation by introducing a viscosity correction factor, $(\mu_b/\mu_w)^i$ for liquids and $(T_b/T_w)^j$ for gases, into the final correlation. Fand and Keswami [122] recently proposed a third method which applies a correction factor to each dimensionless group, Nu, Re, Pr, etc. The correction factor is the ratio of the dimensionless group evaluated at the bulk temperature to the group

evaluated at the wall temperature raised to a power, e.g., $(Pr_b/Pr_w)^i$; if the viscosity is the primary temperature-dependent variable, this method is similar to the viscosity correction method. These three methods are empirical and are not derivable theoretically from governing equations.

Viscosity temperature variation has been considered in a number of analytical investigations. Considering viscosity as a simple function of temperature, Deissler [25] correlated Nusselt number as a function of the absolute surface to bulk temperature ratio for gases and liquid metals in laminar tube flow. The Nusselt number decreases about 7 percent from the constant property solution as the temperature ratio increases to 1.8 for gases. One realizes that all physical properties vary as a function of temperature; however, practically, the viscosity requires special attention (after density variation is considered). Shannon and Depew [109] indicated that the Nusselt number for liquids can be correlated by $(\mu_w/\mu_b)^i$ when the viscosity is assumed to be exponential in temperature. Other studies of heat transfer which consider viscosity the only temperature-dependent property were reported by Rosenberg and Hellums [38], Test [39], Hwang and Hong [40], and Martin and Fargie [36]. The effect of variable viscosity is to increase heat transfer coefficients for most liquids during heating. It was concluded by Hwang and Hong [40] that Nusselt numbers for systems of variable viscosity were 15 to 20 percent higher than those obtained when constant viscosity was assumed. In spite of these analytical studies, there is no general result that can be employed to predict the heat transfer data.

As indicated in the review in Chapter I, numerous investigations were focused on temperature-dependent density and associated free convection in

horizontal, vertical, and inclined tubes. Estimating both density and viscosity as a function of temperature, Lawrence [52] solved analytically the entrance region problem in vertical tubes. It is relatively easy to consider both density and viscosity temperature variation in vertical tube flow since the free convection generated by the buoyancy force is parallel to the axial flow so that the flow field remains two-dimensional. In horizontal tubes, however, there is no analytical solution available to predict the effect of temperature variation of viscosity and density. The previous report of work in this program [97] established that accurate correlation of experimental data is not possible without considering the temperature dependency of transport properties. The present chapter is, therefore, aimed at two goals: 1) Obtaining a more accurate analytical solution to predict laminar flow heat transfer results in horizontal tubes by considering both density and viscosity temperature variation, and 2) Introducing a parameter which is derivable from the governing equations so that the experimental correction factor has an analytical basis.

A Parameter to Account for Variable Viscosity

If viscosity is temperature-dependent, the viscous force in the momentum equation becomes

$$\frac{\partial \tau_{xy}}{\partial Y} = \frac{\partial}{\partial Y}\left(\mu \frac{\partial U}{\partial Y}\right) = \mu \frac{\partial^2 U}{\partial Y^2} + \frac{\partial U}{\partial Y}\frac{\partial \mu}{\partial Y} \qquad (3\text{-}1)$$

The second term in the right hand side of Eq. (3-1) can be neglected for

the traditional constant viscosity assumption. In general, however, viscosity is a function of temperature and pressure. For most applications, the pressure-dependence of viscosity can be neglected. With $\mu = \mu(T)$, the second term in the right hand side of Eq. (3-1) becomes

$$\frac{\partial \mu}{\partial Y}\frac{\partial U}{\partial Y} = \frac{\partial \mu}{\partial T}\frac{\partial T}{\partial Y}\frac{\partial U}{\partial Y} = \left(\frac{1}{\mu}\frac{d\mu}{dT}\Delta T\right)\left(\frac{\partial \phi}{\partial Y}\mu\frac{\partial U}{\partial Y}\right) \tag{3-2}$$

where ϕ is a dimensionless temperature defined as

$$\phi = \frac{T - T_b}{\Delta T}$$

It is clear that the coefficient $(\frac{1}{\mu}\frac{d\mu}{dT}\Delta T)$ appears always in the normalized momentum equation for fluids having temperature-dependent viscosity.

This coefficient can be redefined as a dimensionless viscosity parameter

$$Be = \gamma \Delta T \tag{3-3}$$

where $$\gamma = \frac{-1}{\mu}\left(\frac{d\mu}{dT}\right) \tag{3-4}$$

It is readily seen that this parameter is similar to $\beta \Delta T$ in the Grashof number which accounts for density variation; γ is similar to the bulk modulus β. ΔT in Eq. (3-1) is a reference temperature difference which can be $\bar{T}_w - T_b$ or q"a/k, depending on the tube wall boundary condition.

Values of the viscosity parameter Be may exceed unity when the viscosity is a strong function of temperature and temperature differences are large. For tetraethylene glycol, for example, the viscosity variation coefficient γ equals 0.01431 $^{\circ}F^{-1}$ at 125 $^{\circ}F$. The value of Be is then 0.572 for ΔT = 42 $^{\circ}F$ and is greater than 1.0 when ΔT exceeds 70 $^{\circ}F$. The numeri-

cal values of γ for water and air are 1.14×10^{-2} and $-1.25 \times 10^{-3}\ ^{\circ}F^{-1}$, respectively, at 100 °F. For most gases, Be is negative for heating due to the increase in gas viscosity with increasing temperature. For liquids, whose viscosity decreases as temperature increases, Be is greater than zero for heating and less than zero for cooling. It is noted that zero Be corresponds to the traditional constant viscosity case.

It is of interest that the viscosity parameter can be approximately reduced to a viscosity ratio for small ΔT as follows:

$$Be = \frac{-1}{\mu}\frac{d\mu}{dT}\Delta T \approx \frac{-1}{\mu_b}\left(\frac{\mu_w - \mu_b}{\Delta T}\right)\Delta T$$

$$= 1 - \frac{\mu_w}{\mu_b} \qquad (3\text{-}5)$$

The viscosity variation coefficient γ is in general a function of temperature. However, in practical applications, it is a reasonable approximation to assume that γ is constant over the operating temperature range. For constant heat flux, and thus constant ΔT, this is equivalent to specifying that the viscosity is an exponential function of temperature.

$$\mu = \mu_b\, e^{-\gamma(T-T_b)} \qquad (3\text{-}6)$$

This expression is essentially the same as that used by Shannon and Depew [112].

Formulation of the Problem Using a Boundary Layer Approximation

Introductory remarks

Consideration is given to the problem of the steady, fully developed, laminar flow of a Newtonian fluid in horizontal circular tubes. The fluid is assumed to have temperature-dependent density and viscosity. Both of the usual heat flux boundary conditions are considered: uniform axial average heat flux throughout, with uniform circumferential wall temperature (Case 1), and uniform heat flux axially and circumferentially (Case 2). For sufficiently long tubes, a fully developed condition is reached in which the heat transfer coefficient changes only due to variation in the fluid temperature level. The secondary flow, which is caused by buoyancy forces, is essentially two-dimensional.

The equations of conservation of mass, momentum, and energy for this problem are still too complicated to solve analytically and would require enormous expenditures of computer time. Accordingly, an alternate solution technique is utilized. The results of Siegwarth et al. [31] and Mori and Futagami [30] indicate that a thermal boundary layer exists when the Raleigh number is high. It can then be assumed that the secondary flow is composed of two regions: a thin boundary layer near the pipe wall and a core which is enclosed by the boundary layer. These investigators have been successful in using boundary layer integration techniques to solve the fully developed combined free and forced convection problem.

Since the boundary layer equations for free convection in a horizontal pipe are similar to those of the classical vertical plate, it should be possible to use the same type of dimensional reasoning for both problems.

The problem of free convection on vertical plates is considered in Appendix C to demonstrate the reasons for choosing certain dimensionless groups. The dimensional analysis adopted to analyze the boundary layer and core equations for the present study will be discussed in the following order: First, the dimensional core and boundary layer equations are given. Next, the general nature of the core solution is discussed. The dimensionless boundary layer equations are derived for the thermal boundary layer. Then the viscous boundary layer is considered and the governing equations are presented. Finally, the solutions for the simplified case of large Prandtl number are given for the two different boundary conditions.

Formulation of problem, Case 1

It is important to note that two different coordinate systems are used as shown in Fig. 3-1. A curvilinear orthogonal coordinate system (X, Y, Z) is applied to the boundary layer, and rectangular coordinates(X^+, Y^+, Z) are used in the core. The Z coordinate is coincident with, or parallel to, the tube axis for the core and boundary layer regions, respectively. Since the flow is assumed to be fully developed, the velocity components are invariant in the Z direction.

Neglecting axial conduction and viscous dissipation, one can write the two-dimensional conservation equations for the general flow field as follows:

Continuity equation:

$$\frac{\partial U}{\partial X} + \frac{\partial V}{\partial Y} = 0 \qquad (3\text{-}7)$$

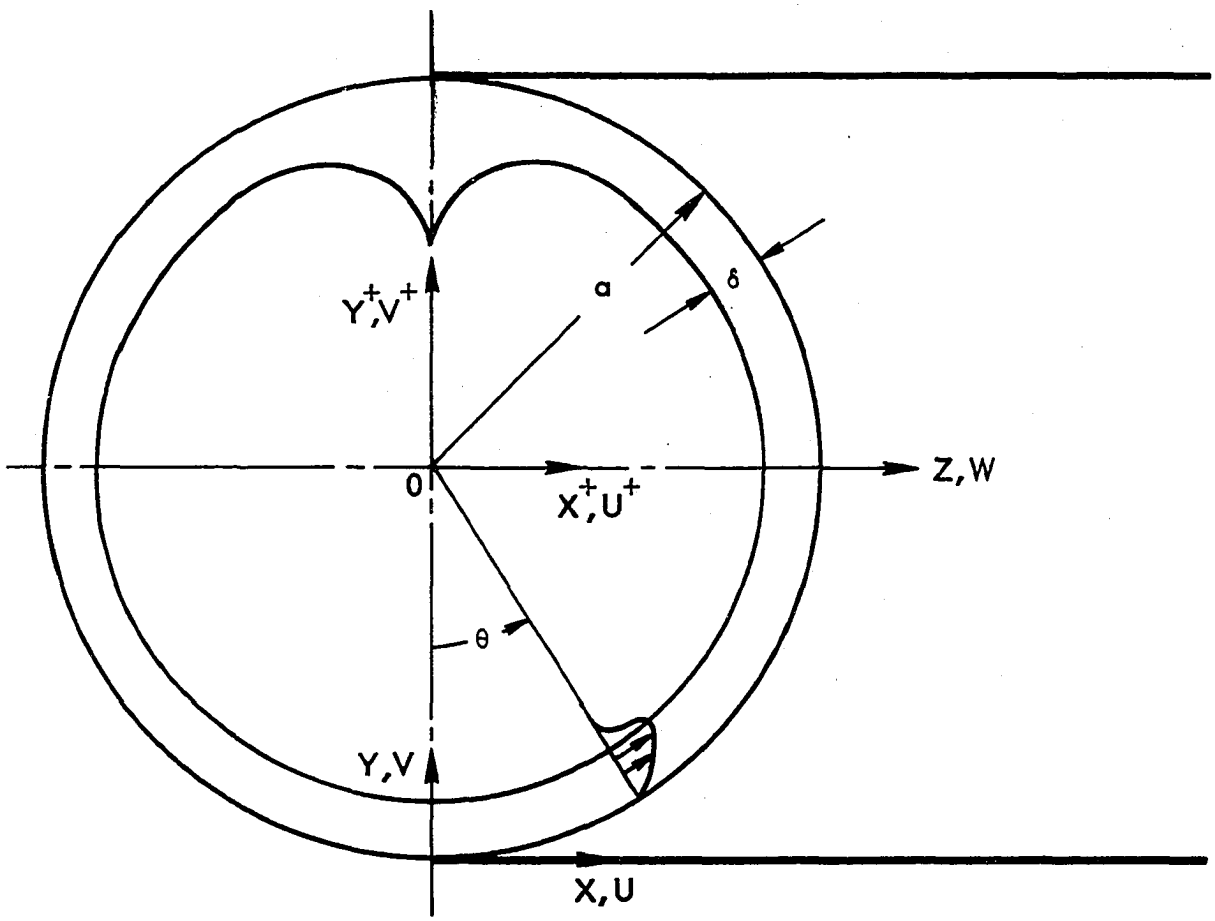

Fig. 3-1 Coordinate system for boundary layer and core regions in horizontal tube

Momentum equation in X-direction:

$$\rho[U \frac{\partial U}{\partial X} + V \frac{\partial U}{\partial Y}] = - \frac{\partial P}{\partial X} + \frac{\partial}{\partial X} [2\mu \frac{\partial U}{\partial X}] + \frac{\partial}{\partial Y} [\mu(\frac{\partial U}{\partial Y} + \frac{\partial V}{\partial X})] + \frac{\partial}{\partial Z} [\mu(\frac{\partial W}{\partial X} + \frac{\partial U}{\partial Z})] + \rho g_x \quad (3\text{-}8)$$

Momentum equation in Y-direction:

$$\rho[U \frac{\partial V}{\partial X} + V \frac{\partial V}{\partial Y}] = - \frac{\partial P}{\partial Y} + \frac{\partial}{\partial X} [\mu(\frac{\partial U}{\partial Y} + \frac{\partial V}{\partial X})] + \frac{\partial}{\partial Y} [2\mu \frac{\partial V}{\partial Y}] + \frac{\partial}{\partial Z} [\mu(\frac{\partial V}{\partial Z} + \frac{\partial W}{\partial Y})] + \rho g_y \quad (3\text{-}9)$$

Momentum equation in Z-direction:

$$\rho[U \frac{\partial W}{\partial X} + V \frac{\partial W}{\partial Y}] = - \frac{\partial P}{\partial Z} + \frac{\partial}{\partial X} [\mu(\frac{\partial W}{\partial X} + \frac{\partial U}{\partial Z})] + \frac{\partial}{\partial Y} [\mu(\frac{\partial V}{\partial Z} + \frac{\partial W}{\partial Y})] \quad (3\text{-}10)$$

Energy equation:

$$\rho C_p[U \frac{\partial T}{\partial X} + V \frac{\partial T}{\partial Y} + W \frac{\partial T}{\partial Z}] = k[\frac{\partial^2 T}{\partial X^2} + \frac{\partial^2 T}{\partial Y^2}] \quad (3\text{-}11)$$

In these equations, the physical properties are considered constant except for the viscosity and the density, as it appears in the buoyancy term.

Core region equations

As shown in Chapter II and as indicated by Siegwarth et al. [31], the main flow will not be affected by secondary flow for high Prandtl number fluid flow. Thus, the inertial force in the axial momentum equation [Eq. (3-10)] for the core region can be neglected. Siegwarth further indicated that the two-dimensional isotherms are horizontal. The axial momentum equation, therefore, can be reduced to

$$\nabla_1^2 w = Be \frac{\partial w}{\partial y^+} \frac{\partial \phi^+}{\partial y^+} + \frac{a^2}{\mu \bar{W}} \frac{\partial P}{\partial Z} \tag{3-12}$$

where the following dimensionless variables are utilized:

$$w = \frac{W}{\bar{W}}, \quad y^+ = \frac{Y^+}{a}, \quad Be = -\frac{1}{\mu}\left(\frac{d\mu}{dT}\right) \Delta T$$

$$\Delta T = \bar{T}_w - T_b, \quad \phi^+ = \frac{T^+ - T_b}{\Delta T} \tag{3-13}$$

The solutions of the previous chapter indicate that the temperature distribution in the core region is more or less isothermal for high Rayleigh number flow. Thus, it is easily seen that the first term on the right hand side of Eq. (3-12) can be neglected. With this simplification and the assumption of linear axial pressure gradient, the solution of Eq. (3-12) is simply a Poiseuille flow, that is

$$w^+ = 2(1 - x^{+2} - y^{+2}) \tag{3-14}$$

With the assumption that $\phi^+ = \phi(y^+)$, $v^+ = v(y^+)$, and $u^+ = 0$, the energy equation in the core region can be obtained as

$$v^+ \frac{\partial \phi^+}{\partial y^+} + \frac{Nu}{(PrGr)^{1/4}} w^+ = \frac{1}{(PrGr)^{1/4}} \frac{\partial^2 \phi^+}{\partial y^{+2}} \tag{3-15}$$

where

$$v^+ = \frac{V^+}{U_c^+}, \quad U_c^+ = \frac{\mu}{\rho a} \left(\frac{Gr}{Pr^3}\right)^{1/4}, \quad Gr = \frac{g\beta \Delta T a^3}{\nu^2}, \quad Pr = \frac{\mu C_p}{k}$$

The reasons for choosing the characteristic velocity U_c^+ are given in Appendix C. With Siegwarth's result $Nu = c_1 Ra^{1/4}$, and assuming a large Rayleigh number, one can further simplify Eq. (3-15) as

$$v^+ \frac{\partial \phi^+}{\partial y^+} + C_1 w^+ = 0 \tag{3-16}$$

Boundary layer region equations

The two-dimensional conservation equations for the boundary layer region are represented by Eqs. (3-7) through (3-11). As indicated in Chapter II, the pressure is assumed to be separated as follows:

$$P(X,Y,Z) = P(Z) + P(X,Y) \tag{3-17}$$

The traditional boundary layer assumption is made that the pressure gradient in the X-direction is independent of Y so that the pressure in the boundary layer equals the pressure in the core evaluated at the wall. As indicated by Siegwarth, the pressure variation in the core is hydrostatic. The pressure gradient in the X-direction can thus be assumed to be

$$\frac{\partial P}{\partial X} = \rho_c g \sin(\frac{X}{a}) \tag{3-18}$$

where the subscript c is used to designate the core solution evaluated at the pipe wall. Employing Eq. (3-18) and the thermal expansion coefficient β as indicated in Chapter II, one can combine the pressure gradient and gravitational force in the X-direction momentum equation and reduce the equation as follows:

$$-\frac{\partial P}{\partial X} - \rho g \sin\frac{X}{a} = \rho_b g\beta (T - T_c) \sin\frac{X}{a} \tag{3-19}$$

Assuming viscosity is a function of temperature only and employing continuity and Eq. (3-19), one can express the X-direction secondary flow momentum equation [Eq. (3-8)] as

$$U\frac{\partial U}{\partial X} + V\frac{\partial U}{\partial Y} = \nu\nabla^2 U - \gamma\nu\left[2\frac{\partial U}{\partial X}\frac{\partial T}{\partial X} + (\frac{\partial U}{\partial Y} + \frac{\partial V}{\partial X})\frac{\partial T}{\partial Y}\right]$$

$$+ g\beta(T - T_c)\sin\frac{X}{a} \tag{3-20}$$

The Y-direction momentum equation can be dropped according to the traditional boundary layer assumption.

To normalize the momentum and energy equations, the following dimensionless variables have been utilized

$$x = \frac{X}{a},\ y = \frac{Y}{\Delta},\ \phi = \frac{T - T_b}{\Delta T}$$

$$u = \frac{U}{U_c} \ , \ v = \frac{V}{V_c} \ , \ w = \frac{W}{W} \tag{3-21}$$

where the characteristic variables U_c, V_c, and Δ are chosen as follows:

$$U_c = \frac{\mu}{\rho a} \left(\frac{Gr}{Pr}\right)^{1/2}$$

$$V_c = \frac{\mu}{a\rho} \left(\frac{Gr}{Pr^3}\right)^{1/4} \tag{3-22}$$

$$\Delta = \frac{a}{(GrPr)^{1/4}}$$

The detailed discussion of the procedure for choosing these variables is given in Appendix C. The X-direction momentum equation can thus be expressed in dimensionless form as follows:

$$\frac{\partial^2 u}{\partial y^2} + \left(\frac{\Delta}{a}\right)^2 \frac{\partial^2 u}{\partial x^2} - Be \left[2\left(\frac{\Delta}{a}\right)^2 \frac{\partial u}{\partial x}\frac{\partial \phi}{\partial x} + \frac{\partial u}{\partial y}\frac{\partial \phi}{\partial y} + \frac{1}{(GrPr)^{1/2}} \frac{\partial u}{\partial x}\frac{\partial \phi}{\partial y}\right]$$

$$+ (\phi - \phi_c) \sin x = \frac{1}{Pr} \left[u \frac{\partial u}{\partial x} + v \frac{\partial u}{\partial y}\right] \tag{3-23}$$

Since Δ is assumed to be very small compared with the tube radius a, the term involving $(\Delta/a)^2$ in Eq. (3-23) becomes negligible. When a large value of Gr Pr is assumed Eq. (3-23) can be reduced to

$$\frac{\partial^2 u}{\partial y^2} - Be \frac{\partial u}{\partial y}\frac{\partial \phi}{\partial y} + (\phi - \phi_c) \sin x = \frac{1}{Pr} \left[u \frac{\partial u}{\partial x} + v \frac{\partial u}{\partial y}\right] \tag{3-24}$$

Equation (3-24) is a general governing equation for most fluids.

It is easily seen that the inertia terms comprising the right hand side of Eq. (3-24) can be ignored. With these further simplifications, Eq. (3-24) can be simplified to

$$\frac{\partial^2 u}{\partial y^2} - Be \frac{\partial u}{\partial y} \frac{\partial \phi}{\partial y} + (\phi - \phi_c) \sin x = 0 \tag{3-25}$$

It should be noted that for large Prandtl number fluids the simple Poiseuille flow distribution in the axial direction shown in Eq. (3-13) is valid throughout the tube, including the boundary layer region.

The energy equation in the boundary layer region can be simplified by introducing the above-mentioned dimensionless variables as follows:

$$\frac{\partial^2 \phi}{\partial y^2} + \left(\frac{\Delta}{a}\right)^2 \frac{\partial^2 \phi}{\partial x^2} = u \frac{\partial \phi}{\partial x} + v \frac{\partial \phi}{\partial y} + w \frac{Nu}{(PrGr)^{1/2}} \tag{3-26}$$

For the very thin boundary layer assumption, the conduction in X-direction vanishes as $(\Delta/a)^2$. Furthermore, the convection due to main flow Eq. (3-26) becomes negligible for high Rayleigh numbers. Therefore, the energy equation in boundary layer region can be simplified to

$$\frac{\partial^2 \phi}{\partial y^2} = u \frac{\partial \phi}{\partial x} + v \frac{\partial \phi}{\partial y} \tag{3-27}$$

Equation (3-27), which is the same equation as for free convection over a vertical plate, indicates that the major heat transfer from the wall is carried away by conduction perpendicular to the wall and by convection due to the secondary flow.

For convenience, the governing equations of core and boundary layer region are summarized as follows:

Core Region:

Energy
$$v^+ \frac{\partial \phi^+}{\partial y^+} + C_1 w^+ = 0 \qquad (3\text{-}18)$$

Boundary Layer Region:

Continuity
$$\frac{\partial u}{\partial x} + \frac{\partial v}{\partial y} = 0 \qquad (3\text{-}7)$$

Momentum
$$\frac{\partial^2 u}{\partial y^2} - Be \frac{\partial u}{\partial y} \frac{\partial \phi}{\partial y} + (\phi - \phi_c) \sin x = 0 \qquad (3\text{-}25)$$

Energy
$$\frac{\partial^2 \phi}{\partial y^2} = u \frac{\partial \phi}{\partial x} + v \frac{\partial \phi}{\partial y} \qquad (3\text{-}27)$$

Nusselt number

The heat transfer coefficient can be obtained by considering the energy balance at the tube wall. The axial heat rate is given as

$$q' = 2\pi a \bar{h} (\bar{T}_w - T_b) = 2\pi a \bar{h} \Delta T \qquad (3\text{-}28)$$

Also, q' can be obtained by applying the Fourier equation at the tube wall

$$q' = 2k \int_0^{\pi a} \frac{\partial T}{\partial Y}\Big|_{Y=0} dX = \frac{2ka\Delta T}{\Delta} \int_0^{\pi} \frac{\partial \phi}{\partial y}\Big|_{y=0} dx \qquad (3\text{-}29)$$

The Nusselt number can thus be obtained by combining Eqs. (3-28) and (3-29).

$$Nu = \frac{2a\bar{h}}{k} = \frac{2a}{\pi\Delta}\int_0^{\pi} \frac{\partial\phi}{\partial y}\Big|_{y=0} dx$$

$$= \frac{2}{\pi}\int_0^{\pi} \frac{\partial\phi}{\partial y}\Big|_{y=0} dx(GrPr)^{1/4} \qquad (3\text{-}30)$$

Let

$$C_1 = \frac{2}{\pi}\int_0^{\pi} \frac{\partial\phi}{\partial y}\Big|_{y=0} dx \qquad (3\text{-}31)$$

Then, as was assumed originally, the Nusselt number is obtained as

$$Nu = C_1\, Ra^{1/4} \qquad (3\text{-}32)$$

Since only one parameter, Be, appears in the governing equations, it is concluded that C_1 in Eq. (3-31) is a function of Be. Thus, Eq. (3-32) can be rewritten as

$$Nu = C_1(Be)Ra^{1/4} \qquad (3\text{-}33)$$

To obtain C_1, one must solve the differential momentum equation [Eq. (3-25)], which is, of course, coupled with the energy equation [Eq. (3-27)].

Analytical Solution Using Integral Method for Case 1

The governing equations are given by Eqs. (3-7), (3-16), (3-25), and (3-27) with the following boundary conditions:

$$\text{at } y = 0, \quad u = v = 0$$

$$\phi = 1 \text{ for Case 1} \tag{3-34}$$

$$y = \delta, \quad \frac{\partial u}{\partial y} = \frac{\partial \phi}{\partial y} = 0, \quad \phi = \phi_c$$

where ϕ_c is the dimensionless core region temperature evaluated at the wall (assuming the boundary layer to be very thin). It is noted that the boundary condition of the traditional free convection is $u = 0$ at $y = \delta$. However, it is apparent that the secondary flow velocity in the core is not zero. Therefore, it is more appropriate to set the velocity gradients equal to zero at $y = \delta$. Since the secondary flow is created by free convection, which is similar to the upward flow of free convection along vertical plates, the hydrodynamic boundary layer thickness of the secondary flow along the tube wall is essentially the same as the thermal boundary layer thickness.

Following the usual boundary layer integration technique, it is assumed that the temperature variation through the boundary layer is a polynomial in y. The dimensionless temperature ϕ can be expressed as

$$\phi = a_0 + a_1 y + a_2 y^2 + a_3 y^3 \tag{3-35}$$

with boundary conditions of Eq. (3.34) and,

$$\text{at } y = 0 \qquad \frac{\partial^2 \phi}{\partial y^2} = 0 \tag{3-36}$$

The coefficients in Eq. (3-35) can be determined by utilizing the boundary conditions of Eqs. (3.34) and (3-36) with the following result:

$$\phi = 1 - \frac{3}{2}(1 - \phi_c)\frac{y}{\delta} + \frac{1}{2}(1 - \phi_c)\left(\frac{y}{\delta}\right)^3 \tag{3-37}$$

where the boundary layer thickness δ is a function of x.

Differentiating Eq. (3-37) with respect to y yields the following expression:

$$\frac{\partial \phi}{\partial y} = \frac{3}{2}\frac{1 - \phi_c}{\delta}\left(\left(\frac{y^2}{\delta^2}\right) - 1\right) \tag{3-38}$$

With the substitution of ϕ and $\frac{\partial \phi}{\partial y}$ into Eq. (3-25) a differential equation is obtained for modified u, with the subscript denoting a differentiation, as follows:

$$u^*_{\eta\eta} + A(1 - \eta^2)\, u^*_{\eta} + 1 - \frac{3}{2}\eta + \frac{1}{2}\eta^3 = 0 \tag{3-39}$$

where

$$u = u^*(\eta) \sin x\, \delta^2(1 - \phi_c) \tag{3-40}$$

$$\eta = \frac{y}{\delta}$$

$$A = \frac{3}{2} * Be(1 - \phi_c)$$

Equation (3-39) is a second-order ordinary differential equation with boundary conditions

$$\begin{aligned} &\text{at } \eta = 0, \qquad u^* = 0 \\ &\qquad \eta = 1, \qquad u^*_\eta = 0 \end{aligned} \tag{3-41}$$

Equation (3-39) can be easily solved by expanding u^* in terms of an infinite series of η and determining the coefficients from the boundary conditions [Eq. (3-41)]. The resulting expression for the velocity u in the boundary layer is

$$u = \sin x \; \delta^2 \; (1 - \phi_c)\eta \sum_{k=0}^{7} \frac{a_k}{k+1} \eta^k \tag{3-42}$$

where the coefficients a_k are obtained from the following linear equations:

$$\begin{bmatrix} A & 1 & 0 & 0 & 0 & 0 & 0 & 0 \\ 0 & A & 2 & 0 & 0 & 0 & 0 & 0 \\ -A & 0 & A & 3 & 0 & 0 & 0 & 0 \\ 0 & -A & 0 & A & 4 & 0 & 0 & 0 \\ 0 & 0 & -A & 0 & A & 5 & 0 & 0 \\ 0 & 0 & 0 & -A & 0 & A & 6 & 0 \\ 0 & 0 & 0 & 0 & -A & 0 & A & 7 \\ 1 & 1 & 1 & 1 & 1 & 1 & 1 & 1 \end{bmatrix} \begin{bmatrix} a_0 \\ a_1 \\ a_2 \\ a_3 \\ a_4 \\ a_5 \\ a_6 \\ a_7 \end{bmatrix} = \begin{bmatrix} -1 \\ 3/2 \\ 0 \\ -1/2 \\ 0 \\ 0 \\ 0 \\ 0 \end{bmatrix} \tag{3-43}$$

It was found that eight terms in Eq. (3-43) give acceptable accuracy. Since ϕ_c is a very small value, the value of A in Eq. (3-43) can be approximated by $\frac{3}{2}$ Be.

Integrating Eq. (3-27) with respect to y from y = 0 to y = δ and eliminating v by means of Eq. (3-7) yields

$$\frac{\partial \phi}{\partial y}\Big|_0^{\delta} = \frac{\partial}{\partial x}\int_0^{\delta} \phi u \, dy - \phi_c \frac{\partial}{\partial x}\int_0^{\delta} u dy \tag{3-44}$$

Now, if Eqs. (3-42) and (3-37) for u and ϕ are substituted into Eq. (3-44), the following differential equation for δ is obtained:

$$D_4(1 - \phi_c)\delta^3 \sin x \frac{d\phi_c}{dx} + 3 D_5(1 - \phi_c)^2 \sin x \, \delta^2 \frac{d\delta}{dx}$$

$$= \frac{3}{2}\frac{1 - \phi_c}{\delta} - D_5 (1 - \phi_c)^2 \delta^3 \cos x \tag{3-45}$$

where

$$D_1 = \int_0^1 \eta \sum_{k=0}^{7} \frac{a_k}{k+1} \eta^k \, d\eta = \sum_{k=0}^{7} \frac{a_k}{(k+1)(k+2)}$$

$$D_2 = \int_0^1 \eta^2 \sum_{k=0}^{7} \frac{a_k}{k+1} \eta^k \, d\eta = \sum_{k=0}^{7} \frac{a_k}{(k+1)(k+3)}$$

$$D_3 = \int_0^1 \eta^4 \sum_{k=0}^{7} \frac{a_k}{k+1} \eta^k \, d\eta = \sum_{k=0}^{7} \frac{a_k}{(k+1)(k+5)}$$

$$D_4 = - D_1 + 3D_2 - D_3$$

$$D_5 = D_1 - \frac{3}{2} D_2 + \frac{D_3}{2}$$

Equation (3-45) expresses the variation of the boundary layer thickness around the circumference of the pipe. To solve Eq. (3-45), an expression for the variation of ϕ_c with respect to x must be obtained. The boundary condition for Eq. (3-45) is obtained by assuming the symmetry of the boundary layer at x =0 i.e., $\frac{d\delta}{dx} = \frac{d\phi_c}{dx} = 0$ which yields

$$\delta = \left[\frac{3}{2(1 - \phi_c)D_5}\right]^{1/4} \qquad \text{at } x = 0 \tag{3-46}$$

The core temperature evaluated at the wall, ϕ_c, is obtained by integrating Eq. (3-16) with respect to x^+ from $x^+ = 0$ to $x^+ = \sqrt{1 - y^{+2}}$, with the following result:

$$\frac{d\phi_c}{dy^+} \int_0^{\sqrt{1 - y^{+2}}} v^+ dx^+ = - C_1 \int_0^{\sqrt{1 - y^{+2}}} w^+ dx^+ \tag{3-47}$$

A mass balance at any height in the pipe reveals that the flow rate downward in the core must equal the flow rate in the boundary layer at that value of x. Therefore, the temperature variation in core is given by

$$B \frac{\partial \phi_c}{\partial y^+} = - C_1 \int_0^{\sqrt{1 - y^{+2}}} w^+ dx^+ \tag{3-48}$$

where

$$B = - \int_0^{\sqrt{1 - y^{+2}}} v^+ dx^+ = \int_0^1 u d\eta$$

By substitution of Eqs. (3-42) and (3-13) for u and w^+, respectively, Eq. (3-48) can be solved for $\frac{d\phi_c}{dy^+}$. This derivative can be written in terms of the boundary layer coordinate x by recognizing that

$$y^+ = - \cos x \tag{3-49}$$

The resulting expression is

$$\frac{d\phi_c}{dx} = \frac{4}{3} \frac{C_1 \sin^3 x}{(1 - \phi_c)\delta^3 D_1} \tag{3-50}$$

Once the core temperature distribution is determined, the bulk temperature, or dimensionless mixing cup temperature, can be obtained by integrating the product of the core temperature times the axial velocity profile as follows:

$$\phi_b = \int_{-1}^{1} \int_{0}^{\sqrt{1 - y^{+2}}} \phi_c \, w^+ dx^+ dy^+ = 0 \tag{3-51}$$

Substituting Eq. (3-13) for w^+ and utilizing Eq. (3-49) to transform the coordinate system in Eq. (3-51) yields:

$$\phi_b = \frac{4}{3} \int_{0}^{\pi} \phi_c \sin^4 x \, dx = 0 \tag{3-52}$$

This equation is used as a constraint to determine the boundary values of ϕ_c at x = 0.

The coefficient C_1 is obtained by introducing Eqs. (3-31) and (3-38) into Eq. (3-32), and the result is given as

$$C_1 = \frac{1}{\pi}\int_0^{\pi} \frac{3(1 - \phi_c)}{\delta}\, dx \tag{3-53}$$

Equation (3-53) can be integrated, provided that ϕ_c and δ are given as functions of x.

Equations (3-50) and (3-45) represent the system of two coupled ordinary differential equations to be solved for ϕ_c and δ. Since ϕ_c and δ are symmetrical about a vertical axis through the center of the pipe, it is only necessary to integrate Eqs. (3-50) and (3-45) from $x = 0$ to $x = \pi$. The initial value of δ at $x = 0$ is given in Eq. (3-46); however, the initial value of ϕ_c at $x = 0$ is not available. An initial value of ϕ_c at $x = 0$ can be obtained by using Eq. (3-52) as one constraint. The value of C_1 for each fixed value of Be is, therefore, determined by solving Eqs. (3-50), (3-45), and (3-53). This solution requires an interaction procedure.

Equations (3-50) and (3-45) were integrated numerically by using the Fourth-Order Runge-Kutta method and assuming initial arbitrary value of ϕ_c and initial condition of Eq. (3-46) for δ at $x = 0$. With an initial value of C_1 assumed the new value of C_1 is obtained by means of Simpson's rule. This new value of C_1 is carried on for the next calculation. In this manner, the procedure is repeated until the new calculated value of C_1 is equal to the previous C_1. Thus, δ and ϕ_c are determined as the iterative procedure completed. More details of the calculation procedure are given in Appendix D. A computing time of 15 seconds was required for one Be with 100 divisions around the circumference, using the Iowa State IBM 360/65.

Formulation and Solution for Case 2

The second boundary condition considered in this analysis is uniform heat flux axially and circumferentially (Case 2). It is assumed that for high Rayleigh number flow, the boundary layer method is still valid for Case 2. The assumptions made in Case 1 will also hold for this second boundary condition. The solutions of laminar free convection from a vertical plate with uniform surface heat flux [123] indicate that average Nusselt number is proportional to $Ra^{1/4}$ for high Prandtl number fluid flow. With this conclusion, one may expect that the Nusselt number of Case 2 will also be proportional to $Ra^{1/4}$.

The derivations of Case 2 are exactly the same for Case 1, and the governing equations are represented by Eqs. (3-7), (3-16), (3-25), and (3-27). The notation used in Case 2 is the same as for Case 1, except that the temperature difference ΔT is taken as $\bar{T}_w - T_b$. The procedures of integration are similar to Case 1, where it is assumed that the dimensionless temperature in the boundary layer region can be expressed as a function of y.

$$\phi = a_0 + a_1 y + a_2 y^2 + a_3 y^3 + a_4 y^4 \tag{3-54}$$

The coefficients of Eq. (3-54) are determined by the following boundary conditions:

$$\text{at } y = 0,\ \frac{\partial \phi}{\partial y} = \frac{-C_1}{2},\ \frac{\partial^2 \phi}{\partial y^2} = 0$$

$$\text{at } y = \delta,\ \phi = \phi_c,\ \frac{\partial \phi}{\partial y} = 0,\ \frac{\partial^2 \phi}{\partial y^2} = 0 \tag{3-55}$$

The result for ϕ is, then,

$$\phi - \phi_c = \frac{C_1}{4} \delta(1 - 2\eta + 2\eta^3 - \eta^4) \tag{3-54}$$

where

$$\eta = y/\delta$$

$\frac{\partial \phi}{\partial y}$ in Eq. (3-27) can be easily obtained by differentiating Eq. (3-54) with respect to y with the following result:

$$\frac{\partial \phi}{\partial y} = \frac{C_1}{2} (-1 + 3\eta^2 - 2\eta^3) \tag{3-55}$$

Substituting Eqs. (3-54) and (3-55) into Eq. (3-27) yields the differential equation for u as follows:

$$\frac{\partial^2 u}{\partial y^2} + \frac{C_1}{2} \text{Be} (1 - 3\eta^2 + 2\eta^3) \frac{\partial u}{\partial y} + \frac{C_1}{4} \delta(1 - 2\eta + 2\eta^3 - \eta^4) \sin x = 0 \tag{3-56}$$

The boundary conditions of Eq. (3-56) are chosen as

$$\begin{aligned} y = 0, \quad & u = 0 \\ y = \delta, \quad & \frac{\partial u}{\partial y} = 0 \end{aligned} \tag{3-57}$$

Integrating Eq. (3-56) using a series solution yields the velocity profile in the boundary layer as:

$$u = \delta \sin x \sum_{k=0}^{7} \frac{b_k}{k+1} \eta^{k+1} \tag{3-58}$$

where b_k are the solutions of the following linear equations:

$$\begin{bmatrix} A & 1 & 0 & 0 & 0 & 0 & 0 & 0 \\ 0 & A & 2 & 0 & 0 & 0 & 0 & 0 \\ -3A & 0 & A & 3 & 0 & 0 & 0 & 0 \\ 2A & -3A & 0 & A & 4 & 0 & 0 & 0 \\ 0 & 2A & -3A & 0 & A & 5 & 0 & 0 \\ 0 & 0 & 2A & -3A & 0 & A & 6 & 0 \\ 0 & 0 & 0 & 2A & -3A & 0 & A & 7 \\ 1 & 1 & 1 & 1 & 1 & 1 & 1 & 1 \end{bmatrix} \begin{bmatrix} b_0 \\ b_1 \\ b_2 \\ b_3 \\ b_4 \\ b_5 \\ b_6 \\ b_7 \end{bmatrix} = \begin{bmatrix} -\frac{C_1}{4} \\ \frac{C_1}{2} \\ 0 \\ -\frac{C_1}{2} \\ \frac{C_1}{4} \\ 0 \\ 0 \\ 0 \end{bmatrix} \tag{3-59}$$

and $A = C_1/2\ Be$.

By substitution of Eqs. (3-54) and (3-58) for ϕ and u into Eq. (3-44), an ordinary differential equation in δ is obtained as follows:

$$\frac{C_1}{2} = \delta^2 \sin x\, E_4 \frac{d\phi_c}{dx} + \frac{C_1}{4}(\delta^4 \cos x + 4\, \delta^3 \sin x \frac{d\delta}{dx})E_5 \tag{3-60}$$

where

$$E_4 = \sum_{k=0}^{7} \frac{b_k}{(k+1)(k+2)}$$

$$E_5 = \sum_{k=0}^{7} \frac{b_k}{k+1} \left(\frac{1}{k+2} - \frac{1}{2} \frac{1}{k+3} + \frac{2}{k+5} - \frac{1}{k+6} \right)$$

The temperature distribution in the core region ϕ_c which appears in Eq. (3-60) can be obtained by integrating the energy equation [Eq. (3-47)].

By substitution of Eqs. (3-58) and (3-13) for u and w into Eq. (3-47) and changing the variable y^+ to x by Eq. (3-49), the ordinary differential equation for ϕ is obtained, as follows:

$$\frac{d\phi_c}{dx} = \frac{4}{3} \frac{C_1 \sin^3 x}{\delta^3 E_4} \tag{3-61}$$

The initial condition of Eq. (3-60) is taken as:

$$\text{at } x = 0, \quad \delta = \left[\frac{2}{E_5} \right]^{\frac{1}{4}} \tag{3-62}$$

for the same reason indicated in the previous section. The initial condition for ϕ_c at x = 0, however, is not known. It is possible to start by assuming an initial value for ϕ_c at x = 0 until the constraint condition of Eq. (3-52) is met. Equations (3-60) and (3-61) are coupled and can be solved numerically by the fourth-order Runge-Kutta method. The constant C_1 is obtained from the dimensionless wall temperature defined as:

$$\phi_w = \frac{T_w - T_b}{\overline{T}_w - T_b} \tag{3-63}$$

Integrating Eq. (3-63) with respect to x from 0 to π yields

$$\int_0^{\pi} \phi_w \, dx = \pi \tag{3-64}$$

The constant C_1 can therefore be obtained by substituting ϕ_w from Eq. (3-54), with y = 0, into Eq. (3-64), and the result is

$$C_1 = \frac{\pi - \int_0^{\pi} \phi_c \, dx}{\frac{1}{4} \int_0^{\pi} \delta \, dx} \tag{3-65}$$

The detailed computing procedures for solving Eqs. (3-60), (3-61), and (3-65) are given in the program listing shown in Appendix D.

Heat Transfer Results

The heat transfer results for the present problem can be generally indicated as

$$Nu = C_1(Be) \, Ra^{\frac{1}{4}} \tag{3-33}$$

The computed values of the coefficient C_1 are tabulated in Table 3-1 for various values of Be.

The effect of viscosity variation on the heat transfer coefficient is clearly shown in Table 3-1 and in Fig. 3-2. It is noted that Be = 0 in the present analysis considers viscosity to be constant. The constant viscosity solution for Case 1 has a numerical value of $C_1 = 0.8781$, which is lower than the value of $C_1 = 0.942$ given in Ref. 31. The disagreement between these solutions is due to the utilization of different profiles for the secondary velocity u and the temperature profile in the boundary layer. It is noted that the asymptotic Nusselt number given in the previous chapter, Eq. (2-74), can be converted to the present notation, and this solution and the present solution for Be = 0 are restated as follows:

Table 3.1 Coefficient C_1 for various Be

Case 1				Case 2			
Be ≥ 0		Be ≤ 0		Be ≥ 0		Be ≤ 0	
Be	C_1	Be	C_1	Be	C_1	Be	C_1
0.0	0.8781	0.0	0.8781	0.0	0.6643	0.0	0.6643
0.1	0.8854	-0.1	0.8713	0.1	0.6752	-0.1	0.6547
0.2	0.8942	-0.2	0.8653	0.2	0.6873	-0.2	0.6466
0.3	0.9047	-0.3	0.8596	0.3	0.7006	-0.3	0.6398
0.4	0.9175	-0.4	0.8542	0.4	0.7149	-0.4	0.6347
0.5	0.9330	-0.5	0.8487	0.5	0.7302	-0.5	0.6312
0.6	0.9519	-0.6	0.8433	0.6	0.7465	-0.6	0.6291
0.7	0.9748	-0.7	0.8378	0.7	0.7636	-0.7	0.6286
0.8	1.002	-0.8	0.8322	0.8	0.7816	-0.8	0.6274
0.9	1.035	-0.9	0.8265	0.9	0.8006	-0.9	0.6265
1.0	1.074	-1.0	0.8208	1.0	0.8205	-1.0	0.6247
1.1	1.1209			1.1	0.8414		
1.2	1.1748			1.2	0.8635		
1.3	1.2359			1.3	0.8870		
1.4	1.2979			1.4	0.9120		
1.5	1.3368			1.5	0.9388		
				1.6	0.9680		
				1.7	1.0000		
				1.8	1.0356		
				1.9	1.0759		
				2.0	1.1227		

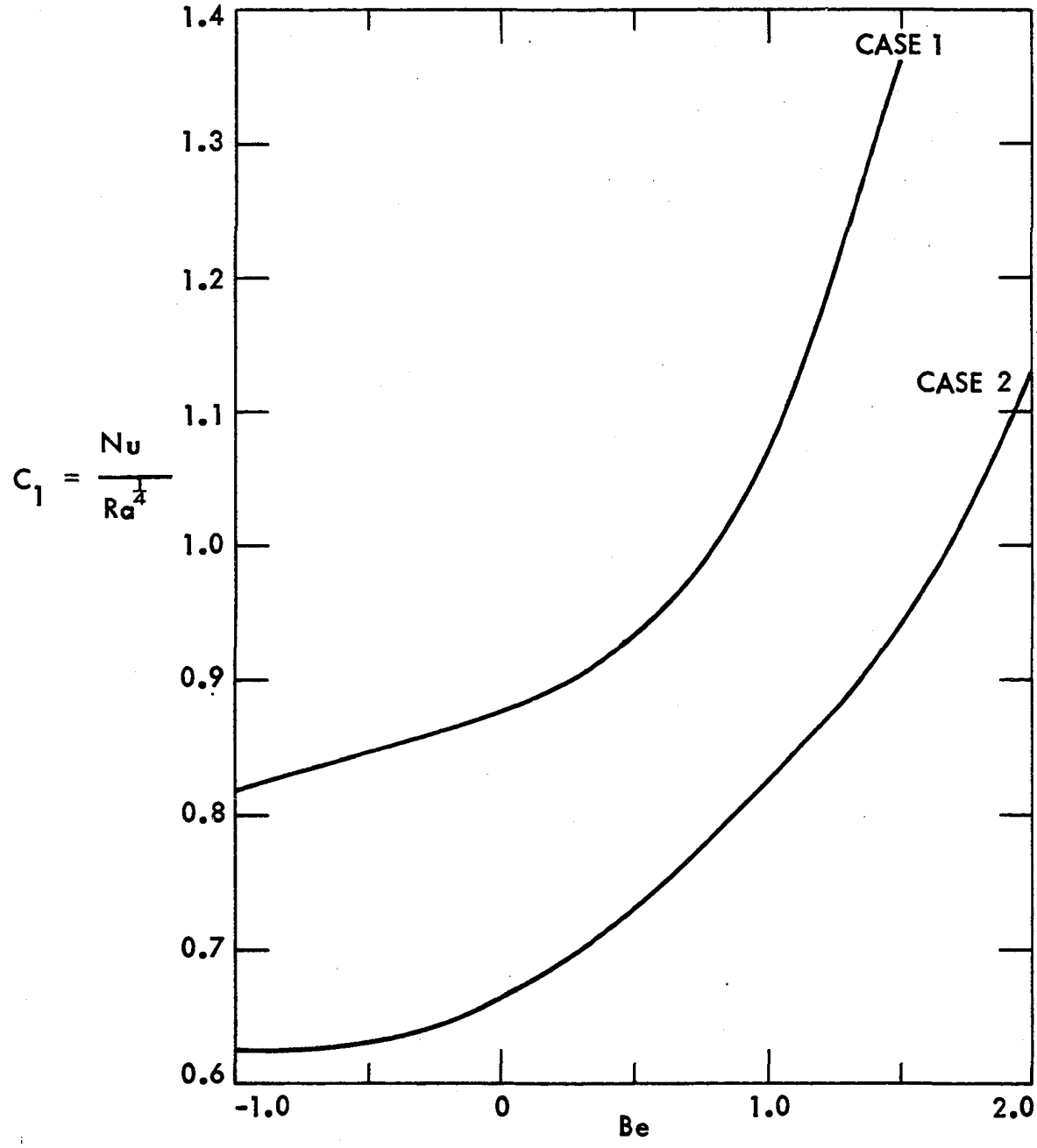

Fig. 3-2 Coefficient C_1 as function of viscosity parameter Be

$$Nu = 0.585\ Ra^{0.215} \qquad (2\text{-}74)$$

$$Nu = 0.6643\ Ra^{0.25} \qquad (3\text{-}33)$$

The prediction of Eq. (2-74) utilized the boundary conditions of Case 2. The lower exponential power in Eq. (2-74) is probably due to the high Rayleigh number assumption in the present analysis.

For Be > 0, which corresponds to heating, with viscosity decreasing as temperature increases, C_1 increases with increasing Be for both boundary conditions. Be can usually be increased by increasing heat flux and thus increasing ΔT. For fixed ΔT, the Be value of a high viscosity temperature sensitive fluid is higher than that of a low-viscosity temperature-dependent fluid. In Case 1, for example, the coefficient C_1 for Be = 1.5 is about 55 percent higher than that for the constant viscosity prediction. In Case 2, the constant C_1 for Be = 2.0 is more than 70 percent above the constant viscosity value. Computation instability is observed when Be is greater than 1.5 in Case 1.

Under cooling conditions (Be < 0 for most liquids), C_1 decreases as the absolute value of Be increases. The difference of C_1 between Be = 0.0 and -1.0 is about seven percent in both cases.

The physical reason for the higher prediction of Nu with temperature-dependent viscosity is the thinner boundary layer associated with stronger secondary flow along the tube wall. Figure 3-3 presents the boundary layer thickness around the tube circumference for Case 1. The boundary layer is thinner at the bottom of the tube; it gradually becomes thicker at $x = \pi/2$ and suddenly becomes very thick near the top of the tube wall. Figure 3-3 also indicates that the boundary layer thickness decreases with

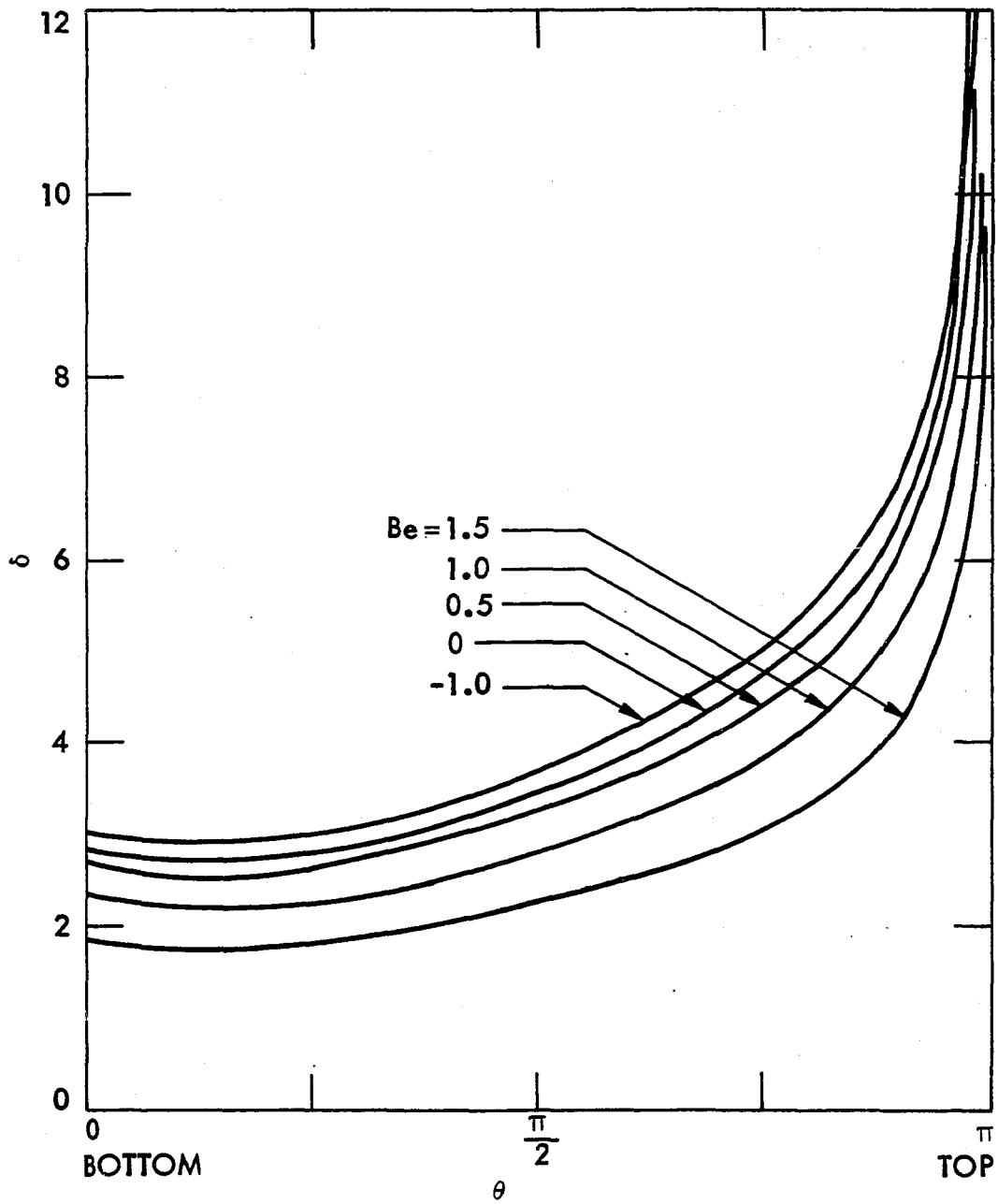

Fig. 3-3 Boundary layer thickness distribution along tube wall with Be as parameter

increasing Be. Since the Nusselt number is inversely proportional to the boundary layer thickness for constant Rayleigh number, the Nusselt number increases as Be increases. For most fluids, the viscosity gradient is large for higher Be due to larger ΔT. Thus, there is less resistance to motion along the tube wall. The increased velocity along the tube wall creates a stronger secondary flow which, in turn, increases the heat transfer coefficient.

The temperature and velocity profiles in the boundary layer for Case 1 are given by Eqs. (3-37) and (3-42), respectively. The secondary velocity and dimensionless temperature profiles are seen to be similar to those profiles for the fully developed case discussed in the previous chapter. Figure 3-4 indicates the temperature distribution in the core region at the vertical centerline for Case 1. Since it is assumed that the isotherms in the core region are horizontal, Fig. 3-4 actually shows the temperature variation in the whole core region for various Be. The temperature distribution near the wall is shown in Fig. 3-5. The viscosity parameter has a minor effect on the temperature distribution in the core region since there is a small temperature gradient in that region. The parameter Be has a significant effect on the secondary velocity as shown in Fig. 3-5. It is clearly seen that secondary velocity increases as Be increases.

The final heat transfer results are tabulated in Table 3-1 and shown in Fig. 3-6. For practical application, these results can be correlated by the following equations within 99 percent of accuracy [124]:

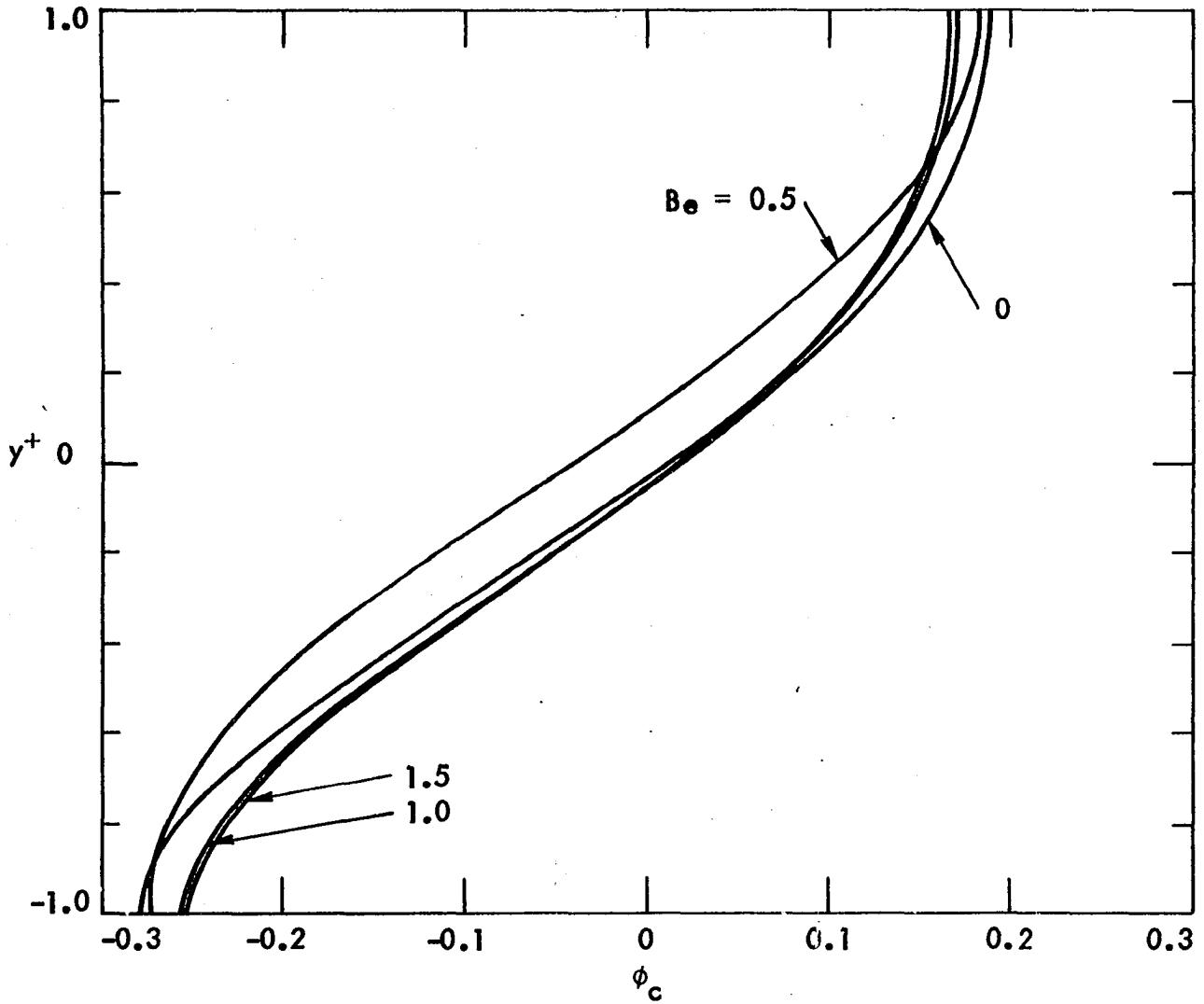

Fig. 3-4 Temperature distribution in the core region with Be as parameter

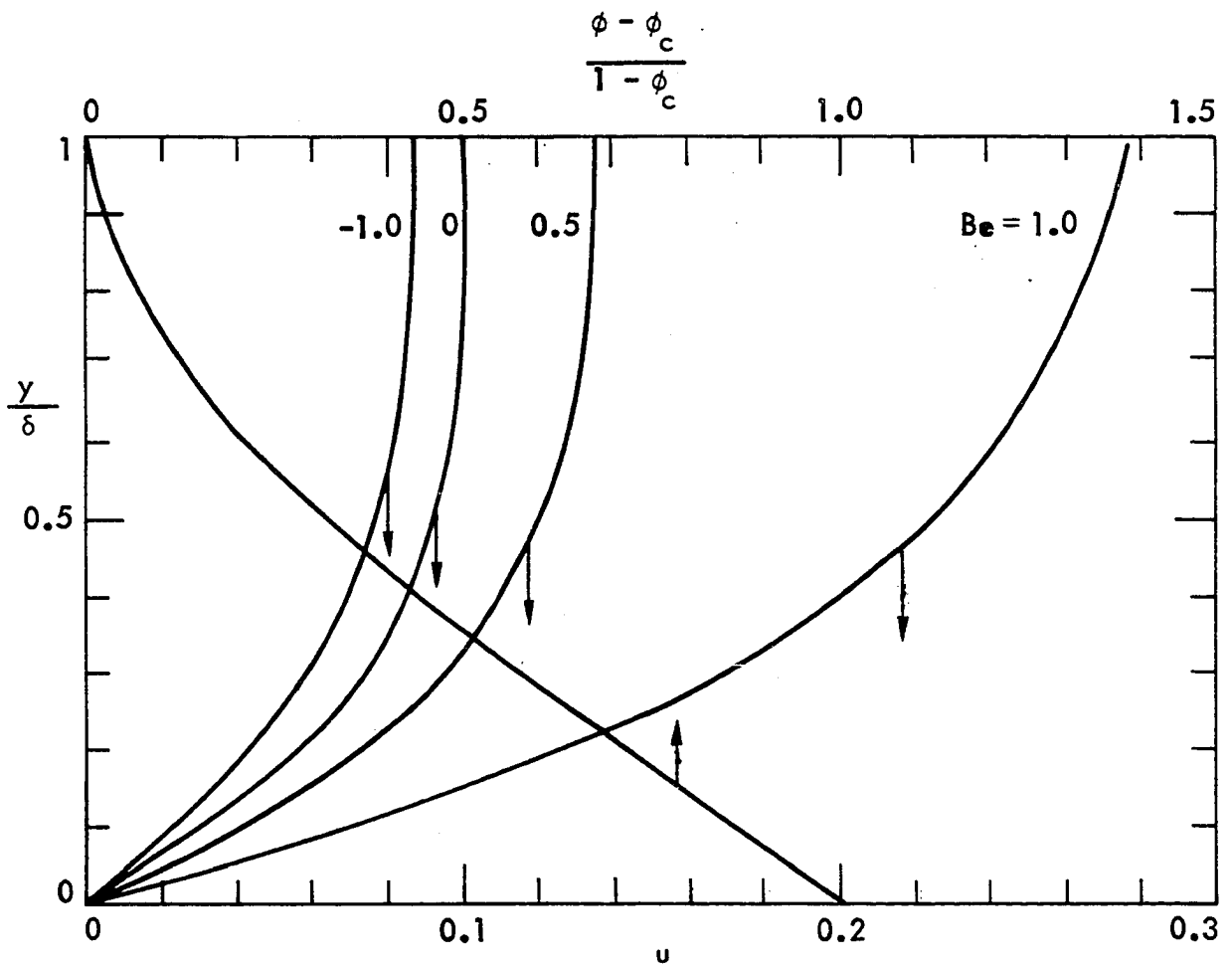

Fig. 3-5 Secondary velocity and temperature distributions in boundary layer region with Be as parameter

Case 1

$1.5 \geq Be \geq 0$ $$Nu = (0.8823 + 0.0153\ Be + 0.1481\ Be^2 + 0.00334\ Be^3)\ Ra^{1/4} \quad (3\text{-}66)$$

$0 > Be \geq -1.0$ $$Nu = (0.877 + 0.0563\ Be)\ Ra^{1/4} \quad (3\text{-}67)$$

Case 2

$2.0 \geq Be \geq 0$ $$Nu = (0.661 + 0.140\ Be - 0.0098\ Be^2 + 0.027\ Be^3)\ Ra^{1/4} \quad (3\text{-}68)$$

$0 > Be \geq -1.0$ $$Nu = (0.663 + 0.0886\ Be + 0.00526\ Be^2)\ Ra^{1/4} \quad (3\text{-}69)$$

As indicated by Morcos and Bergles [97], a number of experimental investigations have provided data which could be compared with the present analysis. However, since the Morcos and Bergles [97] data are the most recent and fully documented, their data will be compared with the present analysis. Since the film temperature was used in their correlation, it was necessary to utilize bulk mean temperature to recalculate all dimensionless parameters. The comparison is shown in Figs. 3-6 through 3-9.

Figure 3-6 reveals the comparison of the present Case 1 solution and data for a metal tube using water and ethylene glycol as the working fluids. It is clear that the constant viscosity solution, Be = 0, is valid only for Be < 0.5 and that the experimental results depart from the constant viscosity prediction as Be increases.

A similar comparison for water and ethylene glycol with the glass tube, which approximates the Case 2 boundary condition, is indicated in Fig. 3-7. The agreement of the present analysis and experimental results

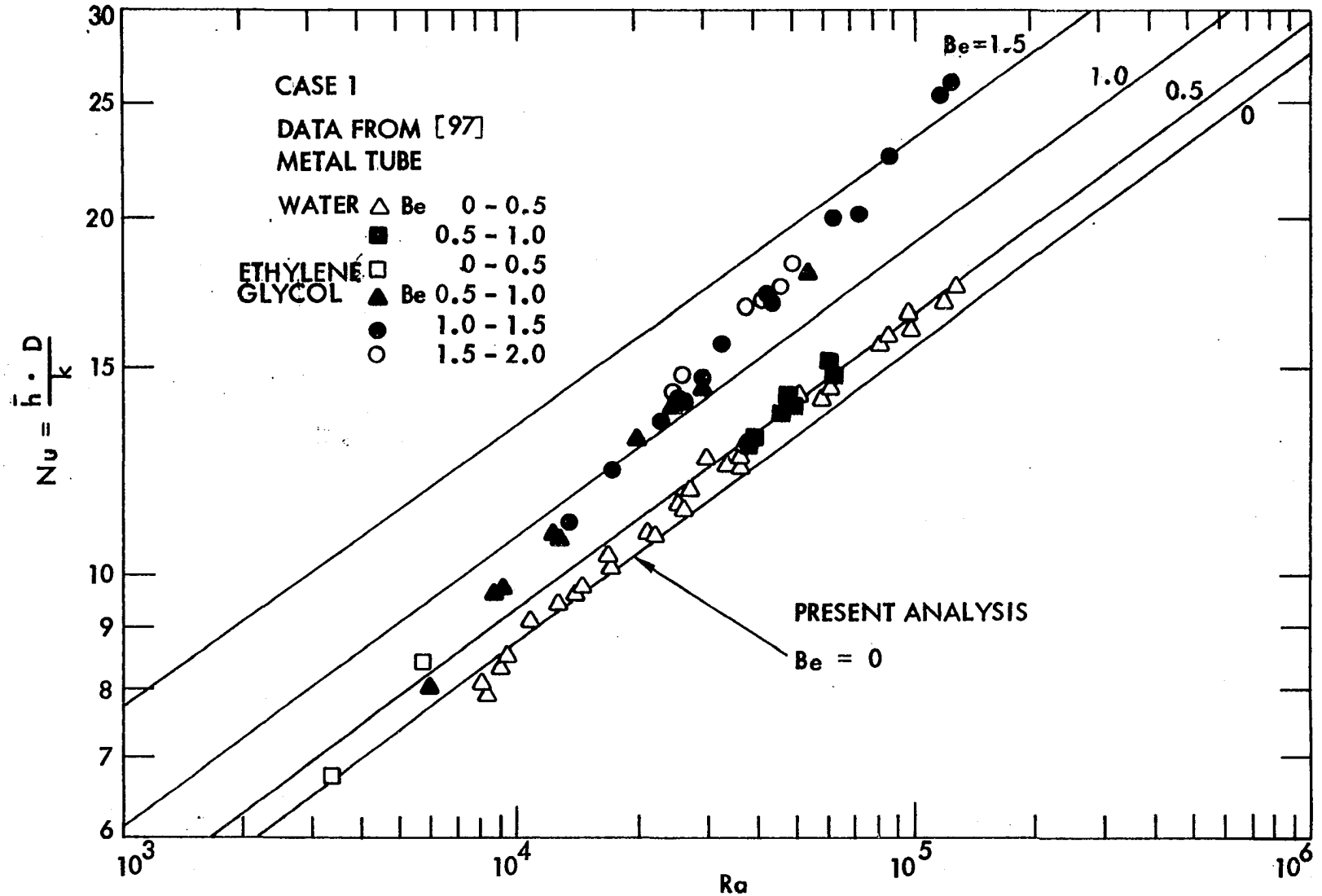

Fig. 3-6 Effect of Be on Nusselt number for Case 1, comparison with data for metal tube

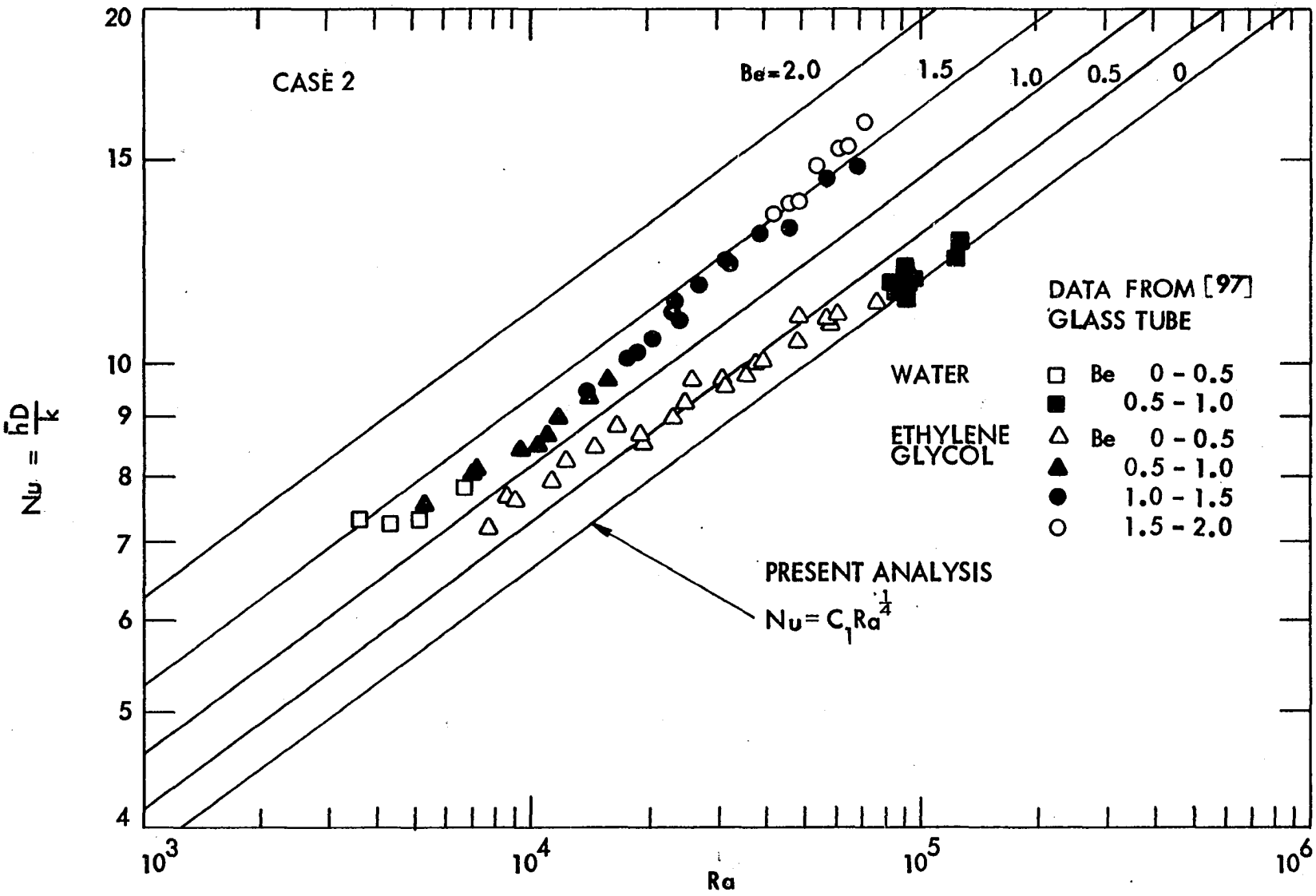

Fig. 3-7 Effect of Be on Nusselt number for Case 2, comparison with data for glass tube

further corroborates the importance of Be in the present investigation. The disagreement of the present analysis and experimental results in the lower Rayleigh number region seems to be due to the high Rayleigh number assumption in this analysis and the small ΔT in the experimental work, which increases the uncertainty of the measurements.

A more graphic comparison of experimental results and analytical prediction is presented in Figs. 3-8 and 3-9 for the metal tube and glass tube, respectively. The excellent agreement between the solution of Case 1 and the experimental results for the metal tube is clearly shown in Fig. 3-8. The deviation of experimental data from the analytical solution is seen to be within 10 percent. The correlation of Eq. (3-66) has thus verified to be valid for intermediate and high Rayleigh number flow.

A comparison of the present Case 2 solutions with glass tube experimental results is shown in Fig. 3-9. A larger discrepancy between prediction and experiment is observed, about 20 percent at low Rayleigh numbers and about 10 percent at high Rayleigh numbers. The larger deviation appearing in Fig. 3-9 for Case 2 seems to be caused by the tube wall effects. The experimental data from Ref. [97] shows that metal tube data are closer to boundary conditions of Case 1 than glass tube data corresponding to Case 2. The tube wall parameter suggests that in order to have uniform circumference tube wall temperature (Case 1), a thicker tube wall and higher thermal conductivity of tube should be utilized.

In general, the deviation between the present analysis and experimental data from Morcos and Bergles [97] may come from the three sources listed below:

(1) Other temperature-dependent properties, such as k and c_p, are not

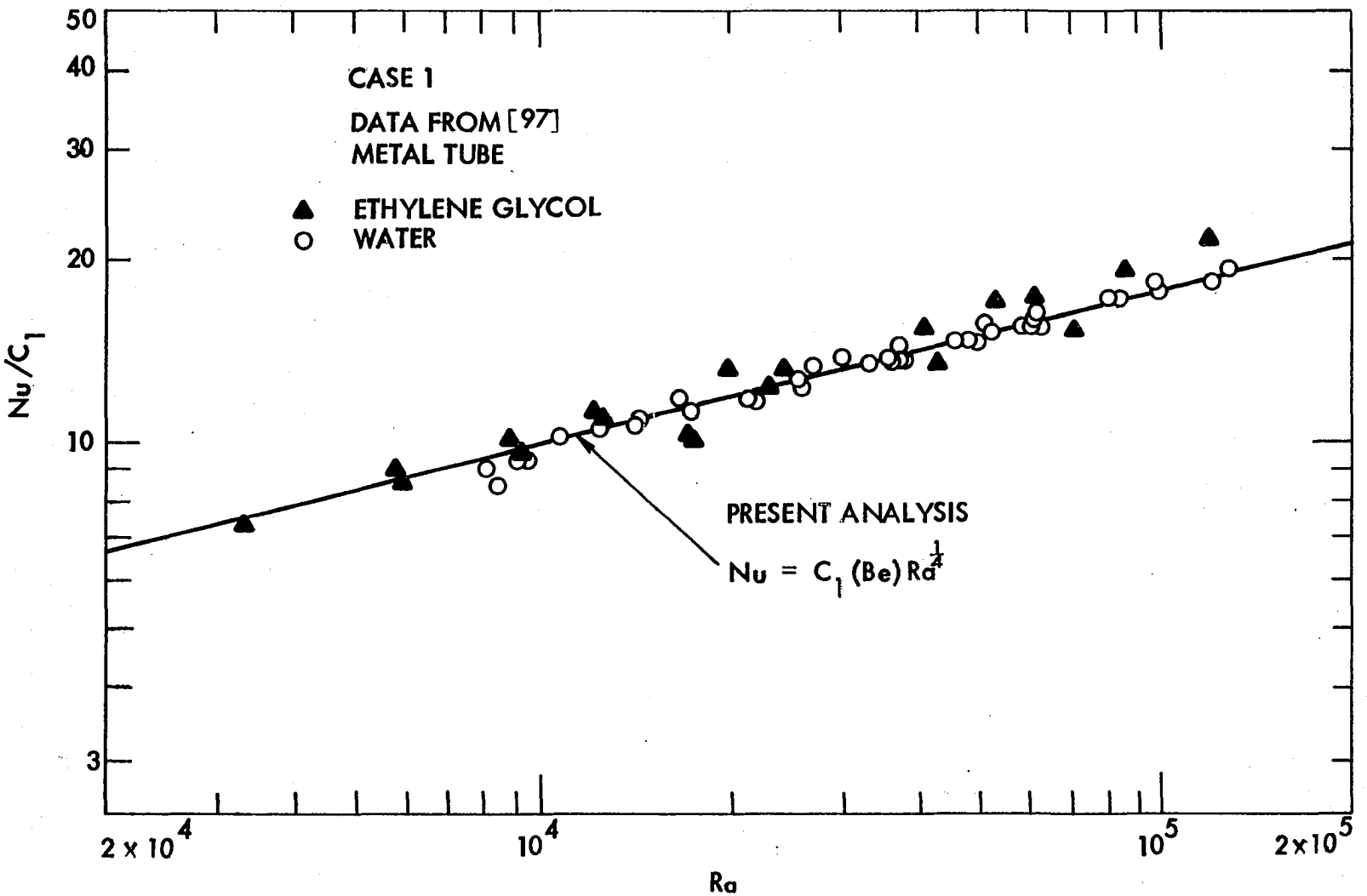

Fig. 3-8 Comparison of present analytical solution of Case 1 with experimental data for metal tube

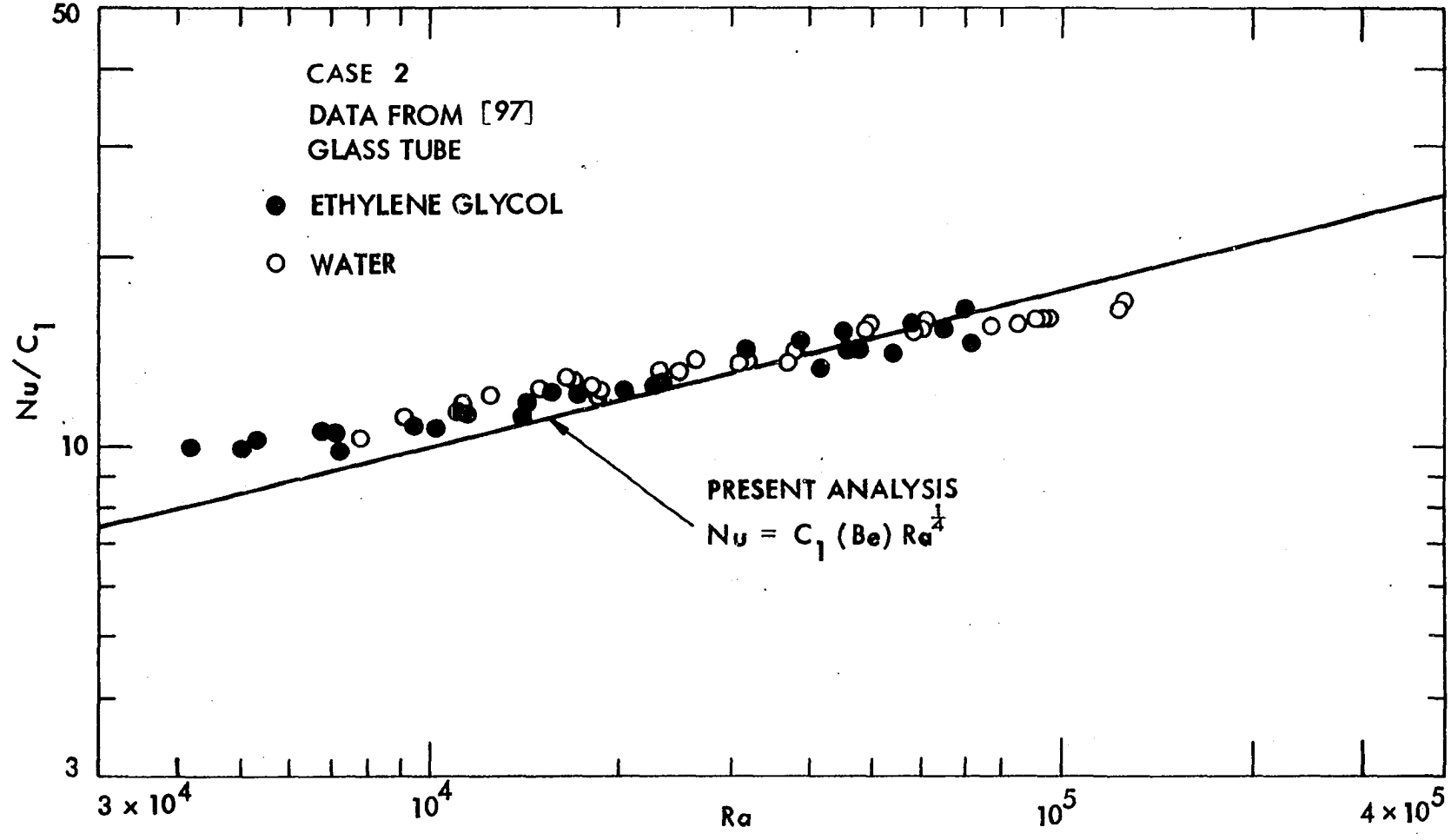

Fig. 3-9 Comparison of present analytical solution of Case 2 with experimental data for glass tube.

considered in the present analysis.

(2) The present simple correlation of Eq. (3-33) is based on high Prandtl and Rayleigh number assumptions.

(3) The thermal boundary conditions of Case 1 and Case 2 in the present analysis correspond to values of the tube wall parameter P_w^* (which was utilized by Morcos and Bergles [97] to correlate the tube wall effect) of infinity and zero, respectively. Since P_w^* was finite for both metal and glass tubes, the experimental data should actually lie between the predictions of Case 1 and Case 2.

Conclusions and Remarks

1. A new viscosity parameter, $Be = (-1/\mu)(d\mu/dT)\,\Delta T$, has been successfully employed in the present analysis to study temperature dependence of viscosity. For most liquids, Be is greater than zero and varies from 0 to about 2 for heating condition. Constant viscosity solutions, Be = 0, are valid only when fluid viscosity is not a strong function of temperature. However, when fluid viscosity varies strongly with temperature, ethylene glycol, for example, constant viscosity solutions are no longer valid. The conventional empirical viscosity temperature-dependent parameter $(\mu_b/\mu_w)^n$ can now be replaced by introducing Be. Be is obtained directly from the governing equation by considering viscosity as temperature-dependent. Be should be useful in solving convective heat transfer processes with temperature-dependent viscosity.

2. Boundary layer assumptions in which tube flow field is divided into two parts, boundary layer region and core region, seem to be valid for the

present analysis. Characteristic variables taken from natural convection at a vertical plate have been verified to be reasonable.

3. The Nusselt number for laminar convection in horizontal tubes with large Prandtl number fluids is proportional to $Ra^{1/4}$ for both limiting boundary conditions, and the proportionality constant C_1 increases as Be increases. The heat transfer results for Be = 1.5 in Case 1 and Be = 2.0 in Case 2 are about 55 percent and 70 percent, respectively, above the constant viscosity predictions. The final correlations are given in Eqs. (3-66) and (3-68) for Cases 1 and 2, respectively.

4. The present analysis and the experimental data for water and ethylene glycol generally agree to within 10 percent. The correlation given by Eq. (3-66) is therefore acceptable for design purposes, for fluids with Prandtl numbers greater than 3.

CHAPTER IV. LAMINAR FLOW HEAT TRANSFER IN THE ENTRANCE REGION OF SEMI-CIRCULAR TUBES WITH UNIFORM HEAT FLUX

Introduction

Analytical results for laminar flow heat transfer in circular tubes, for both developing and fully developed conditions, have been well discussed in previous chapters. A need has been established in the present program for predictions of heat transfer in other geometries, specifically, the semi-circular tube representing a circular tube with a twisted tape insert of infinite pitch.

Laminar flow heat transfer in ducts of various shapes has been cataloged by Shah and London [2] for different kinds of thermal boundary conditions. The thermally and hydrodynamically fully developed flow in semi-circular tubes has been considered by Eckert et al. [125] and Sparrow and Haji-Sheikh [126]. Entrance region solutions published in the literature, using highly sophisticated mathematical and numerical techniques, are generally focused on circular tubes, rectangular ducts, or parallel plates. However, the thermally developing flow region in semi-circular tubes does not appear to have been described in the literature. Laminar flow in tubes containing twisted tapes is one of the applications for this semi-circular tube flow. As twist ratio (defined as H/D) increases, the tape becomes straight, and the flow inside the tube will be similar to the flow in semi-circular tubes.

Consideration in this chapter is given to a solution of this problem which uses the constant properties assumption with uniform axial heat flux. Two thermal boundary conditions around the walls are considered: one for uniform wall temperature all around the semi-circular tubes, another for

uniform wall temperature around the circular part of the tube and thermal insulation in the straight section of tube. These two circumferential boundary conditions represent the extremes of the fin effect of twisted tapes.

Formulation of Problem

The system of coordinates for steady laminar flow in the entrance region of a horizontal semi-circular tube is shown in Fig. 4-1. The flow is assumed to be hydrodynamically fully developed and thermally developing. This assumption is seen to be applicable for most liquids (except liquid metals) with a high or intermediate Prandtl number. To facilitate the theoretical analysis, the following assumptions are made:

1. Physical properties of the fluid are considered to be constant so that no free convection or temperature-dependent viscosity is taken into account.
2. Viscous dissipation is negligible.
3. The axial pressure gradient is constant.
4. The fluid is Newtonian.

When cylindrical coordinates (R, θ, Z) as shown in Fig. 4-1 are introduced and the assumptions stated above are applied, the governing differential equations are:

Momentum equation:

$$\frac{\partial^2 W}{\partial K^2} + \frac{1}{R}\frac{\partial W}{\partial K} + \frac{1}{K^2}\frac{\partial^2 W}{\partial \theta^2} = \frac{1}{\mu}\frac{\partial P}{\partial Z} \tag{4-1}$$

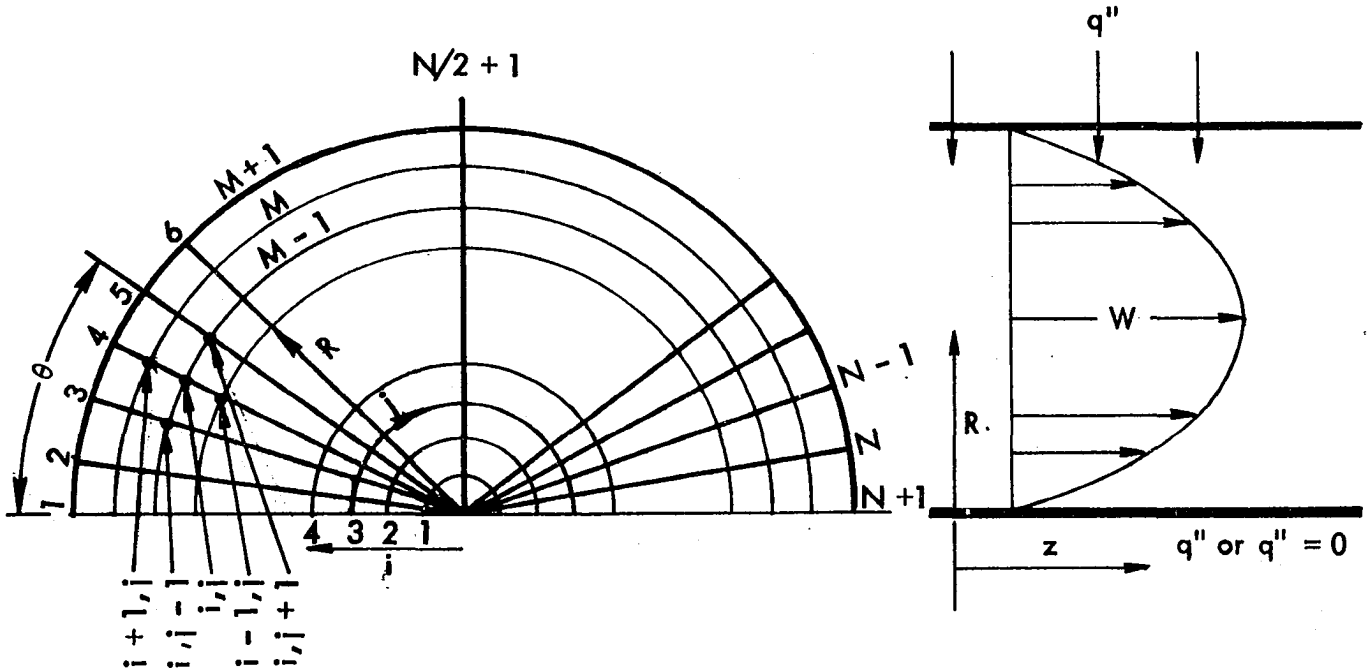

Fig. 4-1 Coordinate system and numerical grid for semi-circular tube

Energy equation:

$$\frac{\rho C_p}{k} W \frac{\partial T}{\partial Z} = \frac{\partial^2 T}{\partial R^2} + \frac{1}{R}\frac{\partial T}{\partial R} + \frac{1}{R^2}\frac{\partial^2 T}{\partial \theta^2} \tag{4-2}$$

Two different thermal boundary conditions are considered:

Case 1. Axially uniform heat flux and uniform wall temperature around the entire semi-circular tube.

Case 2. Axially uniform heat flux, uniform wall temperature around the wall except from $\theta = \pi$ to $\theta = 0$, where an insulated wall is assumed.

To nondimensionalize the governing partial differential equations the following dimensionless dependent variables, constants and parameters were used:

Dimensionless radius, $r = R/a$

Dimensionless velocity, $w = W/\bar{W}$

Dimensionless temperature, $\phi = \dfrac{T - T_b}{q''a/k}$

Reynolds number based on radius, $Re_a = \dfrac{\bar{W}\rho a}{\mu}$

Prandtl number, $Pr = \dfrac{\mu C_p}{k}$

Dimensionless axial distance, $z = \dfrac{Z}{a\, Re_a\, Pr}$

Dimensionless pressure drop constant, $C = \dfrac{a^2}{\mu \bar{W}} \dfrac{\partial P}{\partial Z}$

The momentum and energy equations can thus be simplified to the following dimensionless forms:

$$\nabla_1^2 w = C \tag{4-3}$$

$$\nabla_1^2 \phi = w \left(\frac{\partial \phi}{\partial z} + C_1\right) \tag{4-4}$$

where $\nabla_1^2 = \frac{\partial^2}{\partial r^2} + \frac{1}{r}\frac{\partial}{\partial r} + \frac{1}{r^2}\frac{\partial^2}{\partial \theta^2}$ is the Laplacian operator and

$C_1 = 2(\pi + 2)/\pi$ for Case 1

$C_1 = 2$ for Case 2

The boundary conditions for Eqs. (4-3) and (4-4) are as follows:

At the wall, $w = 0$ for both cases

Case 1. $\phi = \phi_w$ = some constant to be determined at wall

Case 2. $\phi = \phi_w$ at $r = 1$, $0 < \theta < \pi$

$\frac{\partial \phi}{\partial \theta} = 0$ at $\theta = 0$ and π, $0 \leq r \leq 1$

The initial condition is $\phi = 0$, at $z = 0$.

It is noted that Eq. (4-3) is Poisson's equation and can be solved by the Successive Over-Relaxation (SOR) method. Equation (4-4) is a parabolic equation, and the DuFort-Frankel method utilized in Chapter II is applicable to this equation.

Numerical Solution and Heat Transfer Results

DuFort-Frankel and SOR Method

The DuFort-Frankel scheme has been well described in Chapter II. Equation (4-4) is similar to Eq. (2-30) in Chapter II, except that no secondary velocity terms appear in Eq. (4-4). Since the axial velocity w is symmetric with respect to the axis $\theta = \frac{\pi}{2}$, the temperature profile is also expected to be symmetric with this axis. Using a non-equal space derivative in the axial direction and an equal space derivative in the radial and circumferential directions, Eq. (4-4) can be written in finite-difference form with grid points as shown in Fig. 4-1, as follows:

$$w_{i,j}\left[\frac{\Delta z^{-2}\,\phi_{i,j}^{k+1} - \Delta z^{+2}\,\phi_{i,j}^{k-1} + \phi_{i,j}^{k}(\Delta z^{+2} - \Delta z^{-2})}{\Delta z^{-}\,\Delta z^{+}\,(\Delta z^{-} + \Delta z^{+})}\right]$$

$$= \frac{1}{r_i}\frac{1}{\Delta r}\left[\left(\frac{r_i + r_{i+1}}{2}\right)\left(\frac{\phi_{i+1,j}^{k} - \frac{\phi_{i,j}^{k+1} + \phi_{i,j}^{k-1}}{2}}{\Delta r}\right) - \left(\frac{r_i + r_{i-1}}{2}\right)\left(\frac{\frac{\phi_{i,j}^{k+1} + \phi_{i,j}^{k-1}}{2} - \phi_{i-1,j}^{k}}{\Delta r}\right)\right] \tag{4-5}$$

$$+ \frac{1}{r_i^{2}}\left[\frac{\phi_{i,j+1}^{k} + \phi_{i,j-1}^{k} - \phi_{i,j}^{k+1} - \phi_{i,j}^{k-1}}{\Delta\theta^{2}}\right] = C_1 w_{i,j}$$

Since Eqs. (4-3) and (4-4) are uncoupled, the momentum equation associated with axial velocity w can first be solved independently without knowledge of the temperature distribution. The temperature distribution at the previous step, $\phi_{i,j}^{k}$, $\phi_{i,j}^{k-1}$ is considered to be given. The present temperature can

be calculated by rearranging Eq. (4-5) as follows:

$$A_1 \phi_{i,j}^{k+1} = A_2 \phi_{i+1,j}^{k} + A_3 \phi_{i-1,j}^{k} + A_4 \phi_{i,j}^{k-1} + A_5 \phi_{i,j}^{k}$$

$$+ A_6 \phi_{i,j-1}^{k} + A_7 \phi_{i,j+1}^{k} - C_1 w_{i,j} \qquad (4\text{-}6)$$

where

$$A_1 = \frac{w_{i,j} z_1}{z_{12}} + \frac{r_{i+1} + 2r_i + r_{i-1}}{4r_i \Delta r^2} + \frac{1}{(r_i \Delta\theta)^2}$$

$$A_2 = \frac{r_i + r_{i+1}}{2r_i \Delta r^2}$$

$$A_3 = \frac{r_i + r_{i-1}}{2r_i \Delta r^2}$$

$$A_4 = \frac{w_{i,j} z_2}{z_{12}} - \frac{r_{i+1} + 2r_i + r_{i-1}}{4r_i \Delta r^2} - \frac{1}{(r_i \Delta\theta)^2}$$

$$A_5 = -w_{i,j} \frac{z_2 - z_1}{z_{12}}$$

$$A_6 = \frac{1}{(r_i \Delta\theta)^2}$$

$$A_7 = \frac{1}{(r_i \Delta\theta)^2}$$

$$z_1 = \Delta z^{-2}, \quad z_2 = \Delta z^{+2}, \quad z_{12} = \Delta z^{-} \Delta z^{+} (\Delta z^{-} + \Delta z^{+})$$

Right at the entrance, a simple explicit method is employed to solve the energy equation for several steps, due to the three space level requirement of the DuFort-Frankel scheme.

The Poisson equation [Eq. (4-3)] for the axial velocity distribution can be easily solved by employing the SOR method. The constant C is calculated as follows:

Let

$$g = \frac{w}{C}$$

Equation (4-3) then becomes

$$\nabla_1^2 g = 1 \tag{4-8}$$

The average velocity $\bar{W}$ is defined as

$$\bar{W} = \frac{2\iint WdA}{\pi a^2} = \frac{2}{\pi}\int\int WRdRd\theta \tag{4-9}$$

Thus

$$\frac{\pi}{2} = \frac{\iint_{WRdRd\theta}}{\bar{W}} = \iint wrdrd\theta = C\int\int grdrd\theta$$

This implies

$$C = \frac{\pi}{2\iint grdrd\theta} \tag{4-10}$$

Wall temperature

The temperature inside the duct, except at the wall, can be easily evaluated from Eq. (4-6). To predict the temperature at the wall from the values at other points inside the duct, it is necessary to satisfy the boundary condition. For Case 1, it is assumed that the axial heat input is uniform and thus the wall temperature is uniform for each section. To satisfy the energy balance, the heat transferred across the surface must equal the heat transferred by conduction through the wall. Thus

$$\int_s k \left.\frac{\partial T}{\partial N}\right|_{wall} dS = q'' \cdot S \tag{4-11}$$

where S indicates the heated perimeter length and q'' is the uniform heat input per unit area. By introducing dimensionless parameters Eq. (4-11) can be written as

$$\int \left.\frac{\partial \phi}{\partial n}\right|_w ds = \pi + 2 \tag{4-12}$$

The temperature gradient at the wall can be evaluated from the temperature distribution inside the tube as follows:

$$\left.\frac{\partial \phi}{\partial n}\right|_w = \frac{3\phi_{M+1} - 4\phi_M + \phi_{M-1}}{2\Delta r} \tag{4-13}$$

If this relation is employed Eq. (4-12) can be expressed in finite-difference form as:

$$\sum_{j=2}^{N}(3\phi_w - 4\phi_{M,1} + \phi_{M-1,j})\frac{\Delta\theta}{2\Delta r} + \sum_{i=2}^{M}(3\phi_w - 4\phi_{i,2} + \phi_{i,3})$$

$$\frac{\Delta r}{2r_i\Delta\theta} + \sum_{i=2}^{M}(3\phi_w - 4\phi_{i,N} + \phi_{i,N-1})\frac{\Delta r}{2r_i\Delta\theta} + (3\phi_w - 4\phi_{2,N/2+1}$$

$$+ \phi_{3,N/2+1})(\frac{\Delta r}{2\Delta r}) = \pi + 2 \qquad (4\text{-}14)$$

where $\phi_w = \phi_{M+1}$ is the dimensionless wall temperature. The temperature of the wall can hence be calculated from Eq. (4-14).

Similarly, the wall temperature for Case 2 can be obtained by equating the heat balance around the perimeter as follows:

$$\int k \left.\frac{\partial T}{\partial N}\right|_w dS' = q''S' \qquad (4\text{-}15)$$

where S' is the heated perimeter $2\pi a$. For Case 2, it is assumed that there is no heat transfer from the tube wall along straight side, $\theta = 0$ and π. Applying Eq. (4-13) produces a similar expression for the tube wall temperature for Case 2 as follows:

$$\sum_{j=2}^{N}(3\phi_w - 4\phi_{M,j} + \phi_{M-1,j})\frac{\Delta\theta}{2\Delta r} = \pi \qquad (4\text{-}16)$$

Along $\theta = 0$ and π, however, ϕ_w is determined by the assumption of $\left.\frac{\partial\phi}{\partial n}\right|_w = 0$. Thus, for Case 2

$$\phi_w = \frac{1}{3}(4\phi_{i,2} - \phi_{i,3}) \text{ along } \theta = 0 \text{ and } \pi \qquad (4\text{-}17)$$

Hence, ϕ_w can be determined at any point in the duct from Eqs. (4-14), (4-16), and (4-17) for both cases.

Nusselt number

The Nusselt number, as discussed in Chapter II, can be obtained in two alternative ways depending on the method of obtaining the rate of heat transfer. The energy balance requires that the heat input from the wall must equal the enthalpy increase of the fluid. By definition, the coefficient of convective heat transfer is stated as

$$\bar{h} = q''/(\bar{T}_w - T_b) \tag{4-18}$$

The first Nusselt number for both cases can thus be evaluated as

$$(Nu)_I = \frac{\bar{h}\ 2a}{k} = \frac{q''\ 2a}{k(\bar{T}_w - T_b)} = \frac{2}{\bar{\phi}_w} \tag{4-19}$$

The heat transfer in an elemental length of duct dZ is

$$q = \bar{h}\ (\bar{T}_w - T_b)s \cdot dZ \tag{4-20}$$

The change in enthalpy is

$$\Delta H = \int \rho C_p \frac{\partial T}{\partial Z} W \quad dAdZ \tag{4-21}$$

Introducing the dimensionless parameters and the appropriate value of S for the two cases yields the Nusselt number, as follows:

$$(Nu)_{II} = \frac{2[\frac{\pi}{2} \left| \overline{\frac{\partial \phi}{\partial z} w} \right| + (\pi + 2)]}{\bar{\phi}_w (\pi + 2)} \quad \text{for Case 1} \tag{4-23}$$

$$(Nu)_{II} = \frac{[\left| \overline{\frac{\partial \phi}{\partial z} w} \right| + 2]}{\left| \overline{(\phi_w - \phi) \cdot w} \right|} \quad \text{for Case 2} \tag{4-24}$$

The final local Nusselt numbers are predicted by averaging these two alternative Nusselt numbers to reduce the uncertainty.

The detailed computational procedures used to obtain the local Nusselt numbers are shown in Appendix F. A 20 by 20 mesh size has been used in the present calculation. The axial step size Δz is determined by the following equation, which yields a finer step size near the entrance where the axial temperature gradient is expected to be large:

$$(\Delta z)_n = e^{-8} + 0.05\ n \qquad n = 1,2,3...$$

$$z_n = \sum_{n=1}^{n} (\Delta z)_n$$

No unstable situation was observed when this axial step size was used. The final numerical solutions for local Nusselt number are presented in Appendix G.

Heat transfer results

Axial velocity distributions for different θ values are indicated in Fig. 4-2. The velocity profiles are parabolic and have maximum values near the middle of the radius. The present numerical solutions agree exactly

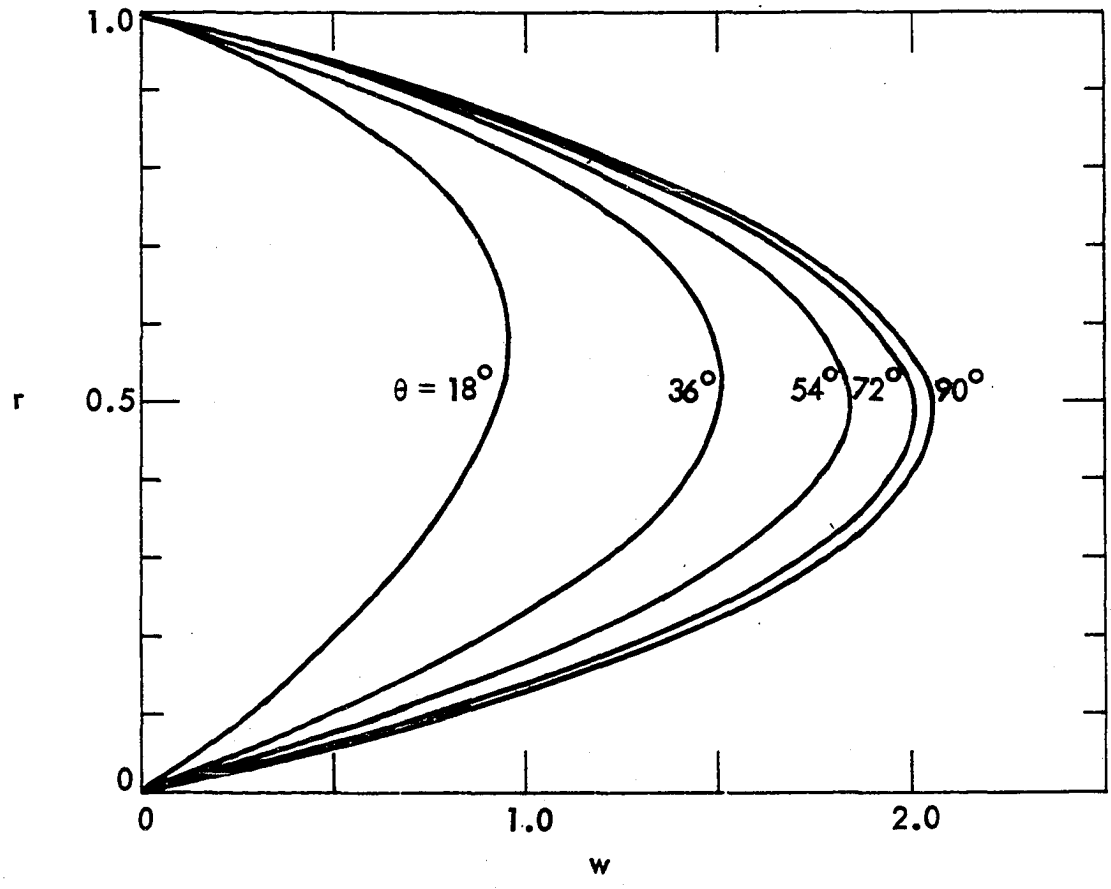

Fig. 4-2 Axial velocity profile at various circumferential locations

with the analytical solutions in Ref. 126. In accordance with the assumptions made in this analysis, these velocity profiles are valid throughout the entrance region for both thermal boundary conditions.

Figure 4-3 shows the temperature distribution of Case 1 at $\theta = \frac{\pi}{2}$ for various axial locations. It is clear that at the entrance of the duct the fluid temperature is more uniform. Since the wall temperature is assumed circumferentially uniform, the fluid temperature becomes parabolic as the fluid moves further downstream, and, finally, the dimensionless temperature profile reaches a fully developed condition. This developing process is similar to the thermally developing flow in circular tubes.

For the case of an insulated wall at the straight section of the circular duct (Case 2), the temperature development in the entrance region at $\theta = \frac{\pi}{2}$ is demonstrated in Fig. 4-4. The temperature gradients at $r = 0$ are seen to be zero for no heat transfer across the wall. Once again, the temperature profiles are more uniform at the tube entrance than further downstream.

The final heat transfer results are presented in Fig. 4-5. As for circular tubes, the Nusselt number at the entrance region is well above the asymptotic solution. The present solution for the fully developed Nusselt number for Case 1 is 6.724, which agrees well with Sparrow and Haji-Shaikh's solution of 6.692 [126]. An asymptotic Nusselt number of 5.2 has been reported by Date and Singham [75] for their limiting case of $y = \infty$ ($y = H/D$) for fully developed laminar flow in tubes containing twisted tapes. This limiting Nusselt number obviously conflicts with the present solution and Sparrow and Haji-Shaikh's solution as stated above.

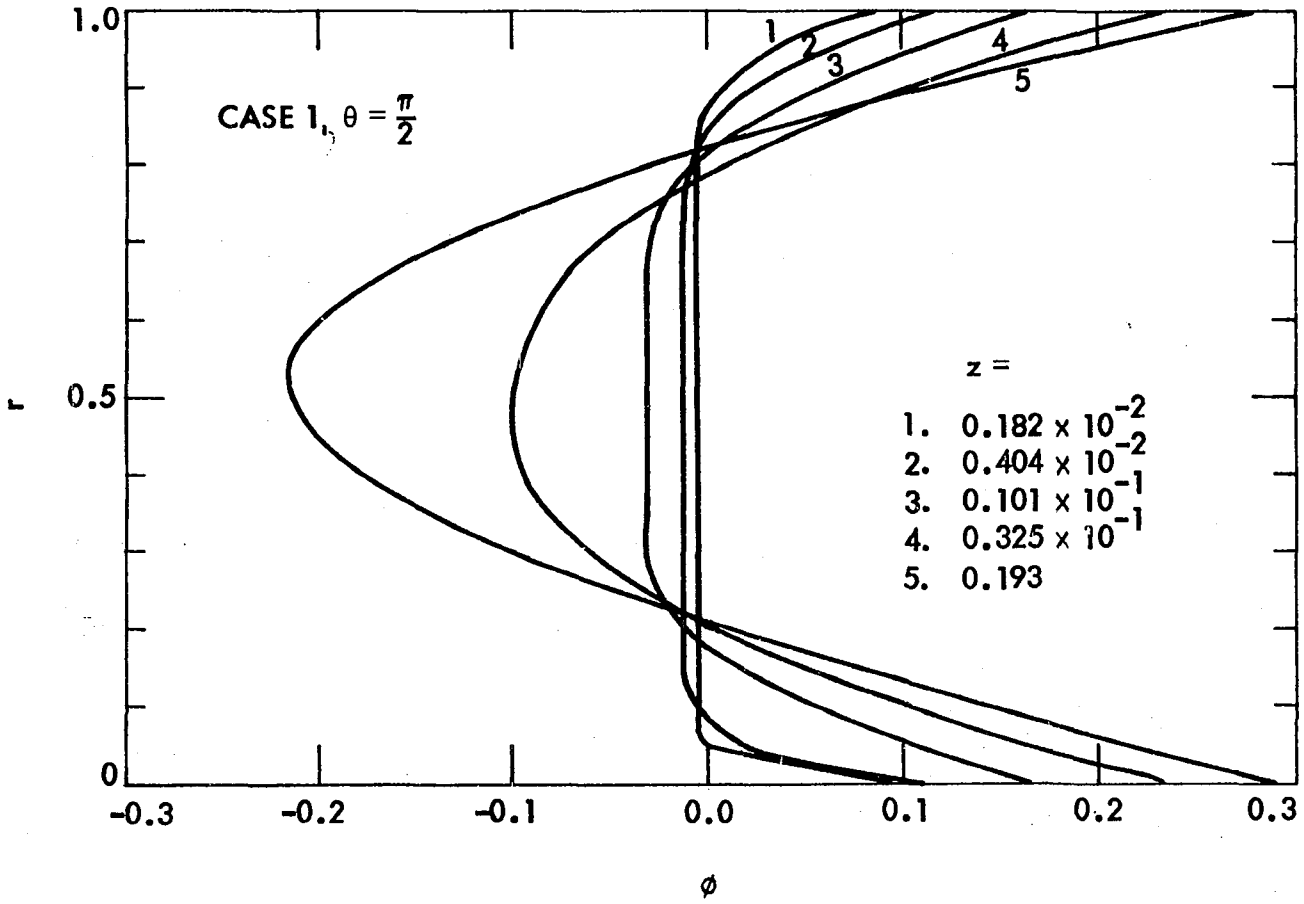

Fig. 4-3 Temperature profile development along the tube for Case 1

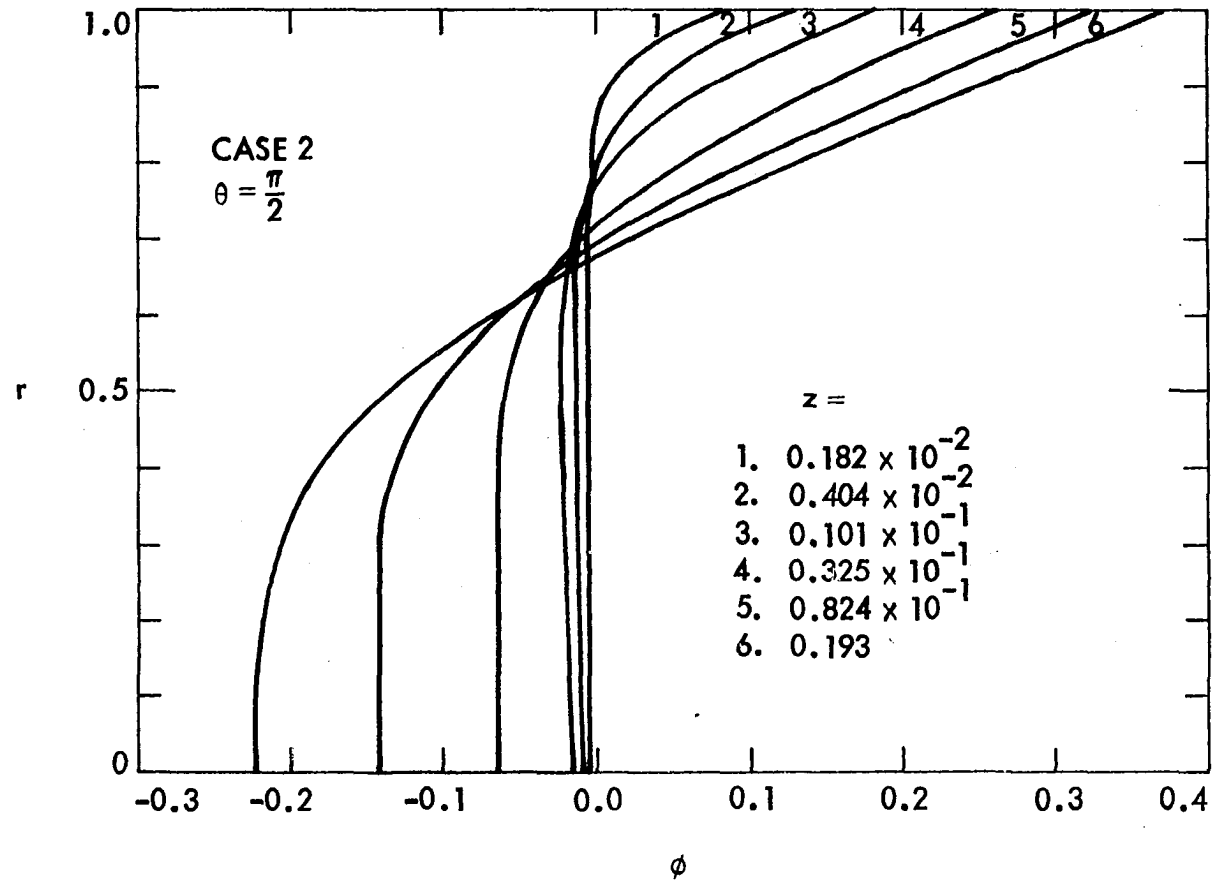

Fig. 4-4 Temperature profile development along the tube for Case 2

Heat transfer coefficients for both cases seem close at the duct inlet. Somewhere downstream, the Nusselt number of Case 1 is seen to be higher than the Nusselt number of Case 2, which is due to the larger heat transfer area of Case 1. An interesting comparison of the present solution with the heat transfer results given in Chapter II for circular tubes is also illustrated in Fig. 4-5. It is seen that the Nusselt numbers for semi-circular tubes are higher than those for circular tubes. The present analytical solution for semi-circular tubes will be utilized in the following chapter.

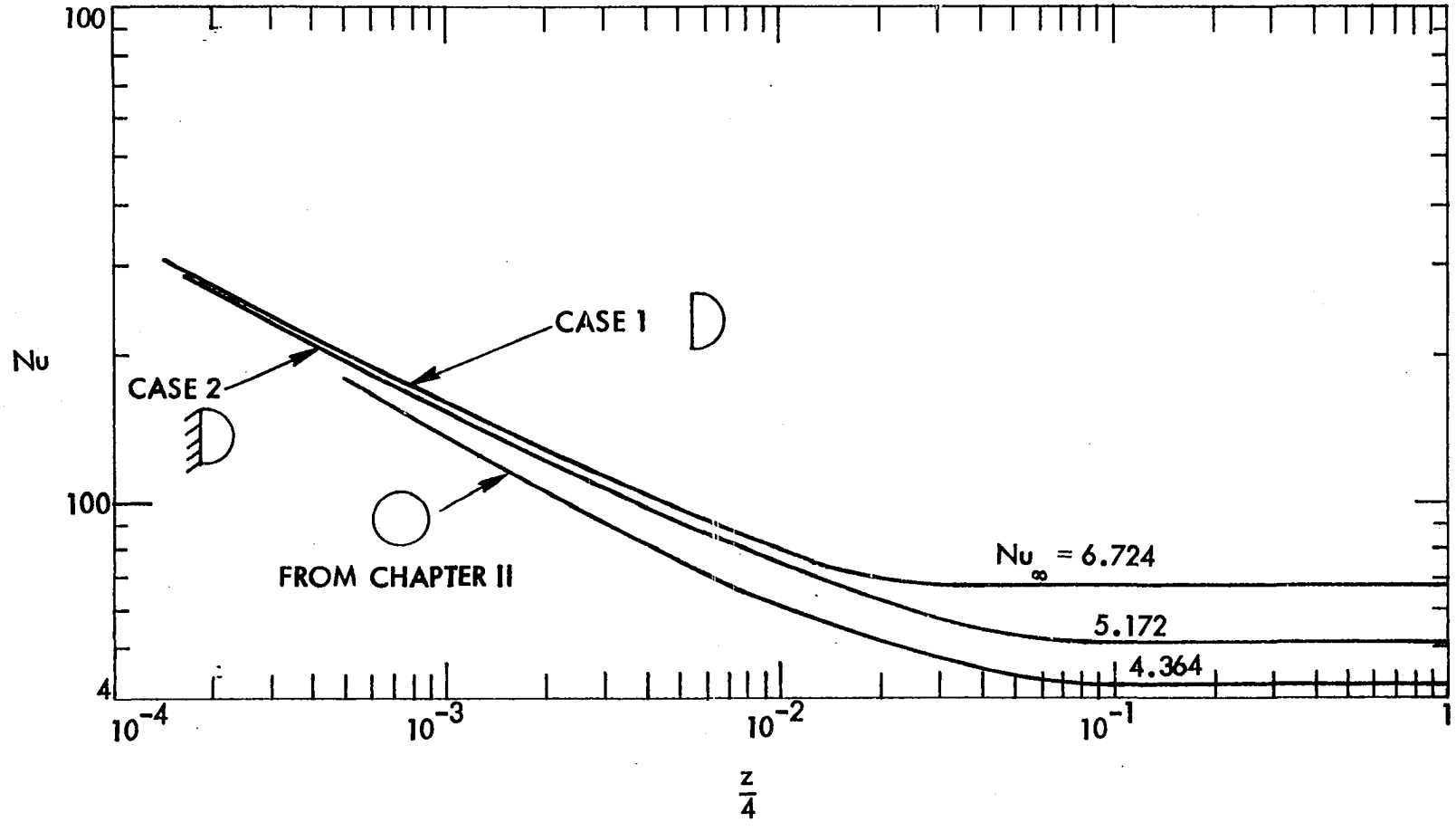

Fig. 4-5 Nusselt number in thermal entrance of semi-circular tube and circular tubes

CHAPTER V. LAMINAR FLOW HEAT TRANSFER AUGMENTATION IN TUBES BY MEANS OF TWISTED TAPE INSERTS

Introduction

Laminar flow heat transfer in horizontal straight tubes has been considered in detail in previous chapters. Unfortunately, the heat transfer coefficients predicted and observed are relatively low. In recent years, the requirement for more efficient heat transfer systems has stimulated interest in augmentative heat transfer methods. Artificially roughened surfaces, extended surfaces, vortex generators, vibration of the surface or fluid, application of electrostatic fields, and the insertion in tubes of objects such as coiled wire, spinners, or twisted tapes are a few examples of such augmentative techniques.

Existing systems can often be improved by using an augmentative method. But in other applications, an augmentative scheme may be mandatory in order for the system to function properly within the limited space. Since the friction factor and cost per foot of tubing are higher for augmented tubes, the designer must make a careful study in order to determine the net improvement available for such a method.

As noted in Chapter I, devices which establish a swirl in the fluid to increase the heat transfer coefficient are particularly attractive augmentative schemes for forced convection systems. Swirl flow generated by twisted tape inserts appears to offer significant benefits since improvements in heat transfer are obtainable at relatively low cost (installation and pumping power). Laminar swirl flow generated by twisted

tape inserts was therefore chosen for the final phase of this study.

To better explain the phenomena of swirl laminar flow heat transfer, the final goals of present study were set as follows:

1. Take data under carefully controlled conditions and from these data develop the first experimentally-based correlation for predicting the associated heat transfer coefficients.
2. Obtain reliable pressure drop data.
3. Evaluate the usefulness of tape-generated swirl flow as an augmentative heat transfer technique by employing standard performance evaluation criteria.

Experimental Apparatus

Test loop

The test facility utilized in this investigation was constructed in the ISU Heat Transfer Laboratory by Dr. Morcos for his straight tube studies [97]. The facility was designed to allow flexibility in testing different kinds of fluids and tubes.

A schematic layout of the test loop is shown in Fig. 5-1. Figure 5-2 presents a photograph of the experimental apparatus. It is a closed loop, low pressure system with all piping made of copper tube and brass fittings. The fluid was stored in a five-gallon stainless steel tank, which also served as a degassing tank. The loop was also equipped with a dimineralizer to prevent fouling of the heated tubes when distilled water was used.

The working fluid was circulated with a small centrifugal pump. A one-gallon accumulator, charged with nitrogen, was installed at the pump outlet

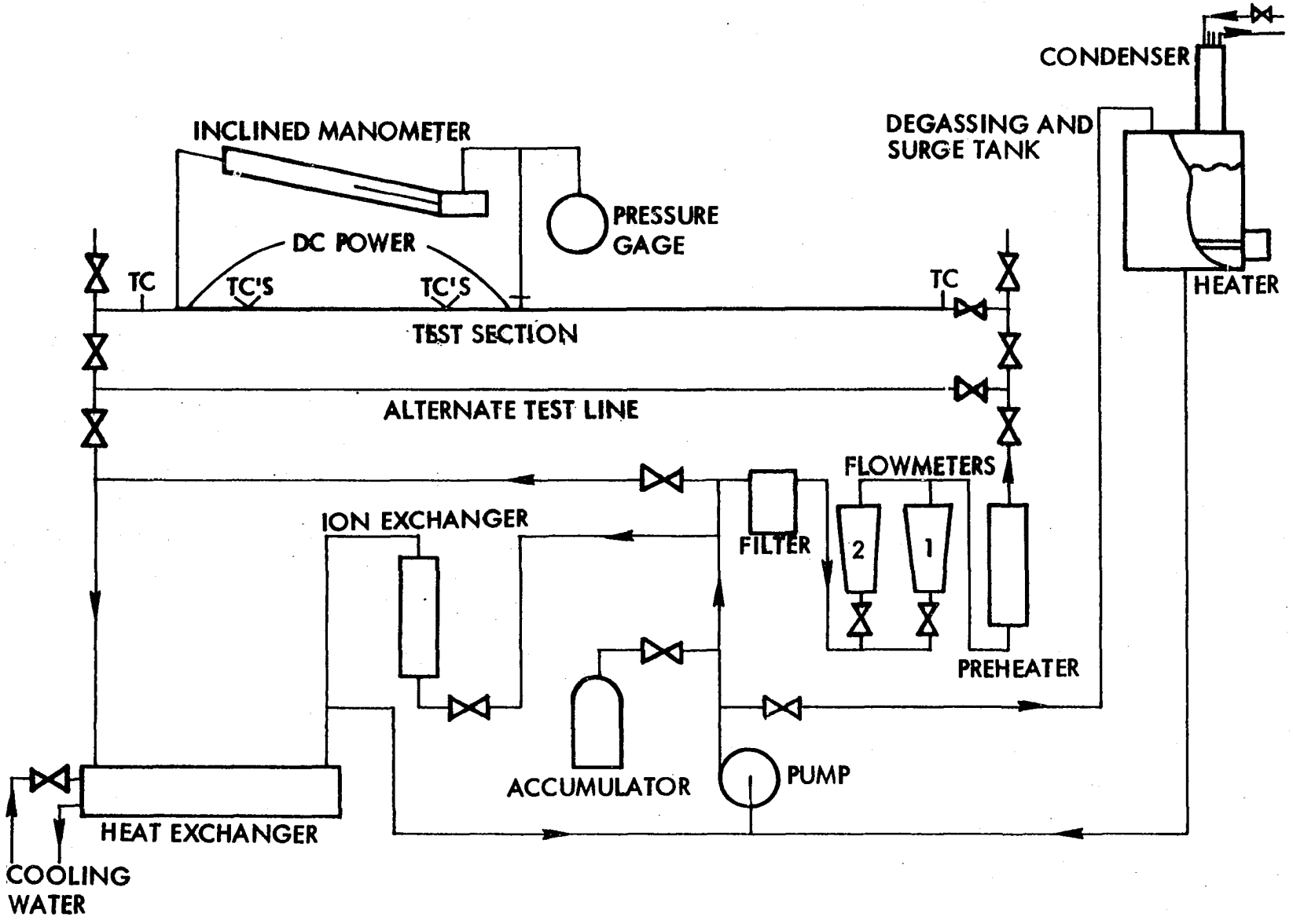

Fig. 5-1 Schematic layout of test loop

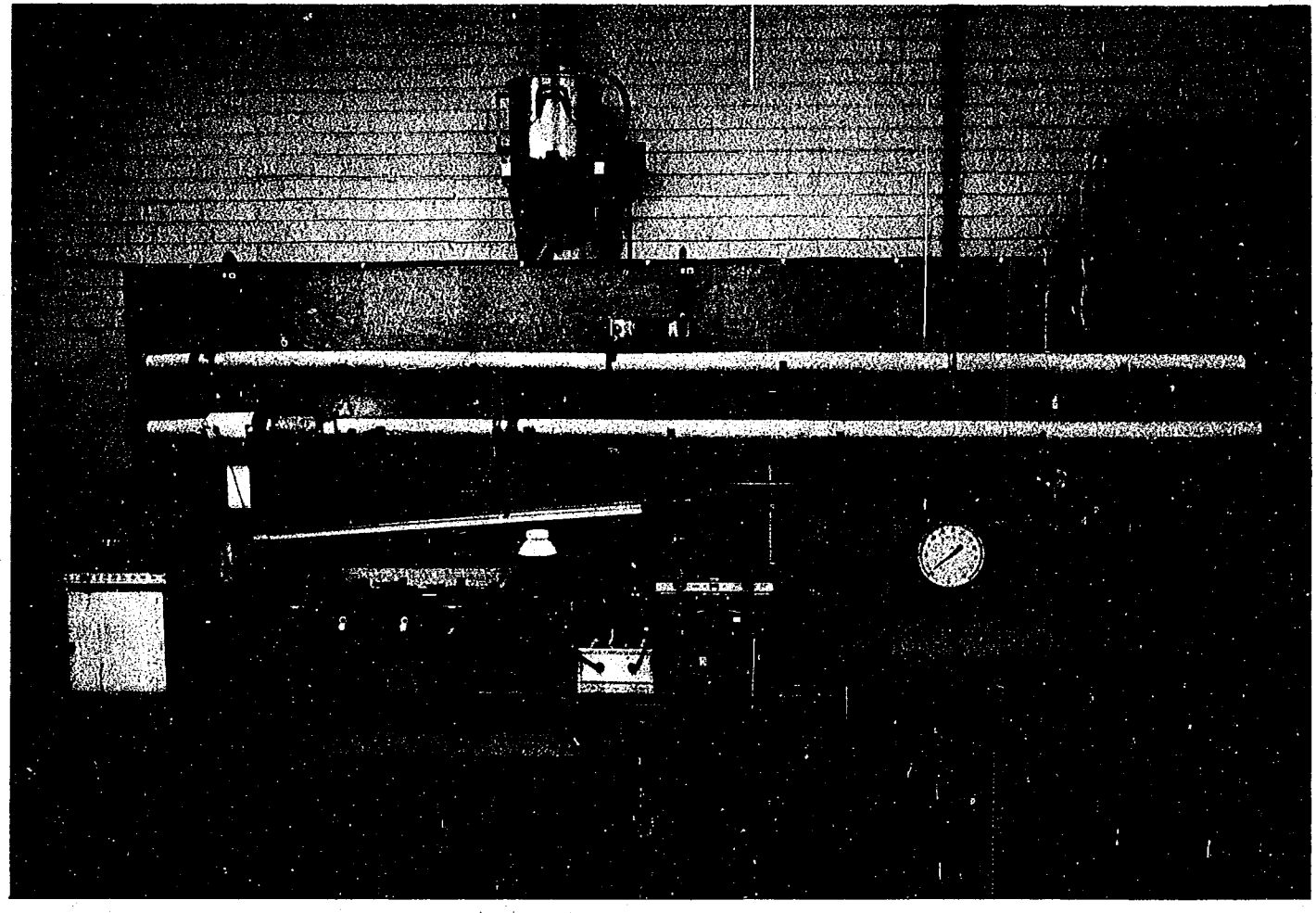

Fig. 5.2. Photograph of experimental apparatus

to dampen pressure fluctuations. The small, high speed pump and the accumulator ensured a stable flow. After passing the accumulator, the flow split into a test-section line and a by-pass line for flow control.

In the test-section line, fluid passed through a filter, a flowmeter and a preheater; it then flowed through the test section and merged with the fluid from the by-pass line. After passing through a heat exchanger, the fluid returned to the pump. Two flowmeters were installed in parallel to measure a wide range of flow rates. The first flowmeter used was Model 1307, size 7, Brooks rotameter with two spherical floats. A Pyrex float that could measure a maximum of 0.17 GPM of water and a Monel float with a maximum flow of 0.39 GPM of water had been calibrated for water and ethylene glycol. The second flowmeter was Model 1110, size 8, Brooks Rotameter with RV type float. The 8-RV-14 stainless steel type float had a maximum flow rate of 1.45 GPM of water. This flowmeter was used to extend the range of ethylene glycol tests. Flowmeter calibration curves are shown in Appendix J.

The test section was a thin-walled stainless steel tube with a full length twisted tape insert. The detail specifications for this test section will be presented later. Two ball valves, one placed upstream and one downstream of the test section, were used to roughly adjust the flow rate and control the pressure level in the heated section. The flow rate was more precisely controlled by a needle valve installed upstream of the test section. An inlet section of about 6.5 ft was used to ensure that the flow was hydrodynamically developed before it entered the heat section. The ends of the test section were electrically insulated from the rest of

the loop by means of short pieces of Buna N pressure hose.

The inlet fluid temperature was measured by a thermocouple probe installed directly in the fluid stream 6 ft prior to the heated section. The bulk temperature of the exit fluid was measured by a thermocouple probe at the exit of the test section. All fluid and tube wall temperatures were measured by 30-gage copper-constantan thermocouples fabricated from the same reel of Leeds and Northrup duplex wire. The thermocouples were connected through selector switches to a common ice bath and a precision potentiometer. Eight of the thermocouples (four from each location) were monitored continuously on a multi-point recorder to ensure that steady-state conditions were reached.

To measure inlet pressure and pressure drop, pressure taps of 0.02 in. diameter were installed 1 in. away from both sides of the heated test section. The pressure drop across the test section was measured with an inclined manometer with a resolution of 0.005 in. of mercury.

The 304 stainless steel tube was the same one used in Morcos' straight tube investigation [97]. The metal tube was chosen in preference to the glass tube used in his investigation because it was feared that tape insertion would break the glass tube. In addition, thermal stratification effects are expected to be negligible with swirl flow; hence, circumferential heat flow effects should not be important. The inside tube diameter and wall thickness were 0.401 in. and 0.02 in., respectively. The wall thickness was a compromise between provision of the minimum thickness required for maximum electrical resistance and provision of sufficient mechanical strength and circumferential conductance.

The tapes used for this investigation were made of a 60 in. sheared strip of 302 stainless steel sheet of width approximately 0.38 in. with a thickness of 0.0182 in. and an RMS roughness of 0.0015 in. The strips were covered at both edges by 0.100 in. wide strips of black No. 33 Scotch electric tape. To assure good electric insulation, the tape assemblies were baked in an electric furnace at 500 ^{o}F for about 1 minute to set the adhesive. The tapes were then twisted by clamping each tape to the ceiling and suspending 50 to 100 lbs of weights from one end. The weights were turned to produce the desired tape twist. The tapes were lubricated with a soap solution and pulled into the tube. After tape installation, the total clearance between the tube wall and the tape was approximately 0.010 in. The electrical resistance between the twisted tape and the test tube was measured to be 5-10 KΩ before and after testing. With this electrical resistance it was reasonable to assume that there was no heat generated in the tape. This situation closely approximates real applications where tapes are inserted in existing heat exchanger tubes. Figure 5-3 shows the two twisted tapes prepared in this study. The twist ratio y is defined as the ratio of tube diameters per 180^{o} rotation of the tape.

The test section was heated by a dc current passed directly through the tube wall. The electric power supply was a 25 kw dc, 125V, 200 amp compound-wound generator driven by an induction motor. Power cables were connected to two brass bushings soldered on each end of the heated test section. A dummy load was constructed in series with the test section in order to boost the resistance and provide better control.

The power input to the test section was determined by measuring the

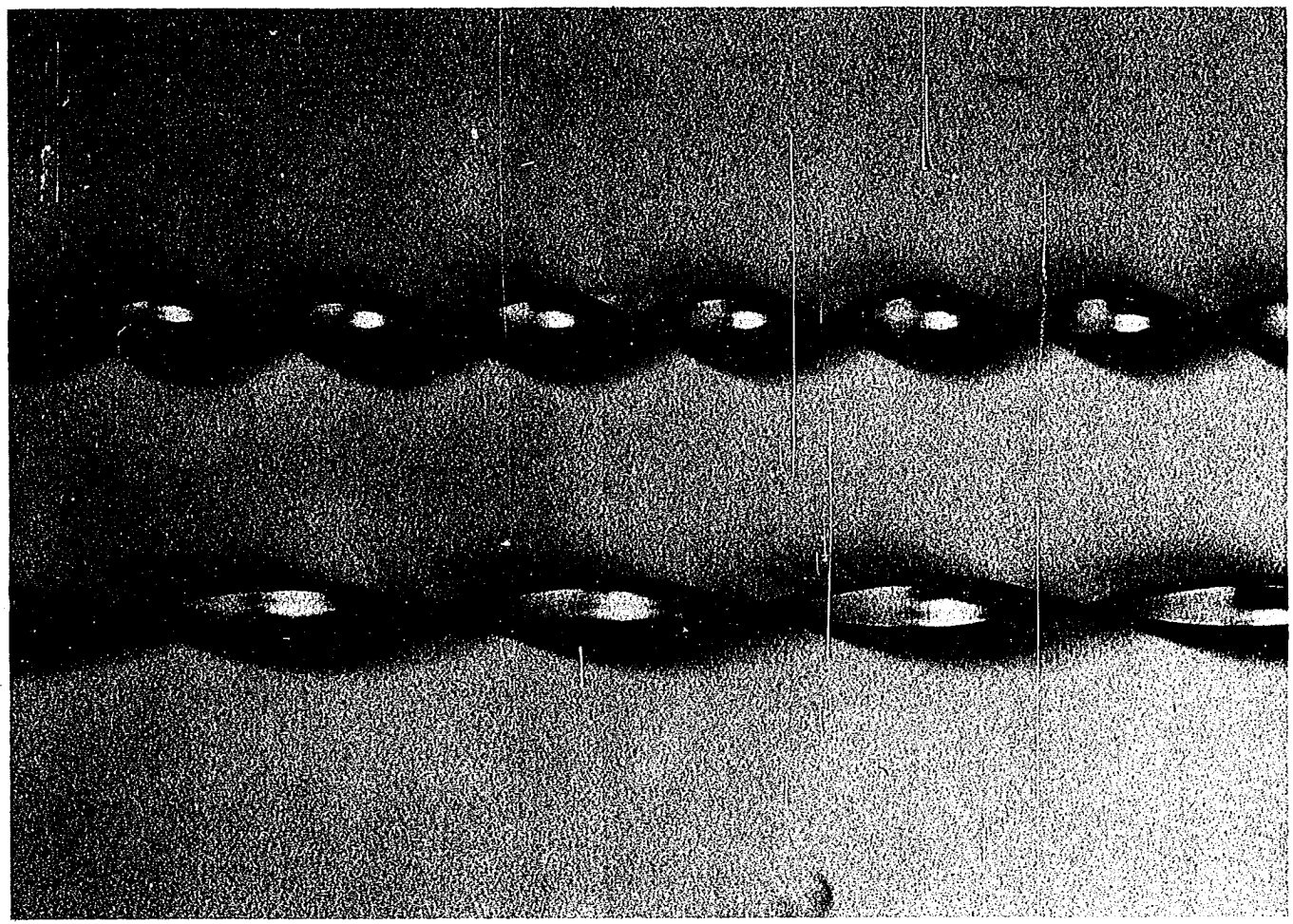

Fig. 5.3. Photograph of twisted tapes, y = 2.45 and 5.08

current and the total voltage drop across the test section. This voltage drop across the heated section was measured by a Digitec Model 204 dc digital voltmeter with an accuracy of ± 1 percent and 0.005 v resolution. The current was measured by means of a calibrated Esterline Angus Shunt (240 amp/100 mv) connected in series with the test section. The voltage across the shunt resistance was monitored with a Leeds and Northrop 8690 potentiometer with a resolution of 0.02 mv.

The outside wall temperature was measured at two axial locations, 19 in. and 44 in. from the onset of heating point. Eight thermocouples were placed 45^{o} apart, circumferentially insulated from the tube with thin strips of insulating paper to prevent erroneous thermocouple readings. The tube was then heavily insulated with 1 in. thick glass fiber insulation to minimize heat loss.

Experimental Procedure

Test fluids

Distilled water was the first working fluid to be tested because of its availability and wide application. Selection criteria for a second fluid required that it not only provide a substantial variation in Prandtl number but also extend the range of Reynolds number to lower values than those obtained with water. Several fluids were considered, and ethylene glycol was found to be the most suitable. It lowers the range of the Reynolds number and has a Prandtl number value as much as 30 times that of water. The physical properties of both fluids, as function of temperature, are given in Appendix I.

Operating procedure

At the beginning of a run, the loop was filled with the test fluid from the top of the degassing tank, and air was bled from all high points of the system. The test fluid in the degassing tank was then heated to eliminate the gas content while the loop fluid was circulated. Degassing was accomplished by bleeding a portion of the loop fluid into the top of the heated degassing tank. The degassing tank was occasionally vented to permit the vapor and gases to escape. A small condenser was used to condense vapor back to the tank. This was continued for about eight hours before initial data-taking. As noted in Ref. [97], evolution of dissolved gas could appreciably enhance heat transfer coefficients.

The gas content of the fluid was measured by a Seaten-Wilson Model AD-4003 B Aire-Ometer and was below 10 cc/liter for water and 6 cc/liter for ethylene glycol. After the water data was completed for the first twist ratio ($y = 5.08$), the water was flushed out with compressed air and dry nitrogen. After the first twisted tape was replaced by a new tape with a different twist ratio, these experimental procedures were then repeated.

The experiments generally proceeded by increasing power to the heated section (the flow rate and inlet temperature remaining constant). The fluid flow rate was controlled by the needle valve at the test-section inlet. The inlet temperature could be adjusted by controlling the heat exchanger cooling water rate and varying the preheater power supply. At each power setting, data were recorded concerning the test-section flow rate, inlet and exit fluid temperatures, current, voltage drop, outer tube wall temperatures and pressure drop. The dc power supply in the

laboratory had a tendency to oscillate. A continuous adjustment of the shunt field rheostat of the generator was required to keep the generator output fairly constant, and the average reading was always recorded. From 30 to 45 minutes were usually required per run in order to establish steady-state conditions and record the data.

Isothermal pressure drop data were obtained by varying the flow rate at room temperature and recording the reading of the inclined differential manometer. The present system variables for water and ethylene glycol were as follows:

Twist ratio: $y = 2.45, 5.08$

Inlet temperature: 50-80 ^{o}F

Water: Flow rate: 45 - 74.97 lbm/hr

Heat flux: 162 - 12237 Btu/hr-ft^2

(Prandtl number: 3-8)

(Reynolds number: 83-2461)

Ethylene Glycol: Flow rate: 14.4 - 299.1 lbm/hr

Heat flux: 1648 - 8745 Btu/hr-ft^2

(Prandtl number: 97-191)

(Reynolds number: 13-390)

Data Reduction

Heat input could be determined in two separate ways: from the measured electrical power input and from the enthalpy rise of the fluid. Theoretically, those two independent methods should agree with each other.

However, due to the uncertainties in calculation of the heat loss through the insulation and lack of a suitable mixing chamber at the test-section exit, the heat balance error was as much as 15 percent at very low flow rates. Generally, the error was about 7 percent. In view of this uncertainty, the heat input was taken from the electrical power input as corrected for the heat loss through the insulation. The heat loss to the surroundings was estimated to be about 1.5 percent of the total power input [97].

The local bulk temperature at the measuring section was computed from the inlet temperature, flow rate, and actual power input. A linear variation in bulk temperature from the inlet to the exit of the heated length was assumed. The tube wall temperature drop was calculated by considering the steady-state, one-dimensional heat conduction equation with uniform heat generation inside the cylindrical tubes. As suggested by Morcos, this correction, less than 1 ^{o}F, was applied uniformly around the circumference of the metal tube. The circumferential average wall temperature was computed from the eight inner wall temperature readings by Simpson's rule of numerical integration.

The average heat transfer coefficient was then calculated by employing the measured heat flux based on the inside tube surface area, the average inner wall temperature, and the calculated bulk fluid temperature at the measuring section. The average heat transfer coefficient associated with Nusselt number can thus be calculated as follows:

$$\bar{h} = \frac{q''}{\bar{T}_w - T_b} \tag{5-1}$$

$$Nu_s = \frac{\bar{h}D}{k} \tag{5-2}$$

where D is the empty tube inner diameter and k is the fluid thermal conductivity evaluated at the bulk fluid temperature.

The pressure drop for water was so small that it was not possible to read it with sufficient accuracy from the inclined mercury manometer. Hence, the pressure drop data were obtained only for ethylene glycol, under both isothermal and non-isothermal conditions. The fluid bulk temperature at the mid-point of the heated section was utilized to evaluate all physical properties. The mercury differential head was employed to calculate the pressure drop across the test section. The friction factor was then obtained according to the following relation:

$$f = 2g_c \frac{D}{\rho \bar{W}^2} \frac{\Delta P}{L} \tag{5-3}$$

It is noted that a linear variation in pressure from the inlet to the exit pressure tap was assumed. Since the pressure taps were on the tube wall within the swirl channel, the pressure they read would include the swirl contribution to the total static pressure. The flow established before entering the heated section and thermal field had little effect on axial velocity profiles. Eq. (5-3) was thus expected to be suitable for the fully developed region. The details of the computational procedure are shown in Appendix J.

A FORTRAN IV computer program was written to facilitate the data reduction and present it in a useful form. It was run on the IBM 360/65 computer in the ISU Computation Center. A sample of the calculation procedure is presented in Appendix K. Similar records of all data obtained

in this investigation are on file in the ISU Heat Transfer Laboratory. About 70 percent of all data, which represents the whole range of this investigation, are given in Appendix L.

Heat Transfer and Pressure Drop Results

Wall temperature variation

Typical temperature variations around the tube wall for various flows and heat fluxes are shown in Figs. 5-4 and 5-5. Figure 5-4 indicates the data for water for two different twist ratios. The local tape locations are 90° and 120° for y = 5.08 and 2.45, respectively. The locations of maximum and minimum for the two tape twists (upper two sets of curves) are different in such a way to suggest that the temperature profiles are related to tape orientation rather than tube orientation. This is as expected since the secondary flow generated by the tapes should be much stronger than any buoyancy-induced secondary flow. In any event, the circumferential variation of tube wall temperature is small, with the maximum and minimum temperatures generally differing by less than 10 $^{\circ}$F.

A rather uniform wall temperature is reasonable due to the possibility of cross flow mixing through the tube-tape gap, and also due to the rather high conductance of the tube wall.

Heat transfer results

The experimental laminar swirl flow heat transfer results are presented in Fig. 5-6 in terms of the traditional dimensionless groups, Nu, Pr, Re_s, and z, as well as twist ratio y. All physical properties are evaluated at the local bulk fluid temperature, and Pr, Re_s and z are

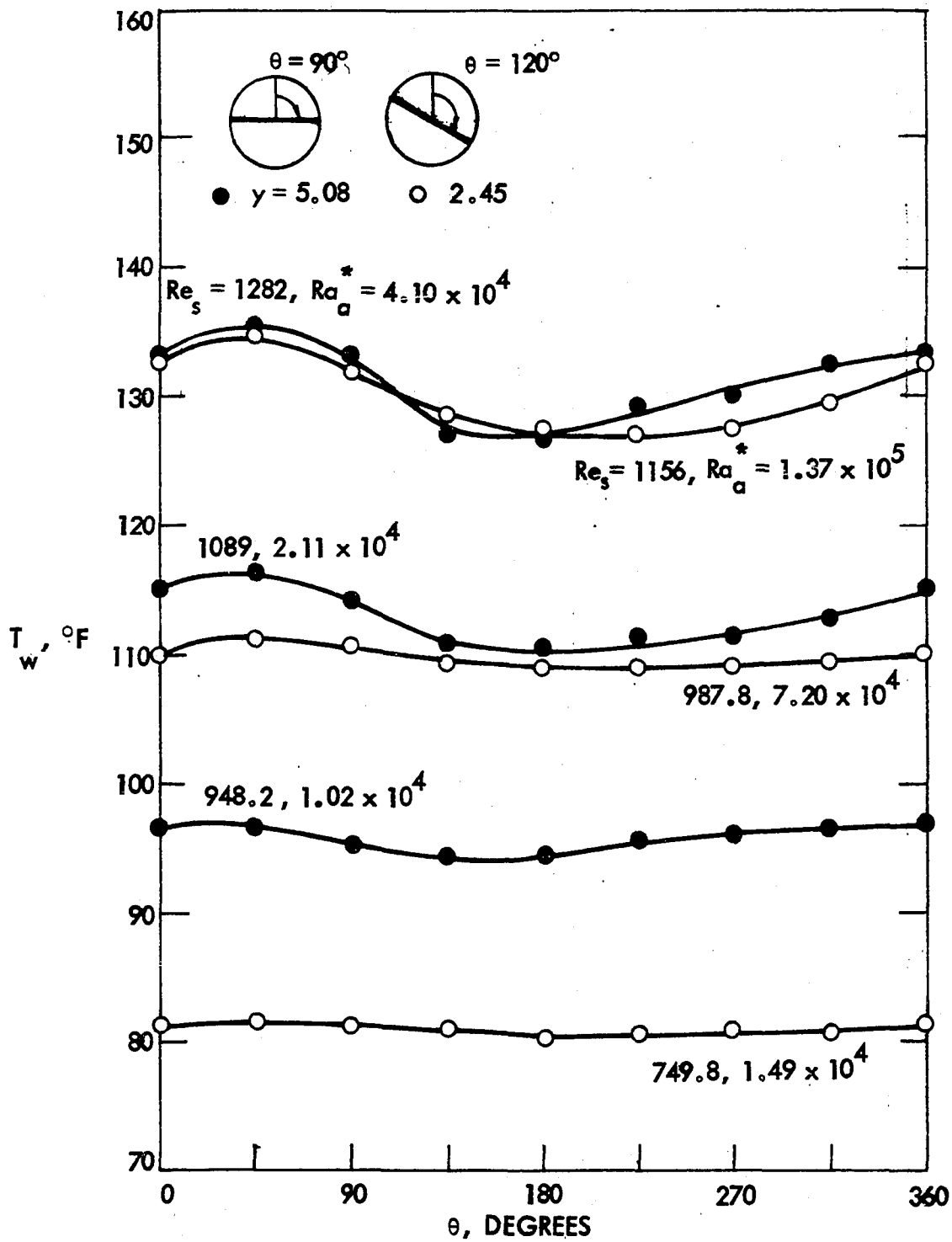

Fig. 5-4 Circumferential wall temperature variation with various Re_s, Ra_a^*, and y for water

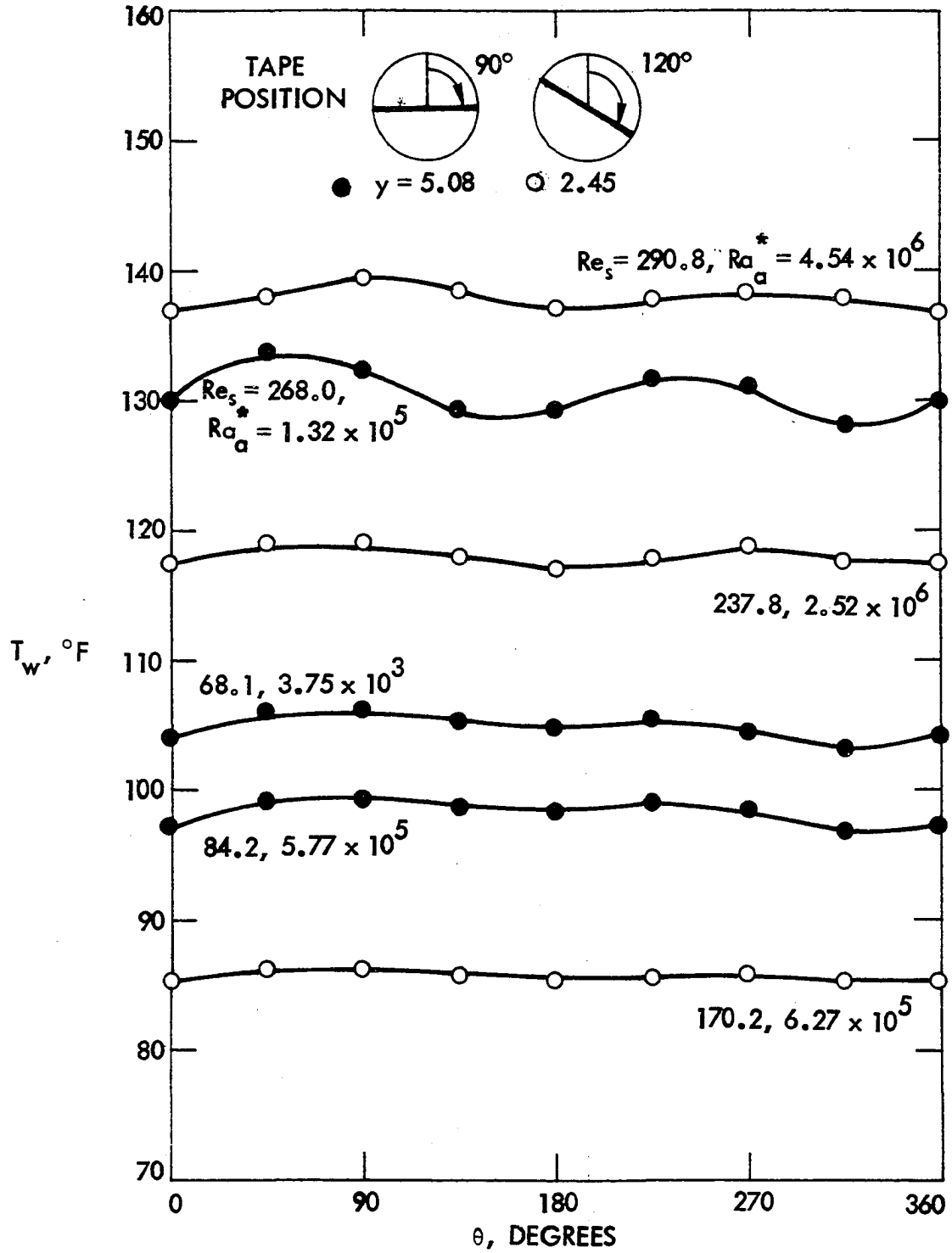

Fig. 5-5 Circumferential wall temperature variations with various Re_s, Ra_a^*, and y for ethylene glycol

defined as follows:

$$\text{Prandtl number: } Pr = \frac{\mu C_p}{k}$$

$$\text{Reynolds number: } Re_s = \frac{G D}{\mu}$$

$$\text{Dimensionless axial distance } z = \frac{Z}{D\, Re_s\, Pr}$$

where G is average mass flux and D is inside tube diameter. The inside tube diameter rather than the hydraulic diameter was used in these parameters in order to best show the improvement obtainable with swirl flow over a comparable empty tube flow. Since the tape blocks free convection, the Grashof number associated with the Rayleigh number, an important parameter in the empty tube laminar flow, is insignificant in swirl flow. The fin parameter suggested in Ref. 75 and the tube wall parameter developed in Ref. 97 were ignored.

The variation of the Nusselt number as a function of reduced length z for various Re_s and y is shown in Fig. 5-6 for water and ethylene glycol. The baseline shown in Fig. 5-6 represents the limiting analytical solution for $y \to \infty$, as obtained in Chapter IV for pure forced convection in a semicircular tube with the flat side insulated. It is evident from Fig. 5-6 that for constant y, and with essentially constant Prandtl number and Reynolds number, Nusselt number is weakly dependent on reduced length. A constant Nusselt number represents the classical interpretation of the fully developed condition; hence, it is concluded that fully developed conditions were obtained prior to the first measuring section. Assuming

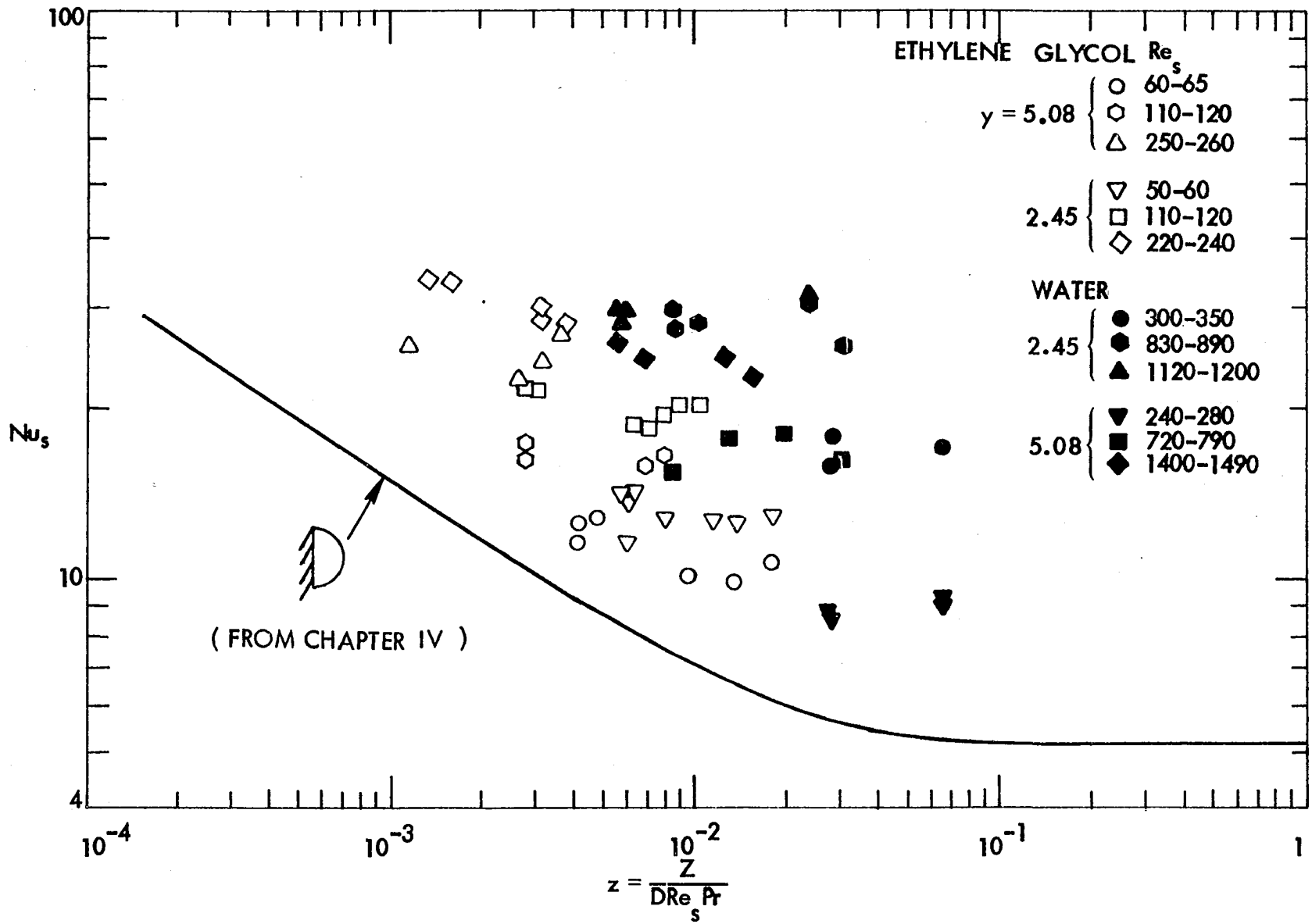

Fig. 5-6 Nusselt number as a function of reduced axial length for water and ethylene glycol

that Nusselt number is independent of axial length Z for fixed Re_s, Pr, and y, a correlation of the following form will be sought:

$$Nu = f(Re_s, Pr, y) \tag{5-4}$$

Plots with this interpretation of all the data are shown in Figs. 5-7 and 5-8 for y = 5.08 and 2.45, respectively. It is apparent that tighter tape twists (lower y value) produce an increase in heat transfer coefficient. It may also be observed that Nu varies essentially as Re_s^m for high Reynolds number flow. This would suggest a linearized correlation for the high Reynolds number region, similar to the usual correlation for turbulent flow in empty tubes. Estimated straight-line representations of the four sets of data are indicated in Fig. 5-9; the maximum deviation of the data from each line is 20 percent. The heat transfer coefficient clearly increases with increasing Reynolds and Prandtl number and decreasing twist ratio.

Correlation of data

As shown in Fig. 5-9, the ethylene glycol data for both twist ratios are well above the water data at constant Reynolds number. In view of a suggestion from Refs. 75 and 127, the parameters Re_s and y were combined as one single parameter Re_s/y. This parameter is similar to the Dean number in curved pipe flow, which accounts for the centrifugal force effect. The final straight line correlation for water and ethylene glycol with two twist ratios is shown in Fig. 5-10. After many trials, it was found that the following equation suitably represented the experimental data for $Re_s/y > 10$:

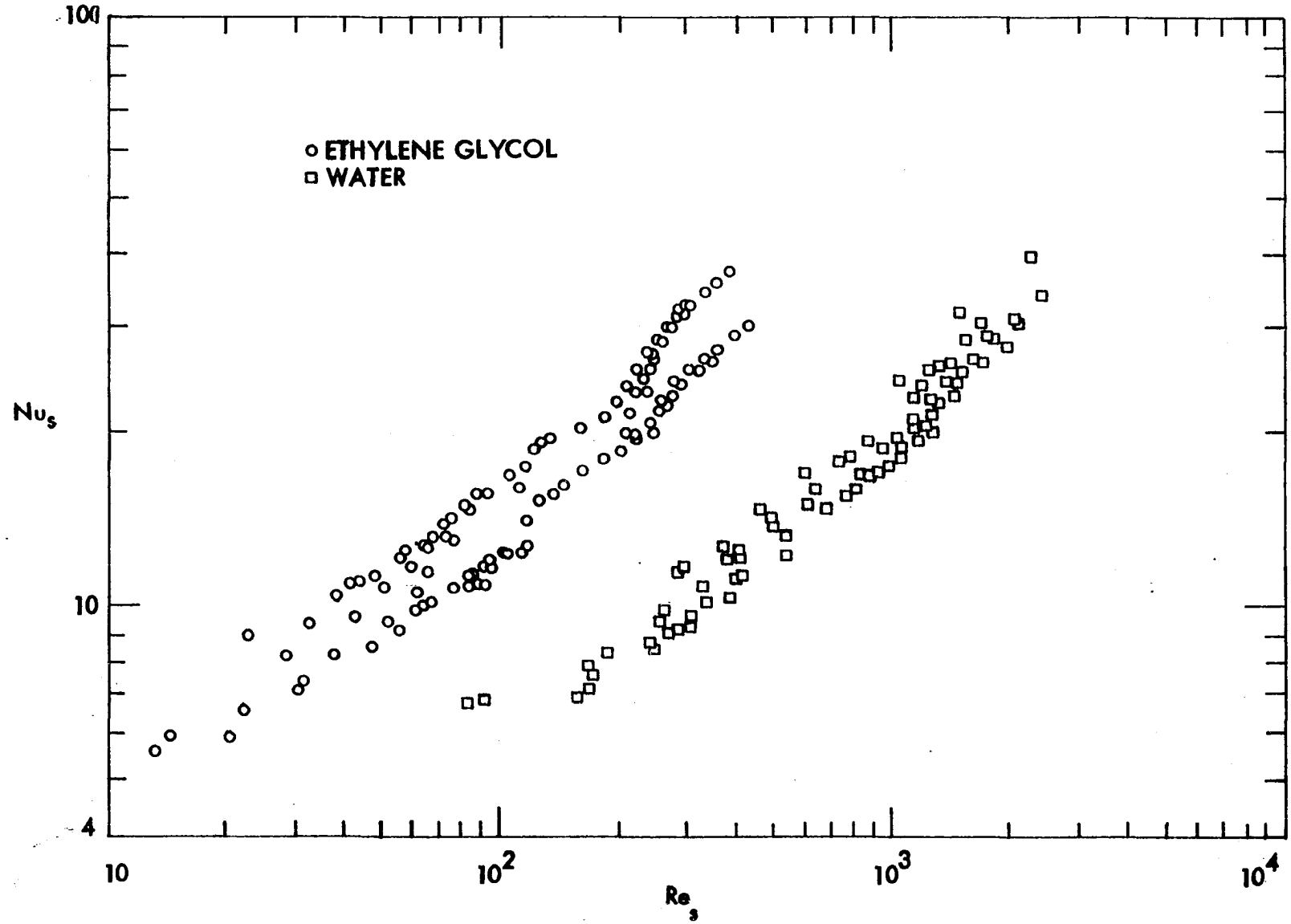

Fig. 5-7 Fully-developed heat transfer results for water and ethylene glycol with y = 5.08

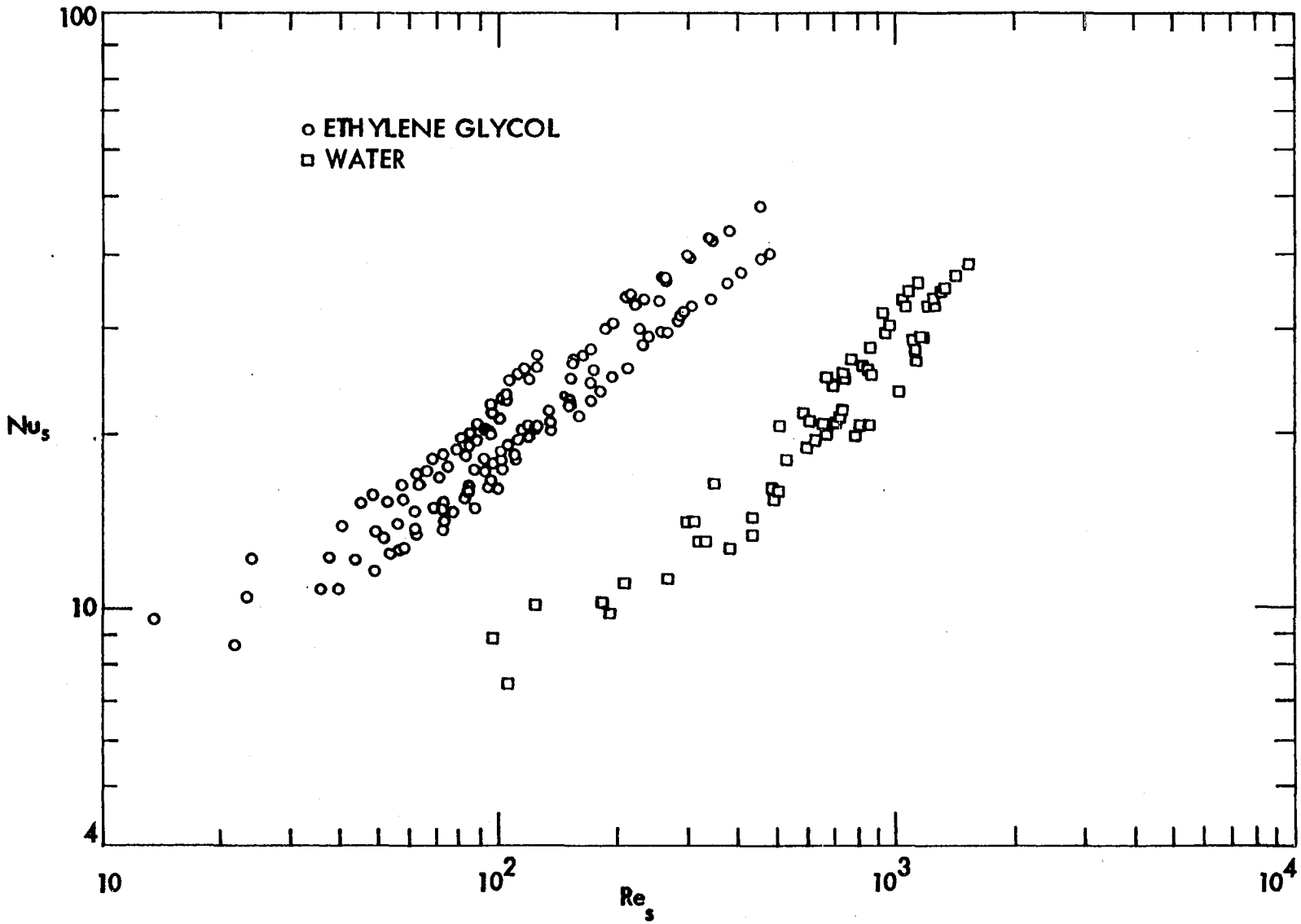

Fig. 5-8 Fully-developed heat transfer results for water and ethylene glycol with y = 2.45

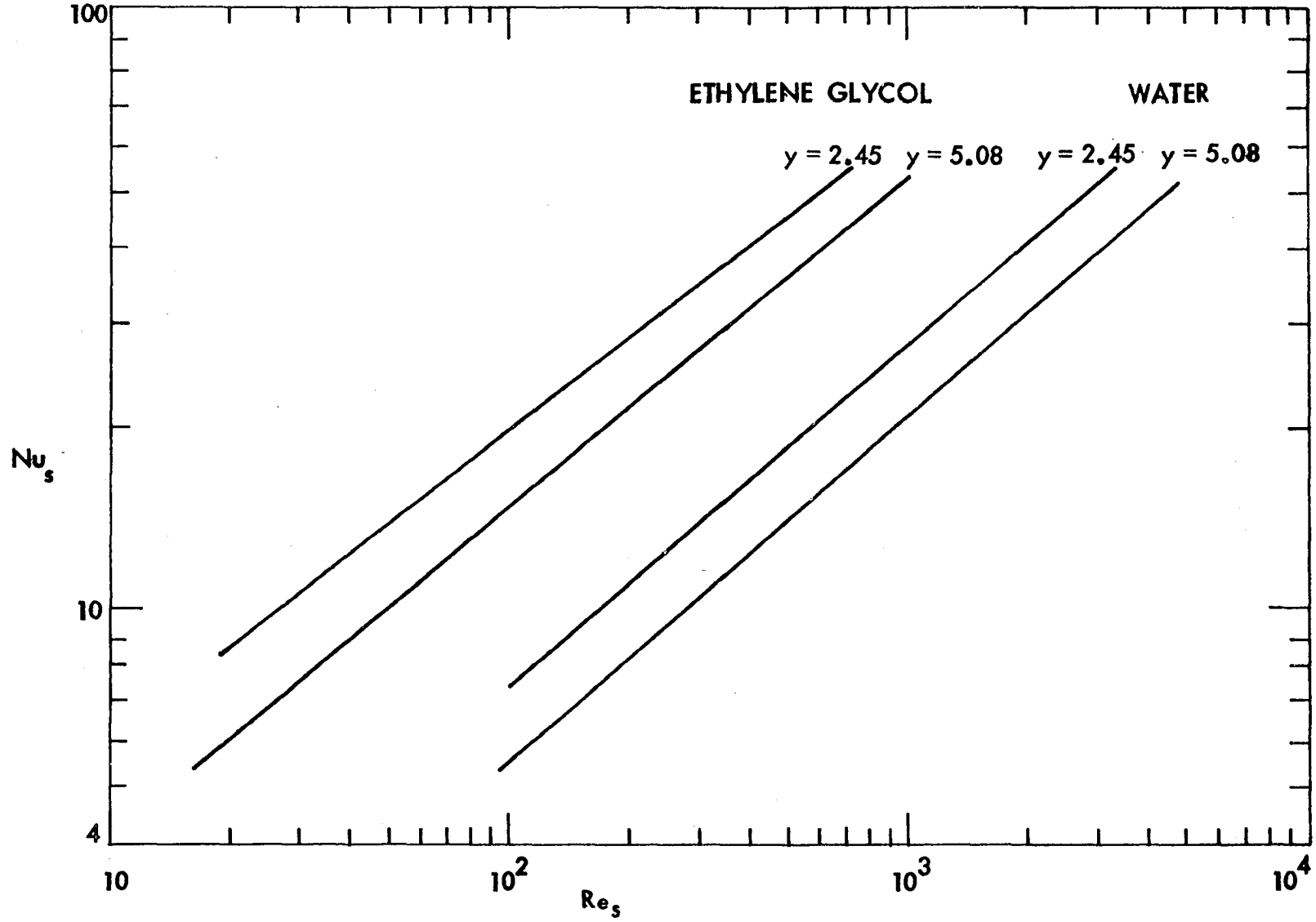

Fig. 5-9 Linearized representation of data for water and ethylene glycol

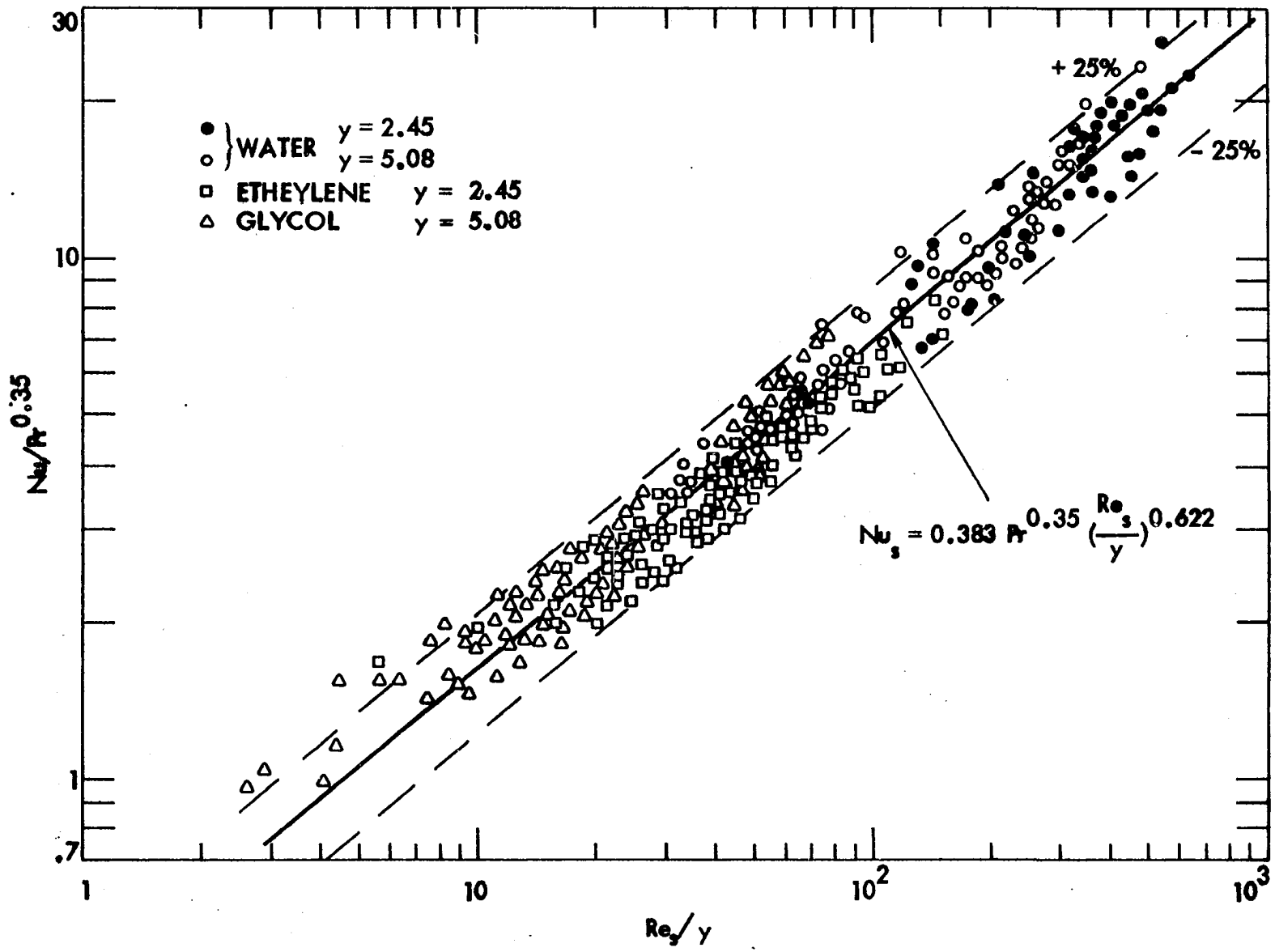

Fig. 5-10 Correlation of heat transfer results for laminar swirl flow

$$Nu_s = 0.383\ Pr^{0.35}(Re_s/y)^{0.622} \qquad (5\text{-}5)$$

where all physical properties are evaluated at the bulk fluid temperature.

In order to reduce the scatter of experimental data, different procedures were tried for producing the four sets of heat transfer data. To account for variable fluid properties, the temperature-dependent viscosity parameter Be discussed in Chapter III was first tried. It was found that including Be as a correlation parameter did not produce a significant improvement. The Be data for water and ethylene glycol are presented in Appendix L for reference.

Another attempt was made to improve the correlation through evaluation of all fluid properties at the film temperature, $T_f = 1/2\ (\bar{T}_w + T_b)$. However, the film temperature did not give a significant improvement over the correlation presented in Fig. 5-10. It was therefore decided to simply use bulk fluid temperature for evaluation of all fluid properties. The inadequacy of the viscosity correlation parameter and the film temperature correlation for the variable fluid properties is probably due to the fact that the fluid in the tube is so well mixed by the twisted tape.

It is evident that Eq. (5-5) is not suitable for correlation of low Re_s/y values. As Re_s/y decreases, the Nusselt number should approach the asymptotic value of 5.172, which was obtained analytically in the previous chapter. The limits are then

$$\begin{aligned} Nu_s &= 5.172 && \text{as } Pr(Re_s/y)^{1.78} \to 0 \\ Nu_s &= 0.383(Pr(Re_s/y)^{1.78})^{0.35} && \text{as } Pr(Re_s/y)^{1.78} \to \infty \end{aligned} \qquad (5\text{-}6)$$

Churchill and Usagi [128] suggest that with these two boundaries a single expression

$$Nu_s = \left\{ 5.172^n + [0.383(Pr\ Re_s/y^{1.78})^{0.35}]^n \right\}^{1/n} \qquad (5\text{-}7)$$

is usually suitable for interpolation. The right side of Eq. (5-7) can be interpreted as the nth-order sum of the two asymptotic solutions. The exponent n can be evaluated from a single intermediate value of $Nu(Pr\ Re_s/y^{1.78})$. However, Eq. (5-7) is relatively insensitive to n, and an integer value of n = 2 is found to be satisfactory. With n = 2, Eq. (5-7) can be rewritten as:

$$Nu_s = 5.172 \left\{ 1 + 5.484 \times 10^{-3}\ Pr^{0.7}(Re_s/y)^{1.25} \right\}^{1/2} \qquad (5\text{-}8)$$

The final correlation plot with Nu versus $Pr(Re_s/y)^{1.78}$ is presented in Fig. 5-11. It is seen that Eq. (5-8) shows reasonable correlation for all values of Re_s/y. The standard deviation of the data from the condition is 16.4 percent.

Comparison with analytical prediction

The only analytical prediction of laminar swirl flow generated by twisted tape inserts is given by Date and Singham [75] and Date [129]. One important parameter used in their analysis is the fin parameter, representing the fin effect of the twisted tape, which is defined as:

$$C_{fin} = \frac{k_w \delta}{k\ D} \qquad (5\text{-}9)$$

In the present investigation, the twisted tape was covered by electrical

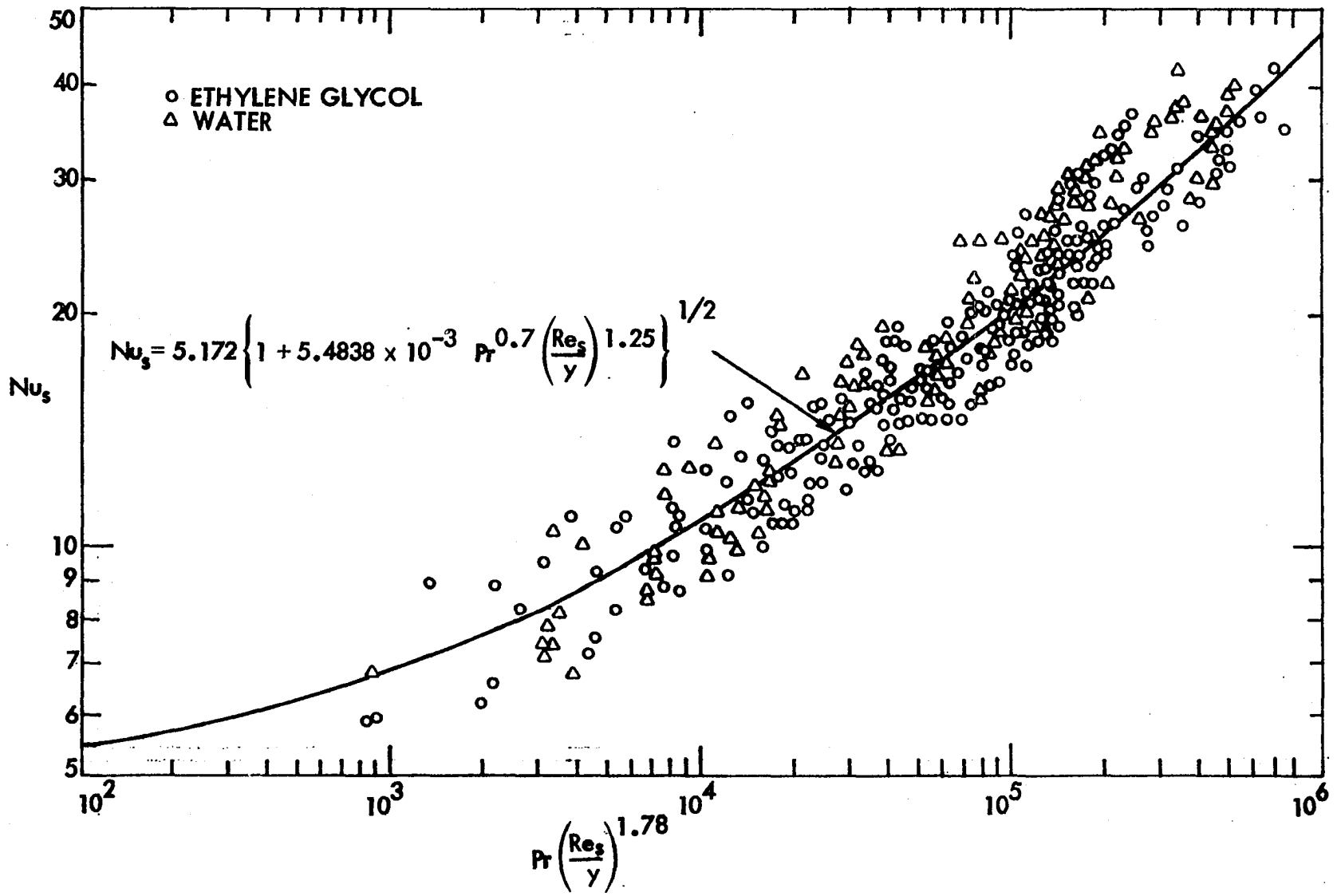

Fig. 5-11 Final correlation of heat transfer results

insulation tape to prevent electric contact between the tape and the tube wall. C_{fin} in this study therefore approaches zero (approximately 0.124 for ethylene glycol). A low value of C_{fin} is also expected to be the case in many practical applications since loose-fitting tapes are desirable from the standpoint of insertion and removal for tube cleaning.

A comparison of the present heat transfer correlation with the analytical results obtained by Date and Singham [75] and Date [129] is presented in Fig. 5-12. The analytical results were presented for $C_{fin} = 1.85$ and ∞ for a range of Prandtl numbers. The analytical results for $C_{fin} = 0$ apparently were computed only for Pr = 1.0. All of the solutions presented by Date and Singham, with the exception of results for Pr = 0.1, are included in Fig. 5-12.

It is evident from Fig. 5-12 that C_{fin} has a large effect on the predicted value of Nu, with Nu increasing with increasing C_{fin}. Since the results for Pr = 1.0 suggest that Nu for $C_{fin} = 1.85$ is approximately the same as Nu for $C_{fin} = 0$, it is appropriate to compare the present results with the data for $C_{fin} = 1.85$.

As shown in Fig. 5-12, the present correlation agrees well only with analytical results for Pr = 100. The analytical predictions at Pr = 500 are seen to be far above the present correlation and those for other values of Pr are well below the correlation.

Due to complexity and lack of published detail, it is not possible to check the solutions given in Refs. 75 and 129. However, some indication of the accuracy of these solutions can be obtained by comparing the results for $y = \infty$ and $C_{fin} = \infty$ with other data. Date and Singham [75] reported Nu = 5.3 for $y = \infty$ and $C_{fin} = \infty$,

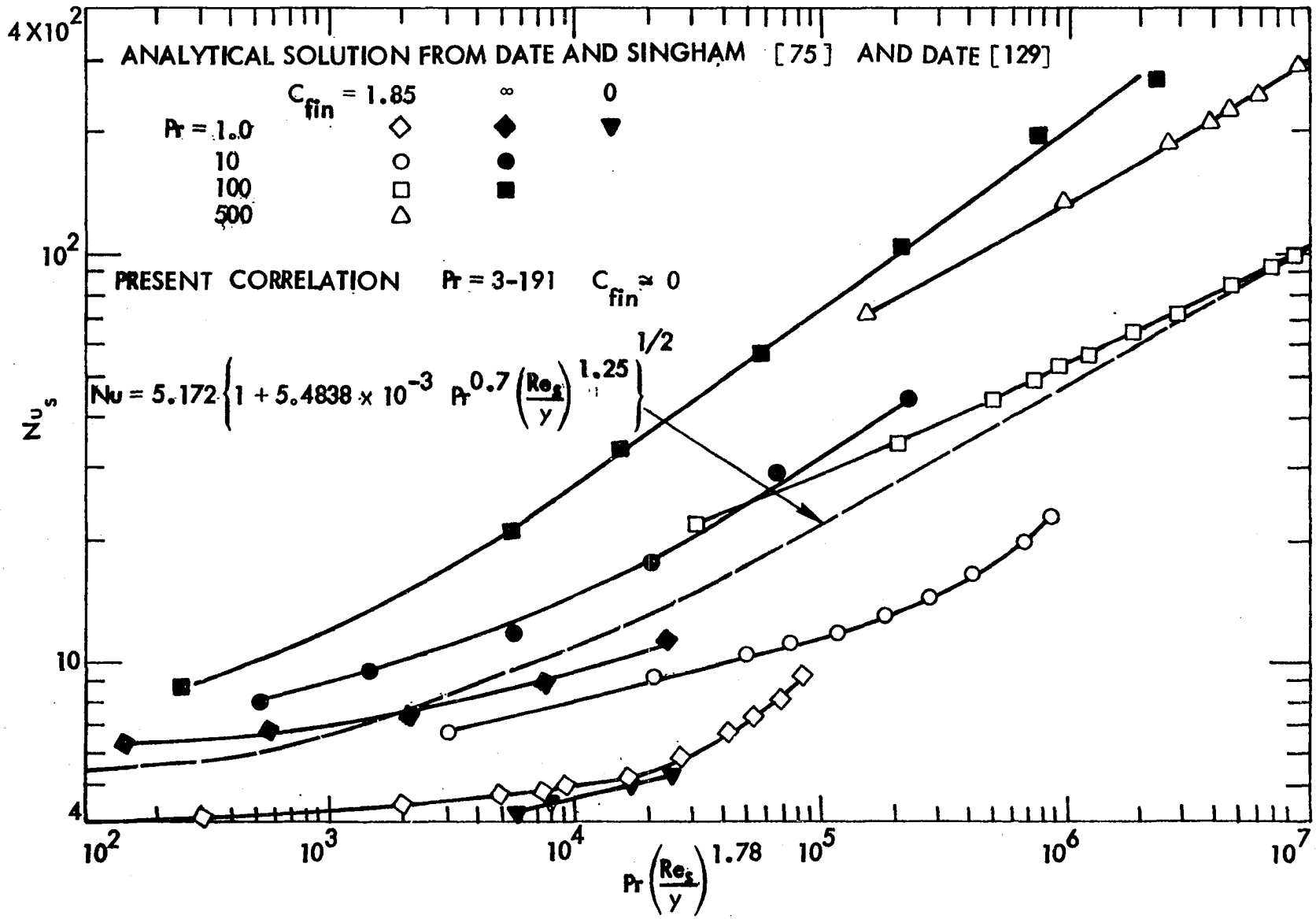

Fig. 5-12 Comparison of present heat transfer correlation with previous analytical predictions

as compared to the exact value of 6.692 obtained by Sparrow and Haji-Sheikh [126]. This disagreement leads one to question the accuracy of Date and Singham's solution. The present experimental correlation is therefore recommended for design.

Pressure drop

Morcos and Bergles [97] found that the pressure drop for water in an empty tube was too low to permit detection of pressure drop variations due to heating. Swirl flow generated by the twisted tape insert does not increase pressure drop significantly. It was therefore decided that pressure drop measurements would be taken only for ethylene glycol runs, since the pressure drop level for ethylene glycol was more than ten times that for water. Mercury was the indicating fluid used in the inclined manometer. All fluid properties for heating runs were evaluated at the bulk mean temperature at an axial location halfway along the heated section.

The Darcy friction factor data for ethylene glycol with and without heating are presented in Fig. 5-13 for the two twist ratios. No consistent difference between isothermal and non-isothermal runs was observed. Friction factor is seen to be independent of heat flux.

The analytical prediction of friction factor for $y = \infty$ is given by Sparrow and Haji-Sheikh [126] as follows:

$$f \cdot Re_D = C = 168.9 \qquad (5\text{-}10)$$

Date and Singham [75] suggest that C = 159; the disagreement may possibly

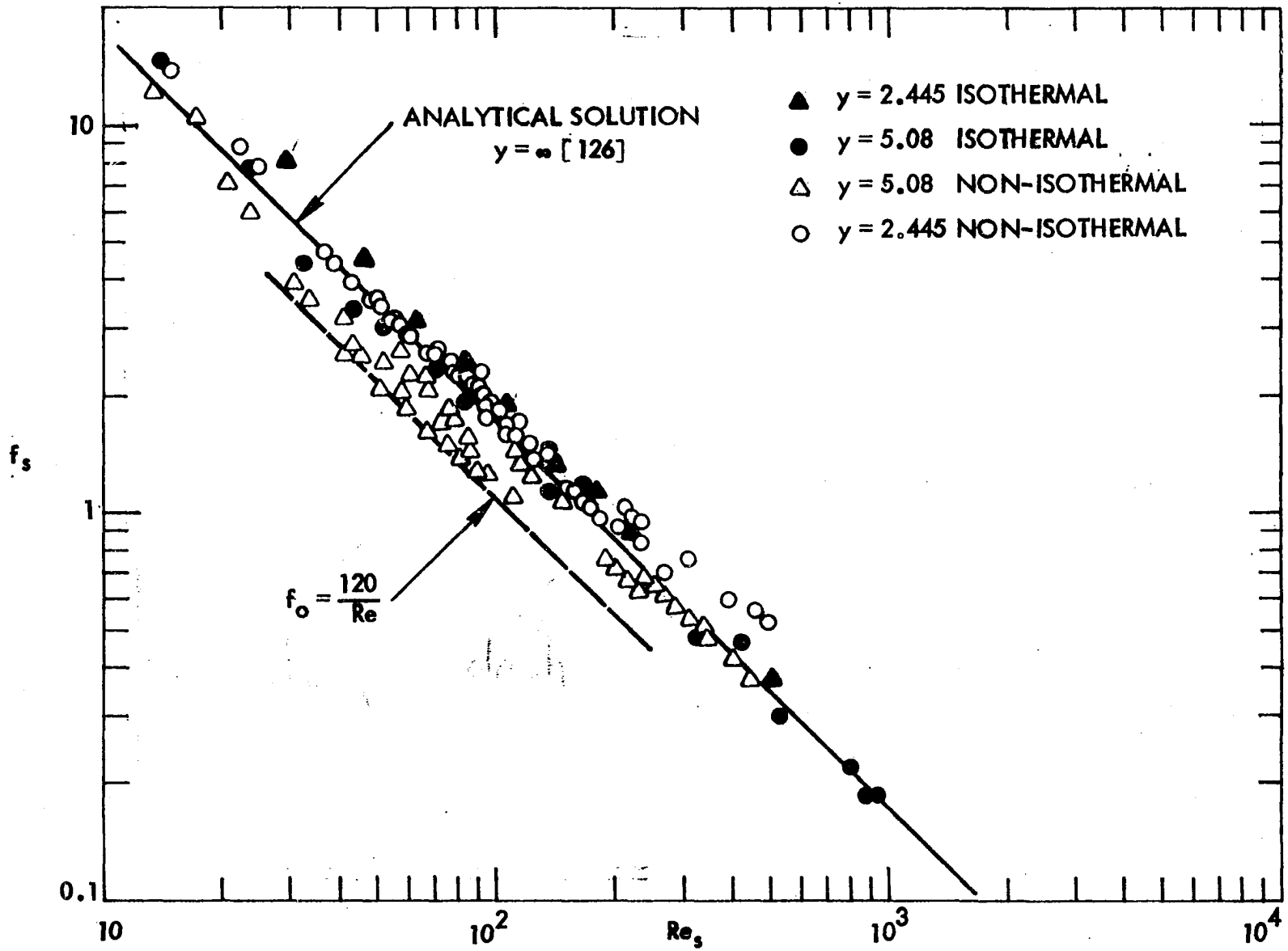

Fig. 5-13 Friction factor verus Re_s for ethylene glycol

be due to computational error, as mentioned above. Sparrow and Haji-Sheikh [126] further suggest that constant C in Eq. (5-10) decreases as the cross-sectional area of a circular segment decreases by decreasing the cord. Since a tube with a tape insert has a cross-section smaller than a semi-circular of the same diameter, the experimental results of constant C in Eq. (5-10) for $y = \infty$ of twisted tape insert is also expected to be less than analytical prediction of 168.9. The friction factor for $y = \infty$ was approximated by drawing a line parallel to the exact analytical prediction shown in Fig. 5-13 and bounding the lower values of the experimental data. This line for $y = \infty$ is estimated to be

$$f_o = \frac{120}{Re_s} \tag{5-11}$$

Increases in friction factor above the line of Eq. 5-11 are considered to be dependent on Re_s/y.

Utilizing the technique recommended by Churchill and Usagi [128] yields the final best correlation for friction factor:

$$\frac{f_s}{f_o} = \left\{ 1 + 0.121(Re_s/y)^{0.65} \right\}^{0.77} \tag{5-12}$$

where f_o is given by Eq. (5-11). The comparison of this correlation and experimental data is shown in Fig. (5-14). Equation (5-12) correlates the data with a maximum deviation of 30 percent.

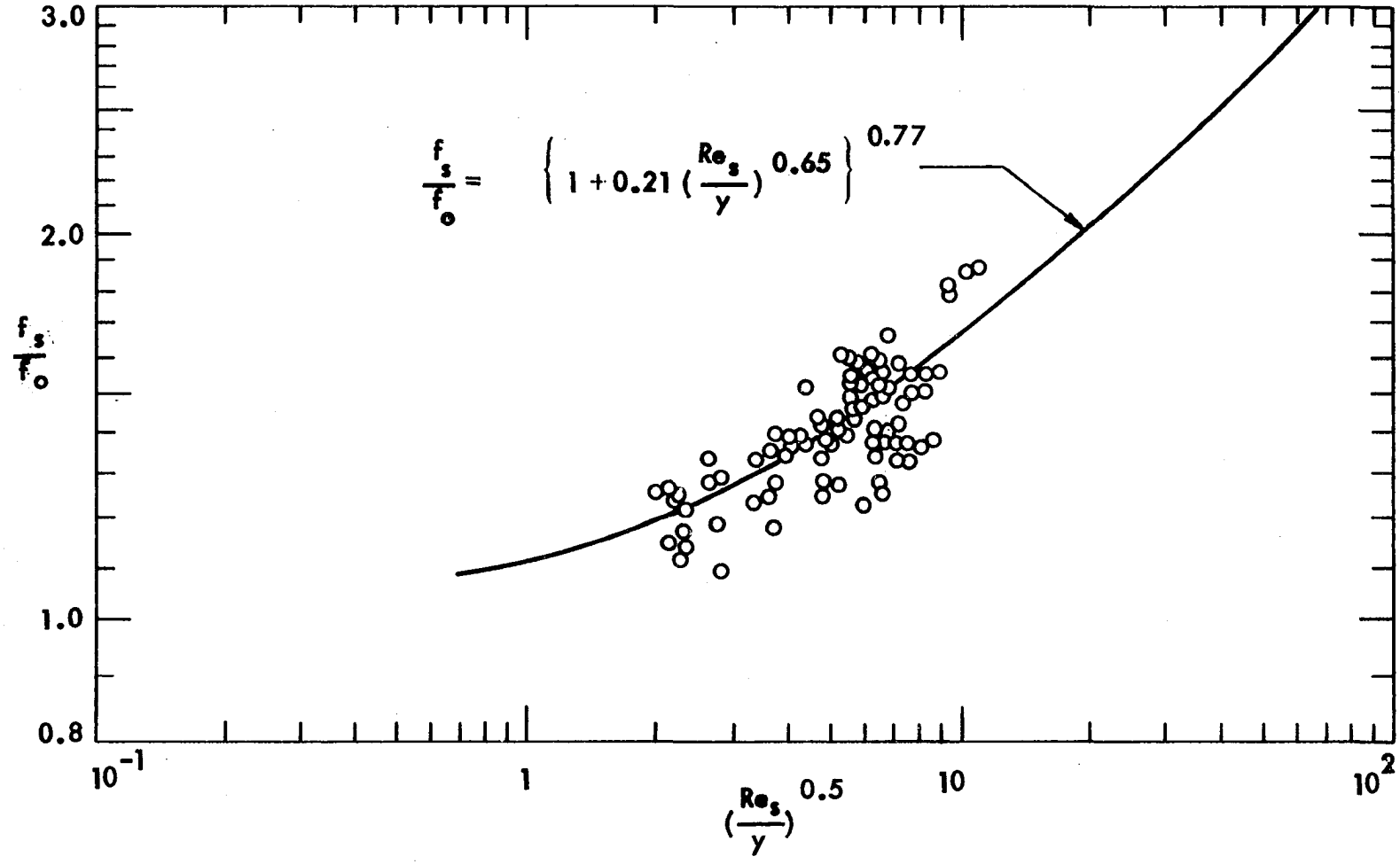

Fig. 5-14 Final correlation of friction factor data

Applications

The final objective in the present chapter is to compare the swirl flow results with the heat transfer performance of ordinary tubes. The heat transfer results in an empty metal tube presented by Morcos and Bergles [97] were correlated as follows:

$$Nu_f = 0.377\ Gr_f^{0.256}\ Pr_f^{0.31}/Pw_f^{*\,0.09} \tag{5-13}$$

where $Pw^* = (k/k_w)\ (D/t)$ and the subscript f indicates that all physical properties are evaluated at film temperature. By introducing $\Delta T^* = q''a/k$ into Grashof number, Eq. (5-13) can be rewritten as follows:

$$Nu_f = 0.45\ Gr_f^{*0.204}\ Pr_f^{0.256}/Pw_f^{*0.072} \tag{5-14}$$

It is seen that the Nusselt number for an ordinary tube depends on Grashof, Prandtl number, and the tube wall parameter. However, in the laminar swirl tube flow Nusselt number is a function only of Pr and Re_s/y as indicated by Eq. (5-4).

In practical applications, the objectives mainly focus on increasing heat transfer, reducing pumping power, or reducing exchanger size. Consider the first objective of increasing heat transfer for fixed geometry. The heat transfer coefficient ratio of tubes with twisted tape and without twisted tape is obtained from Eqs. (5-4) and (5-13) as follows:

$$\frac{q_s}{q_o} = \frac{Nu_s}{Nu_f}\bigg|_{\Delta T, A} = \frac{1.015\ Pr^{0.35}(Re_s/y)^{0.622}\ .\ Pw_f^{*\,0.09}}{Gr_f^{0.256}\ Pr_f^{0.31}} \tag{5-15}$$

Eq. (5-15) reveals that the Nusselt number ratio depends rather strongly on Re_s/y and Gr_f and weakly on Pw^* and Pr for the same working fluid. For high flow rates and low heat fluxes, a large improvement in heat transfer coefficient is obtained. Since the Nusselt number for the empty tube flow is independent of Reynolds number, the usual coupling of augmented and empty tubes is not present. Hence, Eq. (5-15) is valid for a constraint of fixed flow rate, pressure drop, or pumping power. A Nusselt number ratio of 1.9 is achieved for ethylene glycol with $Re_s = 216.5$, $Gr_f = 2.708 \times 10^3$, $y = 5.08$, $Pr = 159$, and $Pw_f^* = 0.167$.

A practical interest frequently encountered in equipment design is to reduce exchanger size. This goal is usually associated with a fixed heat duty. With this objective and the constraint of fixed flow rate, pressure drop, pumping power, or fixed both flow rate and pressure drop, the Nusselt number ratio is obtained as follows:

$$\frac{A_o}{A_s} = \frac{N_o L_o}{N_s L_s} = \frac{Nu_s}{Nu_f}\Bigg|_{\Delta T,q} = \frac{0.851\ Pr^{0.35}\ (Re_s/y)^{0.622}\ Pw_f^{*\,0.072}}{Gr_f^{*\,0.204}\ Pr_f^{0.246}} \qquad (5\text{-}16)$$

where N_o and N_s are number of exchanger tubes for without twisted tape and with twisted tape, respectively. A length ratio, L_s/L_o of 0.37 is obtained for water with $Pr = 6.85$, $Re_s = 805.3$, $Gr_f^* = 1.69 \times 15^4$, $y = 2.45$ and $Pw_f^* = 0.386$ for fixed q and the constraint of fixed flow rate, pressure drop, or pumping power.

Concluding Remarks

An experimental study has been conducted to investigate heat transfer augmentation by means of a twisted tape insert in laminar flow. The investigation is focused on fully developed laminar flow heat transfer and pressure drop in horizontal tubes with uniform axial heat flux. The available test apparatus allowed maximum flexibility in testing various fluids and different twist ratio. The following conclusions may be drawn from the results presented in this chapter:

1. The Nusselt number is shown to be a function of tape twist ratio, Reynolds number, and Prandtl number.

2. The final heat transfer correlation is as follows:

$$Nu_s = 5.172 \left\{ 1 + 5.484 \times 10^{-3} \, Pr^{0.7} (Re_s/y)^{1.25} \right\}^{1/2} \qquad (5\text{-}7)$$

3. The present heat transfer correlation conflicts with the analytical predictions suggested by Date and Singham [75] and Date [129] for both high and low Prandtl number fluids, and is in good agreement only with the prediction for Pr = 100.

4. The constant-condition comparison of Nusselt numbers for tubes with twisted tape inserts and without tapes is given by Eq. (5-15). If the objective is to increase heat transfer rate, two to three times of heat transfer improvement might be achieved, depending on flow and heat conditions. With fixed heat duty, the exchanger may be reduced in size by inserting twisted tapes according to the ratio given in Eq. (5-16). The performance ratios are valid regardless of the constrain (constant

flow rate, constant pumping power, etc.).

5. The pressure drop data indicate that the friction factor depends mainly on Reynolds numbers, slightly on twist ratio and is independent of heat flux. The final correlation for friction factor is presented in Eq. (5-12).

Although this study has verified the application of the twisted tape insert technique for improvement of heat transfer, the following areas need further investigation:

1. The present heat transfer correlation development is based on the four sets of data for two working fluids and two twist ratio tapes. Even though the final result seems to be a good correlation of these data, a testing of higher viscosity fluids, under both heating and cooling conditions, would provide a more extensive check of the present correlation.

2. Tape fin and tube wall effects, which were ignored in this study, need further investigation.

3. Use of a visible glass tube with a twisted tape is recommended for further study of swirl flow in tubes.

4. Other heat transfer augmentation techniques, such as utilizing internally finned tubes or artificial roughness tubes, should be tested for comparison with the very effective twisted tape technique.

CHAPTER VI. CONCLUSIONS AND RECOMMENDATIONS

Laminar flow heat transfer with uniform heat flux in ordinary and augmented tubes has been studied analytically and experimentally to investigate 1. the effect of buoyancy on heat transfer in the thermal entry region of horizontal circular tubes; 2. the effects of temperature dependent properties, particularly density and viscosity, on heat transfer in the fully-developed region of horizontal circular tubes; 3. heat transfer for constant property flow in the thermal entrance region of semi-circular tubes; 4. and augmentation of heat transfer by means of twisted tape inserts. The following conclusions can be drawn from this study:

1a. An analytical solution for heat transfer in the entrance region of circular tubes was carried out assuming that a) density is the only temperature-dependent property, b) the fluid is characterized by a large Prandtl number, and c) the wall heat flux is uniform circumferentially and axially. The explicit DuFort-Frankel method was successfully applied to the set of governing partial differential equations (three-dimensional, non-linear, cylindrical, parabolic). An important consideration in the solution was to insure that the step size in the axial direction was limited by the stability criterion given in Eq. (2.64).

1b. The results indicate that the traditional constant property thermal entrance region solutions are valid only for very low heat fluxes associated with low Rayleigh numbers (less than 10^3) in which the temperature profiles are near parabolic. At higher Rayleigh numbers, $Ra_a^* = 10^6$ for example, the Nusselt number in the fully-developed region is about 200 percent above the constant property solution and the thermal entrance length is about

one-tenth that predicted by the constant property solution.

1c. Rayleigh number is the most significant parameter for correlating the heat transfer results. Increasing Rayleigh number decreases the thermal entrance length and increases Nusselt number. The final heat transfer results, Nusselt number versus reduced axial length with Ra_a^* as parameter, are presented in Fig. 2-12 and Appendix B.

2a. A new viscosity parameter, Be, defined in Eq. (3.3), has been successfully employed to study the temperature dependence of viscosity for laminar flow heat transfer. This parameter is derived directly from governing partial differential equations and can be utilized to correlate experimental data.

2b. A boundary layer solution was carried out for fully-developed laminar flow in a horizontal circular tube, assuming large Prandtl number and temperature-dependent viscosity and density. The Nusselt number is proportional to $Ra^{1/4}$ for both heat flux boundary conditions, and the proportional coefficient C_1 increases as Be increases. The Nusselt number for Be = 1.5 in Case 1 (heat flux uniform axially, wall temperature uniform circumferentially) and Be = 2.0 in Case 2 (heat flux uniform circumferentially and axially) are about 55 percent and 70 percent, respectively, higher than the constant viscosity predictions at the same Rayleigh number. The final correlations are given in Eqs. (3-66) and (3-68). In actual applications, the Nusselt number is expected to lie between these predictions, as demonstrated by a comparison with recent data.

3a. Laminar flow heat transfer in the thermal entrance region of a semicircular tube has been solved numerically for constant property fluid flow. The boundary conditions were chosen to approximate electrically heated

tubes with a strip insert: uniform heat flux and uniform circumferential wall temperature and uniform axial heat flux with uniform circumferential wall temperature except the insulated straight section. The final heat transfer results, Nusselt number versus reduced axial length, for both cases are presented in Fig. 4-5 and Appendix G. The asymptotic Nusselt numbers are 6.724 and 5.172 for the two respective boundary conditions.

4a. The heat transfer coefficient for laminar flow in a metal tube with two twisted tape inserts has been determined experimentally. The Nusselt number is shown to be a function of tape twist ratio, Reynolds number, and Prandtl number. The bulk temperature could not be improved upon as a reference temperature for evaluation of properties. Correlations of the data are given in Figs. 5-4 and 5-7.

4b. The present correlation of swirl flow generated by a twisted tape insert does not agree with the only available analytical prediction of Date and Singham [75]. The accuracy of their solution seems questionable.

4c. The pressure drop data with twisted tape inserts indicates that the friction factor depends mainly on Reynolds number, slightly on twist ratio, and is independent of heat flux. A correlation for friction factor is presented in Eq. (5-10).

4d. The constant condition comparison of Nusselt number for tubes with twisted tape inserts relative to empty tubes is given in Eq. (5-12). Several hundred percent improvements in heat transfer coefficient are readily achieved depending on flow and heating conditions.

Although the present investigation has resolved many questions concerning laminar flow heat transfer in horizontal tubes, the following areas

are recommended for further study:

1. The present thermal entrance region analysis considering buoyancy effects can be extended to curved and rotating pipes with centrifugal force and coriolis force effects, respectively.

2. Although the large Prandtl number assumption employed in Chapters II and III is shown to be valid even for water, a more general analysis including Prandtl number effects in the thermal entry and fully-developed regions could be worthy of investigation. The present analysis in Chapter II with uniform heat flux boundary condition can also be extended to the circumferentially uniform wall temperature boundary condition.

3. The numerical stability criterion given by Eq. (2-64) was obtained by employing the von Neumann condition for the present three-dimensional non-linear cylindrical coordinate system. The reason that numerical oscillation and divergence appeared after the fully developed condition is not clear; however, it appears that other investigators have observed similar behavior, generally without conceding that the results may be inaccurate. A further numerical stability analysis is necessary to verify the applicability of extending the available numerical schemes, namely ADI or DuFort-Frankel, to more complicated problems.

4. Two working fluids, water and ethylene glycol, have been used to verify the applicability of the new viscosity parameter, Be, to correlate experimental data in Chapter III. More experiments, using different working fluids with heating and cooling conditions, are required to verify that this parameter can be employed in general for correlation.

5. The heat transfer correlation developed in Chapter V is based on four sets of data for two working fluids and tapes with two twist ratios.

Even though the final correlation represents these data reasonably well, testing of higher viscosity fluids under both heating and cooling conditions with variable tape fin effects would be desirable.

6. Other heat transfer augmentation techniques, such as utilizing internally finned tubes and tubes with artificial roughness, should be studied.

REFERENCES

1. Sabersky, R. H. "Heat Transfer in the Seventies." International Journal of Heat and Mass Transfer 14 (1971): 1927-1949.

2. Shah, R. K., and London, A. L. "Thermal Boundary Conditions for Laminar Duct Flow Forced Convection Heat Transfer." Journal of Heat Transfer 96 (1974): 159-165.

3. Marco, S. M., and Han, L. S. "A Note on Limiting Laminar Nusselt Number in Ducts With Constant Temperature Gradient by Analogy to Thin Plate Theory." Transactions of ASME 77 (1955): 624-630.

4. Sparrow, E. M., and Siegel, R. S. "A Variational Method for Fully Developed Laminar Heat Transfer in Ducts." Journal of Heat Transfer 81 (1959): 157-167.

5. Reynolds, W. C. "Heat Transfer to Fully-Developed Laminar Flow in a Circular Tube With Arbitrary Circumferential Heat Flux." Journal of Heat Transfer 82 (1960): 108-112.

6. Cheng, K. C., "Analogy Solution of Laminar Heat Transfer in Non-Circular Ducts by Moire Method and Point Marching." Journal of Heat Transfer 88 (1966): 175-182.

7. Faris, G. N., and Viskanta, R. "An Analysis of Laminar Combined Forced and Free Convection Heat Transfer in a Horizontal Tube." International Journal of Heat and Mass Transfer 12 (1969): 1295-1309.

8. Graetz, L. "Über die Wärmeleitungsfähigkeit von Flüssigkeiten." Annalen der Physik 25 (1885): 337-357.

9. Clark, S. H., and Kays, W. M. "Laminar-Flow Forced Convection in Rectangular Tubes." Transactions of ASME 75 (1953): 859-866.

10. Kays, W. M. "Numerical Solutions for Laminar Flow Heat Transfer in Circular Tubes." Transactions of ASME 77 (1955): 1265-1274.

11. Sellars, J. R., Tribus, M., and Klein, J. S. "Heat Transfer to Laminar Flow in a Round Tube or Flat Conduit - The Graetz Problem Extended." Transactions of ASME 78 (1956): 441-448.

12. Siegel, R., Sparrow, E. M., and Hallman, T. M. "Steady Laminar Heat Transfer in a Circular Tube With Prescribed Wall Heat Flux." Applied Scientific Research A7 (1958): 386-392.

13. Singh, R. "Heat Transfer by Laminar Flow in a Cylindrical Tube." Applied Scientific Research A7 (1958): 325-340.

14. Sparrow, E. M., and Siegel, R. S. "Application of Variational Methods to the Thermal Entrance Region of Ducts." International Journal of Heat and Mass Transfer 1 (1960): 161-172.

15. Tien, C., and Pawelek, R. A. "Laminar Flow Heat Transfer in the Entrance Region of Circular Tubes." Applied Scientific Research A13 (1964): 317-331.

16. Hwang, C. L., and Fan L. T. "Finite Difference Analysis of Forced-Convection Heat Transfer in Entrance of a Flat Rectangular Duct." Applied Scientific Research A13 (1964): 401-422.

17. Ulrichson, D. L., and Schmitz, R. A. "Laminar-Flow Heat Transfer in the Entrance Region of Circular Tubes." International Journal of Heat and Mass Transfer 8 (1965): 253-258.

18. Hornbeck, R. W. "An All-Numerical Method for Heat Transfer in the Inlet of a Tube." ASME Paper No. 65-WA/HT-36 (1965).

19. Roy, D. N. "Development of Laminar Flow in Circular and Coaxial Tubes With and Without Heat Transfer." Ph.D. Thesis, University of Calcutta, Bengal Engineering College (1966).

20. McMordie, R. K., and Emery, A. F. "A Numerical Solution for Laminar Flow Heat Transfer in Circular Tubes with Axial Conduction and Developing Thermal and Velocity Field." Journal of Heat Transfer 89 (1967): 11-16.

21. Montgomery, S. R., and Wibuls "Laminar Flow Heat Transfer in Ducts of Rectangular Cross-Section." Proceedings of the Third International Heat Transfer Conference I (1966): 107-113.

22. Butterworth, D., and Hazell, T. D. "Forced Convective Laminar Flow Heat Transfer in the Entrance Region of a Tube." AERE-R 6057 (1969).

23. Manohar, R. "Analysis of Laminar-Flow Heat Transfer in Entrance Region of Circular Tubes." International Journal of Heat and Mass Transfer 12 (1969): 15-22.

24. Hsu, C. J. "An Exact Analysis of Low Peclet Number Thermal Entry Region Heat Transfer in Transversely Non-Uniform Velocity Fields." AICHE Journal 17 (1971): 732-740.

25. Deissler, R. G. "Analytical Investigation of Fully Developed Laminar Flow in Tubes With Heat Transfer With Fluid Properties Variable Along the Radius." NACA TN 2410 (1951).

26. Morton, B. R. "Laminar Convection in Uniformly Heated Horizontal Pipes at Low Rayleigh Number." Quarterly Journal of Mechanics and Applied Mathematics 12 (1959): 401-420.

27. Kettleborough, C. F. "Poiseuille Flow With Variable Fluid Properties." ASME Paper No. 66-WA/FE-22 (1966).

28. Koppel, L. A., and Smith, J. M. "Laminar Flow Heat Transfer for Variable Physical Properties." Journal of Heat Transfer 84 (1962): 157-163.

29. Bradley, D., and Entwistle, A. G. "Developed Laminar Flow Heat Transfer From Air for Variable Physical Properties." International Journal of Heat and Mass Transfer 8 (1965): 621-632.

30. Mori, Y., and Futagami, K. "Forced Convective Heat Transfer in Uniformly Heated Horizontal Tubes, 2nd Report - Theoretical Study." International Journal of Heat and Mass Transfer 10 (1967): 1801-1813.

31. Siegwarth, D. P., Mikesell, R. P., Readal, T. C., and Hanratty, T. J. "Effect of Secondary Flow on the Temperature Field and Primary Flow in a Heated Horizontal Tube." International Journal of Heat and Mass Transfer 12 (1969): 1535-1553.

32. Cheng, K. C., and Hwang, G. J. "Numerical Solution for Combined Free and Forced Laminar Convection in Horizontal Rectangular Channels." Journal of Heat Transfer 91 (1969): 59-66.

33. Newell, P. H., Jr., and Bergles, A. E. "Analysis of Combined Free and Forced Convection for Fully Developed Laminar Flow in Horizontal Tubes." Journal of Heat Transfer 92 (1970): 83-89.

34. Siegwarth, D. P., and Hanratty, T. T. "Computational and Experimental Study of the Effect of Secondary Flow on the Temperature Field and Primary Flow in a Heated Horizontal Tube." International Journal of Heat and Mass Transfer 13 (1970): 27-42.

35. Hwang, G. J., and Cheng, K. C. "Boundary Vorticity Method for Convective Heat Transfer With Secondary Flow - Application to the Combined Free and Forced Laminar Convection in Horizontal Tubes." Heat Transfer 1970 Vol. 4, NC35, Elsevier Publishing Company, Amsterdam (1970).

36. Martin, B. W., and Fargie, D. "Effect of Temperature-Dependent Viscosity on Laminar Forced Convection in the Entrance Region of a Circular Pipe." Proceedings of the Institution of Mechanical Engineers 186 (1972): 307-316.

37. Yang, K. T. "Laminar Forced Convection of Liquids in Tubes With Variable Viscosity." Journal of Heat Transfer 84 (1962): 353-362.

38. Rosenberg, D. E., and Hellums, J. D. "Flow Development and Heat Transfer in Variable Viscosity Fluids." I and EC Fundamentals 4 (1965): 417-422.

39. Test, F. L. "Laminar Flow Heat Transfer and Fluid Flow for Liquids With Temperature-Dependent Viscosity." Journal of Heat Transfer 90 (1968): 385-392.

40. Hwang, S. T., and Hong, S. W. "Effect of Variable Viscosity on Laminar Heat Transfer in a Rectangular Duct." Chemical Engineering Progress Symposium Series 66, No. 102 (1970): 100-108.

41. Schade, K. W., and McEligot, D. M. "Cartesian Graetz Problem With Air Property Variation." Journal of Heat Transfer 93 (1971): 432-440.

42. Swearingen, T. B., and McEligot, D. M. "Internal Laminar Heat Transfer With Gas-Property Variation." Journal of Heat Transfer 93 (1971): 432-440.

43. Cheng, K. C., Hong, S. W., and Hwang, G. J. "Buoyancy Effects on Laminar Heat Transfer in the Thermal Entrance Region of Horizontal Rectangular Channels With Uniform Wall Heat Flux for Large Prandtl Number Fluid." International Journal of Heat and Mass Transfer 15 (1972): 1819-1836.

44. Metzner, A. B. and Gluck, D. F. "Heat Transfer to Non-Newtonian Fluids under Laminar-Flow Conditions." Chemical Engineering Science 12 (1960): 185-190.

45. Oliver, D. R. and Jenson, V. G. "Heat Transfer to Pseudo-Plastic Fluids in Laminar Flow in Horizontal Tubes." Chemical Engineering Science 19 (1964): 115-129.

46. Mckillop, A. A. "Heat Transfer for Laminar Flow of Non-Newtonian Fluids in Entrance Region of a Tube." International Journal of Heat and Mass Transfer 7 (1964): 853-862.

47. DeYoung, S. H., and Scheele, G. J. "Natural Convection Distorted Non-Newtonian Flow in a Vertical Pipe." AIChE Journal 16 (1970): 712-717.

48. Hallman, T. M. "Combined Forced and Free-Laminar Heat Transfer in a Vertical Tube with Uniform Internal Heat Generation." Transactions of ASME 78 (1956): 1831-1841.

49. Lu, P. C. "Combined Free and Forced Convection Heat Generating Laminar Flow Inside Vertical Pipe with Circular Sector Cross Sections." Journal of Heat Transfer 82 (1960): 227-232.

50. Tao, L. N. "On Combined Free and Forced Convection in Channels." Journal of Heat Transfer 82 (1960): 233-238.

51. Rosen, E. M., and Hanratty, T. T. "Use of Boundary Layer Theory to Predict the Effect of Heat Transfer on the Laminar Flow Field in a Vertical Tube with a Constant Temperature Wall." AIChE Journal 7 (1961): 112-123.

52. Lawrence, W. T. "Entrance Flow and Transition from Laminar to Turbulent Flow in Vertical Tubes with Combined Free and Forced Convection." M.I.T. Engineering Project Laboratory Report No. DSR 9365 (1965).

53. Marner, W. J. "Combined Free and Forced Laminar Non-Newtonian Convection in a Vertical Tube." Ph.D. Thesis, College of Engineering, University of South Carolina (1969).

54. Allen, P. H. G., and Finn, A. H. "Profile Development with Mixed Convection in a High Prandtl Number Fluid." Journal of Heat Transfer 92 (1970): 299-304.

55. Zeldin, B., and Schmidt, F. W. "Developing Flow with Combined Forced and Free Convection in an Isothermal Vertical Tube." Journal of Heat Transfer 94 (1972): 211-223.

56. Iqbal, M., Aggarwala, B. D., and Khatry, A. K. "On the Conjugate Problem of Laminar Combined Free and Forced Convection through Vertical Non-Circular Ducts." Journal of Heat Transfer 94 (1972): 52-56.

57. Iqbal, M., and Stachiewicz, J. W. "Influence of Tube Orientation on Combined Free and Forced Laminar Convection Heat Transfer." Journal of Heat Transfer 88 (1966): 109-116.

58. Iqbal, M., and Stachiewicz, J. W. "Variable Density Effects in Combined Free and Forced Convection in Inclined Tubes." International Journal of Heat and Mass Transfer 10 (1967): 1625-1629.

59. Hong, S. W. "Numerical Solution for Combined Free and Forced Laminar Convection with and without Heat Sources in Inclined Tubes." Master of Science Thesis, Dept. of Mechanical Engineering, University of Alberta, Edmonton, Alberta, Canada (1971).

60. Cheng, K. C., and Hong, S. W. "Combined Free and Forced Laminar Convection in Inclined Tubes." Applied Scientific Research A27 (1972): 19-38.

61. Bergles. A. E. "Survey and Evaluation of Techniques to Augment Convective Heat Transfer." Progress in Heat and Mass Transfer Vol. 1, Edited by H. Grigull and E. Hahne. New York: Pergamon Press, 1969.

62. Bergles, A. E. "Recent Developments in Convective Heat Transfer Augmentation." Applied Mechanics Reviews 26 (1973): 675-682.

63. Cope, W. F. "The Friction Factor and Heat Transfer Coefficients of Rough Pipes." Proceedings of the Institution of Mechanical Engineers 145 (1941): 99-105.

64. Nunner, W. "Druckverlust and Wärmeübergang in Rauhen Rohren." VDI-Forschungsheft 22, No. 455, Series B (1956): 5-39. Also AERE Lib. Trans. 786 (1958).

65. Koch. R. "Druckverlust und Wärmeübergang bei Verwirbelter Strömung." VDI-Forschungsheft 24, No. 469, Series B (1958): 1-44.

66. Blumenkrantz, A., and Taborek, J. "Heat Transfer and Pressure Drop Performance of Turbotec Spirally-Grooved Tube in the Laminar and Transition Regime." Heat Transfer Research, Inc. Report No. 2439-300-8 (1971).

67. Zappa, R. F., and Geiger, G. E. "Effect of Artificial Surface Roughness on Heat Transfer and Pressure Drop for a High Prandtl Number Fluid in Laminar Flow." ASME Paper No. 71-HT-36 (1971).

68. DeLorenzo, B., and Anderson, E. D. "Heat Transfer and Pressure Drop of Liquids in Double Pipe in Tube Exchangers." ASME Paper No. 44-A-64 (1944).

69. Kun, L. C. "Friction Factor and Limiting Nusselt Number for Laminar Flow in Internally Finned Tubes by Means of Green's Fuction." Ph.D. Thesis, University of New York at Buffalo (1970).

70. Hu, M. H., and Chang, Y. P. "Optimization of Finned Tubes for Heat Transfer in Laminar Flow." ASME Paper No. 73-HT-M (1973).

71. Watkinson, A. P., Miletti, D. L., and Kubanek, G. R. "Heat Transfer and Pressure Drop of Forge-Fin Tubes in Laminar Oil Flow." Internal Report No. 3.3, Noranda Research Centre, Pointe Claire, Que. (1974).

72. Siegel, R., and Perlmutter, M. "Heat Transfer in Swirling Laminar Pipe Flow." Transactions of ASME 80 (1958): 295-297.

73. Penney, W. R. "The Spiralator - Initial Tests and Correlations." AIChE Preprint 16 for Eighth National Heat Transfer Conference (1965).

74. Kiya, M., and Fukusako, S. "Laminar Swirling Flow in the Entrance Region of a Circular Pipe." Journal of Japan Society of Mechanical Engineers (1971): 659-670.

75. Date, A. W., and Singham, J. R. "Numerical Prediction of Friction and Heat Transfer Characteristics of Fully Developed Laminar Flow in Tubes Containing Twisted Tapes." ASME Paper 72-HT-17 (1972).

76. Sununu, J. H. "Heat Transfer and Pressure Drop Characteristics of a Static, In Line Laminar Mixer." Kinecs Company Report (1971).

77. Genetti, W. E., and Priebe, S. J. "Heat Transfer With a Static Mixer." Proceedings of the Fourth Joint Chemical Engineering Conference, Vancouver, September, 1973.

78. Truesdell, L. C., and Adler, R. J. "Numerical Treatment of Fully Developed Laminar Flow in Helically Coiled Tubes." AICHE Journal 16 (1970): 1010-1014.

79. Dravid, A. N., Smith, K. A., Merrill, E. W., and Brian, P. L. T. "Effect of Secondary Flow Motion on Laminar Flow Heat Transfer in Helically Coiled Tubes." AICHE Journal 17 (1971): 1114-1122.

80. Akiyama, M., and Cheng, K. C. "Boundary Vorticity Method for Laminar Forced Convection Heat Transfer in Curved Pipes." International Journal of Heat and Mass Transfer 14 (1971): 1659-1675.

81. Singh, S. P. N. "Liquid Phase Heat Transfer in Helically Coiled Tubes." Ph.D. Thesis, Chemical Engineering Department, Oklahoma State University (1973).

82. Nakayama, W. "Forced Convective Heat Transfer in a Straight Pipe Rotating Around a Parallel Axis." International Journal of Heat and Mass Transfer 10 (1967): 1179-1194.

83. Mori, Y., and Nakayama, W. "Convective Heat Transfer in Rotating Radial Circular Pipes." International Journal of Heat and Mass Transfer 11 (1968): 1027-1039.

84. Miyazaki, H. "Combined Free and Forced Convective Heat Transfer and Fluid Flow in a Rotating Curved Circular Tube." International Journal of Heat and Mass Transfer 14 (1971): 1295-1309.

85. Scanlan, J. A. "Effects of Normal Surface Vibration on Laminar Forced Convection Heat Transfer." Industrial and Engineering Chemistry 50 (1958): 1565-1568.

86. Raben, I. "The Use of Acoustic Vibrations to Improve Heat Transfer." Proceedings of the 1961 Heat Transfer and Fluid Mechanics Institute. Stanford, Calif.: Stanford University Press, 1961.

87. Nevill, G. E., Commerford, G. E., and Raben, I. A. "Reduction in Convective Heat Transfer Due to Vibration." Journal of the Acoustical Society of America 35 (1960): 928-929.

88. Ogle, J. W., and Engel, A. J. "The Effect of Vibration on a Double-Pipe Heat Exchanger." AIChE Preprint No. 59 for the Sixth National Heat Transfer Conference, Boston (1963).

89. Schmidt, E., and Leidenfrost, W. "Der Einfluss Elektrisches Felder auf den Wärmetransport in Flussigen Elektrischen Nichleitern." VDI-Forschungsheft 19 (1953): 65-80.

90. Velkoff, H. R. "An Exploratory Investigation of the Effect of Ionization on the Flow and Heat Transfer with a Dense Gas." ASD-TDR-63-842 (1963).

91. Velkoff, H. R. "An Analysis of the Effect of Ionization on the Laminar Flow of a Dense Gas in a Channel." RTD-TDR-63-4009 (1963).

92. Levy, E. K. "Effects of Electrostatic Fields on Forced Convection Heat Transfer." S. M. Thesis in Mechanical Engineering, M.I.T. (1964).

93. Moss, R. A., and Grey, J. "Heat Tranfer Augmentation by Steady and Alternating Electric Fields." Proceedings of the 1966 Heat Transfer and Fluid Mechanics Institute. Stanford, Calif.: Stanford University Press, 1966.

94. Petukhov, B. S., and Polyakov, A. F. "Experimental Investigation of Viscogravitational Fluid Flow in a Horizontal Tube." High Temperature 5 (1967): 75-81.

95. Petukhov, B. S., and Polyakov, A. F. "Effect of Free Convection on Heat Transfer during Forced Flow in a Horizontal Tube." High Temperature 5 (1967): 351-384.

96. Bergles, A. E., and Simonds, R. R. "Combined Forced and Free Convection for Laminar Flow in Horizontal Tubes with Uniform Heat Flux." International Journal of Heat and Mass Transfer 14 (1971): 1989-2000.

97. Morcos, S. M., and Bergles, A. E. "Combined Forced and Free Laminar Convection in Horizontal Tubes." Technical Report No. 74008, HTL-1, Engineering Research Institute, Iowa State University (1974).

98. del Casal, E., and Gill, W. N. "A Note on Natural Convection Effects in Fully Developed Horizontal Tube Flow." AIChE Journal 8 (1962): 570-574.

99. Boussinesq, J. "Sur la Maniere Dent les Vitesses, Dans Tube Cylindrique de Section Circulaire, Evases a son Entree, se Distribuent Depuis Cette Entree Jusquaux Endroits ou se Trouve Establi un Regime Uniforme." Comptes Rendus 113 (1891): 49-59.

100. Mikesell, R. D. "The effect of Heat Transfer on the Flow in a Horizontal Pipe." Ph.D. Dissertation, University of Illinois, (1963).

101. Depew, C. A., and August, S. E. "Heat Transfer due to Combined Free and Forced Convection in a Horizontal and Isothermal Tube." Journal of Heat Transfer 97 (1971): 380-384.

102. Shilling, N. Z., and Progelhof, R. C. "Laminar Flow Heat Transfer for Gases in Constant Temperature Cylindrical Tubes at Low Wall to Bulk Temperature Ratios." Proceedings of the Society of Engineering Science Conference, North Carolina State University (1973).

103. Jackson, T. W., Spurlock, J. M., and Purdy, K. R. "Combined Free and Forced Convection in a Constant Temperature Horizontal Tube." AIChE Journal 7 (1961): 38-41.

104. Brown, A. R., and Thomas, M. A. "Combined Free and Forced Convection Heat Transfer for Laminar Flow in Horizontal Tubes." Journal of Mechanical Engineering Science 7 (1965): 440-448.

105. McComas, S. T., and Eckert, E. R. G. "Combined Free and Forced Convection in a Horizontal Circular Tube." Journal of Heat Transfer 88 (1966): 147-153.

106. Mori, Y., Futagami, K., Tokuda, S., and Nakamura, M. "Forced Convective Heat Transfer in Uniformly Heated Horizontal Tubes, 1st Report - Experimental Study on the Effect of Buoyancy." International Journal of Heat and Mass Transfer 12 (1969): 1535-1552.

107. Hussain, N. A., and McComas, S. T. "Experimental Investigation of Combined Convection in a Horizontal Circular Tube with Uniform Heat Flux." Heat Transfer 1970 4, Paper No. NC3.4. Amsterdam: Elsevier Publishing Company, 1970.

108. Lichtarowicz, A. "Combined Free and Forced Convection Effects in Fully Developed Laminar Flow in Horizontal Tubes." Heat and Mass Transfer by Combined Forced and Free Convection. London: Institution of Mechanical Engineers, 1972.

109. Ede, A. T. "The Heat Transfer Coefficient for Flow in a Pipe." International Journal of Heat and Mass Transfer 4 (1961): 105-110.

110. Petukhov, B. S., Polyakov, A. F., and Strigin, B. K. "Heat Transfer in Tubes with Viscous-gravity Flow." Heat Transfer, Soviet Research 1 (1969): 24-31.

111. Shannon, R. L., and Depew, C. A. "Combined Free and Forced Laminar Convection in a Horizontal Tube with Uniform Heat Flux." Journal of Heat Transfer 90 (1968): 353-357.

112. Shannon, R. L., and Depew, C. A. "Forced Laminar Flow Convection in a Horizontal Tube with Variable Viscosity and Free Convection Effects." Journal of Heat Transfer 91 (1969): 251-258.

113. McMordie, R. K., and Emery, A. F. "A Numerical Solution for Laminar Flow Heat Transfer in Circular Tubes with Axial Conduction and Developing Thermal and Velocity Fields." Journal of Heat Transfer 89 (1967): 11-16.

114. Schlichting, H. Boundary Layer Theory. Sixth Edition. New York: McGraw Hill Book Company, 1968.

115. DuFort, E. C., and Frankel, S. P. "Stability Conditions in the Numerical Treatment of Parabolic Differential Equations." Mathematical Tables Aids Computation 7 (1953): 135-153.

116. Peaceman, D. W., and Rachford, H. H., Jr. "The Numerical Solution of Parabolic and Elliptic Differential Equations." Journal Society of Industrial Applied Mathematics 3, No. 1 (1955): 28-41.

117. Douglas, J. Jr. "On the Numerial Integration of $\partial u/\partial t = \partial^2 y/\partial x^2 = \partial^2 u/\partial y^2$ by Implicit Method." Journal Society of Industrial Applied Mathematics 3, No. 1 (1955): 42-65.

118. Thomas, L. H. "Elliptic Problem in Linear Difference Equation Over a Network." Watson Scientific Computation Laboratory Report, Columbia University, New York (1949).

119. Pletcher, R. H. "On a Finite-Difference Solution for the Constant-Property Turbulent Boundary Layer." AIAA Journal 7, No. 2 (1969): 305-311.

120. O'Brien, G. G., Hyman, M. A., and Kaplan, S. "A Study of the Numerical Solution of Partial Difference Equations." Journal of Mathematics and Physics 29 (1951): 223.

121. Richtmyer, R. D., and Mortor, K. W. Difference Methods for Initial Value Problems. 2nd. Ed. New York: Interscience, 1967.

122. Fand, R. M., and Keswami, K. K. "The Influence of Property Variation on Forced Convection Heat Transfer to Liquids." International Journal of Heat and Mass Transfer 15 (1972): 1515-1536.

123. Sparrow, E. M. and Gregg, J. L. "Laminar Free Convection From a Vertical Plate with Uniform Surface Heat Flux." Transactions of ASME 78 (1956): 435-440.

124. Mischke, C. R., and Hall, J. L. "Computer Subroutine ME 0226, Iowa Cadet Algorithm." Mechanical Engineering Department, Iowa State University (1972).

125. Eckert, E. R. G., Irvine, T. F., and Yen, J. T. "Local Laminar Heat Transfer in Wedge-Shaped Passages." Transactions of ASME 80 (1958): 1433-1438.

126. Sparrow, E. M., and Haji-Sheikh, A. "Flow and Heat Transfer in Ducts of Arbitrary Shape with Arbitrary Thermal Boundary Conditions." Journal of Heat Transfer 88 (1966): 351-358.

127. Lopina, R. F., and Bergles, A. E. "Heat Transfer and Pressure Drop in Tape Generated Swirl Flow." M.I.T. Engineering Projects Laboratory Report DSR 70281-47 (1967).

128. Churchill, S. W., and Usagi, R. "A General Expression for the Correlation of Rates of Transfer and Other Phenomena." AIChE Journal 18 (1972): 1121-1128.

129. Date, A. W. "Prediction of Fully-Developed Flow in a Tube Containing a Twisted-Tape." International Journal of Heat Mass Transfer 17 (1974): 845-859.

130. Siegwarth, D. P. "Effect of Free Convection on Laminar Flow Through a Horizontal Pipe." Ph.D. Thesis, University of Illinois (1968).

131. Chen, S. S., Fan, L. T., and Hwang, C. C. "Entrance Region Flow of the Bingham Fluid in a Circular Pipe." AIChE Journal 16 (1970): 293-299.

132. Sylvester, N. D., and Rosen, S. L. "Laminar Flow in the Entrance Region of a Cylindrical Tubes." AIChE Journal 16 (1970): 964-972.

133. Skelland, A. H. Non-Newtonian Flow and Heat Transfer. New York: John Wiley and Sons, Inc., 1967.

134. Tien, C. "Laminar Natural Convection Heat Transfer from Vertical Plate to Power-Law Fluid." Applied Scientific Research A17 (1966): 233-248.

135. Dale, J. D., and Emery, A. F. "The Free Convection of Heat from a Vertical Plate to Several Non-Newtonian 'Pseudoplastic' Fluids." Journal of Heat Transfer 94 (1972): 64-72.

136. A.S.M.E. Steam Tables. New York: Author, 1967.

137. Union Carbide Corporation. Glycols. New York: Author, 1971.

ACKNOWLEDGMENTS

The author wishes to extend his sincere appreciation to:

- Dr. Arthur E. Bergles for his supervision of this work, his many helpful suggestions in directing this study, his editorial comments and recommendations concerning the reporting of this work, and his guidance during three years graduate studies.

- The National Science Foundation for financial support for the research assistantship and for the analytical and experimental program, through Grant GK-36851.

- The Department of Mechanical Engineering and the Engineering Research Institute, Iowa State University, and the School of Mechanical Engineering, Georgia Institute of Technology, for financial assistance during early stages of graduate study.

- Dr. Richard H. Pletcher for his helpful suggestions and discussions regarding numerical techniques.

- Professor Henry M. Black, Dr. William J. Cook, and Dr. Donald F. Young for their comments and suggestions during the Ph.D. program.

- Dr. Samy M. Morcos for providing the major part of the test apparatus, and for his helpful suggestions in carrying out the experimental work.

- Messrs. Leon Girard, Clifford Osam, and George Steininger for their assistance with the test apparatus.

- His wife for her constant encouragement and manuscript typing.

APPENDIX A.

COMPUTER PROGRAM FOR CHAPTER II

```
C
C
C
C     COMPUTER PROGRAM FOR CHAPTER II
C     BUOYANCY EFFECT ON THERMAL ENTRANCE REGION OF CIRCULAR TUBE LAMINAR FLOW
C

      DIMENSION W(21,21),U(21,21),T1(21,21),T2(21,21),T3(21,21),V(21,21)
     1,S(21,21),VO(21,21),R(21),CITA(21),ZA(21),ZB(21),ZC(21),AVS(21),BV
     2S(21),CVS(21),PVS(21),AR(21),BR(21),CR(21),DR(21),HZ(150),SHZ(150)
     3,SS(21,21),WU(21,21),NU1(150),NU2(150),NU12(150),SSS(21,21),TD(10)
     4,SD(10),WNU(21)
      COMMON HR,HR2,HC,HC2,OK,OMEG
      COMMON M,N,MI,NI,MD,ND
      REAL NU1,NU2,NU12
C
C
C     HONGT IS THE SUBROUTINE FOR SOLVING ENERGY EQUATION
C     HONGS IS THE SUBROUTINE FOR SOLVING MOMENTUM EQUATION
C     HONGNU IS THE SUBROUTINE FOR SOLVING NUSSELT NUMBER
C     HONGUV TO SOLVE SECONDARY VELOCITY U AND V
C     HONG MX TO SOLVE THE MAXIMUM VALUE
C     HONGCL TO FIND THE ISOTHERMAL LINE
C     HONGAV TO FIND THE AVERAGE VALUE
C
C

      READ(5,100,END=150) M,N,OK,OMEG,RA,EN,ENN
      WRITE(6,120) RA
C
C     RA IS RAYLEIGH NUMBER
C      W: AXIAL VELOCITY
C     U,V: SECONDARY VELOCITY IN RADIAL AND CIRCUMFERENTIAL DIRECTION
C     T1,T2,T3: THREE LEVEL OF TEMPERATURE
C     VO: VORTICITY FUNCTION
C     S: STREAM FUNCTION
C

      WRITE(6,121) M,N
      WRITE(6,122) OK,OMEG
      WRITE(6,123) EN,ENN
      WRITE(7,127) RA,M,N
      MI=M+1
      MD=M-1
      NI=N+1
      ND=N-1
      N2=N/2+1
      NO=1
      NOO=5
      SZZ=0.0
      Y=-EN
      DO 17 I=1,150
      HZ(I)=EXP(Y)
      SZZ=SZZ+HZ(I)
      SHZ(I)=SZZ
      Y=Y+ENN
   17 CONTINUE
      DO 10 J=1,NI
      DO 10 I=1,MI
      U(I,J)=0.0
      V(I,J)=0.0
      S(I,J)=0.0
      SS(I,J)=0.0
      VO(I,J)=0.0
      T1(I,J)=0.0
      T2(I,J)=0.0
      T3(I,J)=0.0
      W(I,J)=0.0
   10 CONTINUE
      HR=1.0/M
      HR2=HR**2
      PI=3.1415927
      HC=PI/N
      HC2=HC**2
      CITA(1)=0.0
```

```
      DO 9 J=2,NI
    9 CITA(J)=CITA(J-1)+HC
      R(1)=0.0
      DO 8 I=2,MI
      R(I)=R(I-1)+HR
      ZA(I)=HR/(2*R(I))
      ZB(I)=(HR/(HC*R(I)))**2
      ZC(I)=HR**2/(2*R(I)*HC)
      AVS(I)=1-ZA(I)
      BVS(I)=-2*(1+ZB(I))
      CVS(I)=1+ZA(I)
    8 CONTINUE
      AVS(MI)=2.0
      CVS(MI)=0.0
      PVS(2)=CVS(2)/BVS(2)
      DO 5 I=3,M
      PVS(I)=CVS(I)/( BVS(I)-AVS(I)*PVS(I-1))
    5 CONTINUE
      IM=1
      WRITE(6,136)
      WRITE(6,138) (HZ(I),I=1,150)
      WRITE(6,137)
      WRITE(6,138) (SHZ(I),I=1,150)
      DO 6 J=1,NI
      W(MI,J)=0.0
      DO 6 I=1,M
      W(I,J)=2*(1-R(I)**2)
    6 CONTINUE
      WRITE(6,139)
      WRITE(6,140) ((W(I,J),I=1,M),J=1,NI)
      IM=2
      DO 7 I=2,M
      AR(I)=(R(I+1)+2*R(I)+R(I-1))/(4*R(I)*HR2)
      BR(I)=1/((R(I)*HC)**2)
      CR(I)=(R(I+1)+R(I))/(2*R(I)*HR2)
      DR(I)=(R(I)+R(I-1))/(2*R(I)*HR2)
    7 CONTINUE
      SANZ=0.0
      KK=0
      WRITE(6,107)
      WRITE(6,118)
C
C
   20 IM=3
      CALL HONGT(T1,T2,T3,W,U,V,AR,BR,CR,DR,NO,ERRT,HZ,R)
      IF(NO.EQ.1) GO TO 11
      CALL HONGNUI(T1,T2,T3,W,NU1,NU2,NU12,NO,AGWT,AGWZ,BULKT,ENU,ABDT,
     CHZ,R)
      DWB=AGWT-BULKT
      ANZ=NU12(NN)*HZ(NN)
      SANZ=SANZ+ANZ
      ANU=SANZ/SHZ(NN)
      WRITE(6,109) NN,NU1(NN),NU2(NN),NU12(NN),AGWT,AGWZ,BULKT,ABDT,ENU,
     CERRT,NS,ERRS
      WRITE(6,117) HZ(NN),SHZ(NN),DWB,ANU
   11 IM=1
      IF(RA.EQ.0.0) GO TO 12
      CALL HONGS(S,VO,T3,RA,AVS,BVS,CVS,PVS,ERRS,NS,SS,CITA,ZA,ZB,ZC,R)
      CALL HONGUV(S,U,V,R)
      DO 15 J=1,NI
      AU11=U(1,J)+V(1,J)
      WU(1,J)=W(1,J)*HR/ABS(AU11)
      DO 15 I=2,M
      AU1=U(I,J)/HR+V(I,J)/(R(I)*HC)-1/(R(I)*HR)
      WU(I,J)=W(I,J)/ABS(AU1)
   15 CONTINUE
      ADZ=1.0
      DO 16 I=1,M
      DO 16 J=1,NI
      ADZ=AMIN1(ADZ,WU(I,J))
   16 CONTINUE
      ADZ=ADZ*(0.9)
      NOI=NO+1
      HZ(NOI)=AMIN1(HZ(NOI),ADZ)
```

```
      SHZ(NOI)=SHZ(NO)+HZ(NOI)
   12 IM=1
      IF(KK.GT.100) GO TO 99
      IF(ERRT.LT.0.0) KK=KK+1
      IF(NO.EQ.NOO) GO TO 14
      NO=NO+1
      NN=NO-1
      GO TO 20
   14 IM=1
      WRITE(6,108) NO
      WRITE(7,125) NO
      WRITE(6,101)
      WRITE(6,115) ((T3(I,J),I=1,M),J=1,NI)
      WRITE(6,124)
      WRITE(6,115) (T3(MI,J),J=1,NI)
      DO 25 J=1,NI
   25 WNU(J)=2.0/T3(MI,J)
      WRITE(6,128)
      WRITE(6,115) (WNU(J),J=1,NI)
      WRITE(7,126) (T3(I,1),I=1,MI)
      WRITE(7,126) (T3(I,NI),I=1,MI)
      WRITE(7,126) (T3(I,N2),I=1,MI)
      WRITE(7,126) (T3(MI,J),J=1,NI)
      IF(RA.EQ.0.0) GO TO 24
      WRITE(6,104)
      WRITE(6,110) ((U(I,J),I=1,M),J=1,NI)
      WRITE(6,105)
      WRITE(6,110) ((V(I,J),I=1,M),J=1,NI)
      WRITE(7,126) (U(I,1),I=1,MI)
      WRITE(7,126) (U(I,NI),I=1,MI)
      WRITE(7,126) (V(I,N2),I=1,MI)
      WRITE(6,103)
      WRITE(6,110) ((S(I,J),I=2,MI),J=1,NI,2)
      WRITE(6,106)
      WRITE(6,110) ((VO(I,J),I=2,MI),J=1,NI,2)
      CALL HONGMX(IT,JT,XAMT,TD,T3)
      CALL HONGCL(TD,T3)

      DO 22 I=1,MI
      DO 22 J=1,NI
      SSS(I,J)=ABS(S(I,J))
   22 CONTINUE
      CALL HONGMX(IS,JS,XAMS,SD,SSS)
      CALL HONGCL(SD,SSS)
   24 IM=1
      WRITE(6,116)
      WRITE(6,107)
      WRITE(6,118)
      NOC=NOO+5
      NO=NO+1
      NN=NO-1
      GO TO 20
C
   99 IM=1
C
      SANZ=0.0
      DO 23 I=1,NN
      ANZ=NU12(I)*HZ(I)
      SANZ=SANZ+ANZ
      ANU=SANZ/SHZ(I)
      IF(I.EQ.1) WRITE(6,141)
      WRITE(6,142) I,SHZ(I),NU12(I),ANU
   23 CONTINUE
  100 FORMAT(2I5,2F10.5,F10.1,2F5.2)
  101 FORMAT('0','TTT')
  103 FORMAT('0','SSS')
  104 FORMAT('0','UUU')
  105 FORMAT('0','VVV')
  106 FORMAT('0','VO')
  107 FORMAT('0','   NO','    NU1   ','    NU2   ','    NU12  ','   MEAN
     C TW','  D(TW)/DZ','   BULK T ','  (TW-T)*W','  (NU2-NU1)/NU2','
     C     DT/DZ  ',' NO S','    ERROR IN S')
  108 FORMAT('0','NO= ',I5)
  109 FORMAT(' ',I5,3F10.4,4F10.5,2E15.4,I5,E15.4)
  110 FORMAT(' ',10E13.5)
```

```
  115 FORMAT(10F13.6)
  116 FORMAT('0','**********************************************************
     C************************************************************')
  117 FORMAT(' ',40X,2E15.4,F15.6,F11.4)
  118 FORMAT(' ',49X,'HZ',12X,'SHZ',9X,'TW-TB',3X,'AVERAGE NU')
  120 FORMAT('1',//,31X,'RAYLEIGH NUMBER.....',F10.1
     C)
  121 FORMAT(' ',30X,'MESH SIZE M AND N .....',2I10)
  122 FORMAT(' ',30X,'OK AND RELAXATION FACTOR.....',F10.6,
     CF10.2)
  123 FORMAT(' ',30X,'EXP(-Y+DY*N) Y AND DY.....',2F10.2)
  124 FORMAT(' ','TTTHWW')
  125 FORMAT(' ',I5)
  126 FORMAT(8F10.5)
  127 FORMAT(' ',F10.1,2I5)
  128 FORMAT(' ','LOCAL NUSSELT NUMBER')
  136 FORMAT('0','  MARCHING STEP HZ ')
  137 FORMAT('0',' MARCHING LENGTH SHZ ')
  138 FORMAT(' ',10E13.6)
  139 FORMAT('0',' AXIAL VELOCITY W ')
  140 FORMAT(' ',10F13.6)
  141 FORMAT('1',40X,'NO',10X,'Z',10X,'NU',5X,'AVERAGE NU')
  142 FORMAT(' ',39X,I3,E16.6,F9.4,F11.4)
  150 STOP
      END



      SUBROUTINE HONGT(T1,T2,T3,W,U,V,AR,BR,CR,DR,NO,ERRT,HZ,R)
      DIMENSION T1(21,21),T2(21,21),T3(21,21),W(21,21),U(21,21),V(21,21)
     1,AR(21),BR(21),CR(21),DR(21),HZ(150),ZT(21,21),R(21)
      COMMON HR,HR2,HC,HC2,OK,OMEG
      COMMON M,N,MI,NI,MD,ND
      DO 5 J=1,NI
      DO 5 I=1,MI
      T1(I,J)=T2(I,J)
      T2(I,J)=T3(I,J)
    5 CONTINUE
      IF(NO.GT.1) GO TO 20
C
C     STANDARD EXPLICT METHOD
C
      CC1=1/HR2-V(1,1)/(2*HR)
      CC2=1/HR2+V(1,1)/(2*HR)
      CC3=(-1)*(W(1,1)/HZ(NO)-4/HR2)
      T3(1,1)=(CC1*T2(2,1)+CC2*T2(2,NI)+(2/HR2)*T2(2,N/2+1)+CC3*T2(1,1)
     C-2*W(1,1))/(W(1,1)/HZ(NO))
      DO 10 J=1,NI
      T3(1,J)=T3(1,1)
      DO 10 I=2,M
      B1=1/HR2+1/(2*R(I)*HR)-U(I,J)/(2*HR)
      B2=W(I,J)/HZ(NO)-2/HR2-2*BR(I)
      B3=1/HR2-1/(2*R(I)*HR)+U(I,J)/(2*HR)
      B4=BR(I)-V(I,J)/(2*R(I)*HC)
      B5=BR(I)+V(I,J)/(2*R(I)*HC)
      IF(J.EQ.1.OR.J.EQ.NI) GO TO 6
      T3(I,J)=(B1*T2(I+1,J)+B2*T2(I,J)+B3*T2(I-1,J)+B4*T2(I,J+1)+B5*T2(I
     C,J-1)-2*W(I,J))*HZ(NO)/W(I,J)
      GO TO 4
    6 I7=6
      IF(J.EQ.1) T3(I,J)=(B1*T2(I+1,J)+B2*T2(I,J)+B3*T2(I-1,J)+2*BR(I)*
     CT2(I,J+1)-2*W(I,J))*HZ(NO)/W(I,J)
      IF(J.EQ.NI) T3(I,J)=(B1*T2(I+1,J)+B2*T2(I,J)+B3*T2(I-1,J)+2*BR(I)*
     CT2(I,J-1)-2*W(I,J))*HZ(NO)/W(I,J)
    4 IM=4
```

```
   10 CONTINUE
      DO 9 J=1,NI
      T3(MI,J)=(18*T3(M,J)-9*T3(MD,J)+2*T3(M-2,J)+6*HR)/11
    9 CONTINUE
      ERRT=1.0
      GO TO 21
   20 IM=2
C
C
C     DU FORT FRANK METHOD
C
C
      Z1=HZ(NO-1)**2
      Z2=HZ(NO)**2
      Z12=HZ(NO-1)*HZ(NO)*(HZ(NO)+HZ(NO-1))
      Z21=Z2-Z1
      C1=W(1,1)*Z1/Z12+2/HR2
      C2=1/HR2-V(1,1)/(2*HR)
      C3=1/HR2+V(1,1)/(2*HR)
      C4=W(1,1)*Z2/Z12-2/HR2
      C5=W(1,1)*(Z2-Z1)/Z12
      T3(1,1)=(C2*T2(2,1)+C3*T2(2,NI)+(2/HR2)*T2(2,N/2+1)+C4*T1(1,1)-
     CC5*T2(1,1)-2*W(1,1))/C1
      DO 8 J=1,NI
      T3(1,J)=T3(1,1)
      DO 8 I=2,M
      AW1=W(I,J)*Z1/Z12
      AW2=W(I,J)*Z2/Z12
      AW3=W(I,J)*(Z2-Z1)/Z12
      AU=U(I,J)/(2*HR)
      AV=V(I,J)/(2*R(I)*HC)
      A1=AW1+AR(I)+BR(I)
      A2=CR(I)-AU
      A3=DR(I)+AU
      A4=BR(I)-AV
      A5=BR(I)+AV
      A6=AW2-AR(I)-BR(I)
      A7=A2*T2(I+1,J)+A3*T2(I-1,J)+A6*T1(I,J)-2*W(I,J)
      IF(J.EQ.1.OR.J.EQ.NI) GO TO 1
      A8=A4*T2(I,J+1)+A5*T2(I,J-1)
      GO TO 30
    1 IM=1
      IF(J.EQ.1) A8=(A4+A5)*T2(I,J+1)
      IF(J.EQ.NI) A8=(A4+A5)*T2(I,J-1)
   30 IM=1
      T3(I,J)=(A7+A8-AW3*T2(I,J))/A1
    8 CONTINUE
      DO 7 J=1,NI
      T3(MI,J)= (18*T3(M,J)-9*T3(MD,J)+2*T3(M-2,J)+6*HR)/11
    7 CONTINUE
      DO 22 J=1,NI
      DO 22 I=1,MI
      ZT(I,J)=(Z1*T3(I,J)-Z2*T1(I,J)+Z21*T2(I,J))/Z12
   22 CONTINUE
      CALL HONGAV(ZT,ERRT,R)
   21 IM=1
      RETURN
      END
```

```
      SUBROUTINE HONGS (S,VO,T,RA,AVS,BVS,CVS,PVS,ERRS,NS,SS,CITA,ZA,ZB,
     CZC,R)
      DIMENSION S(21,21),SS(21,21),VO(21,21),        T(21,21),AVS(21),
     1BVS(21),CVS(21),PVS(21),TRA(21,21),ZA(21),ZB(21),ZC(21),R(21),
     2CITA(21),DVO(21,21),QVO(21,21),DS(21,21),QS(21,21),VMI(3),SMI(3)
      COMMON HR,HR2,HC,HC2,OK,OMEG
      COMMON M,N,MI,NI,MD,ND
      NS=1
      DO 10 J=2,N
      DO 10 I=2,M
      TRA(I,J)=RA*HR2*(COS(CITA(J))*(T(I,J+1)-T(I,J-1))/(2*R(I)*HC)+SIN(
     CCITA(J))*(T(I+1,J)-T(I-1,J))/(2*HR))*(-1)
   10 CONTINUE
   14 IM=1
      DO 17 J=2,N
      K=0
      VMI(1)=0.0
   20 K=K+1
      VO(MI,J)=VMI(K)
      DO 9 I=2,M
      DVO(I,J)=TRA(I,J)-ZB(I)*(VO(I,J+1)+VO(I,J-1))
      IF(I.EQ.M) DVO(I,J)=DVO(M,J)-CVS(M)*VO(MI,J)
    9 CONTINUE
      QVO(2,J)=DVO(2,J)/BVS(2)
      DO 8 I=3,M
    8 QVO(I,J)=(DVO(I,J)-AVS(I)*QVO(I-1,J))/(BVS(I)-AVS(I)*PVS(I-1))
      VO(M,J)=QVO(M,J)
      DO 4 II=2,MD
      I=MI-II
    4 VO(I,J)=QVO(I,J)-PVS(I)*VO(I+1,J)
      DO 3 I=2,M
      DS(I,J)=(-1)*(ZB(I)*(SS(I,J-1)+SS(I,J+1)))+HR2*VO(I,J)
      IF(I.EQ.2) GO TO 2
      QS(I,J)=(DS(I,J)-AVS(I) *QS(I-1,J))/(BVS(I)-AVS(I)*PVS(I-1))
    2 QS(2,J)=DS(2,J)/BVS(2)
    3 CONTINUE
      DS(MI,J)=(-1)*(ZB(MI)*(SS(MI,J-1)+SS(MI,J+1)))+HR2*VO(MI,J)

      QS(MI,J)=(DS(MI,J)-AVS(MI)*QS(M,J))/(BVS(MI)-AVS(MI)*PVS(M))
      SMI(K)=QS(MI,J)
      IF(K-2) 50,51,52
   50 VMI(2)=-100.0
      GO TO 20
   51 VMI(3)=100*SMI(1)/(SMI(2)-SMI(1))
      GO TO 20
   52 SS(MI,J)=SMI(K)
      DO 18 II=1,MD
      I=MI-II
   18 SS(I,J)=QS(I,J)-PVS(I)*SS(I+1,J)
   17 CONTINUE
      SD=0.0
      SUM=0.0
      DO 15 I=1,MI
      DO 15 J=1,NI
      SSD=SS(I,J)-S(I,J)
      SD=SD+ABS(SSD)
      SUM=SUM+ABS(SS(I,J))
   15 CONTINUE
      IF(SUM.EQ.0.0) SUM=0.0000001
      ERRS=SD/SUM
      IF(ERRS.LT.OK) GO TO 16
      DO 78 J=2,N
      DO 78 I=2,MI
      DI=OMEG*(SS(I,J)-S(I,J))
      S(I,J)=S(I,J)+DI
   78 CONTINUE
    7 NS=NS+1
      GO TO 14
   16 IM=2
      RETURN
      END
```

```
      SUBROUTINE HONGUV(S,U,V,R)
      DIMENSION S(21,21),U(21,21),V(21,21),R(21)
      COMMON HR,HR2,HC,HC2,OK,OMEG
      COMMON M,N,MI,NI,MD,ND
      DO 10 I=2,M
      RH6=R(I)*HC*6
      RH12=R(I)*HC*12
      U(I,1)=(8*S(I,2)-S(I,3))/RH6
      U(I,2)=(-S(I,2)+8*S(I,3)-S(I,4))/RH12
      U(I,NI)=(S(I,ND)-8*S(I,N))/RH6
      U(I,N)=(S(I,N-2)-8*S(I,ND)+S(I,N))/RH12
      DO 10 J=3,ND
      U(I,J)=(S(I,J-2)-8*S(I,J-1)+8*S(I,J+1)-S(I,J+2))/RH12
   10 CONTINUE
      HR12=HR*12
      DO 9 J=2,N
      V(2,J)=(10*S(2,J)-18*S(3,J)+6*S(4,J)-S(5,J))/HR12
      V(M,J)=(S(M-3,J)-6*S(M-2,J)+18*S(M-1,J)-10*S(M,J)-3*S(M+1,J))/HR12
      DO 9 I=3,MD
      V(I,J)=(S(I+2,J)-8*S(I+1,J)+8*S(I-1,J)-S(I-2,J))/HR12
    9 CONTINUE
      V(1,1)=(8*S(2,N/2+1)-S(3,N/2+1))/(6*HR)*(-1)
      DO 8 J=1,NI
      U(1,J)=0.0
    8 V(1,J)=V(1,1)
      DO 7 I=2,MI
      V(I,1)=0.0
    7 V(I,NI)=0.0
      RETURN
      END
      SUBROUTINE HONGNU(T1,T2,T3,W,NU1,NU2,NU12,III,AVEWT,AVGZW,AVGBT,
     CENU,ABDT,HZ,R)
      DIMENSION T1(21,21),T2(21,21),T3(21,21),W(21,21),GZW(21,21),HZ(150
     1),WT(21,21),DWT(21,21),GT(21),NU1(150),NU2(150),NU12(150),R(21)
      COMMON HR,HR2,HC,HC2,OK,OMEG
      COMMON M,N,MI,NI,MD,ND
      REAL NU1,NU2,NU12,NU0

      PI=3.1415927
      NU0=4.364
      II=III-1
      AVEWT=0.0
      DZ1=HZ(III-1)**2
      DZ2=HZ(III)**2
      DZ12=HZ(III-1)*HZ(III)
      DZ22=HZ(III)+HZ(III-1)
      DO 20 J=1,NI
      DO 20 I=1,MI
      WT(I,J)=W(I,J)*T2(I,J)
      GZW(I,J)=(T3(I,J)*DZ1-T1(I,J)*DZ2-T2(I,J)*(DZ1-DZ2))*W(I,J)/(DZ12*
     CDZ22)
   20 CONTINUE
      CALL HONGAV(WT,AVGBT,R)
      CALL HONGAV(GZW,AVGZW,R)
      SWT=0.0
      SWT=SWT+T2(MI,1)+T2(MI,NI)
      DO 19 J=2,N,2
   19 SWT=SWT+T2(MI,J)*4
      DO 18 J=3,ND,2
   18 SWT=SWT+T2(MI,J)*2
      AVEWT=SWT*HC/(3*PI)
      DO 17 J=1,NI
      DO 17 I=1,MI
   17 DWT(I,J)=(AVEWT-T2(I,J))*W(I,J)
      CALL HONGAV(DWT,ABDT,R)
      NU1(II)=2/AVEWT
      NU2(II)=(2+AVGZW)/ABDT
      NU12(II)=(NU1(II)+NU2(II))/2
      IF(II.EQ.1) GO TO 22
      ENU=(NU1(II)-NU1(II-1))/NU1(II)
      ENU=ABS(ENU)
      GO TO 23
   22 ENU=1.0
   23 IM=1
      RETURN
      END
```

```
      SUBROUTINE HONGAV(E,AVG,R)
      DIMENSION EI(21),E(21,21),R(21)
      COMMON HR,HR2,HC,HC2,DK,OMEG
      COMMON M,N,MI,NI,MD,ND
      PI=3.1415927
      DO 7 I=1,MI
      EI(I)=E(I,1)+E(I,NI)
      DO 6 J=2,N,2
    6 EI(I)=EI(I)+E(I,J)*4
      DO 5 J=3,ND,2
    5 EI(I)=EI(I)+E(I,J)*2
      EI(I)=HC*EI(I)/3
    7 CONTINUE
      SE=0.0
      SE=SE+EI(1)*R(1)+EI(MI)*R(MI)
      DO 4 I=2,M,2
    4 SE=SE+EI(I)*R(I)*4
      DO 3 I=3,MD,2
    3 SE=SE+EI(I)*R(I)*2
      AVG=HR*SE*2/(3*PI)
      RETURN
      END
      SUBROUTINE HONGMX(II,JJ,MAXTS,DE,ST)
      COMMON HR,HR2,HC,HC2,DK,OMEG
      COMMON M,N,MI,NI,MD,ND
      REAL MAXST,MAXTS,MINST,MINTS,DE(10),ST(21,21)
      MINST=0.0
      MAXST=0.0
      DO 1 J=1,NI
      DO 1 I=1,MI
      SC=ST(I,J)
      IF(MAXST.LT.SC) II=I
      IF(MAXST.LT.SC) JJ=J
      MAXST=AMAX1(MAXST,ST(I,J))
      MINST=AMIN1(MINST,SC)
    1 CONTINUE
      MAXTS=MAXST
      MINTS=MINST
      MAXST=MAXST-MINST
      EH=0.0
      NJ=1
    7 IM=2
      IF(MAXST.LT.0.00001.OR.MAXST.GT.100.0) GO TO 50
      IF(MAXST.GE.0.00001.AND.MAXST.LT.0.0001) DB=0.00001
      IF(MAXST.GE.0.0001.AND.MAXST.LT.0.001) DB=0.0001
      IF(MAXST.GE.0.001.AND.MAXST.LT.0.01) DB=0.001
      IF(MAXST.GE.0.01.AND.MAXST.LT.0.1) DB=0.01
      IF(MAXST.GE.0.1.AND.MAXST.LT.1.0) DB=0.1
      IF(MAXST.GE.1.0.AND.MAXST.LT.10.0) DB=1.0
      IF(MAXST.GE.10.D.AND.MAXST.LE.100.0) DB=10.0
      DA=DB
      DO 4 I=2,9
      DM=AMIN1(MAXST,DA)
      IF(DM.EQ.DA) DD=DM
      DA=DB*I
    4 CONTINUE
      EH=DD+EH
      IF(NJ.EQ.2) GO TO 8
      MAXST=MAXST-DD
      NJ=NJ+1
      GO TO 7
    8 DC=EH/10.0
      DO 5 J=1,10
      DE(J)=DC*J
    5 CONTINUE
   50 IM=1
      WRITE(6,100) MAXTS,II,JJ
  100 FORMAT('0',20X,'MAXIMUM VALUE IS',E18.6,5X,'IN I-D',I5,'     IN J-
     CO',I5)
      RETURN
      END
```

```
      SUBROUTINE HONGCL(CF,F)
      COMMON HR,HR2,HC,HC2,OK,OMEG
      COMMON M,N,MI,NI,MD,ND
      DIMENSION CF(10),F(21,21),DF(21),CJ(21),PF(21),RI(21),PJ(21),QI(21
     1)
      DI =1.5
      DJ=9.0
      DO 6 K=1,10
      WRITE(6,120) K,CF(K)
      DO 81 I=1,MI
      JK=1
      IF(I.GE.2) GO TO 93
      WRITE(6,105)
   93 DF(1)=CF(K)-F(I,1)
      DO 83 J=2,NI
      DF(J)=CF(K)-F(I,J)
      EE=DF(J)*DF(J-1)
      IF(EE.GT.0.0) GO TO 83
      EF=DF(J-1)/(F(I,J)-F(I,J-1))
      CJ(JK)=J-1+EF
      JK=JK+1
   83 CONTINUE
      IF(JK.EQ.1) GO TO 81
      JKD=JK-1
      QI(I)=DI*(I-1)
      WRITE(6,107) I,QI(I),(CJ(JK),JK=1,JKD)
   81 CONTINUE
      DO 71 J=1,NI
      IK=1
      IF(J.GE.2) GO TO 74
      WRITE(6,108)
   74 PF(1)=CF(K)-F(1,J)
      DO 72 I=2,MI
      PF(I)=CF(K)-F(I,J)
      QF=PF(I)*PF(I-1)
      IF(QF.GT.0.0) GO TO 72
      RF=PF(I-1)/(F(I,J)-F(I-1,J))
      RI(IK)=I-1+RF
      IK=IK+1
   72 CONTINUE
      IF(IK.EQ.1) GO TO 71
      IKD=IK-1
      PJ(J)=DJ*(J-1)
      WRITE(6,107) J,PJ(J),(RI(IK),IK=1,IKD)
   71 CONTINUE
    6 CONTINUE
  105 FORMAT('0',30X,'COORDINATE IN R-DIRECTION',20X,'IN CITA DIRECTION'
     C)
  107 FORMAT(' ',30X,I5,5X,F10.4,20X,4F10.4)
  108 FORMAT('0',30X,'COORDINATE IN CITA DIRECTION',20X,'R-DIRECTION')
  120 FORMAT('0',20X,'NO OF CONSTANT LINE ',10X,I5,10X,'CONSTANT VALUE',
     C10X,F20.5)
      RETURN
      END
```

APPENDIX B.

NUMERICAL RESULTS FOR CHAPTER II

$Ra_a^* = 0$		10^3		10^4		5×10^4	
$z \times 10^3$	Nu	$z \times 10^3$	Nu	$z \times 10^3$	Nu	$z \times 10^3$	Nu
0.3355	47.65	0.3355	47.65	0.3355	47.65	0.3355	47.65
0.6881	32.07	0.7062	31.48	0.7062	31.48	0.7062	31.48
1.059	25.21	1.116	24.46	1.116	24.46	1.116	24.46
1.858	18.69	1.569	20.39	1.569	20.39	1.569	20.39
2.741	15.63	2.069	17.82	2.069	17.82	2.069	17.82
3.718	13.76	2.622	16.02	2.622	16.02	2.622	16.03
4.798	12.45	3.234	14.64	3.909	13.55	3.234	14.64
5.990	11.46	3.909	13.55	5.481	11.90	4.656	12.70
7.308	10.67	4.656	12.65	7.400	10.68	6.062	11.67
8.765	10.01	5.481	11.90	9.745	9.723	7.110	10.83
10.38	9.450	7.400	10.68	12.61	8.942	7.997	10.32
12.15	8.963	9.745	9.714	15.77	8.393	8.792	10.01
14.12	8.533	12.61	8.924	18.29	7.978	9.528	9.794
16.29	8.151	16.11	8.258	20.40	7.627	10.22	9.627
18.70	7.807	20.38	7.687	22.27	7.377	10.88	9.492
21.35	7.494	25.60	7.191	23.99	7.203	11.20	9.433
24.28	7.209	31.97	6.757	25.61	7.086	11.83	9.330
27.53	6.948	39.64	6.382	27.15	6.999	12.44	9.243
31.11	6.708	47.45	6.071	28.62	6.929	13.03	9.169
35.07	6.486	55.12	5.808	30.04	6.871	13.91	9.077
39.44	6.281	62.63	5.593	31.42	6.822	14.77	9.004
44.28	6.090	70.02	5.419	32.77	6.780	15.61	8.944
49.63	5.913	77.30	5.276	34.09	6.744	16.45	8.896
55.53	5.748	84.47	5.156	35.40	6.713	17.29	8.857
62.06	5.594	91.56	5.055	36.68	6.686	18.68	8.807
69.28	5.451	98.57	4.971	37.95	6.662	19.79	8.777
77.25	5.318	105.5	4.901	39.21	6.642	20.64	8.760
86.07	5.193	112.4	4.843	40.47	6.625	21.49	8.745

$Ra_a^* = 0$		10^3		10^4		5×10^4	
$z \times 10^3$	Nu	$z \times 10^3$	Nu	$z \times 10^3$	Nu	$z \times 10^3$	Nu
95.81	5.077	119.2	4.795	41.72	6.610	22.36	8.733
106.6	4.969	126.0	4.756	42.96	6.598	22.94	8.726
118.5	4.869	132.8	4.727	44.20	6.588	24.13	8.715
131.2	4.776	139.5	4.706	45.44	6.580	25.05	8.709
146.1	4.690	146.2	4.693	46.68	6.574	25.98	8.704
162.2	4.612			47.92	6.570	26.94	8.700
178.0	4.540			49.16	6.568	29.72	8.694
199.6	4.476			49.79	6.567		
221.2	4.418						
245.2	4.367 *						

*Last value of Nu corresponds to fully developed condition defined in Eq. (2-56).

$Ra_a^* = 10^5$		3×10^5		5×10^5		10^6	
$z \times 10^3$	Nu	$z \times 10^3$	Nu	$z \times 10^3$	Nu	$z \times 10^3$	Nu
0.3355	47.65	0.335	47.65	0.3355	47.65	0.3355	47.65
0.7062	31.48	0.7062	31.48	0.7062	31.48	0.7062	31.48
1.116	24.46	1.116	24.46	1.116	24.54	1.116	26.01
1.569	20.39	1.569	20.54	1.547	21.39	1.322	23.02
2.069	17.83	2.002	18.64	1.801	19.51	1.466	20.95
2.622	16.04	2.304	17.32	1.994	18.00	1.588	19.91
3.234	14.80	2.544	16.15	2.161	17.15	1.701	19.48
3.780	14.02	2.755	15.44	2.315	16.75	1.805	19.05
4.233	13.34	2.948	15.05	2.458	16.41	1.905	18.75
4.605	12.72	3.129	14.75	2.593	16.15	2.000	18.46
5.270	11.98	3.464	14.31	2.848	15.71	2.181	18.04
5.855	11.58	3.775	13.98	3.088	15.39	2.354	17.72
6.393	11.30	4.070	13.72	3.317	15.14	2.522	17.48
6.896	11.08	4.353	13.52	3.539	14.95	2.686	17.28
7.376	10.91	4.628	13.36	3.756	14.79	2.847	17.12
7.837	10.77	4.896	13.23	4.180	14.55	3.165	16.81
8.285	10.65	5.159	13.12	4.492	14.41	3.401	16.72
8.721	10.55	5.549	12.98	4.803	14.30	3.638	16.59
9.149	10.47	5.934	12.87	5.320	14.14	4.033	16.41
9.571	10.40	6.316	12.78	5.839	14.02	4.435	16.26
10.22	10.31	6.698	12.70	6.368	13.91	4.847	16.12
10.81	10.24	7.206	12.62	6.910	13.82	5.271	16.00

Ra_a^* = 10^5		3×10^5		5×10^5		10^6	
$z \times 10^3$	Nu	$z \times 10^3$	Nu	$z \times 10^3$	Nu	$z \times 10^3$	Nu
11.43	10.18	7.849	12.52	8.046	13.67	5.710	15.89
12.04	10.13	8.505	12.45	8.646	13.60	6.165	15.79
12.65	10.09	9.178	12.39	9.272	13.53	7.133	15.61
13.26	10.06	9.872	12.33	10.62	13.41	8.199	15.43
13.87	10.03	11.34	12.23	12.12	13.30	9.378	15.27
14.70	9.993	12.95	12.14	13.82	13.20	10.58	15.17
15.76	9.959	14.74	12.06	17.41	13.05	11.14	15.03
16.85	9.930	16.77	11.99	18.67	13.01	14.86	14.89
17.98	9.906	19.09	11.93				
20.39	9.867	20.49	11.89				
24.38	9.854						

APPENDIX C.

DERIVATION OF DIMENSIONLESS GROUPS FOR CORE AND BOUNDARY LAYER EQUATIONS

The derivation of the present non-dimensional groups is based on similar derivations from Ref. 130 in which a natural convection boundary layer along a uniformly heated plate has been considered to obtain the characteristic variables. Therefore, the derivation will start from a study of steady boundary layer laminar flow along a vertical plate heated to a uniform temperature T_w.

The dimensional equations that govern the natural laminar convection along a vertical plate, with no dissipation, are given as follows:

$$\frac{\partial U}{\partial X} + \frac{\partial V}{\partial Y} = 0$$

$$U \frac{\partial U}{\partial X} + V \frac{\partial U}{\partial Y} = g\beta(T - T_\infty) + \frac{\mu}{\rho} \frac{\partial^2 U}{\partial Y^2}$$

$$\rho C_p \left[U \frac{\partial T}{\partial X} + V \frac{\partial T}{\partial Y} \right] = k \frac{\partial^2 T}{\partial Y^2} \qquad \text{(C-1)}$$

The X-axis is parallel to the plate, and the origin is at the bottom edge. The Y axis is perpendicular to the plate, with the origin at the plate surface. The velocities U and V are in the X and Y direction velocity components, respectively. The boundary conditions are as follows:

$Y = 0,\ U = V = 0,\ T = T_w$ (uniform wall temperature) (C-2)

$Y = \infty,\ U = V = 0,\ T = T_\infty$

Boundary Layer Region

The following dimensionless variables are introduced:

$$x = \frac{X}{L}, \qquad y = \frac{Y}{\Delta_T}$$

$$u = \frac{U}{U_c}, \qquad v = \frac{V}{V_c} \tag{C-3}$$

$$\phi = \frac{T - T_\infty}{\Delta T}$$

The symbol ΔT will be used to represent the temperature difference $T_w - T_\infty$.

The following hypotheses can be made about the thermal boundary layer:

(1) Both terms in the continuity equation are of the same order of magnitude.

(2) The buoyancy and viscous terms in the X-momentum equation are of the same order of magnitude.

(3) The X and Y convection terms and the conduction terms in the energy equation are of the same order of magnitude.

These hypotheses lead to the following relationships:

$$\frac{U_c}{L} = \frac{V_c}{\Delta_T} \tag{C-4}$$

$$g\beta\Delta T = \frac{\mu U_c}{\rho \Delta_T^2}$$

$$\frac{U_c}{L} = \frac{k}{\rho C_p \Delta_T^2}$$

Solving Eqs. (C-4) simultaneously yields:

$$\Delta_T = \frac{L}{(Gr_L Pr)^{1/4}}$$

$$U_c = \frac{\mu}{\rho L}\left(\frac{Gr_L}{Pr}\right)^{1/2} \qquad \text{(C-5)}$$

$$V_c = \frac{\mu}{\rho L}\left(\frac{Gr_L}{Pr^3}\right)^{1/4}$$

It is noted that Eqs. (C-5) are similar to Eqs. (3-22), from which one obtains the dimensionless variables.

Hydrodynamic Boundary Layer

The dimensionless variables for hydraulic boundary layer are defined as follows:

$$\hat{x} = \frac{X}{L}, \qquad \hat{y} = \frac{Y}{\Delta_h}$$

$$u = \frac{U}{U_h}, \qquad v = \frac{V}{V_h} \qquad \text{(C-6)}$$

$$\phi = \frac{T - T_\infty}{\Delta T}$$

The following hypotheses can be made about the viscous boundary layer:

(1) Both terms in the continuity equation are of the same order of magnitude.

(2) The viscous term and inertia term in the X-momentum equation are of the same order of magnitude.

(3) The characteristic velocity in the hydrodynamic boundary layer, U_h, is the same order of magnitude as U_c.

These hypotheses lead to the following relationships:

$$U_h = U_c = \frac{\mu}{\rho L}\left(\frac{Gr_L}{Pr}\right)^{1/2}$$

$$\frac{(U_h)^2}{L} = \frac{\mu\, U_h}{\rho\, \Delta_h^2} \qquad \text{(C-7)}$$

$$\frac{U_h}{L} = \frac{V_h}{\Delta_h}$$

Solving Eqs. (C-7) simultaneously yields:

$$\Delta_h = L\left(\frac{Pr}{Gr_L}\right)^{1/4}$$

$$V_h = \frac{\mu}{\rho L}\left(\frac{Gr_L}{Pr}\right)^{1/4} \qquad \text{(C-8)}$$

$$U_h = \frac{\mu}{\rho L}\left(\frac{Gr_L}{Pr}\right)^{1/2}$$

From Eqs. (C-5) and (C-7), one obtains

$$\frac{\Delta_h}{\Delta_T} = (Pr)^{1/2} \qquad \text{(C-9)}$$

For large Prandtl number flow, one therefore concludes that the hydrodynamic boundary layer is much thicker than the thermal boundary layer and can be neglected.

Core Region

The characteristic velocity in the core region can be calculated by equating the mass flow in the thermal boundary layer $\bar{\delta}\, U_c$ to the mass flow down in the core, $aU_c^+ \sin x$. Therefore, U_c^+ is obtained and the result is:

$$U_c^+ = \frac{\mu}{a\rho} (Gr/Pr^3)^{1/4} \qquad \text{(C-10)}$$

Equation (C-10) was employed to obtain the dimensionless Eq. (3-14) in the core region.

APPENDIX D.

COMPUTER PROGRAM FOR CHAPTER III

```
C
C
C
C     COMPUTER PROGRAM FOR CHAPER III
C     COMBINED FORCED AND FREE LAMINAR CONVECTION WITH TEMPERATURE DEPENDENT
C     VISCOSITY IN HORIZONTAL TUBES
C
C     HONG1: SUBROUTINE FOR SOLVING BOUNDARY LAYER EQUATION AND HEAT TRANSFER
C
      REAL K1,K2,K3,K4
      DIMENSION X(501),DX(501),EX(501),X3(501),FX(501),Y(501)
   99 READ(5,100,END=200) M,N,BE,RA
      MI=M+1
      PI=3.1415927
      HX=PI/M
      MD=M-1
      CALL HONG1(N,BE,A1)
      WRITE(6,105) A1,M
      A1=ABS(A1)
      X(1)=0.0
      DO 10 I=2,MI
   10 X(I)=X(I-1)+HX
      Y(1)=(3.0/(2*A1))**(1.0/4.0)
      Y(2)=Y(1)
      DO 18 I=2,M
      II=I+1
      AX1=X(I)
      AY1=Y(I)
      K1=1.0/(2*A1*SIN(AX1)*AY1**3)-(COS(AX1)/SIN(AX1))*AY1/3
      AX2=X(I)+HX/2
      AY2=Y(I)+HX*K1/2
      K2=1.0/(2*A1*SIN(AX2)*AY2**3)-(COS(AX2)/SIN(AX2))*AY2/3
      Y(II)=Y(I)+HX*K2
   18 CONTINUE
      WRITE(6,103)
      WRITE(6,101) (Y(I),I=1,MI)
      DO 19 I=1,MI
   19 EX(I)=1.0/Y(I)
      SUMX=EX(1)+EX(MI)
      DO 20 I=2,M,2
   20 SUMX=SUMX+EX(I)*4
      DO 21 I=3,MD,2
   21 SUMX=SUMX+EX(I)*2
      AVG=HX*SUMX/3.0
      ANU=(3.0*AVG)/PI
      WRITE(6,102) AVG,A1
      WRITE(6,104) ANU,BE
      GO TO 99
  100 FORMAT(2I5,F10.5,F10.1)
  101 FORMAT(' ',10E12.5)
  102 FORMAT('0','AVERAGE',5X,F20.6,5X,'A1',F20.6)
  103 FORMAT('0','DEL FUNCTION')
  104 FORMAT('0','COEFFICENT OF NUSSELT NUMBER',F20.6,5X,'BERGLES NUMBER
     C',F10.3)
  105 FORMAT('0','A1',F15.6,5X,'SIZE',I5)
  200 STOP
      END
```

```
      SUBROUTINE HONG1(N,BE,A1)
C     SOLUTION OF SIMULTANEOUS ALGEBRAIC EQUATIONS BY GAUSSIAN ELIMINATI
C     ON.  N IS THE NUMBER OF EQUATIONS.  A(I,J) IS THE COEFFICIENT MATR
C     IX OF THE EQUATIONS.  I IS THE EQUATION NO., J IS THE COEF. NUMBER
      DIMENSION A(20,21),B(20,21),X(20)
C-INPUT--NUMBER OF EQUATIONS
      M=N+1
C-INPUT--EQUATION COEFFICIENTS
      AA=(BE*3.0)/2.0
      A(1,1)=AA
      A(1,2)=1.0
      DO 31 J=3,N
   31 A(1,J)=0.0
      A(2,1)=0.0
      A(2,2)=AA
      A(2,3)=2.0
      DO 32 J=4,N
   32 A(2,J)=0.0
      A(3,1)=-AA
      A(3,2)=0.0
      A(3,3)=AA
      A(3,4)=3.0
      DO 33 J=5,N
   33 A(3,J)=0.0
      A(4,1)=0.0
      A(4,2)=-AA
      A(4,3)=0.0
      A(4,4)=AA
      A(4,5)=4.0
      DO 34 J=6,N
   34 A(4,J)=0.0
      A(5,1)=0.0
      A(5,2)=0.0
      A(5,3)=-AA
      A(5,4)=0.0
      A(5,5)=AA
      A(5,6)=5.0
      DO 35 J=7,N
   35 A(5,J)=0.0
      A(6,1)=0.0
      A(6,2)=0.0
      A(6,3)=0.0
      A(6,4)=-AA
      A(6,5)=0.0
      A(6,6)=AA
      A(6,7)=6.0
      A(6,8)=0.0
      DO 36 J=1,4
   36 A(7,J)=0.0
      A(7,5)=-AA
      A(7,6)=0.0
      A(7,7)=AA
      A(7,8)=7.0
      DO 37 J=1,N
   37 A(8,J)=1.0
      A(1,9)=-1.0
      A(2,9)=1.5
      A(3,9)=0.0
      A(4,9)=-0.5
      DO 38 I=5,N
   38 A(I,9)=0.0
C     SAVE ORIGINAL MATRIX FOR LATER OUTPUT
      DO 17 I=1,N
      DO 17 J=1,M
   17 B(I,J)=A(I,J)
      NN=N-1
C     FIND LARGEST PIVOT ELEMENT
      DO 1 K=1,NN
      MAXA=ABS(A(K,K))
      KK=K+1
      II=K
      DO 2 I=KK,N
      AA=ABS(A(I,K))
      IF(MAXA-AA)3,2,2
```

```
    3 MAXA=AA
      II=I
    2 CONTINUE
      IF(II-K)5,15,5
C     EXCHANGE ROWS TO GET LARGEST ELEMENT TO PIVOT POSITION, IF NEEDED
    5 DO 4 J=K,M
      TEMP=A(II,J)
      A(II,J)=A(K,J)
    4 A(K,J)=TEMP
C     COMPUTE NEW COEFFICIENTS
   15 DO 6 I=KK,N
      ARAT=A(I,K)/A(K,K)
      DO 6 J=K,M
      A(I,J)=A(I,J)-ARAT*A(K,J)
    6 CONTINUE
    1 CONTINUE
C     COMPUTE VARIABLES (SOLUTIONS)
      X(N)=A(N,M)/A(N,N)
      DO 8 MS=1,NN
      I=N-MS
      SUM=0.0
      JJ=I+1
      DO 9 J=JJ,N
    9 SUM=SUM+A(I,J)*X(J)
      X(I)=(A(I,M)-SUM)/A(I,I)
    8 CONTINUE
C-OUTPUT--ORIGINAL EQUATIONS
      WRITE(6,102)
      IF(N-12)20,20,21
   20 DO 12 J=1,N
   12 WRITE(6,103)J    ,(B(I,J),I=1,N)
      WRITE(6,104)(B(I,M),I=1,N)
      GO TO 50
   21 DO 13 J=1,N
   13 WRITE(6,103)J    ,(B(I,J),I=1,12)
      WRITE(6,104)(B(I,M),I=1,12)
      DO 14 J=1,N
   14 WRITE(6,103)J    ,(B(I,J),I=13,N)
      WRITE(6,104)(B(I,J),I=13,N)
   50 WRITE(6,105)
C     COMPUTE VALUE OF EACH EQUATION
      DO 18 I=1,N
      SUM=0.0
      DO 19 J=1,N
   19 SUM=SUM+B(I,J)*X(J)
C-OUTPUT--SOLUTIONS, COMPUTED VALUE OF EQUATION, & ACTUAL VALUE OF EQUAT
      WRITE(6,106)I,X(I),I,SUM,B(I,M)
   18 CONTINUE
      A1=X(1)/10+X(2)/48+X(3)/140+X(4)/320+X(5)/630+X(6)/120+X(7)/1848+
     CX(8)/2880
  102 FORMAT('1',10X,'THE SYSTEM OF SIMULTANEOUS ALGEBRAIC EQUATIONS',//
     1,' THE COEFFICIENTS',//)
  103 FORMAT(' ','X',I2,5X,12F10.5)
  104 FORMAT(' ','C',7X,12F10.5,//)
  105 FORMAT('1',10X,'THE SOLUTION OF THE SYSTEM OF SIMULTANEOUS ALGEBRA
     1IC EQUATIONS',//,39X,'EQUATION #',10X,'COMPUTED VALUE',6X,'ACTUAL
     2VALUE',//)
  106 FORMAT('0',10X,'X',I2,' =',F13.7,16X,I2,13X,F13.7,4X,F13.7)
      RETURN
      END
```

APPENDIX E. NON-NEWTONIAN FLUID EFFECTS ON MIXED CONVECTION HEAT TRANSFER IN TUBES

All those fluids for which the "flow curve" (τ_{xy} versus du/dy) is not linear through the origin at a given temperature and pressure are said to be non-Newtonian. The increasing awareness during recent years of the importance of manufacturing and processing materials, such as plastics, paints, polymers, etc., which exhibit anomalous rheological behavior has resulted in numerous studies of non-Newtonian fluids. Analytical investigations have been presented by DeYoung and Scheele [47], Chen et al. [131], and Sylvester and Rosen [132]. A review of laminar flow heat transfer in tubes with non-Newtonian fluids is given by Skelland [133].

Emphasis in this appendix is given to power law fluids whose shear stress and shear rate is defined as follows:

$$\tau_{xy} = K \left|\frac{du}{dy}\right|^{n-1} \frac{du}{dy} \qquad \text{(E-1)}$$

where n is the flow behavior index, which ranges from unity toward zero for pseudoplastic fluids, and K is the consistency index. For the special case of n = 1, Eq. (E-1) reduces to the standard relation for a Newtonian fluid. The majority of non-Newtonian materials obey Eq. (E-1) which is a relatively simple constitutive equation to use in mathematical analysis. In general, the Nusselt number increases with n.

It has been recognized that boundary layer analysis can be employed to study pseudoplastic fluids in laminar, fully developed tube flow. As indicated in Chapter III, a somewhat similar relationship of Nu versus Ra exists between vertical flat plate natural convection and horizontal tube flow. It

is therefore expected that this similarity may still hold for non-Newtonian fluid flow.

Employing an integral method for laminar natural convection heat transfer between a vertical plate and a power law fluid with high Prandtl number, Tien [134] and Dale and Emery [135] reported that the average Nusselt number could be expressed as follows:

$$\bar{Nu} = C(n)\left[Gr^{\nabla} Pr^{\nabla n}\right]^{\frac{1}{3n+1}} \tag{E-2}$$

The boundary layer thickness along the vertical plate was found to be

$$\delta^{+} = M(n)\left(\frac{1}{Gr^{\nabla} Pr^{\nabla n}}\right)^{\frac{1}{3n+1}} (x^{+})^{\frac{n}{3n+1}} \tag{E-3}$$

where C in Eq. (E-2) and M in Eq. (E-3) are functions of the index n, δ and x^{+} are dimensionless boundary layer thicknesses, and axial distance is defined as follows:

$$\delta^{+} = \frac{\delta}{L}, \quad x^{+} = \frac{x}{L}$$

Gr^{∇} and Pr^{∇} are Grashof and Prandtl numbers, defined in Eqs. (E-14) and (E-15) for non-Newtonian fluids. It is not surprising that Eq. (E-2) agrees with heat transfer results for Newtonian fluid flow with n = 1, $Nu = CRa^{1/4}$.

Formulation of the problem

Consideration is given to steady, laminar, fully developed, combined forced and free convection of a power law fluid in horizontal tubes. Neglecting viscous dissipation, axial conduction, and property variation except for density, one can derive the governing partial differential equation by following the same procedure as shown in Chapter III. Using the same

coordinates for boundary layer and core regions as used in Chapter III, one obtains the field equations as follows:

Boundary layer region

Secondary velocity momentum equation:

$$\rho\left(U\frac{\partial U}{\partial X}+V\frac{\partial U}{\partial Y}\right)=Kn\left(\frac{\partial U}{\partial Y}\right)^{n-1}\frac{\partial^2 U}{\partial Y^2}+g\beta\rho(T-T_c)\sin\theta \tag{E-4}$$

Energy equation

$$\rho C_p\left(U\frac{\partial T}{\partial X}+V\frac{\partial T}{\partial Y}\right)=k\frac{\partial^2 T}{\partial Y^2} \tag{E-5}$$

Continuity equation

$$\frac{\partial U}{\partial X}+\frac{\partial V}{\partial Y}=0 \tag{E-6}$$

The following dimensionless variables are introduced

$$x=\frac{X}{a}\,,\qquad y=\frac{Y}{\Delta}$$

$$u=\frac{U}{U_c}\,,\qquad v=\frac{V}{V_c}$$

$$\phi=\frac{T-T_b}{\Delta T} \tag{E-7}$$

The symbol ΔT will be used to represent the temperature difference $\overline{T}_w - T_b$.

The following hypotheses can be made to derive the reference parameters, Δ, U_c, and V_c in the dimensionless groups:

(1) Both terms in the continuity equation are of the same order of magnitude, hence

$$\frac{U_c}{a}=\frac{V_c}{\Delta} \tag{E-8}$$

(2) The buoyancy term and viscous term are of the same order of magnitude which leads to

$$\beta g \Delta T = \frac{K}{\rho} \frac{U_c^n}{\Delta^{n+1}} \tag{E-9}$$

(3) If the X and Y convective terms and the conduction term are the same order of magnitude in the energy equation, one obtains

$$\frac{U_c}{a} = \frac{k}{\rho C_p \Delta^2} \tag{E-10}$$

Solving Eqs. (E-8), (E-9), and (E-10) simultaneously yields

$$\Delta = \frac{a}{\left(Gr^{\nabla}_{Pr} \nabla n\right)^{\frac{1}{3n+1}}} \tag{E-11}$$

$$U_c = \frac{\alpha}{a}\left(Gr^{\nabla}_{Pr} \nabla n\right)^{\frac{2}{3n+1}} \tag{E-12}$$

$$V_c = \frac{\alpha}{a}\left(Gr^{\nabla}_{Pr} \nabla n\right)^{\frac{1}{3n+1}} \tag{E-13}$$

where Gr^{∇}, and Pr^{∇} are Grashof and Prandtl numbers defined as follows:

$$Gr^{\nabla} = \frac{g\beta\Delta T \; a^{\frac{n+2}{2-n}}}{\left(\frac{K}{\rho}\right)^{\frac{2}{2-n}}} \tag{E-14}$$

$$Pr^{\nabla} = \left(\frac{1}{\alpha}\right)\left(\frac{K}{\rho}\right)^{\frac{1}{2-n}} a^{\frac{2(n-1)}{n-2}} \tag{E-15}$$

Introducing Eqs. (E-11), (E-12), and (E-13) into Eqs. (E-4), (E-5), and (E-6) allows the dimensionless boundary layer equations to be written as follows:

$$\frac{\partial u}{\partial x} + \frac{\partial v}{\partial y} = 0 \tag{E-16}$$

$$\left[\frac{Gr^{\nabla 3(1-n)}}{Pr^{\nabla 2(1+n)}}\right]^{\frac{1}{3n+1}} \left(u \frac{\partial u}{\partial x} + v \frac{\partial u}{\partial y}\right) = (\phi - \phi_c) \sin \theta + n\left(\frac{\partial u}{\partial y}\right)^{n-1} \frac{\partial^2 u}{\partial y^2} \tag{E-17}$$

$$u \frac{\partial \phi}{\partial x} + v \frac{\partial \phi}{\partial y} = \frac{\partial^2 \phi}{\partial y^2} \tag{E-18}$$

The boundary conditions are:

$$y = 0,\ u = v = 0,\ \phi = 1$$

$$y = \delta,\ u = u(\delta),\ v = v(\delta),\ \phi = \phi_c$$

where $u(\delta)$, $v(\delta)$, and ϕ_c are to be determined at the boundary layer edge and can be obtained from solutions of core region. Since n is bounded at zero and unity, the left-hand side in Eq. (E-17) can be neglected for high Prandtl number fluids. Thus, Eq. (E-17) becomes:

$$n\left(\frac{\partial u}{\partial y}\right)^{n-1} \frac{\partial^2 u}{\partial y^2} + (\phi - \phi_c) \sin \theta = 0 \tag{E-19}$$

Equation (E-19) is a non-linear, second-order, ordinary differential equation and may be solved numerically.

The governing equations in the core region can be derived from energy and continuity equations. Since the procedures are exactly the same as derivation of Newtonian fluid flow, the details of the derivation will be omitted.

Nusselt number

The heat transfer coefficient can be obtained from the energy balance along the tube wall. For the axially uniform heat flux boundary condition, one obtains

$$Q = 2\pi a\bar{h}\left(\bar{T}_w - T_b\right) = 2k \int_0^{\pi a} \left.\frac{\partial T}{\partial Y}\right|_{Y=0} dX \tag{E-20}$$

Using the dimensionless variables, one obtains the Nusselt number as follows:

$$\begin{aligned} Nu = \frac{2a\bar{h}}{k} &= \frac{2a}{\pi\Delta} \int_0^{\pi} \left.\frac{\partial \phi}{\partial y}\right|_{y=0} dx \\ &= \frac{2}{\pi}\left(Gr_{Pr}\nabla n\right)^{\frac{1}{3n+1}} \int_0^{\pi} \left.\frac{\partial \phi}{\partial y}\right|_{y=0} dx \\ &= C(n)\left(Gr_{Pr}\nabla n\right)^{\frac{1}{3n+1}} \end{aligned} \tag{E-21}$$

where

$$C(n) = \frac{2}{\pi} \int_0^{\pi} \left.\frac{\partial \phi}{\partial y}\right|_{y=0} dx \tag{E-22}$$

Since the governing equations [Eqs. (E-19) and (E-18)] are functions of n only, one concludes that the constant C in Eq. (E-21) is a function of n. It is obvious that Eq. (E-21) reduces to that for a Newtonian fluid for $n = 1$. One way to obtain the constant C in Eq. (E-21) is to solve Eq. (E-19) with Eq. (E-18), coupling it to the core equation by an iterative process. The detailed solution procedure will be similar to that described in Chapter III.

APPENDIX F.

COMPUTER PROGRAM FOR CHAPTER IV

```
C
C
C
C     COMPUTER PROGRAM FOR CHAPER IV
C     LAMINAR FLOW HEAT TRANSFER IN THERMAL ENTRANCE REGION OF SEMI-CIRCULAR
C     TUBES
C
C
C     W: AXIAL VELOCITY
C     T1,T2,T3,: THREE LEVEL OF TEMPERATURE
C     HONGT: SUBROUTINE FOR ENERGY EQUQTION
C
      DIMENSION W(21,21),          T1(21,21),T2(21,21),T3(21,21),
     1                     R(21),CITA(21),ZA(21),ZB(21),ZC(21),
     2                       AR(21),BR(21),CR(21),DR(21),HZ(300),SHZ(300)
     3,NU1(300),NU2(300),NU12(300)
      COMMON HR,HR2,HC,HC2,OK,OMEG
      COMMON M,N,MI,NI,MD,ND
      REAL NU1,NU2,NU12
C
C
C
C
      READ(5,100,END=150) M,N,OK,OMEG,RA,EN,ENN
C
C     RA IS RAYLEIGH NUMBER
C
      WRITE(6,121) M,N
      WRITE(6,122) OK,OMEG
      WRITE(6,123) EN,ENN
      MI=M+1
      MD=M-1
      NI=N+1
      ND=N-1
      N2=N/2+1
      NO=1
      NOO=5
      SZZ=0.0
      Y=-EN
      DO 17 I=1,150
      HZ(I)=EXP(Y)
      SZZ=SZZ+HZ(I)
      SHZ(I)=SZZ
      Y=Y+ENN
   17 CONTINUE
      DO 10 J=1,NI
      DO 10 I=1,MI
      T1(I,J)=0.0
      T2(I,J)=0.0
      T3(I,J)=0.0
   10 CONTINUE
      READ(5,102) ((W(I,J),I=1,MI),J=1,NI)
      HR=1.0/N
      HR2=HR**2
      PI=3.1415927
      HC=PI/N
      HC2=HC**2
      CITA(1)=0.0
      DO 9 J=2,NI
    9 CITA(J)=CITA(J-1)+HC
      R(1)=0.0
      DO 8 I=2,MI
      R(I)=R(I-1)+HR
      ZA(I)=HR/(2*R(I))
      ZB(I)=(HR/(HC*R(I)))**2
      ZC(I)=HR**2/(2*R(I)*HC)
    8 CONTINUE
      ADZ=1.0
      DO 16 I=2,M
      DO 16 J=2,N
      AD1=W(I,J)*R(I)*HR
      ADZ=AMIN1(ADZ,AD1)
   16 CONTINUE
```

```
      WRITE(6,103) ADZ
      IM=1
      WRITE(6,136)
      WRITE(6,138) (HZ(I),I=1,150)
      WRITE(6,137)
      WRITE(6,138) (SHZ(I),I=1,150)
      WRITE(6,139)
      WRITE(6,140) ((W(I,J),I=1,M),J=1,NI)
      IM=2
      DO 7 I=2,M
      AR(I)=(R(I+1)+2*R(I)+R(I-1))/(4*R(I)*HR2)
      BR(I)=1/((R(I)*HC)**2)
      CR(I)=(R(I+1)+R(I))/(2*R(I)*HR2)
      DR(I)=(R(I)+R(I-1))/(2*R(I)*HR2)
    7 CONTINUE
      SANZ=0.0
      KK=0
      CALL HONGAV(W,AVW,R)
      WRITE(6,104) AVW
C
C
   20 IM=3
      CALL HONGT(T1,T2,T3,W,ANU,AR,BR,CR,DR,NO,ERRT,HZ,R,ANU2,AVW)
      IF(NO.EQ.1) GO TO 21
      NU1(NN)=ANU
      NU2(NN)=ANU2
      NU12(NN)=(NU1(NN)+NU2(NN))/2.0
      WRITE(6,107) NN,HZ(NN),SHZ(NN),NU1(NN),NU2(NN),NU12(NN),ERRT
   21 IM=1
      IF(NO.GT.149) GO TO 99
      IF(NO.EQ.NOO) GO TO 14
      NO=NO+1
      NN=NO-1
      GO TO 20
   14 IM=1
      WRITE(6,108) NO
      WRITE(6,101)
      WRITE(6,115) ((T3(I,J),I=2,MI),J=1,NI)
      NOC=NOO+5
      NO=NO+1
      NN=NO-1
      GO TO 20
C
   99 IM=1
C
      WRITE(6,141)
      DO 23 I=1,NN
      SHZD4=SHZ(I)/4.0
      WRITE(6,142) I,SHZ(I),SHZD4,NU1(I),NU2(I),NU12(I)
   23 CONTINUE
  100 FORMAT(2I5,2F10.5,F10.1,2F5.2)
  101 FORMAT('0','TTT')
  102 FORMAT(20A4)
  103 FORMAT('0','ADZ=',5X,E16.7)
  104 FORMAT('0','AVERAGE VELOCITY',5X,E14.5)
  107 FORMAT('0','NO',I5,2X,'HZ',E14.5,2X,'AHZ',E14.5,2X,'NU1',F10.4,2X,
     C'NU2',F10.4,2X,'NU12',F10.4,2X,'ERRT',E14.5)
  108 FORMAT('0','NO= ',I5)
  115 FORMAT(10F13.6)
  121 FORMAT(' ',30X,'MESH SIZE M AND N .....',2I10)
  122 FORMAT(' ',30X,'OK AND RELAXATION FACTOR.....',F10.6,
     CF10.2)
  123 FORMAT(' ',30X,'EXP(-Y+DY*N) Y AND DY.....',2F10.2)
  136 FORMAT('0','  MARCHING STEP HZ ')
  137 FORMAT('0','  MARCHING LENGTH SHZ ')
  138 FORMAT(' ',10E13.6)
  139 FORMAT('0','  AXIAL VELOCITY W ')
  140 FORMAT(' ',10F13.6)
  141 FORMAT('1',10X,'NO',10X,'Z',14X,'Z/4',12X,'NU1',10X,'NU2',10X,'NU
     C12')
  142 FORMAT(' ', 9X,I3,E16.6,E16.6,3F12.4)
  150 STOP
      END
```

```
      SUBROUTINE HONGT(T1,T2,T3,W,ANU,AR,BR,CR,DR,NO,ERRT,HZ,R,ANU2,AVW)
      DIMENSION T1(21,21),T2(21,21),T3(21,21),W(21,21),DWT(21,21)
     1,AR(21),BR(21),CR(21),DR(21),HZ(150),ZT(21,21),R(21),WT(21,21)



      COMMON HR,HR2,HC,HC2,OK,OMEG
      COMMON M,N,MI,NI,MO,ND
      PI=3.1415927
      C=(PI+2.0)*2.0/PI
      DO 5 J=1,NI
      DO 5 I=1,MI
      T1(I,J)=T2(I,J)
      T2(I,J)=T3(I,J)
    5 CONTINUE
      IF(NO.GT.1) GO TO 20
C
C     STANDARD EXPLICT METHOD
C
      DO 10 J=2,N
      DO 10 I=2,M
      B1=1/HR2+1/(2*R(I)*HR)
      B2=W(I,J)/HZ(NO)-2/HR2-2*BR(I)
      B3=1/HR2-1/(2*R(I)*HR)
      B4=BR(I)
      B5=BR(I)
      T3(I,J)=(B1*T2(I+1,J)+B2*T2(I,J)+B3*T2(I-1,J)+B4*T2(I,J+1)+B5*T2(I
     C,J-1)-C*W(I,J))*HZ(NO)/W(I,J)
   10 CONTINUE
      ERRT=1.0
      GO TO 21
   20 IM=2
C
C
C     DU FORT FRANK METHOD
C
      Z1=HZ(NO-1)**2
      Z2=HZ(NO)**2
      Z12=HZ(NO-1)*HZ(NO)*(HZ(NO)+HZ(NO-1))
      Z21=Z2-Z1
      DO 8 J=2,N
      DO 8 I=2,M
      AW1=W(I,J)*Z1/Z12
      AW2=W(I,J)*Z2/Z12
      AW3=W(I,J)*(Z2-Z1)/Z12
      A1=AW1+AR(I)+BR(I)
      A2=CR(I)
      A3=DR(I)
      A4=BR(I)
      A5=BR(I)
      A6=AW2-AR(I)-BR(I)
      A7=A2*T2(I+1,J)+A3*T2(I-1,J)+A6*T1(I,J)-C*W(I,J)
      A8=A4*T2(I,J+1)+A5*T2(I,J-1)
      T3(I,J)=(A7+A8-AW3*T2(I,J))/A1
    8 CONTINUE
   21 IM=1
      SS1=0.0
      SS2=0.0
      SS3=0.0
      SS4=0.0
      DO 6 I=2,M
      SS1=SS1+1.0/R(I)
      SS3=SS3+(-4*T3(I,2)+T3(I,3))/R(I)
      SS4=SS4+(-4*T3(I,N)+T3(I,ND))/R(I)
    6 CONTINUE
      AAT1=3*HC*(N-1)/(2*HR)+3*HR*SS1/HC+3.0/2.0
      AAT3=SS3*HR/(2.0*HC)
      AAT4=SS4*HR/(2.0*HC)
      NC=N/2+1
      AAT5=(-4*T3(2,NC)+T3(3,NC))/2.0
      DO 7 J=2,N
```

```
 7 SS2=SS2-(4*T3(M,J)-T3(MD,J))
   AAT2=SS2*HC/(2*HR)
   TW=(PI+2.0-AAT5-AAT4-AAT3-AAT2)/AAT1
   DO 9 J=1,NI
   T3(1,J)=TW
 9 T3(MI,J)=TW
   DO 4 I=1,MI
   T3(I,1)=TW
   T3(I,NI)=TW
 4 CONTINUE
   IF(NO.EQ.1) GO TO 23
   DO 22 J=1,NI
   DO 22 I=1,MI
   ZT(I,J)=(Z1*T3(I,J)-Z2*T1(I,J)+Z21*T2(I,J))/Z12
   WT(I,J)=ZT(I,J)*W(I,J)
   DWT(I,J)=(TW-T2(I,J))*W(I,J)
22 CONTINUE
   CALL HONGAV(ZT,ERRT,R)
   CALL HONGAV(WT,AVWT,R)
   CALL HONGAV(DWT,AVBT,R)
   ANU=(2.0*AVW)/AVBT
   ANU2=(PI*AVWT+2.0*(PI+2.0))/(AVBT*(PI+2.0))
23 IM=1
   RETURN
   END
   SUBROUTINE HONGAV(E,AVG,R)
   DIMENSION EI(21),E(21,21),R(21)
   COMMON HR,HR2,HC,HC2,OK,OMEG
   COMMON M,N,MI,NI,MD,ND
   PI=3.1415927
   DO 7 I=1,MI
   EI(I)=E(I,1)+E(I,NI)
   DO 6 J=2,N,2
 6 EI(I)=EI(I)+E(I,J)*4
   DO 5 J=3,ND,2
 5 EI(I)=EI(I)+E(I,J)*2
   EI(I)=HC*EI(I)/3
 7 CONTINUE
   SE=0.0
   SE=SE+EI(1)*R(1)+EI(MI)*R(MI)
   DO 4 I=2,M,2
 4 SE=SE+EI(I)*R(I)*4
   DO 3 I=3,MD,2
 3 SE=SE+EI(I)*R(I)*2
   AVG=HR*SE*2/(3*PI)
   RETURN
   END
```

APPENDIX G. NUMERICAL RESULTS FOR CHAPTER IV

$\frac{Z}{D\ Re_D\ Pr}$	Nusselt Number	
	Case 1	Case 2
0.171×10^{-3}	28.98	28.52
0.356	22.45	21.94
0.557	19.31	18.61
0.775	17.27	16.49
0.101×10^{-2}	15.72	14.96
0.140	13.87	13.30
0.184	12.64	12.07
0.234	11.68	11.11
0.290	10.73	10.33
0.353	10.31	9.675
0.477	9.527	8.786
0.628	8.831	8.076
0.812	8.309	7.494
0.104×10^{-1}	7.801	7.101
0.131	7.467	6.607
0.165	7.248	6.269
0.206	6.998	6.033
0.256	6.901	5.798
0.317	6.801	5.605
0.392	6.750	5.450
0.484	6.739	5.343
0.595	6.724	5.250
0.732		5.190
0.898		5.173
0.975		5.172

APPENDIX H.

WORKING FLUID PROPERTIES

This appendix contains the physical and transport properties of both water and ethylene glycol. Seven properties were evaluated for each fluid: density, isobaric thermal expansion coefficient, enthalpy, viscosity, thermal conductivity, Prandtl number, and viscosity thermal coefficient. The working fluid properties depend strictly on two state variables, pressure and temperature. Since the pressure variations in the system were too small to affect the fluid properties, they were adequately represented by functions of temperature.

All properties were put in analytical form by fitting a power polynomial through the data points. The polynomial expression for each property has been compared with the reference data and, within the listed temperature range, has been found to deviate by no more than the percentage error indicated.

Distilled Water

The data points listed below were taken from the ASME Steam Tables [136] corresponding to 20 psia.

Density

Data points:

T (^{o}F)	ρ (lbm/ft^3)
50	62.4220
100	61.9963
150	61.1995
200	60.0962

Equation:

$$\rho = 62.422 - 0.21862\ \theta - 0.21785\ \theta^2 + 0.01077\ \theta^3 \text{ lbm/ft}^3 \qquad \text{(H-1)}$$

where

$$\theta = \frac{T - 50\ ^{\circ}F}{50\ ^{\circ}F} \qquad \text{(H-2)}$$

Temperature range: 50-200 $^{\circ}$F

Maximum error: 0.02%

Isobaric thermal expansion coefficient

The isobaric thermal expansion coefficient is defined by the equation

$$\beta = -\frac{1}{\rho}\left(\frac{\partial \rho}{\partial T}\right)_p \qquad \text{(H-3)}$$

By using Eq. H-1, one can write β as

$$\beta = -\frac{-0.21862 - 0.43570\ \theta + 0.03231\ \theta^2}{50(62.422 - 0.21862\ \theta - 0.21785\ \theta^2 + 0.01077\ \theta^3)}\ \frac{1}{^{\circ}F} \qquad \text{(H-4)}$$

where

$$\theta = \frac{T - 50\ ^{\circ}F}{50\ ^{\circ}F} \qquad \text{(H-5)}$$

Enthalpy

Data points:

T ($^{\circ}$F)	h (Btu/lbm)
50	18.11
200	168.11

Equation:

$$h = T - 31.89 \text{ Btu/lbm} \qquad \text{(H-6)}$$

Temperature range: 50-200 ^{o}F

Maximum error: 0.03%

In the data reduction, an expression for fluid temperature as a function of enthalpy was needed. Eq. (H-6) was rearranged to yield

$$T = h + 31.89\ ^{o}F \tag{H-7}$$

Viscosity

Data points:

T (^{o}F)	μ (lb-sec/ft^2)
50	271.4×10^{-7}
100	142.0
150	89.1
200	62.6

Equation:

$$\mu = \exp(5.6036 - 0.76097\ \theta + 0.1245\ \theta^2 - 0.01133\ \theta^3) \times 0.0115826\ \text{lbm/ft-hr} \tag{H-8}$$

where

$$\theta = \frac{T - 50\ ^{o}F}{50\ ^{o}F} \tag{H-9}$$

Temperature range: 50-200 ^{o}F

Maximum error: 0.74%

Thermal conductivity

Data points:

T (^{o}F)	k (Btu/hr-ft-^{o}F)
50	0.3392
100	0.3633
150	0.3806

Equation:

$$k = 0.3392 + 0.0275\ \theta - 0.0034\ \theta^2 \quad \text{Btu/hr-ft-}^{\circ}\text{F} \tag{H-10}$$

where

$$\theta = \frac{T - 50\ ^{\circ}\text{F}}{50\ ^{\circ}\text{F}} \tag{H-11}$$

Temperature range: 50-200 $^{\circ}$F

Maximum error: 0.13%

Prandtl number

Data points:

T ($^{\circ}$F)	Pr
50	9.28
100	4.52
150	2.71
200	1.86

Equation:

$$Pr = \exp(2.2279 - 0.84747\ \theta + 0.14015\ \theta^2 - 0.012083\ \theta^3) \tag{H-12}$$

where

$$\theta = \frac{T - 50\ ^{\circ}\text{F}}{50\ ^{\circ}\text{F}} \tag{H-13}$$

Temperature range: 50-200 $^{\circ}$F

Maximum error: 0.28%

Viscosity thermal coefficient

The definition of the isobaric viscosity thermal coefficients is similar to that for the isobaric thermal expansion coefficient:

$$\gamma = -\frac{1}{\mu}\left(\frac{\partial \mu}{\partial T}\right)_p \tag{H-14}$$

By using Eq. (H-8), one can write γ as

$$\gamma = \frac{1}{50} (0.76097 - 0.2490\ \theta + 0.03399\ \theta^2) \tag{H-15}$$

where

$$\theta = \frac{T - 50\ ^{o}F}{50\ ^{o}F} \tag{H-15}$$

Ethylene Glycol

The physical properties of ethylene glycol were taken from Ref. 137.

Density

Equation: The following expression for the specific volume v, cm^3/gm, as a function of temperature T, ^{o}C, was reported in Ref. 137.

$$v = 0.924848 + 6.2796 \times 10^{-4}\ \theta + 9.2444 \times 10^{-7}\ \theta^2 + 3.057 \times 10^{-9}\ \theta^3\ cm^3/gm \tag{H-16}$$

where

$$\theta = T - 65\ ^{o}C \tag{H-17}$$

The density can be obtained from Eq. (H-14), according to the relation

$$\rho = \frac{62.43}{v}\ lbm/ft^3 \tag{H-18}$$

Temperature range: 40-340 ^{o}F

Maximum error: 0.18%

Isobaric thermal expansion coefficient

The definition of β, as given by Eq. (H-3), can also be rearranged to read

$$\beta = \frac{1}{v}\left(\frac{\partial v}{\partial T}\right)_p \qquad \text{(H-19)}$$

Using Eq. (H-16), one can express β as

$$\beta = \frac{6.2795 \times 10^{-4} + 1.84888 \times 10^{-6}\ \theta + 9.171 \times 10^{-9}\ \theta^2}{1.8(0.924848 + 6.2796 \times 10^{-4}\ \theta + 9.2444 \times 10^{-7}\ \theta^2 + 3.057 \times 10^{-9}\ \theta^3)}\ \frac{1}{^{o}F} \qquad \text{(H-20)}$$

Enthalpy

Data points:

T (^{o}F)	c_p (Btu/lbm-^{o}F)
60	0.553
140	0.598
220	0.650

Equation:

$$c_p = 0.553 + 0.04150\ \theta + 0.0035\ \theta^2 \quad \text{Btu/lbm-}^{o}\text{F} \qquad \text{(H-21)}$$

where

$$\theta = \frac{T - 60\ ^{o}F}{80\ ^{o}F} \qquad \text{(H-22)}$$

Equation (H-19) was integrated along the isobar p = 0 psig and the enthalpy was arbitrarily chosen to be zero at the freezing point T = 9.14 ^{o}F. The final result is given by

$$h = 27.4786 + 44.24\ \theta + 1.66\ \theta^2 + 0.09333\ \theta^3 \quad \text{Btu/lbm} \qquad \text{(H-23)}$$

Temperature range: 40-300 ^{o}F

Maximum error: For specific heat at constant pressure, the maximum error was 0.12%. The expression for enthalpy was numerically differentiated and compared with the computed values of specific heat. The comparison showed no difference within the accuracy of computation.

Equation (H-21) was also rearranged to yield an expression for temperature as a function of enthalpy.

Viscosity

Data points:

T (^{o}F)	μ (centipoise)
40	45.0
100	10.38
160	3.86
220	1.89
280	1.10

Equation:

$$\mu = \exp(3.80666 - 1.79809\ \theta + 0.38590\ \theta^2 - 0.05878\ \theta^3 + 0.004173\ \theta^4) \times 2.42 \quad \text{lbm/hr-ft} \qquad \text{(H-24)}$$

where

$$\theta = \frac{T - 40\ ^{o}F}{60\ ^{o}F} \qquad \text{(H-25)}$$

Temperature range: 40-300 ^{o}F

Maximum error: 0.56%

Thermal conductivity

Data points:

T (^{o}F)	k (Btu/hr-ft-^{o}F)
50	0.1710
150	0.1480

Equation:

$$k = 0.1825 - 2.3 \times 10^{-4} T \quad \text{Btu/hr-ft-}^{o}\text{F} \qquad \text{(H-26)}$$

Temperature range: 40-350 ^{o}F

Maximum error: There is no difference between the computed value and the input data within the accuracy of computation.

Prandtl number

Data points:

T (^{o}F)	Pr
40	340.587
120	65.754
200	26.468
280	15.620

Equation:

$$Pr = \exp(5.83067 - 2.12950\ \theta + 0.54344\ \theta^2 - 0.058687\ \theta^3) \quad \text{(H-27)}$$

where

$$\theta = \frac{T - 40\ ^{o}F}{80\ ^{o}F} \quad \text{(H-28)}$$

Temperature range: 40-300 ^{o}F

Maximum error: 0.69%

Viscosity thermal coefficient

The definition of γ is given in Eq. (H-14). Using Eq. (H-24), one can express γ as

$$\gamma = \frac{1}{60}\left[1.79809 - 0.7718\ \theta + 0.17634\ \theta^2\right] \quad \text{(H-29)}$$

APPENDIX I.

CALIBRATION OF FLOWMETER

The flowmeter used was a Brooks Rotameter, Model 1307, size 7, serial No. 7210-36292. Two spherical floats of Pyrex (specific gravity 2.20) and Monel (specific gravity 8.84) were used to provide accurate measurements of the flow rate within the range of interest. The flowmeter was calibrated by weighing the fluid collected for a measured time interval at different flow settings. A constant-head tank was used to supply the desired flow rate. Since the viscosity immunity ceiling of both floats in 5 centistokes, it was necessary to calibrate the flowmeter when using water and ethylene glycol. The calibration data for both fluids are given below.

Distilled Water

The Pyrex and Monel floats were both calibrated with distilled water. The duration of each calibration run ranged from 5 to 15 minutes for the Pyrex float, and from 3 to 10 minutes for the Monel float. The calibration data, taken at an average temperature of 68 ^{o}F, are given in Table I-1 and the calibration curve is shown in Fig. I-1.

A polynomial expression of the mass flow rate as a function of the float position was obtained by fitting a power polynomial through the experimental data points. The final expression for the Pyrex float is given by

$$\dot{m} = 0.0750 + 0.507333\ FP - 0.0504\ FP^2 + 0.003867\ FP^3 \text{ lbm/min} \qquad \text{(I-1)}$$

Table I-1 Flowmeter calibration data for distilled water

Flowmeter reading (percent)	Actual flow rate (lbm/min)	
	Pyrex float	Monel float
10.0	0.075	0.320
20.0	0.244	0.703
30.0	0.395	1.067
40.0	0.536	1.405
50.0	0.670	1.730
60.0	0.794	2.039
70.0	0.919	2.336
80.0	1.035	2.576
90.0	1.142	2.841
100.0	1.248	3.100

where

$$FP = \frac{\text{Pyrex float reading - 10}}{30} \tag{I-2}$$

The expression for the Monel float is given by

$$\dot{m} = 0.703 + 1.473\ FM - 0.137\ FM^2 \quad \text{lbm/min} \tag{I-3}$$

where

$$FM = \frac{\text{Monel float reading - 20}}{40} \tag{I-4}$$

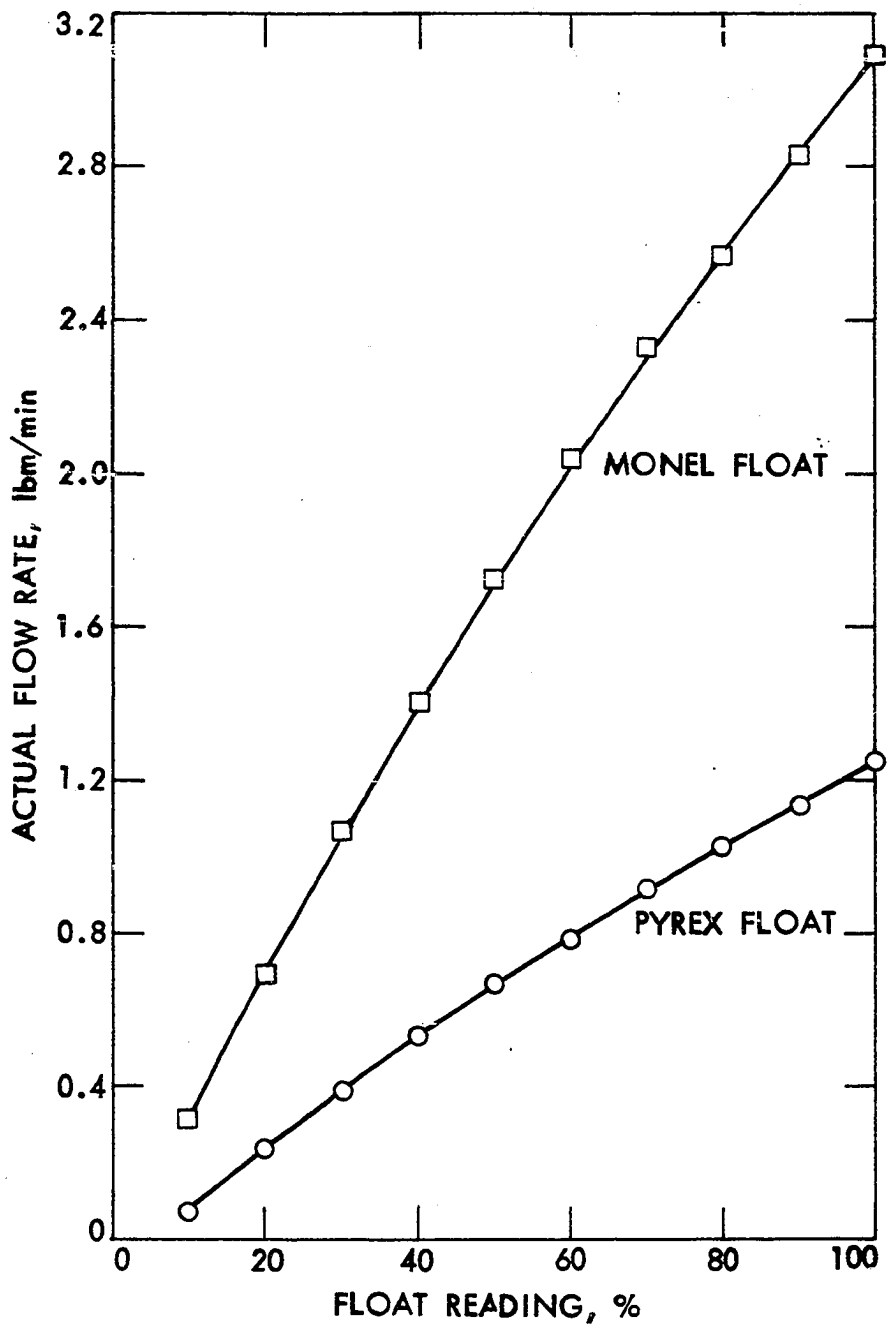

Fig. I-1 Calibration curve for flowmeter with water

Ethylene Glycol

In order to obtain the desired range of flow rate for ethylene glycol, it was only necessary to calibrate the Monel float. Since the flow rates were generally lower than those of water, the duration of each run was increased to range from 5 to 18 minutes. The calibration data for an average fluid temperature of 78 ^{o}F are given below; the calibration curve is shown in Fig. I-2.

Table I-2 Flow meter calibration data for ethylene glycol

Flowmeter reading (percent)	Actual flow rate (lbm/min)
10.0	0.0287
20.0	0.1109
30.0	0.2405
40.0	0.4159
50.0	0.6869
60.0	0.9417
70.0	1.1726
80.0	1.3728
90.0	1.5860
100.0	1.8406

During the heat transfer and pressure drop runs, provisions were made to keep the inlet fluid temperature to the flow meter as close as possible to 78 ^{o}F to avoid any errors in the calibration data. Due to the nature of the calibration curve, it was not possible to fit an accurate power polynomial through the data points. However, numerical interpolation of the data points was performed whenever needed.

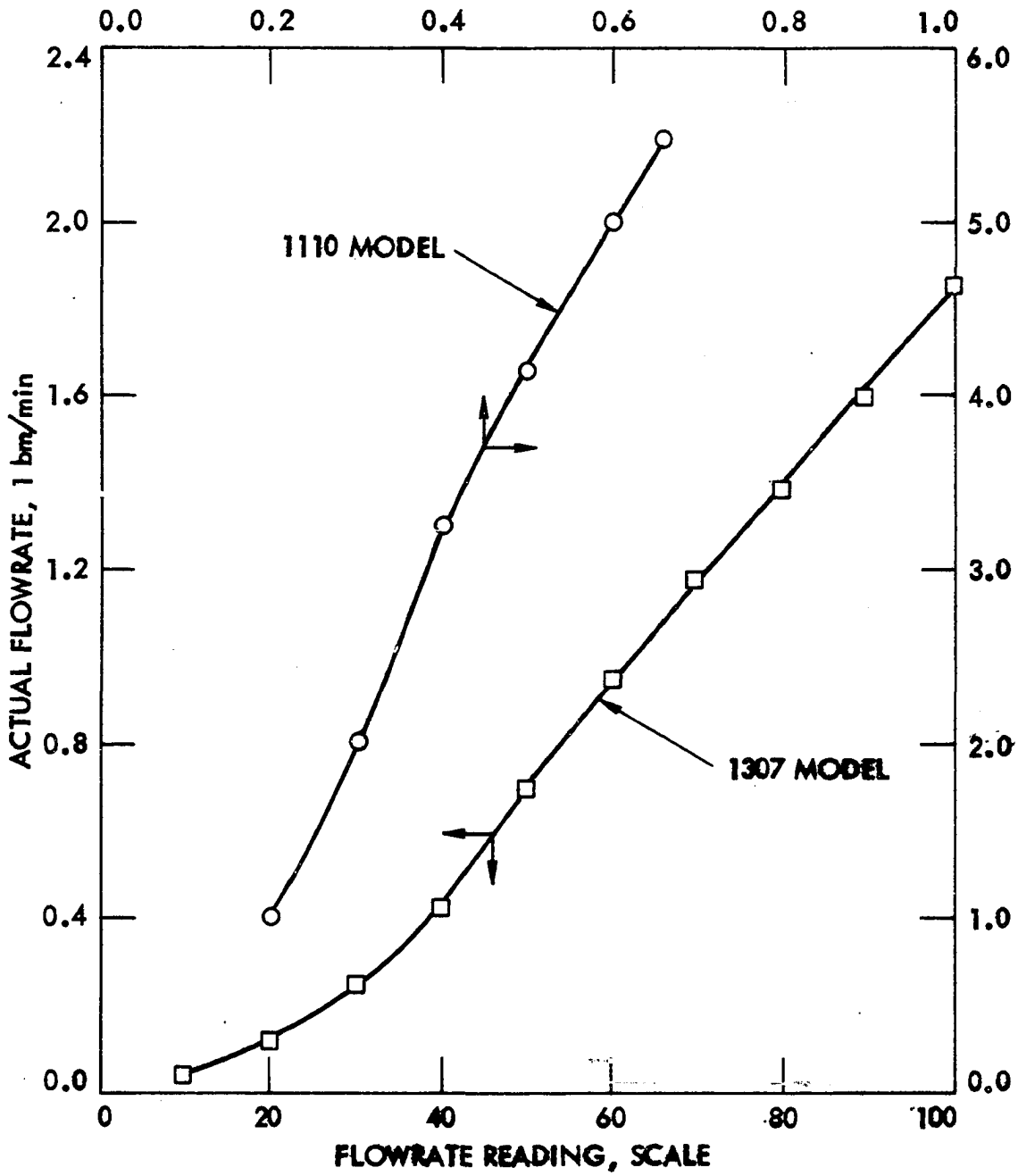

Fig. I-2 Calibration curve for flow meter with ethylene glycol

APPENDIX J.

COMPUTATION PROCEDURE FOR DATA REDUCTION IN CHAPTER V

```
C
C
C
C     COMPUTATION PROCEDURE FOR DATA REDUCTION IN CHAPTER V
C
C
      REAL NU,NUF,NUO,L1,LO,LT,NUOF
      DIMENSION EMF(10),TEMP(10),TWI(10)
      DATA D1,D2,TL1,TL2,TL/0.033417,0.03675,1.583333,3.666667,4.0/,
     1THCTB/9.4/
      DATA PI,G,PCF /3.141593,32.174,3.4129/
      DATA RHONG,RHOFL/874.12,69.34/
      DATA DD1,DD2,DD3,DD4/-1.798086,0.385912,-0.05878,0.004173/
      L1=1.125/12.0
      LO=1.0/12.0
      LT=46.875/12.0
      AREA     = PI*D1*D1/4.0
      DAL=0.0182/12.0
      AS=PI*D1**2/4.0-DAL*D1
      READ (5,110) Y
      D13      = D1**3
      DH=(PI*D1+4.0*DAL)/(PI+2.0*(1.0-DAL/D1))
C
    1 READ (5,2,END=500) NR,NS,M,RFN,VLT,VLS,H2
    2 FORMAT (3I5,2F10.4,F9.4,F11.4)
      AMP      = 2.4*VLS
      RT       = VLT/AMP
      WAT      = 0.985*VLT*AMP
      QTOT     = WAT*PCF
      QPUA     = QTOT/(PI*D1*TL)
      FLOW     = FLOWR(M,RFM)
      G=FLOW/(PI*D1**2/4.0-DAL*D1)
      GOO=FLOW/AREA
      QPUV     = 4.0*QTOT/(PI*(D2*D2-D1*D1)*TL)
      DTW      = QPUV*(D2*D2*ALOG(D2/D1)-(D2*D2-D1*D1)/2.0)/(8.0*THCTB)
C     WALL TEMPERATURE
C
      READ (5,5) (EMF(I),I=1,10)
    5 FORMAT (10F8.4)
      CALL THCPL(EMF,TEMP,10)
      DO 10 I = 1,8
   10 TWI(I)   = TEMP(I)-DTW
      TWM=(TWI(1)+TWI(3)+TWI(5)+TWI(7)+2.0*(TWI(2)+TWI(4)+TWI(6)+TWI(8))
     C)/12.0
C
C     FLUID BULK TEMPERATURE
C
      HFI      = HFL(TEMP(9))
      HFE      = HFL(TEMP(10))
      DHFL     = (HFE-HFI)*FLOW
      TLTC     = TL1
      IF (NS.EQ.2) TLTC = TL2
      QIN      = QTOT*TLTC/TL
      HFB      = HFI+QIN/FLOW
      TFB      = THL(HFB)
      TFLM     = (TFB+TWM)/2.0
C
      DTWB     = TWM-TFB
      CT=(TFB-40.0)/60.0
      ALPHA=(DD1+2*DD2*CT+3*DD3*CT**2+4*DD4*CT**3)*(-1)/60.0
      BE=ALPHA*DTWB
      DTQ=(QPUA*D1)/THCNL(TFB)
      HTC      = QPUA/DTWB
      VISC     = VISCL(TFB)
      VISCF=VISCL(TFLM)
      VISCW=VISCL(TWM)
      BETA     = BETAL(TFB)
      BETAF=BETAL(TFLM)
      VRHO2    = (VISC/RHOL(TFB))**2
      VRHOF2=(VISCF/RHOL(TFLM))**2
      PR       = PRND(TFB)
      PRF=PRND(TFLM)
```

```
      VISWB=VISCW/VISC
C
      NU       = HTC*D1/THCNL(TFB)
C
      NUF=HTC*D1/THCNL(TFLM)
      RES=G*D1/VISC
      REO=GOO*D1/VISC
      RE=REO
      REY=RES/Y
      REF=G*D1/VISCF
      REFY=REF/Y
      REH=G*DH/VISC
      REHF=G*DH/VISCF
      GR=4.94*REH**2*DH*BETA*DTWB/(Y**2*D1)
      GRF=4.94*REHF**2*DH*BETAF*DTWB/(Y**2*D1)
      GRQ=GR*DTQ/DTWB
      GRQF=GRF*DTQ/DTWB
      RA=GR*PR
      RAF=GRF*PRF
      RAQ=GRQ*PR
      RAQF=GRQF*PRF
      GZ       = TLTC/(D1*RES*PR)
      GZF=TLTC/(D1*REF*PRF)
      GRO=GC*BETA*D13*DTWB*3600.0*3600.0/VRHO2
      GROF=GC*BETA*D13*DTWB*3600.0**2/VRHOF2
      RAC=GRO*PR
      RACF=GROF*PRF
      RAO=ABS(RAO)
      RAOQ=RAO*DTQ/DTWB
      RAOQF=RAOF*DTQ/DTWB
      RAOQ=ABS(RAOQ)
      GRO =ABS(GRO)
      GROF=ABS(GROF)
      NUO=0.2515*RAOQ**0.2675
      RATO=NU/NUO
      NUOF=0.3836*GROF**0.256*PRF**0.31
      RATOF=NUF/NUOF
      REPGR=REY/(GRO**0.25)
      REPGRF=REFY/(GROF**0.25)
C
C     MEASURED FRICTION FACTOR
C
      HP=H2
      DPFL     = HP*(RHOHG-RHOFL)/1728.0
      TFBI=TEMP(9)
      QINM=QTOT/2.0
      HFBM=HFI+QINM/FLOW
      HFB2=HFI+QTOT/FLOW
C
      TFBIO=TEMP(9)
      TFBM=THL(HFBM)
      TFE=THL(HFB2)
      RHOI=RHOL(TFBIO)
      RHOM=RHOL(TFBM)
      RHOE=RHOL(TFE)
      VELI=G/RHOI
      VELM=G/RHOM
      VELE=G/RHOE
      REI=G*D1/VISCL(TFBIO)
      REM=G*D1/VISCL(TFBM)
      REE=G*D1/VISCL(TFE)
      FRINI=175.6/REI**0.95
      FRINM=175.6/REM**0.95
      FRINE=175.6/REE**0.95
      DPI      =FRINI*RHOI*VELI*VELI/(D1*GC*2.0*3600.0*3600.0*1728.0)
     C*LG
      DPO=FRINE*RHOE*VELE**2/(D1*GC*2.0*3600.0**2*1728.0)*LO
C
      DPH      = DPFL-DPI-DPO
      FRS=288.0*3600.0**2*GC*D1*DPH/(TL*RHOM*VELM**2)
      FRES=FRS*RES
      FRS=ABS(FRS)
      AA1=(FRS*AS/(14.64*AREA))**0.5
      RECP=AA1*RES**1.5*(NUO/RAOQ)**0.065
```

```
      VELM=VELM/3600.0
C
C
C
      WRITE(6,15) NR,NS,FLOW,RFM,VLT,AMP,RT,WAT,QPUA,VELM,Y
      WRITE (6,20) TWI(1),TWI(2),TWI(8),TWI(3),TWI(7),TWI(4),TWI(6),
     CTWI(5)
      WRITE (6,60) TEMP(9),TEMP(10),TFB,TWM,HTC,QTOT,DHFL,NU,NUF,PR,PRF,
     CRES,REF,FRS,REM ,GRQ,GRQF,RAOQ,RAOQF,GZ,GZF
      WRITE(6,100) NUO,NUOF,RATO,RATOF,BE,VISWB,REY,REFY,RECP
      WRITE(7,101) NR,NS,RFM,VLT
      WRITE(7,102) NU,NUF,NUO,RATO,PR,PRF,VISWB
      WRITE(7,103) GR,GRF,GRQ,GRQF,GZ,GZF,RA,RAF,RAO,RAOQ,RAQ,RAQF,
     CRES,REF,REH,REHF,BE,REY,RATOF,FRS,FRES,RECP,NUOF,REO,REFY,RAOF
     C,REM
C
C
   15 FORMAT (1H1,35X,60HCOMBINED FORCED AND FREE CONVECTION IN HORIZONT
     1AL METAL TUBE,//,10X,5HRUN: ,I2,/,10X,9HSECTION: ,I1,///,5X,17HSYST
     2EM PARAMETERS,/,5X,17H****************,//,
     310X,27HWATER FLOW RATE           = ,F10.4,7H LBM/HR,F10.3,/,
     410X,27HVOLTAGE ACROSS THE TUBE   = ,F10.4,6H VOLTS,/,
     510X,27HCURRENT THROUGH THE TUBE  = ,F10.4,5H AMPS,/,
     610X,27HTUBE ELECTRIC RESISTENCE  = ,E10.4,5H OHMS,/,
     710X,27HELECTRIC POWER INPUT      = ,F10.4,6H WATTS,/,
     810X,27HHEAT FLUX                 = ,F10.4,15H BTU/(HR.SQ.FT),/,
     910X,27HVELOCITY,TWIST RATIO, H/D= ,E10.4,7H FT/SEC,F10.3,/)
   20 FORMAT (5X,36HINSIDE WALL TEMPERATURE DISTRIBUTION,/,5X,36H******
     1**************************,//,40X,F10.4,//,25X,F10.4,18X,F10.4,
     2//,23X,F10.4,22X,F10.4,//,25X,F10.4,18X,F10.4,//,40X,F10.4,//)
   60 FORMAT (5X,16HSYSTEM VARIABLES,/,5X,16H****************,//,
     110X,27HFLUID INLET TEMPERATURE   = ,F10.4,2H F,/,
     210X,27HFLUID EXIT TEMPERATURE    = ,F10.4,2H F,/,
     310X,27HFLUID BULK TEMPERATURE    = ,F10.4,2H F,/,
     410X,27HMEAN WALL TEMPERATURE     = ,F10.4,2H F,/,
     510X,27HHEAT TRANSFER COEFFI.     = ,F10.4,17H BTU/(HR.SQ.FT.F),//,
     610X,27HTOTAL POWER INPUT         = ,F10.4,7H BTU/HR,/,
     710X,27HTOTAL ENTHALPY CHANGE     = ,F10.4,7H BTU/HR,//,
     810X,27HNUSSELT NUMBER BULK, FILM= ,2F15.4,/,
     910X,27HPRANDTL NUMBER   "   "    = ,2F15.4,/,
     110X,27HREYNOLDS NUMBER  "   "    = ,2E15.6,//,
     210X,27HFRICTION FACTOR FRS,REM   = ,2E15.6,/,
     210X,27HGRASHOF NUMBER OF CENT. F= ,2E15.6,/,
     310X,27HRAYLEIGH NUMBER DQ RAOQ   = ,2E15.6,/,
     410X,27HGRAETZ NUMBER D  "   "    = ,2E15.6,/)
  100 FORMAT('0', 9X,'NUSSELT NO FOR EMPTY B,F  =',2F15.4,/,
     210X,'NU NO. RATIO, NUS/NUO B,F =',2F15.4,/,
     310X,'BERGLES NUMBER BE         =',F15.4,/,
     410X,'VISCOSITY RATIO W/B       =',E15.5,/,
     510X,'RE/Y,BULK,FILM            =',2E15.5,/,
     610X,'RE BASE ON CONS. POWER    =',E15.5)
  101 FORMAT(2I5,F10.1,F10.4)
  102 FORMAT(4F10.5,2F10.4,F10.6)
  103 FORMAT(20A4)
  110 FORMAT(F10.3)
      GO TO 1
  500 STOP
      END
```

```
      SUBROUTINE THCPL(EMF,TEMP,N)
C             THERMOCOUPLE TEMPERATURE (F) AS A FUNCTION OF
C             ELECTROMOTIVE FORCE (MV)
C
      DIMENSION EMF(N),TEMP(N)
      DATA X1,X2,X3 /32.35441,45.69075,-0.84649/
C
      DO 1 I  = 1,N
    1 TEMP(I) = (X3*EMF(I)+X2)*EMF(I)+X1
      RETURN
      END
      FUNCTION FLOWR(N,R)
C             ACTUAL FLOW RATE IN LBM/HR
C
C
      IF (N. EQ. 2) GO TO 1
C
C     MONEL FLOAT (1485) FOR ETHELENE GLYCOL
C
      IF(R.GT.9.99.AND.R.LT.10.01) FLOWR= 0.0287
      IF(R.GT.19.99.AND.R.LT.20.01) FLOWR=0.1109
      IF(R.GT.29.99.AND.R.LT.30.01) FLOWR=0.2405
      IF(R.GT.39.99.AND.R.LT.40.01) FLOWR=0.4159
      IF(R.GT.49.99.AND.R.LT.50.01) FLOWR=0.6869
      IF(R.GT.59.99.AND.R.LT.60.01) FLOWR=0.9417
      IF(R.GT.69.99.AND.R.LT.70.01) FLOWR=1.1726
      IF(R.GT.79.99.AND.R.LT.80.01) FLOWR=1.3728
      IF(R.GT.89.99.AND.R.LT.90.01) FLOWR=1.5860
      IF(R.GT.99.99.AND.R.LT.100.01) FLOWR=1.8406
      FLOWR=FLOWR*60.0
      RETURN
C
C
    1 IM=1
      IF(R.GT.0.19.AND.R.LT.0.21) FLOW=0.99826
      IF(R.GT.0.29.AND.R.LT.0.31) FLOW=2.01665
      IF(R.GT.0.39.AND.R.LT.0.41) FLOW=3.33088
      IF(R.GT.0.49.AND.R.LT.0.51) FLOW=4.13934
      IF(R.GT.0.59.AND.R.LT.0.61) FLOW=4.98561
      IF(R.GT.0.65.AND.R.LT.0.67) FLOW=5.48973
      FLOWR=FLOW*60.0
      RETURN
      END
      FUNCTION RHOL(T)
C             DENSITY AS A FUNCTION OF TEMPERATURE (F) FOR ETHELENE GLYCOL
C                     UNITS LBM/QU.FT
C
      DATA X1,X2,X3,X4 /0.924848,6.2796E-04,9.2444E-07,3.057E-09/
      TC    = (T-32.0)/1.8
      DT    = TC-65.0
      VOL   =((X4*DT+X3)*DT+X2)*DT+X1
      RHOL  = 62.43/VOL
      RETURN
      END
      FUNCTION BETAL(T)
C             COEFFICIENT OF THERMAL EXPANSION AS A FUNCTION OF
C             TEMPERATURE (F) FOR ETHELENE GLYCOL
C                     UNITS 1/F
C
      DATA X1,X2,X3,X4 /0.924848,6.2796E-04,9.2444E-07,3.057E-09/
      TC    = (T-32.0)/1.8
      DT    = TC-65.0
      VOL   =((X4*DT+X3)*DT+X2)*DT+X1
      DVOL  = (3.0*X4*DT+2.0*X3)*DT+X2
      BETAL= DVOL/(1.8*VOL)
      RETURN
      END
      FUNCTION HFL(T)
C             ENTHALPY AS A FUNCTION OF TEMPERATURE (F) FOR ETHELENE GLYCOL
C                     UNITS BTU/LBM
C
      DATA X1,X2,X3,X4 /27.47863,44.24,1.66,0.093333/,T0,DT /60.0,80.0/
      THETA = (T-T0)/DT
      HFL   = ((X4*THETA+X3)*THETA+X2)*THETA+X1
```

```
      RETURN
      END
      FUNCTION THL(H)
C             TEMPERATURE AS A FUNCTION OF ENTHALPY (BTU/LBM) FOR
C             ETHELENE GLYCOL
C                       UNITS F
      DATA X1,X2,X3,X4 /27.47863,44.24,1.66,0.093333/,T0,DT /60.0,20.0/
      P     = X3/X4
      Q     = X2/X4
      R     = (X1-H)/X4
      P2    = P*P
      A     = Q-P2/3.0
      B     = (2.0*P*P2-9.0*P*Q+27.0*R)/27.0
      C     = SQRT(B*B/4.0+A*A*A/27.0)
      A1    = (-B/2.0+C)**(1.0/3.0)
      B1    = (B/2.0+C)**(1.0/3.0)
      THETA= A1-B1-P/3.0
      THL   = THETA*DT+T0
      RETURN
      END
      FUNCTION VISCL(T)
C             VISCOSITY AS A FUNCTION OF TEMPERATURE (F) FOR
C             ETHELENE GLYCOL
C                       UNITS LBM/(FT.HR)
C
      DATA X1,X2,X3,X4,X5 /3.80666,-1.798086,0.385912,-0.05878,0.004173/
     1,T0,DT /40.0,60.0/
      THETA = (T-T0)/DT
      VISCL = 2.42*EXP((((X5*THETA+X4)*THETA+X3)*THETA+X2)*THETA+X1)
      RETURN
      END
      FUNCTION THCNL(T)
C             THERMAL CONDUCTIVITY AS A FUNCTION OF TEMPERATURE (F)
C             FOR ETHELENE GLYCOL
C                       UNITS BTU/(HR.FT.F)
C
      DATA X1,X2 /0.1825,-2.3E-04/
      THCNL = X1+X2*T
      RETURN
      END
      FUNCTION PRNO(T)
C             PRANDTL NUMBER AS A FUNCTION OF TEMPERATURE (F) FOR
C             ETHELENE GLYCOL
C
      DATA X1,X2,X3,X4 /5.83067,-2.129503,0.54344,-0.058687/,T0,DT /40.0
     1,80.0/
      THETA = (T-T0)/DT
      PRNO = EXP(((X4*THETA+X3)*THETA+X2)*THETA+X1)
      RETURN
      END
//
```

APPENDIX K .

SAMPLE CALCULATIONS

Heat Transfer

Run 36 for ethylene glycol with y = 2.45 is used to illustrate the details of data reduction procedure.

Physical dimensions and properties of tube and tape

Inside tube diameter, D_i = 0.401 in.

Outside tube diameter, D_o = 0.441 in.

Total heated length, L_T = 48.0 in.

Length to measuring section, L_s = 44.0 in.

Thermal conductivity of tube and tape, k at 100 ^oF = 9.4 Btu/hr ft ^oF

Thickness of tape δ = 0.0182 in.

Length of pressure tap (1 in. away from heating section) = 50 in.

Measured quantities

The tube wall thermocouple readings at the measuring section were numbered 1 through 8. These locations were 45^o apart, starting clockwise from the top of the tube. The tape was located at 120^o from the top of the tube. The two thermocouples placed in the flow at the inlet and outlet sections were numbered 9 and 10. The measured data were as follows:

e_1 = 1.417 mv

e_2 = 1.412 mv

e_3 = 1.444 mv

e_4 = 1.438 mv

e_5 = 1.414 mv

e_6 = 1.434 mv

e_7 = 1.432 mv

e_8 = 1.414 mv

e_9 = 0.777 mv

e_{10} = 1.195 mv

Flow meter reading, FMR = 100%

Voltage across the test section, V_T = 3.00 V

Voltage across the shunt, V_s = 28.42 V

Pressure drop reading, ΔP = 1.014 in. Hg

Mean Wall temperature

The wall and fluid temperature were obtained from the corresponding thermocouple reading using NBS Circular 561.

$T_{w,1}$ = 95.40 °F

$T_{w,2}$ = 95.27 °F

$T_{w,3}$ = 96.05 °F

$T_{w,4}$ = 96.14 °F

$T_{w,5}$ = 95.30 °F

$T_{w,6}$ = 96.30 °F

$T_{w,7}$ = 96.56 °F

$T_{w,8}$ = 95.18 °F

T_i = 67.35 °F

T_o = 85.75 °F

The electric current through the heat test section is obtained from the voltage across the shunt with calibration of 240 amp/100 mv.

$$I = 2.4\ V_s$$
$$= 2.4 \times 28.42 = 68.208 \text{ amp}$$

The test section insulation limited the heat loss to about 1.5 percent of the total power generated in the tube wall. Accordingly, the net heat input to the fluid can be calculated as follows:

$$q = 0.985\ V_T\ I$$
$$= 0.985 \times 3.00 \times 68.208 \times 3.4129$$
$$= 687.89 \text{ Btu/hr}$$

The average heat flux, q", based on the inside tube surface area, is given as

$$q'' = \frac{q}{\pi D_i L_T}$$

$$= \frac{687.89 \times 144}{\pi \times 0.401 \times 48} = 1638.1 \text{ Btu/hr ft}^2$$

The rate of volumetric heat generation may be calculated according to the relation

$$\dot{q}'' = \frac{q}{\frac{\pi}{4}\left(D_o^2 - D_i^2\right) L_T}$$

$$= \frac{4 \times 687.89 \times 12^3}{\pi[(0.441)^2 - (0.401)^2] \times 48}$$

$$= 9.351 \times 10^5 \text{ Btu/hr ft}^3$$

The temperature drop across the tube wall can then be calculated from the results suggested by Morcos and Bergles [97] as follows:

$$\Delta T_w = \frac{q''}{2 k_w}\left[r_o^2 \ln \frac{r_o}{r_i} - \frac{1}{2}\left(r_o^2 - r_i^2\right)\right]$$

$$= \frac{9.315 \times 10^5}{2 \times 9.4 \times 144 \times 4}\left\{(0.441)^2 \ln\left(\frac{0.441}{0.401}\right) - \frac{1}{2}\left[(0.441)^2 - (0.401)^2\right]\right\}$$

$$= 0.14 \ ^{o}F$$

The above temperature drop was applied uniformly around the circumference of the tube so as to obtain the following inside wall temperatures:

$T_{w,1} = 95.26\ ^{o}F$ $\quad$ $T_{w,5} = 95.16\ ^{o}F$

$T_{w,2} = 95.13\ ^{o}F$ $\quad$ $T_{w,6} = 96.16\ ^{o}F$

$T_{w,3} = 95.91\ ^{o}F$ $\quad$ $T_{w,7} = 96.42\ ^{o}F$

$T_{w,4} = 96.00\ ^{o}F$ $\quad$ $T_{w,8} = 95.04\ ^{o}F$

The circumferentially averaged inside tube wall temperature was calculated from the above eight values using Simpson's integration:

$$\bar{T}_w = \frac{1}{12}\left[T_{w,1} + T_{w,3} + T_{w,5} + T_{w,7} + 2\left(T_{w,2} + T_{w,4} + T_{w,6} + T_{w,8}\right)\right]$$

$$= 95.61\ ^{o}F$$

Fluid bulk temperature

Using the flowmeter calibration curve gives the fluid flow rate:

$$\dot{m} = 110.44\ lb_m/hr$$

An energy balance over the tube length from the onset of heating up to the measuring section yields:

$$q\frac{L_s}{L_T} = \dot{m}(h_s - h_i) \qquad \text{(K-1)}$$

where h_i and h_s are the fluid enthalpy at the inlet and measuring section, respectively. Equation (K-1) can than be rearranged to yield:

$$h_s = h_i + \frac{qL_s}{\dot{m}L_T}$$

$$= 31.54 + \frac{687.89}{110.44} \times \frac{44}{48}$$

$$h_s = 37.24 \text{ Btu } lb_m$$

From the physical properties of ethylene glycol, the fluid bulk temperature, corresponding to h_s, is found to be:

$$T_b = 77.55\ ^{o}F$$

Nusselt number

The circumferentially averaged heat transfer coefficient is calculated as follows:

$$\bar{h} = \frac{q''}{\bar{T}_w - T_b}$$

$$= \frac{163.8}{95.61 - 77.55}$$

$$= 90.68 \text{ Btu/hr ft}^2\ ^{o}\bar{F}$$

The above calculated $\bar{h}$ and the physical property of ethylene glycol evaluated at the bulk temperature were used to obtain Nusselt number as follows:

$$Nu_s = \frac{\bar{h} \cdot D_i}{k}$$

$$= \frac{90.68 \times 0.401}{0.1645 \times 12} = 18.40$$

Nondimensional parameters

The physical properties of ethylene glycol evaluated at the bulk temperature were employed to calculate the following dimensionless parameters:

$$Gr_D = \frac{g\beta\rho^2 D_i^3 \left(\bar{T}_w - T_b\right)}{\mu^2}$$

$$= \frac{32.2 \times 3.88 \times 10^{-4} \times (66.9)^2 \times (0.401)^3 \times (3,600)^2}{(41.15)^2 \times (12)^3}$$

$$\times (95.61 - 77.55)$$

$$= 0.3329 \times 10^3$$

$$Ra_D = Gr_D \cdot Pr$$

$$= 0.3329 \times 10^3 \times 140.4$$

$$= 0.467 \times 10^5$$

$$Re_s = \frac{GD_i}{\mu} = \frac{\dot{m}}{\left(\frac{\pi}{4} D_i - \delta\right)\mu}$$

$$= \frac{110.44 \times 12}{\frac{\pi}{4} (0.401 - 0.0182) \times 41.15}$$

$$= 110.13$$

$$z = \frac{L_s}{D_i \, Re_s \, Pr}$$

$$= \frac{44}{0.401 \times 110.13 \times 140.4} = 7.094 \times 10^{-3}$$

$$Re_s/y = \frac{110.13}{2.45} = 45.04$$

Nusselt number ratio

Since the correlation from Morcos and Bergles are based on film temperature, it is necessary to convert the present data utilizing bulk mean temperature to film temperature, which is calculated to be

$$T_f = \frac{1}{2} \left(\bar{T}_w + T_b\right)$$

$$= \frac{1}{2} (95.61 + 77.55) = 86.58 \ ^oF$$

The Nusselt number using film temperature in the present experimental data is

$$Nu_{sf} = \frac{\bar{h} \cdot D_i}{k_f}$$

$$= \frac{90.68 \times 0.401}{0.1622 \times 12} = 18.64$$

The heat transfer correlation from Morcos and Bergles [97] for metal tube and ethylene glycol fluid is as follows

$$Nu_{of} = 0.3836\ Gr_f^{0.256} \cdot Pr_f^{0.31}$$

$$= 0.3836 \times (0.5016 \times 10^3)^{0.256} \times (117.1)^{0.31} \qquad \text{(K-2)}$$

$$= 7.921$$

$$\left(\frac{Nu_s}{Nu_o}\right)_f = 2.353$$

Pressure Drop

Midpoint bulk temperature

The friction factor was evaluated at an axial location halfway along the heated section. An energy balance over the first half of the heated section yields

$$\frac{q}{2} = \dot{m}\ (h_b - h_i)$$

where h_b is the fluid enthalpy at the midpoint. The enthalpy at the midpoint can thus be obtained as follows:

$$h_b = h_i + \frac{q}{2\dot{m}}$$

$$= 31.54 + \frac{687.89}{2 \times 110.44}$$

$$= 34.65 \text{ Btu/lb}_m$$

which results in

$$T_b = 72.92\ ^{o}F$$

Friction factor

The Reynolds number at the middle section of the tube is given by

$$Re_M = \frac{\dot{m}}{\left(\frac{\pi}{4} D_i - \delta\right)\mu}$$

$$= \frac{110.44 \times 12}{\frac{\pi}{4} (0.401 - 0.0182) \times 45.85}$$

$$= 98.85$$

The isothermal pressure drop data shown in Fig. 5-13 is found to have the following functional dependence on the Reynolds number:

$$f = \frac{160}{Re_s} \qquad \text{(K-3)}$$

The pressure taps on the metal tube are 50 in. apart, 1 in. outside the 48 in. heated length. Ic is necessary, therefore, to calculate the isothermal pressure drop, using Eq. (K-3) for both of these segments. This pressure drop is subtracted from the total measured pressure drop to yield the pressure drop across the heated section. Using the inlet and outlet fluid temperatures, one can calculate the Reynolds numbers at the inlet and outlet section as follows:

$$Re_i = \frac{110.44 \times 12}{\frac{\pi}{4} (0.401 - 0.0182) \times 52.0}$$

$$= 87.10$$

$$Re_o = \frac{110.44 \times 12}{\frac{\pi}{4}(0.401 - 0.0182) \times 28.2}$$

$$= 160.7$$

The corresponding friction factors are given by

$$f_i = \frac{160}{87.10} = 1.836$$

$$f_o = \frac{160}{160.7} = 0.996$$

The isothermal pressure drop across the unheated inlet and outlet segment can be calculated according to the following equations:

$$\Delta P_i = \frac{g}{g_c} \cdot \frac{f_h \cdot \Delta L}{D_i} \cdot \frac{\rho \bar{w}^2}{2g}$$

$$= \frac{1.836 \times 1 \times 68.43 \times (1.931 \times 10^3)^2}{32.3 \times 0.401 \times 2 \times (3600)^2 \times 12}$$

$$= 1.065 \times 10^{-2} \text{ psi}$$

$$\Delta P_o = \frac{0.996 \times 1 \times 67.62 \times (1.951 \times 10^3)^2}{32.2 \times 0.401 \times 2 \times (3600)^2 \times 12}$$

$$= 0.6275 \times 10^{-2} \text{ psi}$$

The total measured pressure drop, as calculated from the differential mercury head, is given by

$$\Delta P_t = \frac{g}{g_c} \Delta P(\rho_{Hg} - \rho_{Eg})$$

$$= 1.014 \times \frac{(874.12 - 69.34)}{1728} = 0.472 \text{ psi}$$

Finally, the pressure drop across the heated section can be calculated as

$$\Delta P_h = \Delta P_t - \Delta P_i - \Delta P_o$$

$$= 0.472 - 1.065 \times 10^{-2} - 0.6275 \times 10^{-2}$$

$$= 0.460 \text{ psi}$$

which yields

$$f = \frac{2 g_c D_i \Delta P_h}{\rho \bar{w}^2 L_T}$$

$$= \frac{2 \times 32.2 \times 0.401 \times 0.460 \times 144 \times (3600)^2}{67.92 \times (1.942 \times 10^3)^2 \times 48}$$

$$= 1.833$$

A listing of the FORTRAN IV computer program utilized to facilitate the data reduction is given in Appendix J. The experimental results for heat transfer and friction factor are tabulated in Appendix L.

APPENDIX L .

TABULATION OF EXPERIMENTAL RESULTS

Experimental Results for Ethylene Glycol, y = 5.08

Run	$\dot{m}$ lb/hr	q" Btu/hr-ft^2	T_b °F	$\bar{T}_w$ °F	f	Re_s	Pr	Be	Nu_s	$Gr^*_o \times 10^{-3}$	Nu_s/Nu_o	$Re_o)_p$[1]	Ref.[2]
1	14.43	163.8	73.95	79.81	10.99	13.23	151.5	0.138	5.646	0.45	1.147	21.8	7-1
2	14.43	163.8	78.37	83.95	10.99	14.67	138.1	0.128	5.966	0.55	1.174	25.29	7-2
3	24.95	165.4	69.90	75.46	6.300	20.77	165.3	0.135	5.972	0.369	1.246	32.61	10-1
4	24.95	165.4	72.49	77.47	6.300	22.11	156.3	0.119	6.696	0.419	1.371	35.68	10-2
5	41.21	164.8	65.39	69.99	3.779	30.70	182.7	0.115	7.140	0.292	1.544	45.66	13-1
6	41.21	164.8	66.96	71.39	3.779	31.92	176.4	0.110	7.439	0.3168	1.589	48.32	13-2
7	41.21	649.6	74.22	90.17	3.084	38.04	150.6	0.375	8.229	1.791	1.154	52.69	14-2
8	24.95	641.3	83.83	99.73	4.764	28.66	123.7	0.350	8.258	2.776	1.085	42.34	11-2
9	56.50	649.8	70.76	85.96	2.547	48.03	162.2	0.366	8.595	1.512	1.236	68.23	18-2
10	70.36	648.2	68.43	82.62	2.313	56.51	170.7	0.348	9.159	1.342	1.341	83.26	22-2
11	41.21	649.6	68.06	82.02	3.084	32.80	172.1	0.343	9.315	1.320	1.367	42.52	14-1
12	41.21	177.2	88.45	119.7	2.323	52.33	113.0	0.667	9.497	7.574	0.9742	69.80	15-2
13	56.50	649.8	66.25	79.70	2.547	43.00	179.2	0.335	9.654	1.205	1.437	58.16	18-1
14	56.50	179.2	81.07	111.3	2.024	61.05	130.7	0.679	9.813	5.554	1.056	82.77	19-2
15	82.37	652.5	67.63	80.64	2.154	64.86	173.7	0.321	10.04	1.297	1.476	98.87	28-2
16	41.21	1440.4	74.91	102.4	2.324	38.66	148.4	0.644	10.60	4.104	1.195	45.07	15-1
17	41.21	1940.0	96.00	134.4	2.022	62.24	96.70	0.759	10.76	14.82	0.9654	82.47	16-2
18	110.4	656.7	65.00	77.69	1.750	82.69	181.8	0.302	10.84	1.177	1.617	78.36	35-2
19	70.36	648.2	64.81	76.68	2.313	51.65	185.1	0.298	10.89	1.116	1.639	73.12	22-1
20	70.36	2541.1	87.85	135.0	1.471	88.20	114.3	1.010	11.11	13.18	0.9826	118.4	24-2
21	95.16	654.4	66.69	78.42	2.019	73.21	177.4	0.291	11.15	1.240	1.651	114.9	30-2
22	24.95	1422.5	104.9	131.7	3.334	44.20	83.86	0.513	11.19	15.15	1.036	63.73	12-2

[1] Reynolds number for smooth tube computed assuming constant pumping power for swirl and smooth tube.
[2] Heat Transfer Laboratory file number.

Run	$\dot{m}$ lb/hr	q" Btu/hr-ft^2	T_b ^oF	$\bar{T}_w$ ^oF	f	Re_s	Pr	Be	Nu_s	Gr_o^* x10^{-3}	Nu_s/Nu_o	$Re_o)_p$	Ref.
23	95.1.	1459.4	72.43	98.44	1.702	84.19	156.5	0.620	11.31	3.686	1.293	124.3	31-2
24	56.5'	1450.0	71.04	96.88	2.024	48.34	161.2	0.622	11.33	3.433	1.311	59.08	19-1
25	56.50	2520.0	95.70	141.8	1.535	83.45	98.65	0.937	11.39	18.37	0.9588	110.3	20-2
26	82.37	2539.2	84.04	129.1	1.408	95.06	123.1	0.992	11.53	11.10	1.047	130.2	26-2
27	82.37	652.5	64.52	75.56	2.154	60.02	186.3	0.278	11.77	1.106	1.773	88.39	28-1
28	110.4	1457.7	71.67	96.24	1.501	95.93	159.0	0.589	11.94	3.546	1.374	142.1	36-2
29	70.36	1449.2	68.17	92.05	1.868	56.15	171.7	0.586	12.16	2.962	1.439	71.33	32-1
30	95.16	2556.5	81.65	124.4	1.384	104.1	129.2	0.955	12.22	10.01	1.126	148.4	32-2
31	110.4	2550.7	79.65	121.1	1.236	115.5	134.4	0.940	12.52	9.102	1.171	164.2	37-2
32	56.50	2520.0	78.51	119.0	1.535	57.61	137.7	0.926	12.63	8.527	1.195	64.59	20-1
33	82.37	1445.0	67.57	90.22	1.792	64.76	174.0	0.558	12.77	2.864	1.519	86.66	27-1
34	95.16	395.8	87.55	138.7	1.241	118.5	115.0	1.098	12.95	16.47	1.078	167.5	33-2
35	110.4	656.7	63.26	73.30	1.750	77.95	191.7	0.255	13.01	1.043	1.976	118.1	35-1
36	70.36	2541.1	73.85	112.6	1.471	64.36	151.8	0.916	13.22	6.877	1.290	75.10	24-1
37	95.16	654.4	63.98	73.72	2.019	68.41	188.6	0.246	13.38	1.079	2.022	104.2	30-1
38	95.16	1459.4	66.42	87.49	1.702	72.73	178.5	0.524	13.84	2.729	1.656	100.6	31-1
39	82.37	2539.2	72.06	108.9	1.408	72.22	157.7	0.879	13.90	6.296	1.375	87.52	26-1
40	121.0	700.1	77.07	87.11	1.420	119.3	141.8	0.232	14.14	2.213	1.904	197.2	1-2
41	82.37	3202.5	74.09	119.2	1.274	75.79	151.0	1.061	14.36	8.772	1.315	88.28	25-1
42	110.4	1457.7	66.49	86.38	1.501	84.55	178.2	0.494	14.65	2.736	1.753	118.4	36-1
43	95.16	2556.5	71.19	105.5	1.384	81.71	160.7	0.826	14.97	6.073	1.487	104.5	32-1
44	121.0	1100.4	80.04	94.95	1.334	127.7	133.4	0.337	15.03	3.999	1.755	206.3	3-2

Run	$\dot{m}$ lb/hr	q" Btu/hr-ft^2	T_b ^oF	$\tilde{T}_w$ ^oF	f	Re_s	Pr	Be	Nu_s	Gr_o^* x10^{-3}	Nu_s/Nu_o	$Re_o)_p$	Ref.
45	110.4	2550.7	70.64	103.7	1.236	93.59	162.6	0.799	15.49	5.898	1.546	121.2	37-1
46	121.0	1566.0	83.19	103.8	1.254	137.0	125.2	0.456	15.54	6.583	1.615	217.8	2-2
47	95.16	3217.1	74.44	115.6	1.241	88.28	149.9	0.968	15.79	8.961	1.440	109.5	33-1
48	121.0	2125.0	86.98	114.3	1.162	148.9	116.2	0.588	16.02	10.60	1.495	232.9	4-2
49	121.0	700.1	74.82	83.61	1.420	113.2	148.7	0.206	16.10	1.986	2.202	182.8	1-1
50	110.4	3942.0	76.28	124.1	1.018	106.9	144.2	1.109	16.71	11.99	1.425	130.6	38-1
51	121.0	2739.0	91.37	124.6	1.101	163.4	106.9	0.695	17.06	16.59	1.445	256.3	5-2
52	121.0	1100.4	76.50	89.34	1.334	117.8	143.5	0.297	17.36	3.384	2.080	183.6	3-1
53	121.0	1566.0	78.17	95.38	1.254	122.4	138.7	0.394	18.48	5.213	1.990	185.0	2-1
54	121.0	2125.0	80.19	103.2	1.162	128.1	133.0	0.519	18.85	7.778	1.844	187.6	4-1
55	121.0	273.90	82.65	111.3	1.101	135.4	126.6	0.636	19.54	11.23	1.756	195.3	5-1
56	248.4	1572.4	75.99	91.38	0.732	238.9	145.1	0.358	20.69	4.720	2.260	386.6	16-2
57	199.9	2136.4	74.39	95.53	0.771	109.6	146.9	0.470	21.46	6.229	2.170	276.5	9-1
58	248.4	2145.1	79.02	99.09	0.682	256.2	136.2	0.457	21.73	7.434	2.138	406.6	17-2
59	248.4	1105.2	71.81	82.01	0.766	216.5	158.5	0.244	21.82	2.708	2.701	348.6	15-1
60	199.9	2775.9	77.43	102.7	0.721	198.8	140.8	0.581	22.32	8.926	2.073	282.8	10-1
61	199.9	4280.6	91.03	130.7	0.629	268.0	107.6	0.832	22.32	25.53	1.681	398.2	12-2
62	299.1	1571.9	71.48	85.57	0.683	258.5	159.8	0.339	22.41	3.784	2.531	422.8	23-2
63	299.1	1103.8	68.45	77.92	0.683	240.3	170.6	0.232	23.35	2.287	2.965	386.9	22-1
64	299.1	2143.1	73.17	91.60	0.658	269.3	154.0	0.437	23.45	5.612	2.407	433.8	24-2
65	248.4	2772.0	82.63	106.8	0.650	277.8	126.6	0.537	23.46	11.36	2.101	440.7	18-2
66	248.4	1572.4	73.52	86.98	0.732	225.5	152.9	0.318	23.58	4.189	2.623	355.5	16-1

Run	$\dot{m}$ lb/hr	q" Btu/hr-ft^2	T_b ^oF	$\bar{T}_w$ ^oF	f	Re_s	Pr	Be	Nu_s	Gr_o^* $\times 10^{-3}$	Nu_s/Nu_o	$Re_o)_p$	Ref.
67	199.8	5173.6	96.33	141.2	0.589	299.0	97.53	0.910	24.00	38.74	1.661	447.5	13-2
68	248.4	3499.0	85.41	115.0	0.610	295.3	119.9	0.646	24.22	16.27	2.000	461.2	19-2
69	299.1	2772.8	75.67	98.79	0.618	285.6	146.1	0.539	24.27	8.196	2.284	452.0	25-2
70	248.4	2145.1	75.66	93.31	0.682	237.1	146.1	0.411	24.60	6.337	2.479	363.6	17-1
71	248.4	4289.3	89.74	124.2	0.576	324.1	110.2	0.731	25.65	24.19	1.948	507.6	20-2
72	199.8	4280.6	82.77	116.8	0.629	224.3	126.3	0.755	25.72	17.66	2.049	307.9	12-1
73	299.1	1571.8	69.40	81.66	0.683	246.0	167.1	0.298	25.72	3.416	2.951	393.5	23.1
74	299.1	3498.1	78.92	106.4	0.586	307.8	136.5	0.627	25.85	12.06	2.233	484.8	26-2
75	299.1	2143.1	70.37	86.63	0.658	251.8	163.6	0.393	26.48	4.888	2.776	393.7	24-1
76	248.4	5167.3	93.82	134.0	0.539	353.0	102.1	0.828	26.70	34.78	1.878	550.5	21-2
77	299.1	4296.0	82.62	115.4	0.550	334.6	126.7	0.728	26.80	17.60	2.135	525.0	27-2
78	199.9	5173.7	86.40	124.7	0.589	242.8	117.6	0.830	27.72	25.15	2.048	331.4	13-1
79	299.1	5195.8	85.89	124.5	0.517	359.5	118.7	0.838	27.66	24.69	2.048	559.2	28.2
80	248.4	2772.0	78.30	98.50	0.650	252.0	138.3	0.462	27.87	9.286	2.574	382.7	18.1
81	248.4	3499.0	79.95	104.9	0.610	261.6	133.7	0.564	28.59	12.67	2.452	387.2	19-1
82	299.1	2772.8	72.05	91.52	0.618	262.3	157.7	0.465	28.68	6.875	2.771	399.6	25-1
83	299.1	3498.1	74.36	97.60	0.586	277.0	150.1	0.546	30.41	9.707	2.715	416.3	26-1
84	248.4	4289.3	83.08	111.8	0.576	280.6	125.5	0.637	30.49	17.95	2.423	412.2	20-1
85	248.4	5167.3	84.82	113.4	0.539	298.0	118.9	0.729	31.64	24.48	2.347	431.1	21-1
86	299.1	4296.0	77.05	103.8	0.550	294.9	141.9	0.618	32.52	13.56	2.695	437.5	27-1
87	299.1	5195.8	79.17	111.2	0.517	309.6	135.8	0.729	32.96	18.13	2.557	450.6	28-1
88	299.1	6151.2	83.04	119.1	0.478	337.7	125.6	0.798	34.93	25.69	2.521	487.3	7-1
89	299.1	7185.8	85.63	126.4	0.451	357.5	119.3	0.887	36.19	33.76	2.462	510.3	30-1
90	299.1	8263.1	89.13	135.1	0.417	385.4	111.5	0.976	37.11	45.36	2.375	543.3	31-1

Experimental Results for Ethylene Glycol, $y = 2.45$

Run	$\dot{m}$ lb/hr	q" Btu/hr-ft^2	T_b ^oF	$\bar{T}_w$ ^oF	f	Re_s	Pr	Be	Nu_s	Gr_q^* $\times 10^{-3}$	Nu_s/Nu_o	$Re_o)_p$	Ref.
1	24.95	184.8	72.30	76.54	8.750	22.00	156.9	0.101	8.779	0.4637	1.747	41.55	8-1
2	41.21	418.5	76.41	84.11	4.685	40.03	143.8	0.178	11.02	1.281	1.710	71.39	12-2
3	41.21	418.5	72.45	80.08	4.685	36.48	156.4	0.182	11.05	0.1564	1.765	62.40	12-1
4	24.95	184.8	75.19	78.55	8.750	23.56	147.6	0.079	11.13	0.5337	2.169	45.86	8-2
5	56.50	412.4	72.13	79.32	3.654	49.63	157.5	6.172	11.55	1.026	1.857	87.56	17-1
6	41.21	721.2	80.95	93.02	4.344	44.41	131.0	0.271	12.18	2.735	1.483	77.80	13-2
7	56.50	412.4	74.98	81.63	3.654	53.09	148.2	0.156	12.55	1.179	1.976	96.52	17-2
8	41.21	721.3	74.14	85.71	4.344	37.97	150.8	0.272	12.60	1.980	1.718	62.05	13-1
9	56.50	723.9	77.35	88.82	3.425	56.09	141.0	0.264	12.81	2.319	1.706	98.50	18-2
10	70.36	419.9	70.53	77.03	3.104	59.47	163.0	0.157	12.98	15.74	2.102	106.0	23-2
11	41.21	1135.5	88.18	105.8	3.896	52.03	113.6	0.378	13.24	5.977	1.450	90.66	14-2
12	70.36	734.7	73.92	84.80	2.906	64.48	151.6	0.257	13.64	1.996	1.854	112.2	24-2
13	56.50	723.9	72.36	82.97	3.425	49.89	150.7	0.253	13.74	1.822	1.897	83.17	18-1
14	82.37	421.1	72.46	78.57	2.798	72.92	156.3	0.145	13.90	1.065	2.216	136.3	29-2
15	56.50	1141.7	82.97	99.76	3.131	63.69	125.8	0.372	13.91	4.753	1.576	110.7	19-2
16	70.36	419.9	68.19	74.20	3.104	56.18	171.6	0.147	14.02	0.859	2.309	97.63	23-1
17	70.36	1148.5	79.84	96.18	2.688	73.93	134.0	0.370	14.31	4.136	1.654	128.8	25-2
18	82.37	735.9	74.87	85.12	2.666	77.19	148.5	0.240	14.51	2.093	1.959	140.6	30-2
19	41.21	1608.7	96.79	119.7	3.514	62.23	96.72	0.463	14.62	12.28	1.379	109.7	15-2
20	82.37	421.1	70.46	76.18	2.798	69.51	163.3	0.138	14.81	0.965	2.398	127.2	29-1
21	56.50	1141.7	75.12	90.28	3.131	53.26	147.7	0.354	15.24	3.287	1.825	25.52	19-1

Run	$\dot{m}$ lb/hr	q" Btu/hr-ft^2	T_b ^oF	$\bar{T}_w$ ^oF	f	Re_s	Pr	Be	Nu_s	Gr_o^* $\times 10^{-3}$	Nu_s/Nu_o	$Re_o)_p$	Ref.
22	41.21	1608.7	81.78	103.2	3.514	45.24	128.8	0.479	15.31	6.34	1.596	69.19	15-1
23	41.21	2178.1	85.27	114.3	3.185	48.87	120.2	0.633	15.40	10.07	1.444	72.58	16-1
24	95.16	733.5	71.50	80.98	2.309	82.33	159.6	0.227	15.58	1.770	2.157	144.8	36-1
25	70.36	1635.8	84.82	106.1	2.543	82.60	121.2	0.465	15.79	7.409	1.605	144.6	26-2
26	110.4	737.8	71.47	80.75	2.055	95.47	159.7	0.223	15.98	1.777	2.210	170.6	43-2
27	70.36	1148.5	73.49	87.74	2.688	63.82	153.0	0.337	16.26	3.054	1.968	104.1	25-1
28	82.37	735.9	71.38	80.30	2.666	71.06	160.0	0.214	16.59	1.765	2.298	124.8	30-1
29	56.50	2182.1	82.19	108.4	2.612	62.58	127.8	0.584	17.02	8.762	1.630	95.61	21-1
30	82.37	1632.3	83.71	103.2	2.327	94.37	123.9	0.429	17.16	7.029	1.758	169.1	32-2
31	110.4	737.8	68.85	77.33	2.055	89.61	169.1	0.207	17.45	1.560	2.461	155.6	43-1
32	70.36	2213.0	91.65	117.7	2.326	95.57	106.3	0.544	17.59	13.56	1.575	168.2	27-2
33	95.16	1638.1	80.89	99.51	2.124	102.4	131.2	0.419	17.93	6.194	1.872	183.2	38-2
34	121.0	1162.4	66.80	79.62	1.745	93.34	177.0	0.318	18.12	2.215	2.298	149.6	51-1
35	56.50	2815.8	86.88	118.5	2.387	69.36	116.5	0.683	18.29	13.99	1.584	104.8	22-1
36	110.4	1638.1	77.55	95.61	1.833	110.3	140.4	0.415	18.40	5.296	1.967	190.7	45-2
37	56.50	2815.8	105.9	137.8	2.387	102.0	82.46	0.606	18.67	31.20	1.432	182.8	22-2
38	82.37	1632.3	76.02	93.76	2.327	79.29	145.0	0.409	18.79	4.206	2.032	131.5	32-1
39	82.37	2216.4	89.40	113.4	2.155	106.7	111.0	0.510	19.03	12.31	1.728	191.6	33-2
40	95.16	1638.1	74.19	91.36	2.124	87.77	150.7	0.404	19.27	4.508	2.110	146.6	38-1
41	121.0	2262.1	78.26	102.0	1.557	122.7	138.4	0.543	19.37	7.550	1.890	203.1	52-2
42	95.16	2223.1	85.82	109.1	1.993	114.2	118.9	0.507	19.58	10.53	1.821	204.7	39-2
43	110.4	1638.1	71.76	88.33	1.833	96.15	158.7	0.397	19.91	4.004	2.219	156.7	45-1

Run	$\dot{m}$ lb/hr	q'' Btu/hr-ft^2	T_b ^oF	$\bar{T}_w$ ^oF	f	Re_s	Pr	Be	Nu_s	Gr^* $\times 10^{-3}$	Nu_s/Nu_o	$Re_o)_p$	Ref.
44	82.37	2216.4	79.00	101.5	2.155	84.91	136.3	0.513	20.02	7.672	1.953	137.7	33-1
45	70.36	2870.4	98.92	129.8	2.153	113.1	91.46	0.591	20.13	24.95	1.594	203.8	28-2
46	121.0	2906.5	82.90	112.3	1.471	136.0	126.0	0.651	20.23	12.06	1.786	227.0	53-2
47	82.37	2871.9	94.94	124.0	2.007	119.8	100.0	0.595	20.52	20.27	1.677	215.7	34-2
48	121.0	1660.0	69.26	85.41	1.651	199.18	167.6	0.393	20.62	3.584	2.334	156.2	52-1
49	110.4	2233.9	82.94	105.1	1.724	124.4	125.9	0.490	20.64	9.287	1.955	217.2	46-2
50	95.16	2223.1	76.76	98.45	1.993	93.19	142.8	0.502	20.78	6.923	2.058	152.7	39-1
51	82.37	2871.9	81.52	109.3	2.007	89.88	129.5	0.623	21.07	11.18	1.884	142.5	34-1
52	199.9	1168.1	68.77	79.81	1.199	161.8	169.4	0.270	21.20	2.460	2.645	282.3	57-2
53	110.4	2875.8	87.07	114.8	1.600	136.1	116.0	0.598	21.33	14.41	1.835	235.5	47-2
54	82.37	3605.3	101.3	134.9	1.865	136.2	89.19	0.677	21.90	3.324	1.617	247.5	35-2
55	121.0	2906.5	73.57	99.86	1.471	110.0	152.7	0.622	22.31	7.759	2.105	166.6	53-1
56	121.0	3665.0	89.12	122.9	1.351	155.9	111.5	0.717	22.39	20.11	1.781	261.5	54-2
57	82.37	3605.3	84.57	117.6	1.865	96.18	121.8	0.723	22.40	16.15	1.345	149.8	35-1
58	199.9	1658.3	70.86	85.71	1.147	170.3	161.9	0.358	22.44	3.875	2.510	292.2	58-2
59	110.4	2233.9	75.09	95.10	1.724	104.0	147.9	0.468	22.58	6.419	2.260	167.8	46-1
60	110.4	3629.5	92.64	125.5	1.506	153.2	104.4	0.682	22.90	23.22	1.784	267.9	48-2
61	110.4	2875.8	76.98	102.2	1.600	108.7	142.1	0.583	23.11	9.050	2.133	170.1	47-1
62	95.1	3601.0	98.41	139.6	1.735	148.4	93.95	0.642	23.40	29.41	1.761	272.6	41-2
63	199.9	2243.3	73.71	92.88	1.093	182.2	152.2	0.453	23.63	6.031	2.386	310.2	59-2
64	121.0	4501.6	94.22	133.2	1.310	173.4	101.4	0.800	24.01	30.82	1.748	297.3	55-2
65	95.16	3601.0	83.88	114.0	1.735	109.4	123.5	0.663	24.50	15.63	2.029	175.6	41-1
66	95.16	4443.9	105.0	142.8	1.366	168.9	83.71	0.723	24.80	47.51	1.693	288.6	42-2

Run	$\dot{m}$ lb/hr	q" Btu/hr-ft^2	T_b ^oF	$\bar{T}_w$ ^oF	f	Re_s	Pr	Be	Nu_s	Gr^* $\times 10^{-3}$	Nu_s/Nu_o	$Re_o)_p$	Ref.
67	199.9	1168.1	66.47	75.88	1.199	152.9	178.3	0.234	24.83	2.190	3.152	260.1	57-1
68	199.9	2928.0	76.98	100.87	1.038	196.7	142.1	0.552	24.86	9.216	2.283	333.4	60-2
69	110.4	4468.0	99.60	136.41	1.412	176.4	91.97	0.729	25.42	38.34	1.791	314.9	49-2
70	121.0	4501.6	79.88	115.4	1.310	127.3	133.9	0.803	25.82	16.24	2.071	190.2	55-1
71	199.9	3667.6	80.83	109.5	0.986	214.8	131.3	0.644	26.11	13.83	2.198	364.8	61-2
72	199.9	1658.3	67.60	80.28	1.147	157.3	173.9	0.312	26.18	3.293	3.001	260.6	58-1
73	199.9	2243.3	69.32	85.87	1.093	164.0	167.4	0.403	27.18	4.856	2.837	266.4	59-1
74	110.4	4468.0	84.08	117.6	1.412	127.6	123.0	0.738	27.28	19.57	2.129	197.2	49-1
75	199.9	2928.0	71.27	92.10	1.038	171.9	160.4	0.500	28.28	6.984	2.708	274.4	60-1
76	199.9	4510.2	85.45	117.9	0.938	237.9	119.8	0.708	28.48	21.02	2.197	408.4	62-2
77	248.4	2267.5	76.32	92.08	1.009	240.8	144.1	0.365	29.17	6.916	2.882	451.0	65-2
78	248.4	2928.0	79.60	99.64	0.961	259.5	134.7	0.455	29.73	10.42	2.681	484.5	66-2
79	199.9	3667.6	73.69	98.52	0.986	182.2	152.3	0.587	29.81	9.851	2.641	287.6	61-1
80	248.4	1658.3	74.16	85.37	1.059	228.9	150.8	0.264	29.88	4.556	3.261	435.8	64-2
81	199.9	6427.9	94.98	137.6	0.848	290.9	99.96	0.870	31.41	45.45	2.069	510.5	63-2
82	199.9	4510.2	76.70	105.8	0.938	195.5	142.9	0.672	31.46	14.01	2.580	307.5	62-1
83	248.4	4565.9	87.06	115.9	0.713	306.1	116.1	0.623	32.47	22.87	2.469	518.5	67-2
84	248.4	2928.0	75.01	92.46	0.961	233.5	148.1	0.408	33.93	8.383	3.162	415.9	66-1
85	199.9	6427.9	83.60	120.2	0.848	223.4	126.7	0.835	34.96	26.31	2.501	348.8	63-1
86	248.4	6497.0	96.69	134.7	0.774	374.2	96.90	0.769	35.61	49.38	2.313	710.4	68-2
87	248.4	4565.9	79.95	105.2	0.889	261.6	133.7	0.571	36.87	16.53	2.944	461.5	67-1
88	248.4	6497.0	86.65	120.1	0.774	303.4	117.0	0.723	39.91	31.95	2.769	524.7	68-1
89	248.4	8744.6	93.21	135.9	1.049	348.5	103.3	0.884	42.45	57.32	2.605	735.7	69-1

Experimental Results for Water, y = 5.08

Run	$\dot{m}$ lb/hr	q" Btu/hr-ft^2	T_b ^oF	$\bar{T}_w$ ^oF	Re_s	Pr	Be	Nu_s	$Gr^*_q \times 10^{-5}$	Nu_s/Nu_o	Ref.
1	4.500	158.5	76.13	78.36	83.42	6.181	0.029	6.739	0.2675	1.093	33-1
2	9.49	161.6	69.51	71.71	161.3	6.806	0.029	7.026	0.2032	1.184	40-1
3	9.49	161.6	73.24	75.35	169.5	6.443	0.028	7.277	0.2406	1.197	40-2
4	9.49	362.2	73.56	78.26	170.2	6.413	0.061	7.340	0.5471	1.017	52-1
5	9.49	362.0	73.74	78.08	170.6	6.397	0.056	7.925	0.5509	1.097	41-1
6	9.49	362.0	82.09	86.19	189.6	5.689	0.050	8.297	0.7794	1.094	41-2
7	14.65	363.7	69.17	73.27	247.9	6.841	0.055	8.488	0.4499	1.208	51-1
8	14.65	632.1	68.43	75.47	245.5	6.917	0.095	8.604	0.7553	1.096	46-1
9	14.65	632.1	77.88	84.43	277.7	6.031	0.083	9.118	1.148	1.095	46-2
10	14.65	363.7	74.60	78.27	266.3	6.318	0.047	9.407	0.5748	1.294	51-2
11	18.99	630.6	66.64	72.89	310.6	7.106	0.085	9.696	0.6914	1.251	45-1
12	23.70	634.4	66.37	72.27	386.1	7.135	0.081	10.33	0.6866	1.335	37-1
13	18.99	360.5	71.51	74.61	331.5	6.608	0.041	11.08	0.4968	1.557	50-2
14	23.70	360.2	70.40	73.49	407.7	6.717	0.041	11.16	0.4720	1.579	49-2
15	23.70	633.3	73.02	78.34	422.0	6.464	0.070	11.32	0.9337	1.399	44-2
16	14.65	637.5	83.45	88.59	297.6	5.585	0.063	11.62	1.448	1.351	30-2
17	23.70	160.6	65.51	66.79	381.6	7.229	0.018	12.11	0.1665	2.099	36-2
18	23.70	1416.8	72.13	82.90	417.1	6.548	0.142	12.54	2.008	1.316	38-1
19	14.65	1397.7	82.29	92.62	293.4	5.674	0.127	12.72	3.033	1.261	31-1
20	14.65	1397.7	103.2	113.1	372.8	4.352	0.1065	12.88	6.313	1.158	31-2
21	32.15	1416.8	69.03	79.13	492.9	6.855	0.136	13.43	1.742	1.438	25-1

Run	$\dot{m}$ lb/hr	q'' Btu/hr-ft^2	T_b ^oF	$\bar{T}_w$ ^oF	Re_s	Pr	Be	Nu_s	$Gr_q^* \times 10^{-5}$	Nu_s/Nu_o	Ref.
22	14.65	2452.3	134.6	150.4	505.0	3.118	0.139	13.75	2.615	0.9836	32-2
23	23.70	2491.5	80.31	96.33	463.1	5.830	0.200	14.65	4.997	1.301	39-1
24	32.15	2505.4	75.33	91.35	589.8	6.252	0.206	14.84	4.086	1.355	26-1
25	32.15	1416.8	78.68	87.60	615.5	5.963	0.112	15.00	2.660	1.514	25-2
26	47.63	1416.8	66.33	75.21	775.5	7.139	0.121	15.33	1.530	1.672	18-1
27	47.63	2508.4	70.28	85.33	818.0	6.729	0.200	15.93	3.268	1.500	19-1
28	32.15	3871.4	82.85	105.4	648.2	5.630	0.276	16.10	2.589	1.285	27-1
29	32.15	2505.4	92.40	106.8	725.9	4.966	0.165	16.18	7.913	1.350	26-2
30	47.63	1416.8	72.85	80.86	846.1	6.480	0.105	16.84	2.073	1.759	18-2
31	23.70	2491.5	103.3	116.7	604.0	4.344	0.143	17.08	11.31	1.359	39-2
32	47.63	3890.5	75.60	96.77	876.9	6.228	0.272	17.43	6.419	1.448	20-1
33	32.15	5522.9	92.91	121.5	730.2	4.934	0.327	17.93	17.76	1.263	28-1
34	47.63	632.9	67.84	71.19	791.6	6.978	0.045	18.13	0.735	2.319	17-2
35	62.01	2510.0	67.63	80.84	102.8	7.001	0.179	18.22	2.887	1.747	11-1
36	47.63	3890.6	93.49	113.2	1089	4.898	0.225	18.28	12.76	1.383	20-2
37	47.63	5554.1	83.02	110.9	962.3	5.618	0.341	18.72	29.58	1.384	21-1
38	62.01	3894.0	71.88	90.94	1088	6.573	0.251	19.47	5.456	1.656	12-1
39	74.87	635.6	64.09	67.22	1182	7.389	0.043	19.59	0.6138	2.572	1-1
40	62.01	3894.0	89.63	103.9	1293	5.424	0.218	19.97	9.612	1.570	12-2
41	62.01	5559.1	77.76	103.3	1173	6.041	0.323	20.63	10.06	1.570	13-1
42	47.63	9623.4	100.0	142.1	1171	4.520	0.460	21.00	39.26	1.276	23-1
43	62.01	7530.1	85.07	117.9	1284	5.465	0.396	21.46	18.20	1.472	14-1
44	74.87	2520.7	73.02	83.80	1333	6.464	0.141	22.25	3.717	2.058	3-2
45	62.01	5569.0	97.42	120.1	1482	4.664	0.252	22.66	20.88	1.562	13-2

Run	$\dot{m}$ lb/hr	q" Btu/hr-ft^2	T_b ^oF	$\bar{T}_w$ ^oF	Re_s	Pr	Be	Nu_s	Gr^* $\times 10^{-5}$	Nu_s/Nu_o	Ref.
46	62.01	9720.2	92.81	129.9	1407	4.940	0.425	24.30	31.14	1.521	15-1
47	74.87	3914.6	80.87	95.85	1473	5.785	0.186	24.60	8.030	1.981	4-2
48	32.15	5522.9	130.5	150.5	1069	3.241	0.179	24.71	53.41	1.509	28-2
49	62.01	12173	100.9	145.4	1540	4.469	0.482	25.19	51.11	1.451	16-1
50	74.87	5599.0	73.74	94.33	1346	6.397	0.268	25.85	8.522	2.013	5-1
51	74.87	7513.3	79.15	106.2	1442	5.924	0.340	26.19	14.38	1.856	6-1
52	62.01	7530.1	111.7	137.2	1723	3.948	0.259	26.73	43.94	1.632	14-2
53	74.87	5599.0	90.11	109.5	1647	5.114	0.226	26.88	16.31	1.914	5-2
54	62.01	9729.2	127.1	157.7	2000	3.352	0.280	28.42	86.33	1.558	15-2
55	74.87	7513.3	101.1	124.8	1864	4.459	0.257	29.15	31.80	1.856	6-2
56	74.87	9772.5	85.87	116.8	1566	5.407	0.371	29.58	24.34	1.914	7-1
57	74.87	12237	93.43	180.1	1711	4.901	0.419	30.90	40.07	1.838	8-1
58	47.87	9772.5	114.5	142.4	2140	3.828	0.278	31.66	61.78	1.811	7-2
59	47.63	7488.4	125.5	146.1	1514	3.407	0.191	32.52	63.85	1.893	22-2
60	74.87	12237	129.2	160.6	2461	3.283	0.283	34.87	114.6	1.809	8-2

Experimental Results for Water, y = 2.45

Run	$\dot{m}$ lb/hr	q'' Btu/hr-ft^2	T_b ^oF	$\bar{T}_w$ ^oF	Re_s	Pr	Be	Nu_s	Gr^* $\times 10^{-5}$	Nu_s/Nu_o	Ref.
1	4.500	260.3	97.86	101.4	108.1	4.639	0.039	6.851	0.9901	0.8968	49-2
2	9.490	599.4	82.82	88.49	191.3	5.633	0.069	9.919	2.541	1.172	46-1
3	4.500	391.0	110.0	113.5	123.0	4.021	0.036	10.17	2.175	1.163	50-2
4	9.490	345.0	80.47	83.63	185.8	6.772	0.039	10.29	0.6965	1.382	45-1
5	9.49	950.1	87.77	95.62	203.0	5.272	0.093	11.29	2.541	1.181	47-1
6	18.99	612.1	70.89	75.38	328.8	6.669	0.060	13.02	0.8200	1.643	43-1
7	23.70	650.5	75.57	79.68	436.2	6.231	0.053	15.03	1.072	1.818	12-2
8	27.90	654.0	73.45	77.51	499.6	6.424	0.053	15.30	0.9827	1.874	52-2
9	23.70	1419.1	76.11	84.69	439.2	6.183	0.1100	15.67	2.393	1.605	13-1
10	14.65	1465.2	86.51	95.22	308.8	5.361	0.1040	15.73	3.739	1.511	10-1
11	23.70	2478.5	82.88	96.25	478.1	5.628	0.164	17.42	12.14	1.527	14-1
12	44.14	1367.8	75.11	81.89	807.5	6.272	0.087	19.15	2.209	1.988	57-2
13	36.27	1369.5	70.34	77.06	623.3	6.723	0.009	19.46	1.789	2.081	55-1
14	23.70	3814.7	93.56	111.6	542.3	4.894	0.206	19.59	12.54	1.488	15-1
15	32.15	2427.0	78.31	89.52	612.6	5.994	0.141	20.46	4.487	1.848	17-1
16	44.14	1367.8	68.32	74.37	738.4	6.928	0.082	21.66	1.626	2.348	57-1
17	47.63	1371.8	69.12	75.07	805.3	6.846	0.080	22.04	1.693	2.376	20-1
18	32.15	3742.7	84.21	100.9	667.1	5.454	0.189	22.70	9.093	1.771	18-1
19	32.15	3742.7	110.7	124.9	884.9	3.991	0.145	23.93	21.24	1.698	18-2
20	36.27	2418.5	75.60	84.80	667.7	6.228	0.118	24.94	3.990	2.290	56-1

Run	$\dot{m}$ lb/hr	q'' Btu/hr-ft^2	T_b ^oF	$\bar{T}_w$ ^oF	Re_s	Pr	Be	Nu_s	Gr_o^* $\times 10^{-5}$	Nu_s/Nu_o	Ref.
21	23.70	3814.7	128.8	142.3	776.1	3.297	0.123	25.16	3.533	1.670	15-2
22	62.01	1364.9	65.94	71.16	1004.0	7.182	0.071	25.25	1.446	2.784	28-1
23	23.70	2478.5	105.8	114.7	620.0	4.221	0.094	25.27	12.14	1.983	14-2
24	44.14	2431.6	72.29	81.22	778.4	6.533	0.1171	25.94	3.471	2.428	58-1
25	55.14	1365.4	66.26	71.16	897.0	7.147	0.067	26.76	1.470	2.945	24-1
26	67.63	2413.9	71.69	79.69	833.4	6.591	0.109	27.85	3.354	2.621	21-1
27	40.21	5360.4	85.04	103.7	840.6	5.408	0.214	28.14	13.34	2.066	4-1
28	68.53	2050.4	66.76	73.74	1122.0	7.093	0.095	28.23	2.262	2.842	33-1
29	74.87	1200.6	63.70	67.50	1176.0	7.434	0.053	30.44	1.137	3.506	36-1
30	47.63	3777.3	76.23	87.96	884.0	6.173	0.150	30.50	6.402	2.541	22-1
31	40.21	2417.0	86.56	93.91	847.8	5.357	0.088	30.71	6.178	2.655	2-2
32	68.53	3290.2	70.31	80.46	1177	6.726	0.135	30.96	4.292	2.754	34-1
33	40.21	5300.4	115.0	129.9	1156	3.804	0.147	32.65	34.45	2.114	4-2
34	40.21	7228.9	95.36	115.7	939.0	4.785	0.229	32.94	25.29	2.169	5-1
35	47.63	5369.6	83.22	98.20	964.7	5.602	0.183	33.64	12.09	2.502	23-1
36	55.14	3780.1	74.17	84.58	996.7	6.357	0.135	34.53	5.864	2.912	26-1
37	74.87	3513.1	69.50	79.22	1272	6.807	0.130	34.56	4.415	3.049	38-1
38	74.87	2221.8	66.46	72.60	1221	7.126	0.084	34.73	2.414	3.445	37-1
39	40.21	3756.1	99.93	109.7	987.8	4.524	0.107	35.41	15.29	2.622	3-2
40	62.01	3781.1	72.60	82.14	1098	6.503	0.125	37.76	3.215	5.472	30-1
41	62.01	2431.6	68.76	75.13	1043	6.883	0.086	36.53	2.951	3.499	29-1
42	74.87	4933.9	74.00	86.80	1350	6.373	0.166	36.62	7.596	2.923	39-1
43	74.87	6772.9	79.33	95.54	1445	5.909	0.203	39.43	13.06	2.854	40-1